Elucidation and modeling of the *in-vivo* kinetics of enzymes and membrane transporters associated with β-lactam and non-ribosomal peptide production in *Penicillium chrysogenum*

Proefschrift

ter verkrijging van de graad van doctor
aan de Technische Universiteit Delft
op gezag van de Rector Magnificus prof. ir. K.C.A.M. Luyben,
voorzitter van het College voor Promoties
in het openbaar te verdedigen op maandag 8 juli 2013 om 12:30 uur

door

Amit Tatyasaheb DESHMUKH

Master of Science in Chemical Engineering
Technische Universität Dortmund
geboren te Kotul, Akole, India

Dit proefschrift is goedgekeurd door de promotor:
Prof. dr. ir. J.J. Heijnen
Copromotor: Dr. W.M. van Gulik

Samenstelling promotiecommissie:

Rector Magnificus,	voorzitter
Prof. dr. ir. J. J. Heijnen,	Technische Universiteit Delft, promotor
Dr. W. M. van Gulik,	Technische Universiteit Delft, copromotor
Prof. dr. ir. M. H. Zwietering,	Wageningen University & Research Centre
Prof. dr. ing. L. M. Blank,	RWTH Aachen University, Germany
Prof. dr. ir. H. Noorman,	Technische Universiteit Delft & Royal DSM N.V.
Prof. dr. I. J. van der Klei,	Rijksuniversiteit Groningen
Dr. ir. J-M. G. Daran,	Technische Universiteit Delft
Prof. dr. ir. L. A. M. van der Wielen,	Technische Universiteit Delft, reservelid

The research described in this thesis was performed at the Bioprocess Technology Group of the Department of Biotechnology at Delft University of Technology. This project is financially supported by Netherlands Organisation for Scientific Research (NWO) via the IBOS (Integration of Biosynthesis and Organic Synthesis) Programme of Advanced Chemical Technologies for Sustainability (ACTS) (project nr: IBOS 053.63.011) and also by DSM. This project was carried out within the research programme of the Kluyver Centre for Genomics of Industrial Fermentation which is part of the Netherlands Genomics Initiative / Netherlands Organization for Scientific Research.

ISBN: 978-94-6186-169-6

Printed in The Netherlands by Ipskamp Drukkers

Dedicated to my grandfather….

Twenty years from now,
You will be more disappointed by the things you didn't do than by the ones you did do!
So throw off the bowlines. Sail away from the safe harbor. Catch the trade winds in your sails!!
Explore! Dream!! Discover!!!

-Mark Twain

Summary

Even 80 years after the discovery of penicillin, it still holds 16% of total antibiotics market. This makes it crucial, from an economical point of view, to improve our understanding of the production organism *Penicillium chrysogenum* to maximize the penicillin production, as its theoretical yields are far from reached. With the advancement in analytical techniques and detailed knowledge of the metabolic pathways, enough information and tools are available to try to identify possible bottlenecks that limit the penicillin yield, and thus with known genome sequence there are possibilities to modify the strain by using metabolic engineering strategies.

One of the aims of this study was to unravel the *in vivo* enzyme kinetic properties and identify possible bottlenecks in the penicillin biosynthesis pathway in *Penicillium chrysogenum*. To understand the mechanism of the enzymes/transporters under *in vivo* conditions and to estimate parameters, several different studies were carried out that included steady state and stimulus response experiments. The other aim of the study was to use *Penicillium chrysogenum* as a cell factory to produce non-ribosomal peptides. The strain used was an industrial high producing strain.

It has been reported in literature that in low producing strains, one of the bottlenecks limiting the fluxes through the pathway is the availability of one of the precursor amino acid, α-aminoadipate (α-AAA). Therefore, a stimulus response experiment with addition of α-AAA was carried out to investigate whether α-AAA is a limiting precursor to δ-[L-α-aminoadipyl]-L-cysteinyl-D-valine synthetase (ACVS), the first enzyme in the penicillin biosynthesis pathway and hence affecting the penicillin production rate in a high producing *P. chrysogenum* strain (**Chapter 2**). The results showed that even at a 60 fold higher concentration of intracellular α-AAA, the intracellular penicillinG (PenG) level was not affected and no increase of the rate of PenG production was measured. The results indicate that the used high producing strain has lost the L-α-AAA limitation.

To understand the transport mechanisms of the penicillin side chain precursor phenylacetic acid (PAA) and of PenG over the cellular membrane, separate kinetic models were developed **(Chapter 3)**. To estimate the parameters, stimulus response experiments were performed with PAA and PenG in chemostat cultures of *P. chrysogenum* at time scales of seconds to minutes. The results indicated that even at pH of 6.5 PAA is able to enter the cell by passive diffusion

of the undissociated acid at a very high rate (100 times faster than the penicillin production rate), but is at the same time actively excreted, possibly by an ATP-binding cassette (ABC) transporter. This results in a futile cycle, dissipating a significant amount of metabolic energy, which was quantitatively confirmed by increased rates of substrate consumption and of respiration. Furthermore, PenG was found to be rapidly taken up by the cells upon extracellular addition, indicating that PenG export is reversible. The measured concentration difference of PenG over the cell membrane corresponded well with a uniport mechanism transporting the PenG anion.

In order to study the kinetics of the enzymes and the transport mechanisms of the metabolites in the penicillin pathway, experiments were performed to locally perturb the penicillin biosynthesis pathway by PAA (**Chapter 4**). The high producing strain of *P. chrysogenum* was grown in a glucose limited chemostat without supply of PAA and was instantaneously perturbed by a step of 5 mM. Subsequently the intra- and extra- cellular concentrations of all compounds related to the penicillin biosynthesis pathway were measured. The results reveal that in the absence of PAA the rate of total ß-lactam production was almost 50% as compared to ß-lactams produced in the reference conditions (in presence of PAA), but the penicillin pathway enzymes were degenerating faster. After the PAA step, the strain immediately started to produce penicillin-G (PenG) indicating that the biosynthetic machinery needed to produce PenG was already expressed during the cultivation without PAA. Indications for the most likely transport mechanism for the pathway metabolites were obtained from measured transport rates and concentration differences over the cell membrane and thermodynamic analysis. IPN^- transport seems to be mediated by irreversible facilitated diffusion, $6APA^-$ by reversible facilitated transport, and 8-hydoxy-penillic acid ($8HPA^{-2}$) by irreversible facilitated transport. We found indications that formation of 8HPA takes place both inside and outside of the cell while ortho-hydroxy-PAA ($oOHPAA^-$) is formed in the cell and secreted actively.

The studies with *P. chrysogenum* fermentations in the absence of PAA demonstrated significant production of 6APA, which is an important precursor to produce semisynthetic antibiotics such as ampicillin and amoxillin. This insight in the production of 6APA could lead to the development of sustainable one-step fermentation processes to replace the current 2 step process for producing 6APA with penicillin acylase from PenG. This will reduce the

cellular energy burden and waste production associated with the required unit operations of the current industrial processes.

The information obtained from these experiments (Chapter 3 and Chapter 4) was combined to construct a full kinetic model for the penicillin biosynthesis pathway including transport of intermediate metabolites over the cell membrane **(Chapter 5)**. To this end a dynamic model of the pathway, based on Michaelis-Menten type rate equations, was constructed. The model included the formation of several byproducts as well as the transport of PAA, penicillin pathway intermediates, the product PenG and other byproducts over the cytoplasmic membrane. Parameter estimation was carried out by fitting the model to the obtained dynamic metabolite patterns. Finally, the full kinetic model was capable of describing the changes in the levels of intra- and extracellular concentrations of pathway metabolites, and was used to estimate the changes in the enzyme levels of the penicillin pathway and calculating the fluxes through the pathway. It also yielded information about the mechanisms of enzymes and cell membrane transporters present in the pathway. The flux control coefficient based on the model equations showed that in this strain ACVS controls 94% of the flux through the penicillin biosynthesis pathway.

The issue of accurate quantification of thiol compounds such as ACV was solved by using maleimide for derivatizing the reactive sulfhydryl bond in ACV at the time of sampling, as described in **Chapter 6**.

A demonstration to show that *P. chrysogenum* can be used as a fungal cell factory for the production NRP's was carried out in **Chapter 7**. As model NRP - ACV was used, which is the first intermediate in the penicillin biosynthesis pathway. For this purpose a *P. chrysogenum* strain lacking the penicillin gene cluster, but containing only ACVS was constructed and used to study the production of ACV and its secretion mechanism in a glucose limited chemostat. We observed that a significant amount of ACV was produced and secreted, but that the production slowed down significantly during cultivation, due to a five-fold decrease in ACVS enzyme level. A kinetic model is proposed that describes the kinetics of formation of ACV and bisACV and their secretion mechanism. Furthermore, accurate quantification of free glutathione, and the ratio of glutathione to glutathione disulfide elucidated the redox state of the cell.

Several different metabolic engineering targets to decrease the cost of penG production were identified in this whole study.

1) Eliminating the active PAA exporter will decrease the energy consumed by futile cycling of PAA and thus increase the energetic efficiency (and therewith the penicillin yield on glucose) of the strain and saving substantial substrate and O_2 costs for industrial production of PenG.

2) The capacity of the PenG exporter was probably utilized to its maximum, thus identifying and increasing the PenG exporter capacity is identified as metabolic engineering target.

3) Identification and elimination of the transporters of IPN, 6APA and 8HPA will decrease losses towards unwanted by-products, and thus increase the flux through the pathway towards PenG.

4) Finally, ACVS was found to control the flux in the pathway because it is degenerating over a period of cultivation. Thus, ACVS is identified as the main metabolic engineering target for improvement by finding the cause of its genetic and/or protein instability.

Samenvatting

Ruim 80 jaar na de ontdekking van penicilline beslaat het middel nog steeds 16% van de totale markt voor antibiotica. De theoretisch maximale rendementen zijn nog niet behaald, waardoor het vanuit een kosten oogpunt cruciaal is de productie te vergroten door een beter inzicht te krijgen in de producerende stam. Met behulp van verbeterde analytische methoden, alsmede gedetailleerde kennis van metabole routes, kan voldoende informatie verzameld worden om mogelijke knelpunten van het penicilline productieproces te identificeren. Aan de hand van bekende sequenties in het genoom zijn er daardoor mogelijkheden om de stam te verbeteren, bijvoorbeeld door middel van genetische modificatie.

Een van de doelen van dit onderzoek was het ontrafelen van de *in vivo* kinetische eigenschappen van de enzymen van de penicilline biosynthese route in *Penicillium chrysogenum* en het identificeren van mogelijke knelpunten. Om het mechanisme van enzymen/transporteiwitten te begrijpen onder *in vivo* omstandigheden en een schatting te maken van parameters, werden verschillende studies uitgevoerd, waaronder steady state en stimulus respons experimenten. Een tweede doel van het onderzoek was om *Penicillium chrysogenum* als een cell factory (cellulaire fabriek) te gebruiken voor de productie van niet-ribosomale peptides. In deze studie wordt een hoog produceert industriële stam gebruikt.

Het is in het verleden aangetoond dat in laag-producerende stammen, de beschikbaarheid van één van de precursor aminozuren, α-aminoadipate (α-AAA) een van de limiterende factoren voor de flux door de metabole route is. Om te achterhalen of dit ook het geval is voor de in dit onderzoek gebruikte hoog producerende stam werd een stimulus response experiment uitgevoerd om vast te stellen of α-AAA een limiterende precursor is voor δ-[L-α-aminoadipyl]-L-cysteinyl-D-valine synthetase (ACVS), het eerste enzym in de penicilline biosynthetische route, en daarmee de productiesnelheid van penicilline beinvloedt **(Hoofdstuk 2)**. De resultaten wezen uit dat er zelfs bij een 60-voudige concentratieverhoging van intracellulair α-AAA geen verandering optrad van het niveau van intracellulair penicilline-G (PenG) of diens productiesnelheid. De resultaten geven aan dat de gebruikte hoog producerende stam de L-α-AAA limitatie heeft verloren.

Om de transportmechanismen van de penicilline zij-keten precursor phenylazijnzuur (PAA) en PenG over het cellair membraan te begrijpen, werden aparte kinetiekmodellen ontwikkeld

(Hoofdstuk 3). Voor een schatting van de modelparameters werden stimulus respons experimenten met PAA en PenG uitgevoerd in chemostaatculturen van *P. chrysogenum* op een tijdschaal van seconden tot minuten. De resultaten gaven aan dat PAA met zeer hoge snelheid de cel binnentreedt via passieve diffusie (100 keer sneller dan de productiesnelheid van penicilline), maar tegelijkertijd actief wordt uitgescheiden, mogelijk door een zgn. ATP binding cassette (ABC) transport eiwit. Dit resulteert in een energie verbruikende futiele cyclus waarbij een significante hoeveelheid metabole energie verloren gaat, wat kwantitatief werd bevestigd door hogere snelheden van substraatconsumptie en respiratie. Daarnaast werd waargenomen dat PenG acuut door de cellen werd opgenomen wanneer extracellulair toegevoegd, wat aangeeft dat PenG export reversibel is. De gemeten concentratieverschillen van PenG over het celmembraan kwamen goed overeen met een uniport mechanisme voor transport van het PenG anion.

Om enzymkinetiek en transportmechanismen van de penicilline biosynthese te bestuderen werden experimenten uitgevoerd waarin de metabole route lokaal werd verstoord door toevoeging van PAA **(Hoofdstuk 4)**. De stam *P. chrysogenum* werd in afwezigheid van PAA gecultiveerd in een glucose-gelimiteerde chemostaat, en verstoord met een stapsgewijze verhoging tot 5mM PAA**.** Vervolgens werden de intra- en extracellulaire concentraties gemeten van alle stoffen die aan de penicilline biosynthese route gerelateerd zijn. De resultaten wezen uit dat in afwezigheid van PAA de snelheid van totale ß-lactam productie bijna 50% bedroeg van de productiesnelheid onder normale omstandigheden (bij aanwezigheid van PAA). Daarintegen degenereerden de enzymen van de penicilline biosynthese sneller. Na de PAA stap bleek het organisme direct penicilline (PenG) te gaan produceren, wat aangaf dat het benodigde cellulair mechanisme voor PenG productie al tot expressie was gebracht tijdens de cultivatie in afwezigheid van PAA. Uitspraken over de aanwezige transportmechanismen voor de diverse metabolieten van de penicilline biosynthese werden gebaseerd op gemeten transportsnelheden, verschillen van intra- en extracellulaire concentraties over het celmembraan en een thermodynamich analyse. IPN^- transport leek te verlopen middels irreversibel gefaciliteerde diffusie, $6APA^-$ middels reversibel gefaciliteerde diffusie en 8-hydroxy-penillic acid ($8HPA^{-2}$) door irreversibel gefaciliteerd transport. Vorming van 8HPA vond zowel binnen als buiten de cel plaats, terwijl ortho-hydroxy-PAA ($oOHPAA^-$) intracellulair werd gevormd en actief uitgescheden.

De studies met *P. chrysogenum* fermentaties in afwezigheid van PAA demonstreerden significante productie van 6APA, wat een belangrijke precursor is voor de productie van semisynthetische antibiotica zoals ampicilline en amoxilline. Dit inzicht in de productie van 6APA kan leiden tot de ontwikkeling van duurzaam een-staps fermentatieproces, wat het huidige 2 staps proces van 6APA productie met penicilline acylase uit PenG zou kunnen vervangen. Dit zal de energie consumptie verlagen en een vermindering teweeg brengen van productie van afvalstoffen uit de huidige industriële processen.

De informatie verkregen uit deze experimenten (Hoofdstuk 3 en Hoofdstuk 4) werd samengevoegd om een compleet kinetiekmodel te construeren voor de penicilline biosynthese, inclusief transport van intermediaire metabolieten over het celmembraan (Hoofdstuk 5). Hiervoor werd een dynamisch model opgezet, gebaseerd op vergelijkingen van reactiesnelheden in een Michaelis-Menten vorm. De vorming van verscheidene bijproducten werd in het model inbegrepen, evenals het transport over het cell membraan van PAA, intermediairen, het product PenG en bijproducten. Parameters werden geschat aan de hand van gemeten patronen van veranderende metabolietconcentraties tijdens het PAA stap experiment. Het volledige kinetiekmodel was in staat de veranderende intra- en extracellulaire concentraties van metabolieten te beschrijven, veranderende enzymconcentraties in kaart te brengen en fluxen door de penicilline biosynthese te berekenen. Daarnaast verschafte het model ook informatie over de mechanismen van enzymen en membraan transporteiwitten relevant voor de PenG biosynthese pad. De flux controle coefficienten verkregen uit het model toonde aan dat ACVS in deze stam voor 94% de flux door de penicilline biosynthese bepaalt.

Nauwkeurige kwantificering van ACV en andere thiol-houdende stoffen werd bereikt door het gebruik van maleimide voor derivatisatie van de reactieve sulfhydrylbinding in ACV op het moment van monstername zoals beschreven in Hoofdstuk 6.

De inzetbaarheid van *P. chrysogenum* als ‘cell factory’ voor de productie van niet ribosomale eiwitten (non ribosomal proteins of NRP’s) werd gedemonstreerd in Hoofdstuk 7. Als model NRP werd ACV gebruikt, de eerste intermediar in de penicilline biosynthese route. Hiertoe werd een *P. chrysogenum* stam geconstrueerd die als enig enzym van de penicilline biosynthese route ACV synthase (ACVS) bevatte. Vervolgens werd de productie en uitscheiding van ACV van deze stam in een glucose gelimiteerde chemostaat onderzocht. We

vonden dat een significante hoeveelheid ACV werd geproduceerd en uitgescheiden, maar dat de productie geleidelijk daalde door een vijf-voudige vermindering van het ACVS enzymniveau. Een kinetiekmodel werd opgesteld om de vormingskinetiek en uitscheiding van ACV en bisACV te beschrijven. Bovendien werd de verhouding van vrij en gedimeriseerd glutathion nauwkeurig gemeten, welke de redox staat van de cel weerspiegelt.

In deze studie werden verschillende mogelijkheden voor stamverbetering gevonden teneinde de PenG productie te verhogen en dus de productiekosten de verminderen:

1. Eliminatie van de actieve PAA exporter zal de energie die verspild wordt in een cyclus van passieve import en actieve export van PAA verminderen en zo de energie efficiëntie (en daarmee de penicilline opbrengst op glucose) van de stam verhogen.
2. Afgaand op onze bevindingen bleek de capaciteit van de PenG exporter in de hoog producerende stam maar net toereikend, en zijn identificeren en verhogen van deze capaciteit noodzakelijk bij verdere stamverbetering.
3. Identificatie en eliminatie van de transporteiwitten van IPN, 6APA en 8HPA zal ongewenste verliezen naar deze bij-producten verminderen en zo de flux door de metabole route naar PenG verhogen.
4. Tenslotte werd gevonden dat ACVS de flux in de penicilline biosynthese controleert, dit als gevolg van ACVS degeneratie gedurende de cultivatie. Het vaststellen van de oorzaak van genetische en/of eiwit-instabiliteit van ACVS werd daarom aangewezen als een belangrijk doel voor verdere stamverbetering.

The following abbreviations have been used throughout this thesis.

3PG	3-phosphoglycerate
6APA	6-aminopenicillanic acid
6PG	6-phosphogluconate
8HPA	8-hydroxypenicillic acid
α-AAA	L-α -aminoadipic acid
AAT	Acyl-CoA: 6APA Acyltransferase
ABC	ATP-binding cassette
ACV	L-α-(δ-aminoadipyl)-L-α-cysteinyl-D-α-valine
ACVS	L-α-(δ-aminoadipyl)-L-α -cysteinyl-D-α-valine synthetase
ADP	adenosine diposphate
αKG	α-ketogluterate
AMP	adenosine monoposphate
AT	acyl coenzyme A: Isopenicillin-N acyltransferase
ATP	adenosine triposphate
Cys	L-cysteine
bisACV	Bis- L-α-(δ-aminoadipyl)-L-α-cysteinyl-D-α-valine
DBAA	dibutylammonium acetate
DHAP	dihydroxyacetone phosphate
DO	dissolved oxygen
EC/Ex	extracellular
EM	ethyl maleimide
F6P	fructose-6-phosphate
F16bP	fructose-1,6-bisphophate
G6P	glucose-6-phosphate
GAP	glyceraldehyde-3-phosphate
g DW	gram dry weight
Glu	L-Glutamic acid
GSH	glutathione
GSSG	glutathione disulphide
GR	glutathione reductase system
IAH	isopenicillin-N amidohydrolase
IAT	isopenicillin-N acyltransferase
IC/ in	intracellular
IDMS	isotope dilution mass spectrometry
IPN	isopenicillin-N
IPNS	isopenicillin-N synthase
Lys	L-Lysine
MRM	multiple reaction monitoring
NAD(H)	nicotinamide dinucleotide

NADP(H)	nicotinamide dinucleotide phosphate
NRP	non-ribosomal peptides
NRPS	non-ribosomal peptide synthetases
oOHPAA	ortho-hydroxyphenylacetic acid
OPC	6-oxopiperidine-2-carboxylic acid
PA	penicillin amidase
PAA	phenyl acetic acid
PA-CoA	phenylacetyl CoA
PAH	phenylacetate hydroxylase
PCL	phenylacetyl CoA ligase
PEP	phosphoenolpyruvate
PenG	penicillin-G
PIO	penicilloic acid
Ser	L-Serine
SRM	selected reaction monitoring
TCEP	tris(2-carboxy-ethyl)phosphine hydrochloride;
TR	thioredoxin-thioredoxin reductase system
Val	L-valine

Table of contents

Chapter 1

Introduction

1.1 General introduction

The discovery of antibiotics and its introduction to cure diseases had a profound impact on human health and sustainably contributed to increase the human life expectancy. Due to the ever increasing demand for antibiotics, pharmaceutical industries are striving to improve the product yield, titers and productivities by improving the strains and processes. The emergence of bacterial resistant strains also needs to focus on finding novel antibiotics [7,84].

1.1.1 ß-lactam antibiotics

The global antibiotics market was $42 billion in 2009 and is estimated to grow to $66 billion in 2016 with a growth rate of 9.6% [10]. ß-lactams, which include penicillins, carbapenems, and cephalosporins and semi-synthetic penicillins such as amoxycillin and ampicillin, accounts for 45% of the total antibiotics market (Figure 1.1). Of these antibiotics, penicillin alone share 16% of total antibiotics market. This underlines the importance of penicillin in the world of antibiotics and motivates to strive further to understand the obscure regions of the penicillin metabolism. There is still enough room to improve the penicillin production, as its theoretical yields are far from reached. With a detailed knowledge of the metabolic pathways, stoichiometric/kinetic models and with the known genome sequence, it is possible to identify bottlenecks that limit the yield and rate of penicillin production [12,93,123,132,176].

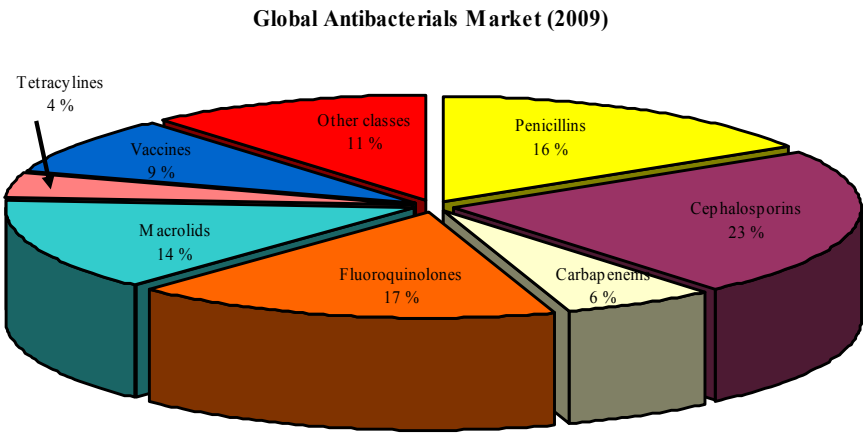

Figure 1.1: Global antibacterial market for year 2009 [10].

1.1.2 History of ß-lactam antibiotics

The history of the ß-lactam antibiotics started with the discovery of penicillin by Sir Alexander Fleming in 1929. The discovery was done accidentally when Fleming found that there was some active compound produced by a fungus that contaminated a Petri dish

inoculated with *Staphylococcus aureus*. This phenomenon inspired him to isolate and culture the mould to produce the active compound, which he named as penicillin, to inhibit the growth of the bacteria [54]. Initially the mould was identified as *Penicillium rubrum* and later corrected to *Penicillium notatum* in 1932. New ways were devised to grow the fungus in large quantities and the antibiotic properties of penicillin were studied [35]. However, a detailed study of penicillin was undertaken much later by Howard Florey and Ernst Chain in 1940 who described the chemotherapeutic effects of penicillin on mice [33]. This was later followed by human trials and Abraham and co workers described the conditions required for effective production of penicillin on large scale [1]. Due to outbreak of World War II, the progress of penicillin research shifted from the UK to the US at Northern Regional Research Laboratory (NRRL) in Peoria, Illinois. A practice of submerged cultivation started which increased the yield of penicillin-G (PenG). The penicillin research continued at NRRL [114-116] and later at University of Wisconsin [155] where the early development of the penicillin producing strains took place. After the end of the war, penicillin was finally available in the open market and several different penicillins were being produced, depending on the composition of the medium, the fungal strain, and the fermentation conditions (Penicillin-G/Penicillin-V). Later the strains were substantially improved during classical strain improvement program. For their significant contribution for the discovery of penicillin and its curative effects, Sir Alexander Fleming, Ernst B. Chain, and Howard W. Florey were awarded with the Nobel Prize for Physiology and Medicine in 1945.

Another important discovery occurred when the penicillin fermentations were carried out in the absence of any side chain precursor. Under such condition the penicillin nucleus 6-aminopenicillanic acid (6APA) [17] was produced. It was also possible to produce 6APA by enzymatic hydrolysis of penicillin [143]. 6APA was the ideal starting material for the preparation of semisynthetic penicillins (ampicillin /amoxillin).

1.1.3 Strain improvement programs

The “Fleming strain” called *P. notatum* strain (NRRL 824) produced 0.13 µg/ml of penicillin and the strain derived from it, NRRL 1249.B21, produced 1.2 µg/ml in submerged cultures. As these quantities were too low to exploit the commercial production of penicillin, several cultures of *P. notatum-chrysogenum* group were screened for penicillin production. This resulted in the promising strain *P. chrysogenum* NRRL producing 60-150 µg/mL. This strain

is the parent of all worldwide industrially used *P. chrysogenum* strains [139]. Several other mutants were created by X-ray or ultraviolet radiation and tested at the Carnegie institution, Cold Spring Harbor, New York and the University of Wisconsin. One of these mutant strains Q-176 was able to produce 550 μg/ml. After several rounds of classical mutagenesis, the improved Wisconsin line of strains were produced of which Wisconsin 54-1255 could produce over 1800 μg/ml of penicillin [40,77,138]. Several industries improved the strains for higher penicillin yields resulting in the high producing strain such as P2/ B14 strains of Penlabs, AS-P-78/ E1 strains of Antibioticos, NMU2/40 of Bitika, BW1952 of Beecham, and DS04825/DS17690 from DSM. The current high producing strains can produce more than 50,000 μg/ml in fed batch cultures.

This random mutagenesis and selection procedure modified the wild type strain with several different aspects. The first change observed was the decrease in the catabolism of phenyl acetic acid thus resulting in increased penicillin production [141]. Secondly there was amplification in the penicillin biosynthetic gene cluster containing the genes *pcbAB*, *pcbC*, and *penD*. There was only a single copy of the penicillin biosynthetic gene cluster in the genome of NRRL 1951 and Wis 54-1255, whereas the high producing industrial strains contain several copies of the penicillin gene cluster. Furthermore, there was also different transport capabilities evolved from Q-176 to Wisconsin 54-1255 [53,126,169]. Recent transcriptome studies indicated that the genes involved in biosynthesis of the amino acid precursors for the penicillin biosynthesis (α-AAA, cysteine and valine) and the genes encoding microbody proteins were upregulated in the high producing strains [171]. Recent proteomics studies comparing NRRL 1951, Wisconsin 54-1255, and the high producing strain AS-P-78, indicated that there was overproduction of the enzymes involved in the pentose phosphate pathway like ribose-5-phosphate isomerase or transketolase which had direct consequence on the production of NADPH and consequently on the production of cysteine. Furthermore, there was loss of certain pathways leading to secondary metabolites such as pigment production [77]. These findings suggest that in order to improve the production of penicillin the strains evolved to optimize the energetic burden and the redox metabolism and increased the supply of precursor amino acids. These improvements were done randomly, but similar strategies can be used through systematic studies of the strain using metabolic engineering tools. Thus, this study uses metabolic engineering strategies to identify the bottlenecks in the penicillin biosynthesis pathway to improve the penicillin production. The strain used for most of the study presented in this thesis was *Penicillium chrysogenum*

DS17690, which is a high producing strain, developed by Gist-Brocades, since 1998 part of DSM. This strain was used for industrial scale penicillin production in the 1980's and is a direct continued cultivation strain of *Penicillium chrysogenum* DS12975 [164,175,176]. It has been extensively used for research on industrial penicillin production over the last decade [37,38,42,65,120,171]. Furthermore, in order to produce ACV as a model NRP, *Penicillium chrysogenum* DS62824 was used that was constructed by removing the penicillin pathway enzymes and then reintroducing only ACV synthetase.

1.2 Metabolic engineering

Because of the limitations of the conventional strain improvement techniques like random mutagenesis and screening, new methodologies and techniques such as metabolic engineering approach are been developed. Metabolic engineering is defined as the improvement of the cellular activities by making changes to the enzymatic, transport and regulatory functions of the cell with the help of recombinant DNA technology [12,123]. Metabolic engineering requires insight about the physiology of the microorganism regarding the metabolic pathways in the cell. It often involves improving the flux through the biosynthesis pathway leading to the antibiotic of interest by overexpressing the genes encoding the penicillin biosynthesis enzymes e.g. through insertion of multiple gene copies, promoter replacement and/or through overexpression of transcriptional activators. The use of metabolic engineering approach could boost yields of production strains that are difficult to overcome by classical strain improvement procedures. However, for directed genetic improvement construction of mathematical models of metabolic pathways is essential in order to absorb the underlying biological processes. These models help to understand the complex kinetic behavior of metabolic reaction networks with respect to metabolite-enzyme interactions. In addition, the mathematical models serve the purpose to predict genetic targets for successful modification and/or optimization of the metabolic reaction network. There are two main classes of models: steady state models and kinetic models.

1.2.1 Steady state stoichiometric models

Steady state stoichiometric models describe the biochemical reactions in the cell as a set of algebraic equations and can be used to calculate steady-state intracellular fluxes [68,176]. The main advantages of stoichiometric models compared with kinetic models are: no kinetic information is needed, comprehensive models of pathway biochemistry are possible, and

these models can be used to test pathway insertions or deletions, *in silico*, with relatively little effort. This last feature of stoichiometric models is particularly useful for metabolic engineering, as it allows a systems approach for planning directed genetic changes. However, the stoichiometric models cannot identify fluxes in parallel pathways and bidirectional fluxes. The solution to such problem is to do flux analysis based on 13C-labeling experiments [184,185]. In addition, it poses limitations to predict the rate of formation for non-catabolic products when the same metabolites are necessary for product formation and for biomass formation. At the branching point, the distribution of flux is based on the kinetic properties of the branching enzymes. An example of this situation is the production of penicillin that requires amino acids, cysteine and valine, in competition with biomass formation. Thus, the flux towards the penicillin biosynthetic pathway will be determined by the kinetic properties of the first enzyme of the pathway, ACVS, with respect to these amino acids and other allosteric effectors.

1.2.2 Kinetic models

The kinetic models describe the biochemical reactions as a set of differential equations instead of algebraic relations as in steady state. Thus, they can describe the time dependent data and determine the fluxes through the enzyme/pathway in consideration. Each individual reaction rate is a function of the enzyme activities, the metabolite concentration and the kinetic function/parameters of the enzyme. Usually the mathematical expressions representing the kinetic behavior of these enzymes are based on the known molecular interactions of the substrate and the enzyme. The simplest mechanistic kinetic equation is a two parameter model showing hyperbolic behavior of the enzyme also known as Michaelis-Menten kinetic expression. For a one substrate and an irreversible reaction it is defined as

$$v = \frac{v^{\max}}{1 + K_m \cdot C_s^{-1}}$$

where, v is the flux through the enzyme, v^{max} is the maximum flux at full saturation of the enzyme's active sites, K_m is the concentration of the substrate that saturates half of the enzyme's active sites, also called as Michaelis-Menten constant. In addition, there can be different allosteric interactions added to the above equation, which can increase the complexity of the model and parameters. Such non-linear mechanistic enzyme kinetics when used to describe the *in vivo* system poses the problem of parameter estimation.

1.2.3 Stimulus response experiments of different timescales

A rich data set of concentration/rates are necessary in order to estimate kinetic parameters *in vivo*, as it is often found that *in vitro* kinetic parameter estimates do not apply to the *in vivo* situations [158]. Such a data set can be generated by performing stimulus response experiments, whereby a perturbation is introduced to a microorganism in a steady state chemostat system. The microorganism rapidly reacts to changes in its environment in order to adjust itself to the new condition, thus providing information about metabolic network regulation during this transient behavior. Perturbations can be induced by changes in extracellular concentrations through the discrete addition of a component or a change in flow rates or a change in extracellular pH or temperature. In addition, the type of perturbation depends on timescales, such as second's timescale in a pulse experiment, minute's time scale in a ramp experiment or hour's time scale in a step experiment. Within a time frame of 300 s in a pulse experiment, enzyme levels can be assumed unchanged and reaction rates can be deduced from the metabolite concentration using dynamic balances and constructing kinetic models. For the larger timescale experiments, a new steady state is obtained after the perturbation, and information regarding rates can be obtained by measuring enzyme levels and metabolite concentrations. [96,108,119,140,179]. Such an approach also allows identifying the membrane transporter mechanisms [38]. For the practical execution of such experiments, accurate sampling of extra- and intracellular samples within seconds is needed to capture the dynamics in metabolite concentration responding to the perturbation.

In this thesis, such data obtained from stimulus response experiments at different timescales are used to understand the *in vivo* kinetics of enzymes and transporters involved in the penicillin biosynthesis pathway. As the dynamic data to be generated was specifically for the penicillin pathway a local perturbation of the pathway was necessary, as the perturbation based on glucose does not provide enough changes in the concentrations of the penicillin pathway metabolites [119]. Therefore, metabolites particular to the penicillin pathway were used as a perturbation agent. This included metabolites such as α-AAA, PAA and PenG. The other metabolites in the penicillin pathway such as ACV, IPN and 6APA were not used because ACV and IPN are not taken up by the cell [56] and 6APA, although taken up by the cell [56], its ability to perturb the penicillin pathway fluxes is obscure.

1.2.4 Identification of possible bottlenecks in the penicillin biosynthesis pathway

The classical strain improvement, that used random mutation and selection, led to high-yielding industrial penicillin producing strains. Improvement of the current industrial strains with the recently available genetic engineering tools is now possible by making use of metabolic engineering strategies. With a detailed knowledge of the metabolic pathways, stoichiometric/kinetic models and with the known genome sequence, it is possible to identify bottlenecks that limit the yield and rate of penicillin production. In order to identify bottlenecks, two general approaches have been applied, metabolic flux analysis and metabolic control analysis [68,80,124]. From various studies, it was concluded that the control of the flux through the pathway was distributed over ACVS and IPNS and that IPNS exerted the main control [45,124,125,159]. Other studies showed that, for high producing industrial strains, the flux through the pathway can be limited by the precursor supply from central carbon metabolism [79,120] or by the supply/regeneration of cofactors [89,176,191]. Some studies also suggested that the activity of IAT [182] or PCL can be limiting [126]. However, one of the important aspects that were not taken into account in these studies was transport of precursors and products across the plasma membrane [125,135]. These transport processes are important for cellular homeostasis and therefore fluxes across the membrane are tightly controlled. They also affect the overall energetic state of the cell. So sufficient understanding of the transport mechanisms is important to accurately identify possible bottlenecks in the metabolic pathway of interest [94].

1.3 Penicillin biosynthesis pathway and compartmentalization

Over several decades, research groups focused on establishing the biosynthesis pathway and identifying the genes/proteins involved in the biosynthesis and regulation of penicillin in *P. chrysogenum* [5,15,21,27,65,122,135,171,189]. A schematic representation of the reactions involved in the penicillin biosynthesis pathway is shown in Figure 1.2. The penicillin biosynthesis pathway encoded in gene cluster (*pcbAB-pcbC-penDE*) consists of three enzymes, α-aminoadipyl-L-cysteinyl-D-valine synthetase (ACVS), isopenicillin-N synthase (IPNS) and acyl-CoA: isopenicillin-N acyltransferase (AT) [41]. The first two enzymes are important for biosynthesis of penicillin and cephalosporin antibiotics and a lot of attention has been focused to characterize them. To investigate the kinetics of these enzymes, several *in vitro* studies were carried out [5,27,161,189].

The localization of the penicillin pathway enzymes is shown in Figure 1.3. The first step of the penicillin biosynthesis pathway is the condensation of the three amino acids, α-aminoadipate (α-AAA), L-cysteine and L-valine, to form α-aminoadipyl-L-cysteinyl-D-valine (ACV) by a multifunctional enzyme ACVS. The first enzyme ACVS is probably located in the cytosol [168]. Intracellularly, ACV accumulated can be spontaneously oxidized to bisACV and can be converted back from bisACV to ACV by a thioredoxin-thioredoxin reductase (TR) system [36]. The next step is the oxidative ring closure of ACV to form isopenicillin-N (IPN) that is catalyzed by isopenicillin-N synthetase (IPNS), which is also located in the cytosol [117]. After the formation of IPN, it is necessary that it be transported to the peroxisomes where AT is located [88,117,168]. In the absence of PAA, IPN is converted into 6-aminopenicillanic acid (6APA) catalyzed by one of the activities of AT called as IAH. 6APA reacts instantaneously with CO_2 to produce 8HPA [69]. In the presence of PAA, the final step of PenG synthesis is the replacement of the α-AAA side chain of IPN with PA-CoA, the activated form of phenylacetic acid (PAA) [92]. The activation of PAA also takes place in peroxisomes where phenylacetate CoA ligase (PCL) is located [58,92,168]. The formation of PenG takes place by two different pathways. The first pathway is the direct replacement of α-AAA by PA-CoA catalyzed by isopenicillin-N acyltransferase (IAT), while in the second pathway 6APA is formed first to which the activated PAA is attached to form PenG [4,5]. In the presence of PAA, there is formation of oOHPAA by phenylacetate hydroxylase (PAH). The transcriptome studies carried out by Harris et al. [65] indicated that transcriptional regulation of *pahA* has been retained that was removed by a point mutation and an increase in transcript level was seen in the presence of PAA. The product PenG and all the intermediate such as IPN, 6APA, 8HPA, and oOHPAA are secreted [37].

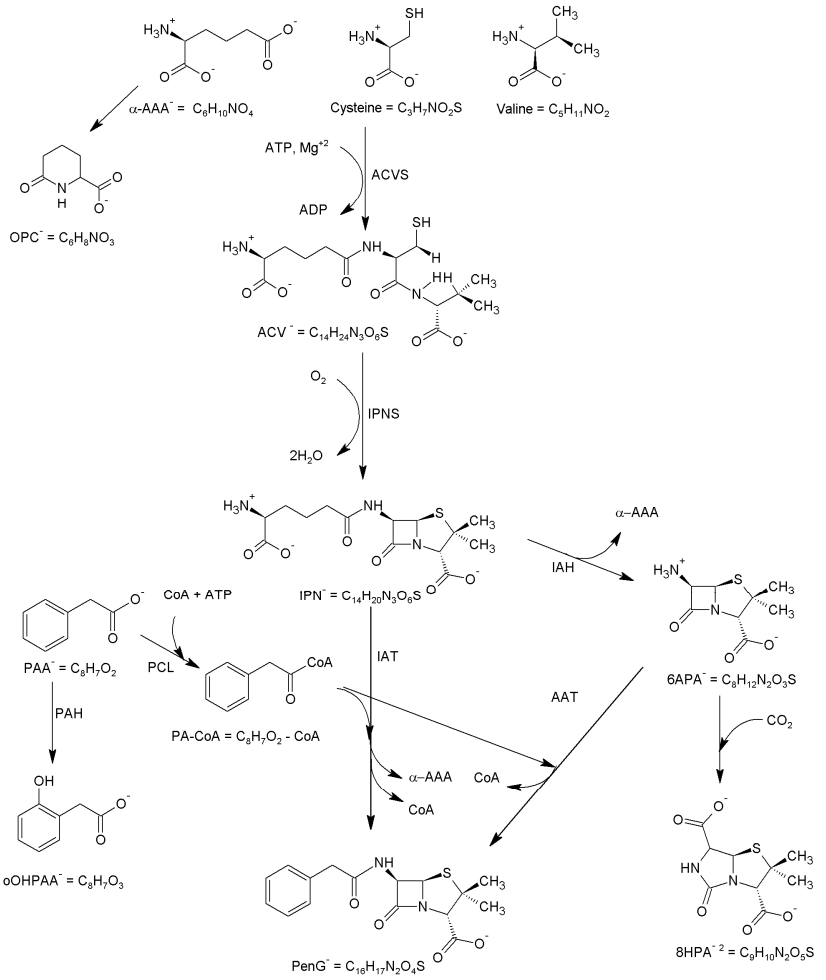

Figure 1.2: Schematic representation of the reaction pathway for synthesis of metabolites during production.

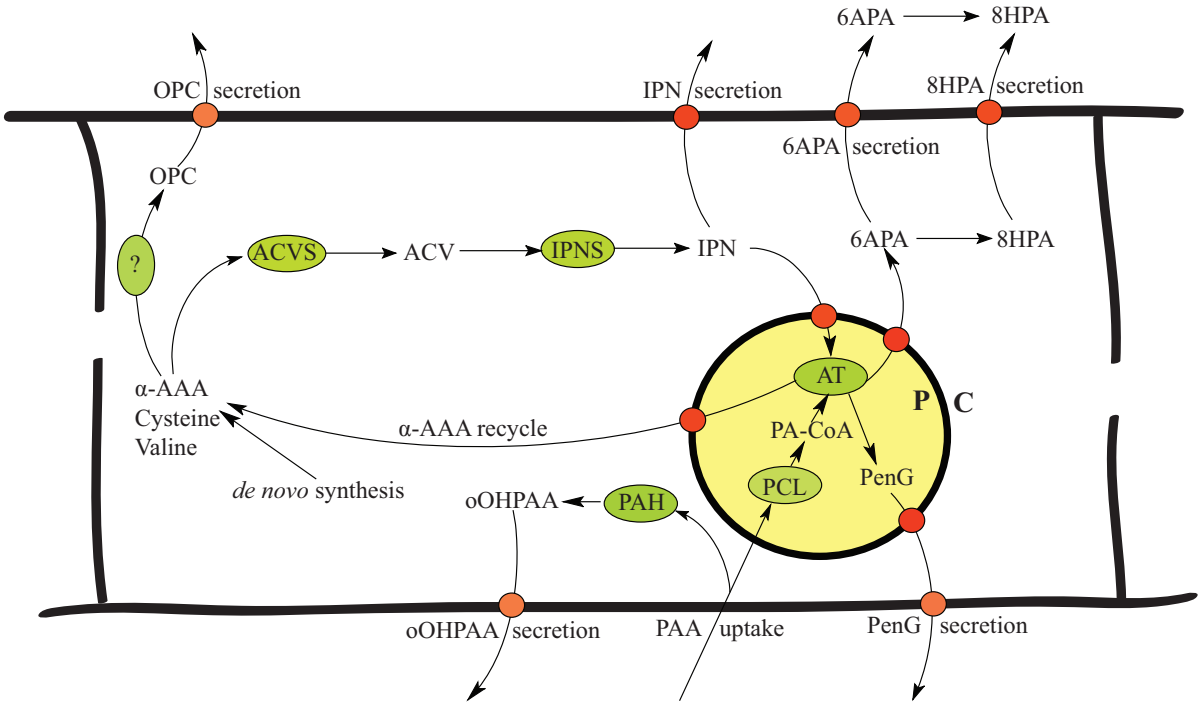

Figure 1.3: Localization of penicillin pathway enzymes in *P. chrysogenum.* ACVS and IPNS are present in cytosol (C), while AT and PCL are present in peroxisomes (P)[49].

1.4 Plasma membrane transport

Transport of substrates and products over the plasma membrane is unfortunately often neglected in the studies to improve a strain, although inefficient transport can have negative effects on the fluxes in the pathway of interest. Although several groups have been studying the transport of antibiotics over the cell membrane very little is known about the transport mechanisms of the penicillin pathway metabolites across the cell membrane which include uptake of precursor PAA and secretion of product PenG and byproducts IPN and 6APA. Understanding the mechanism of the transport of these metabolites can shed insights about the energetic burden on the cell due to the transport processes and their role in flux control through the penicillin biosynthesis pathway. Thus, identifying flux controlling transporters is one of the important aspects of this study. Studies conducted by Hillenga et al. [72] and Eriksen et al. [48] concluded that the uptake of undissociated PAA occurs through passive diffusion over the cell membrane. However, in an earlier study, PAA uptake was attributed to a protein-mediated uptake mechanism for dissociated PAA. [8,48,52,56,72].

Studies performed on various *P. chrysogenum* mutants showed that ACV, IPN were poorly taken up by the cell whereas 6APA was taken up efficiently [56]. Additionally, Ullán et al.[166] have identified the CefT protein which is responsible for IPN secretion and belongs to Family 3 of the Major Facilitator Superfamily (MFS) of membrane proteins as a Drug:H^+ antiporter. The secretion of PenG was always assumed to take place by an ABC transporter, however there is no clear evidence of involvement of an ABC transporter and no transporters are yet identified [8,172].

1.5 *Penicillium chrysogenum*: A cell factory to produce non-ribosomal peptides

P. chrysogenum is the most widely used organism for the production of β-lactams and its metabolism has been studied elaborately. Decades of industrial research on the *P. chrysogenum* strain, has made this strain very robust for industrial scale production of β-lactams (penicillin and cephalosporin). Several mutants were produced and now they can achieve high titers, productivities and yields for ß-lactam production [39]. Furthermore, there have been studies on the genome sequence of *P. chrysogenum,* which highlighted the presence of several other non-ribosomal peptide synthesis proteins (e.g. NRPSs, PKSs) which demonstrate its potential to produce secondary metabolites [171].

One example of *P. chrysogenum* as a cell factory can be demonstrated for the production NRP's, a class of peptides that is produced by a multiple-substrate non-ribosomal peptide synthetase (NRPS). Besides ACVS, over 9 other non-ribosomal peptide synthetases have been found in *P. chrysogenum* [170]. Most of them are expressed at low levels, but their expression opens up possibilities for further research for production of NRP's by *P. chrysogenum*. Non-ribosomal peptides with antibiotic properties include gramicidin S, tyrocidine, cyclosporine and capreomycin [90,112]. Other NRPs are known to act as immunomodulatory, cytostatic, surfactant, siderophore or antifungal agents (Figure 1.4). Approximately 100 NRPs have been known to display anti-tumor activity [15]. Besides this wide range of already known biological functions, other characteristics of NRPs have also sparked the interest of pharmaceutical and food industries. The first is that many NRPs and their function have not been discovered. Furthermore, building blocks of NRP synthesis are not limited to the twenty naturally occurring amino acids as hundreds of other molecules can be incorporated in NRPs [154]. Finally, genetic engineering of the peptide synthetases responsible for the production of these peptides creates an exciting new method of discovering novel antibiotics, cytostatics, antitumor drugs and other beneficial non-ribosomal peptides. A special database named NORINE has been dedicated to categorizing the 1122 currently known NRPs [15,28].

P. chrysogenum is suitable not only for homologous, but also hetrologous secondary metabolites and also homologous and hetrologous proteins [15]. These characteristics along with the information available for the fermentation conditions have made *P. chrysogenum* a suitable host strain for cell factory of novel peptides (NRP's) with possible antibiotic properties.

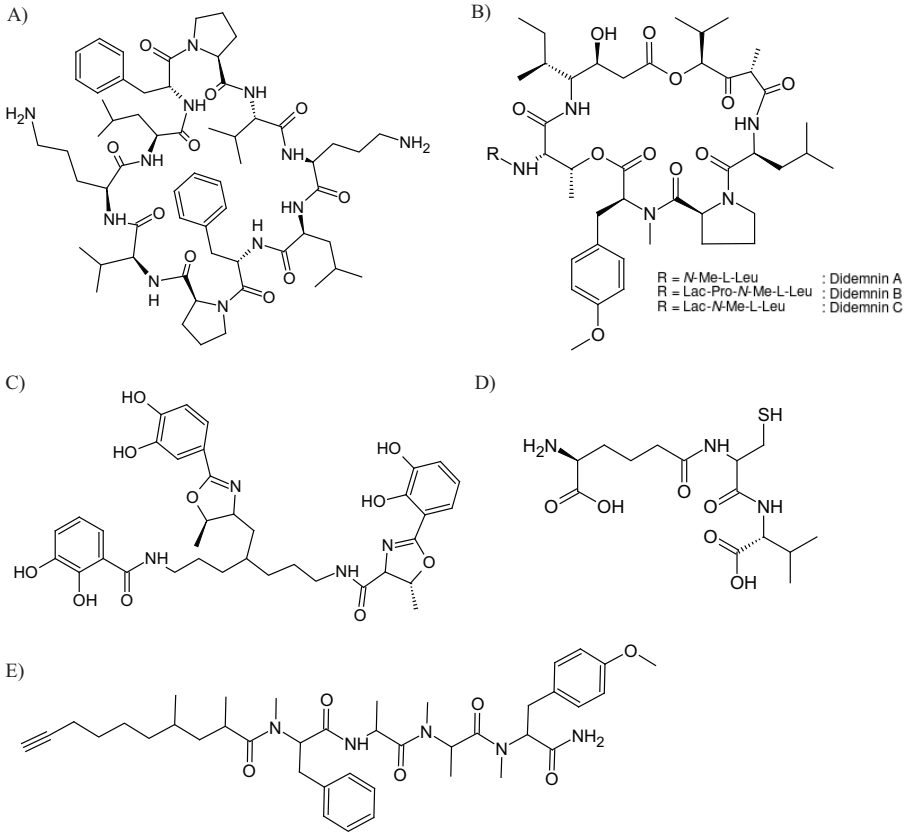

Figure 1.4: Non-ribosomal peptides are known to have a wide range of functions. Shown here are [A] Gramicidin: antibiotic. [B] Didemnin: immunosuppressant and cytotoxic agent. [C] Carbamin A: surfactant. [D] ACV: precursor for penicillin and cephalosporin antibiotics. [E] Vibriobactin: siderophore.

1.6 Aim of the thesis

The aim of the thesis is to understand the *in vivo* enzyme kinetic properties, transport mechanisms of metabolites over the cell membrane, and identify possible bottlenecks in the penicillin product pathway in using *Penicillium chrysogenum* as host strain. This will be achieved by cultivating *P. chrysogenum* in glucose-limited chemostats and using the strategy of stimulus response experiments at different timescales, whereby dynamic information will be obtained by perturbing the steady state. The information obtained from these experiments will be used to construct dynamic models, based on Michaelis-Menten type rate equations of enzymes and transporters. Parameter estimation will be carried out by fitting the model to the obtained dynamic metabolite patterns. Subsequently model parameters obtained from different stimulus experiments will be then integrated to give a complete model for penicillin biosynthetic pathway including transport of metabolites over cell membrane. Metabolic control analysis will be done to identify possible bottlenecks in the penicillin biosynthesis pathway. In the end, a proof of concept to use *P. chrysogenum* as a cell factory to produce non-ribosomal peptides will be shown.

1.7 Outline of the thesis

In chapter 2, we investigated whether the supply of L-α-AAA, which is one of the three precursor amino acids of the tripeptide ACV, would be limiting for the biosynthesis of penicillin. This was performed by investigating the response of the pathway to a sudden supply of DL-α-AAA in a high producing *P. chrysogenum* strain, leading to a local perturbation in the penicillin pathway. Therefore, the strain was grown in a glucose-limited chemostat under penicillin producing conditions in the absence of externally supplied DL-α-AAA. Subsequently, the steady state was perturbed by a stepwise increase of the extracellular DL-α-AAA concentration and the transient response of the intra- and extra-cellular concentrations of all compounds related to the penicillin biosynthesis pathway was followed until a new steady state was reached.

Chapter 3 describes the *in vivo* stimulus response experiments performed, again locally in the penicillin pathway, with the precursor phenylacetic acid (PAA) and the product PenG in chemostat cultures of *P. chrysogenum* to obtain more insight in the nature of the transport mechanism of these metabolites over the cell membrane. To estimate the thermodynamic kinetic properties of the transport of PAA and PenG over the cell membrane, a dynamic mathematical model was constructed.

Chapter 4 was aimed at understanding the pathway enzyme kinetics and secretion mechanisms of metabolites in the penicillin biosynthesis pathway by studying the dynamics in metabolome and fluxome obtained from local stimulus response experiments when a step change in PAA was applied to a steady state *P. chrysogenum* culture. In addition, by calculating ratios of measured extra- and intracellular concentrations, thermodynamics/kinetics for transport mechanisms of penicillin pathway metabolites were validated.

In chapter 5, a dynamic model of the pathway, based on Michaelis-Menten type rate equations, was constructed to unravel the *in vivo* enzyme kinetic properties of the penicillin biosynthetic pathway in *Penicillium chrysogenum*. The model included the formation of several byproducts as well as the transport of precursor, intermediates, the product penicillin-G and byproducts over the cytoplasmic membrane. To estimate the parameters of the model

under *in-vivo* conditions, data from PAA stimulus response experiments was used. The parameters were obtained by fitting the data in both dynamic and pseudo steady states.

Accurate quantification of the total ACV was achieved by using a reducing agent tris(2-carboxyethyl) phosphine hydrochloride (TCEP). For quantification of free ACV/glutathione, derivatizing agent such as maleimides (ethyl maleimide) was used. In chapter 6, the interaction of maleimides and TCEP with the thiol compounds was studied.

Due to potential pharmaceutical and food applications of complex natural and (semi-) synthetic peptides, there is a growing need for their efficient and sustainable synthesis. The majority of these natural complex peptides are synthesized by non-ribosomal peptide synthetases. In chapter 7, we have studied the production of non-ribosomal peptide formation using *P. chrysogenum* as host organism. As a model protein, δ-[L-α-aminoadipyl]-L-cysteinyl-D-valine synthetase (ACVS) was used to produce δ-[L-α-aminoadipyl]-L-cysteinyl-D-valine (ACV). For this purpose a *P. chrysogenum* strain lacking the penicillin gene cluster, but containing only ACVS was constructed. This strain was used to study the production of ACV and its secretion mechanism in a glucose-limited chemostat. Furthermore, a kinetic model was constructed to describe the system and estimate the *in vivo* kinetic parameters for the enzymes and the transporters involved.

Chapter 2

Stimulus response experiments reveal the fate of α-aminoadipate in a high producing strain of *Penicillium chrysogenum*

Deshmukh AT, van der Hoek C, Maleki Seifar R, ten Pierick A, Heijnen JJ and van Gulik WM. Stimulus response experiments reveal the fate of α-aminoadipate in a high producing strain of *Penicillium chrysogenum.* *(submitted for publication)*

Abstract

L-α-aminoadipate (α-AAA) is one of the three precursor amino acids that are converted to the tripeptide δ-[L-α-aminoadipyl]-L-cysteinyl-D-valine (ACV) as the first step in the penicillin biosynthesis pathway. To elucidate a possible α-AAA limitation for the biosynthesis of penicillin, the response of the pathway to a sudden supply of α-AAA in a high producing *Penicillium chrysogenum* strain was investigated. Therefore, the strain was grown in a glucose-limited chemostat under penicillin producing conditions in the absence of α-AAA. Subsequently, the steady state was perturbed by a step change in the extracellular α-AAA concentration and the transient response of the intra- and extra-cellular concentrations of all compounds related to the penicillin biosynthesis pathway was followed until the new steady state was reached.

After addition of the α-AAA, the intracellular concentration of α-AAA showed a rapid 60 fold increase, indicating that it was readily transported into the cell. However, this did not result in increased levels of penicillin pathway intermediates nor an increased penicillin-G production rate. Instead, the α-AAA which was taken up by the cells was assimilated in the lysine pathway. Our results indicate that the endogenous α-AAA synthesis rate was not limiting β-lactam production in the high-producing strain. Finally, the dynamic data was used to construct a kinetic model of α-AAA transport that confirmed H^+ symport as α-AAA import mechanism.

2.1 Introduction

While it is known that classical strain improvement has increased the penicillin productivities by 100,000 fold [142], we are still far away from the maximum theoretical yield of penicillin production based on glucose [80,175]. Limitations with respect to the availability of precursor aminoacids, supply/regeneration of cofactors (NADPH), level of pathway enzymes and level of membrane transporters have often been discussed in literature [55,75,124,135,159,170,176]. Therefore, it is still relevant to identify, and subsequently eliminate, possible rate limiting steps in penicillin biosynthesis. To investigate such limiting factors, stimulus response strategies can be utilized as they provide information about metabolic network regulation and flux capacities when an organism rapidly responds to the imposed changes in its environment [108,140,162,179].

Penicillin is the end product of the penicillin biosynthesis pathway, schematically shown in Figure 2.1, which consists of the enzymes δ-[L-α-aminoadipyl]-L-cysteinyl-D-valine synthetase (ACVS), Isopenicillin-N synthase (IPNS) and Isopenicillin-N acyl transferase (AT) [5,22,137,146]. The first step of the penicillin biosynthesis pathway is the condensation of three precursor amino acids: L-α-aminoadipate, L-cysteine, and L-valine by the enzyme ACVS to produce the non-ribosomal tripeptide ACV [17-20]. Cysteine and valine are proteinogenic amino acids, whereas α-AAA is an intermediate of the lysine biosynthetic pathway in *P. chrysogenum* [19,187]. Only cysteine and valine are finally incorporated in the ß-lactam nucleus, whereas α-AAA can be recycled, as it is being released from Isopenicillin-N (IPN) in the last step of the pathway [5]. Still a considerable amount of α-AAA is lost due to secretion of IPN and the cyclization of α-AAA to 6-oxo-pipridine-2-carboxylic acid (OPC) [79] that is subsequently secreted. *De novo* synthesis of α-AAA is therefore required to maintain a sufficient supply of α-AAA to sustain the penicillin pathway flux.

During the classical strain improvement in the past decades, several studies on low producing strains were carried out to find out the limiting factors for penicillin production. Jacklitsch et al. [75] used four strains of *P. chrysogenum*, the Wisconsin strain Q 176 and three derived mutants, and observed for all cases that *Penicillium* cells that produce increased levels of penicillin contain a higher intracellular concentration of α-AAA. They also observed a linear correlation between the intracellular concentration of α-AAA and the rate of penicillin production, suggesting that α-AAA might be the rate-limiting step in the penicillin production

pathway in these strains. Hollinger et al. [74], who carried out pulse-labeling experiments with (6-^{14}C)-α-aminoadipate in low producing penicillin strains, observed a correlation between the intracellular α-AAA pool size and ACV and IPN biosynthesis. Ten years later metabolic engineering strategies were applied to increase the penicillin production rate by genetically modifying the lysine biosynthesis pathway (see Figure 2.1) in *P. chrysogenum* Wisconsin 54-1255. Strategies such as knocking out the gene *lys2* coding for aminoadipate reductase or overexpressing *lys1* coding for homocitrate synthase were adopted. The former strategy was successful and knocking out the *lsy2* gene increased the penicillin production, thus confirming that L-α-AAA was indeed a rate-limiting precursor in the Wisconsin 54-1255 strain [31,32].

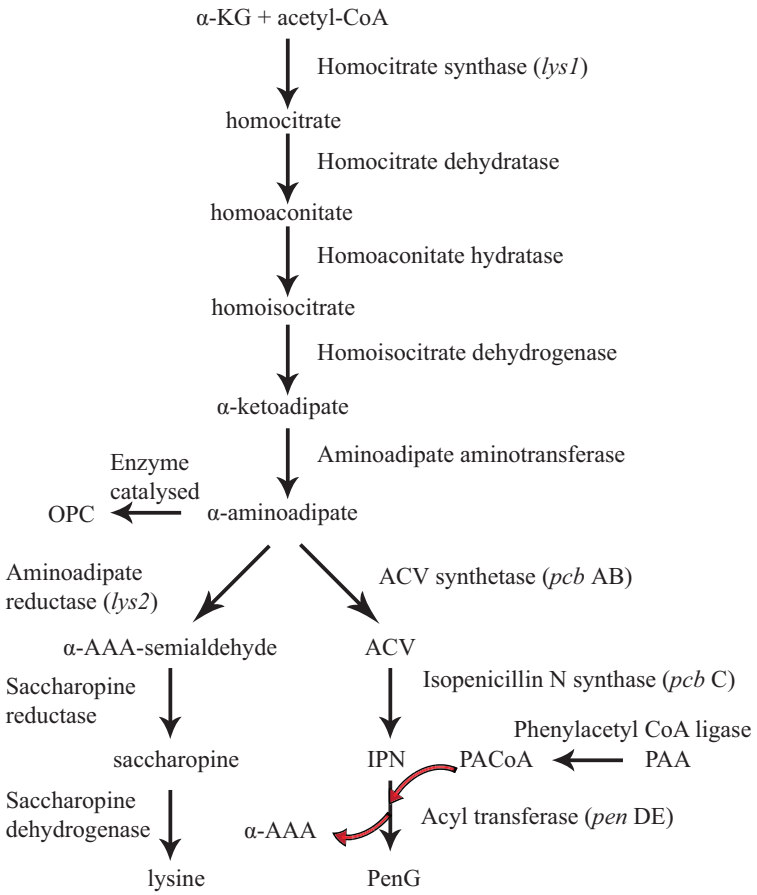

Figure 2.1: The penicillin and lysine pathway. α-AAA is used as a precursor for penicillinG pathway, lysine pathway and OPC production.

Also for high producing strains, it was investigated whether α-AAA could be limiting. Jørgensen et al. [79] performed fed batch fermentations using a high-producing industrial strain whereby the three precursor amino acids were supplied simultaneously through the feed medium. They observed slightly higher specific penicillin-V productivity in these

fermentations compared to specific penicillin-V productivity in fermentations that were not fed with the precursor amino acids. They attributed this increase of the specific penicillin-V productivity to the measured larger intracellular pools of valine and α-AAA. In contrast to these results, Nasution et al. [120] showed that in another high producing industrial strain, penicillin-G production was not correlated with the intracellular α-AAA and valine levels, but with the level of cysteine. The results of Nasution et al. [120] were based on chemostat studies, whereby *P. chrysogenum* was grown on glucose and ethanol as carbon sources. They observed that growth on both carbon sources resulted in similar penicillin production rates, however, the measured intracellular levels of α-AAA and valine were significantly lower in the ethanol-grown cultures than in the glucose-grown cultures. They also observed that the intracellular levels of α-AAA and valine were higher than the reported *in vitro* K_m values for ACVS. (0.045 mM for L-α-AAA, 0.080 mM for L-cysteine and 0.083 mM L-valine) [161]. However, care should be taken when comparing *in-vivo* metabolite measurements with K_m values determined *in-vitro*, because they are not necessarily valid for the actual intracellular conditions [158]. In addition, it has been reported that the amino acid precursors of penicillin are compartmented in vacuoles, which can lead to different concentrations in the vacuoles and in the cytosol [73]. With the sampling techniques used by Nasution et al. [120] only whole-cell average concentrations could be measured, which are not necessarily representative for the concentrations present in the cytosol, which is the compartment where ACVS is located. Direct proof for a possible α-AAA limitation can only be obtained from experiments wherein the effect of extra availability of α-AAA on the penicillin biosynthetic pathway flux is studied.

To resolve the contradictory results of previous studies for high producing industrial strains, a stimulus response experiment was conducted to establish the dependency of the penicillin production rate on the amount of intracellular α-AAA in the high producing industrial strain *P. chrysogenum* DS17690. Therefore, the strain was cultivated under producing conditions in a glucose-limited chemostat with addition of the PenG side chain precursor PAA. After a pseudo steady state was reached, an instantaneous step change in the extracellular concentration of α-AAA (0 → 2 mM) was applied to the culture. Subsequently, the dynamics of the intra- and extra- cellular concentrations of all compounds related to the penicillin biosynthesis pathway were measured with high resolution during a period of 1 h and at a lower resolution for another 80 h until a new steady state was reached. Finally, the dynamic

data obtained during the α-AAA step experiment was used to construct a kinetic model to identify possible α-AAA transport mechanisms.

2.2 Materials and methods

2.2.1 Strain

A high-yielding strain, *P. chrysogenum* DS17690, was used for cultivation. This strain was kindly donated by DSM, Biotechnology Center, Delft, The Netherlands. This strain has been extensively used for research on industrial penicillin production over the last decade [42,65,88,89,120,171].

2.2.2 Chemostat cultivation

The strain *P. chrysogenum* DS17690 was cultivated in aerobic glucose-limited chemostat cultures of 4 L working volume in a 7 L fermentor (Applikon, Schiedam, The Netherlands) at a dilution rate of 0.05 h^{-1}. The pH was controlled at 6.5 with 4 M NaOH and the temperature at 25 ± 0.1 °C. The air flow rate was set at 2 $L.min^{-1}$ (0.5 vvm), with 0.3 bar overpressure and the stirrer speed was 500 rpm. The dissolved oxygen tension was measured with a Mettler Toledo dissolved oxygen sensor (Mettler-Toledo GmbH, Greinfensee, Switzerland) and under these conditions it was known that the dissolved oxygen never dropped below 80% of saturation. Additional details of the fermentor setup and operation have been published previously [37].

2.2.3 Experimental design : α-AAA step experiment

To perform a stimulus response experiment the strain *P. chrysogenum* DS17690 was first cultivated in an aerobic glucose-limited chemostat in the absence of external supply of α-AAA (Figure 2.2), termed as Phase I. To perturb the steady state chemostat system by a step change in concentrations of α-AAA, a racemic D/L mix of α-AAA (DL-2-Aminoadipic acid, 99%, Sigma-Aldrich Chemie BV, Netherlands) was used. This step change was accomplished by replacing the feed medium without DL-α-AAA with an identical medium containing 2 mM DL-α-AAA while simultaneously injecting a solution of DL-aminoadipic acid (8 mmol at pH 6.5 in 20 mL). This resulted in an instantaneous increase of the extracellular DL-α-AAA concentration from virtually zero to 2 mM. The part after the step change in the DL-α-AAA concentration is indicated as Phase II (Figure 2.2). Phase I was carried out for 74 h after

which the step change in extracellular α-AAA was given. After the step change, phase II was carried out for 80 h.

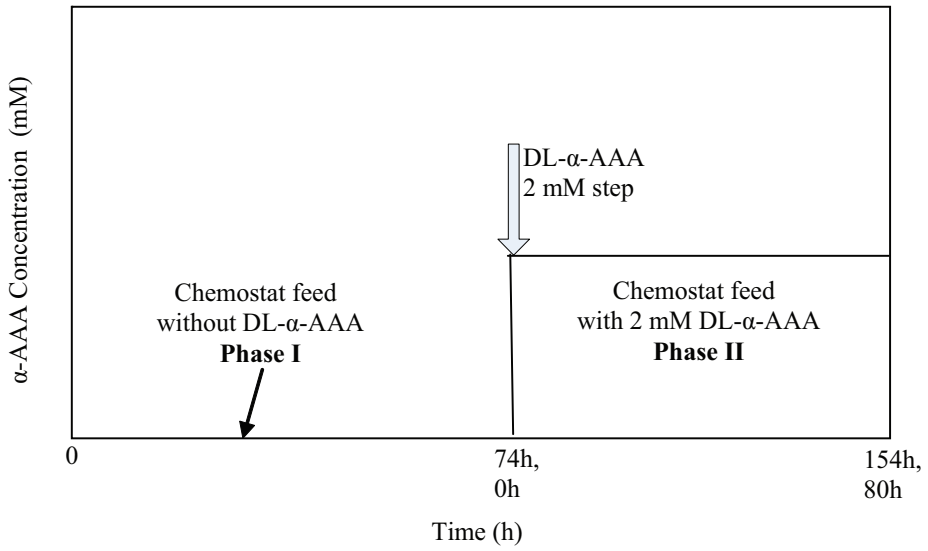

Figure 2.2: Schematic representation of the stimulus response experiment.

2.2.4 Media preparation

The composition of the chemostat medium was designed to support a biomass dry weight concentration of 6 $g.L^{-1}$ and contained 0.5 $Cmol.L^{-1}$ of glucose (16.5 $g.L^{-1}$ glucose monohydrate), 5 $g.L^{-1}$ $(NH_4)_2SO_4$, 1 $g.L^{-1}$ KH_2PO_4, 0.5 $g.L^{-1}$ $MgSO_4 \cdot 7H_2O$ and 2 $ml.L^{-1}$ trace elements solution [43] and 0.680 $g.L^{-1}$ of phenylacetic acid (5 mM). The composition of the medium for the batch phase was the same, except for the concentration of phenylacetic acid, which was 0.408 $g.L^{-1}$ (3 mM). Both batch and chemostat media for phase I of the α-AAA step experiment and for reference chemostats were prepared as described previously [37]. For phase II of α-AAA step experiment, the preparation and composition of chemostat medium was similar to that of the chemostat medium of phase I, except that it contained 0.322 $g.L^{-1}$ (2 mM) of DL-α-AAA.

2.2.5 Rapid sampling for intracellular metabolite quantification

α-AAA step experiment

Approximately 1.2 g of sample was withdrawn from the chemostat using a dedicated rapid sampling device [98] and quenched in 8 mL 40% (v/v) methanol/water solution at -27.5 °C. Directly thereafter to remove the extracellular α-AAA, the mycelium was washed 3 times with 20 mL 40% (v/v) methanol/water solution at -27.5 °C using a modified cold vacuum filtration method as described by Douma et al. [43]. In the modified vacuum filtration method

the methanol concentration was changed from 60% to 40% to avoid leakage of the intracellular metabolites into the quenching solution [38]. With the lower concentration of methanol solution, the temperature was also reduced from -40 °C to -27.5 °C to avoid freezing of the solution.

Reference chemostats

Approximately 5 g of sample was withdrawn within 1 s by means of a peristaltic pump into a cold filtration unit containing 40 mL 40% (v/v) methanol/water solution at -27.5 °C. The sample was subsequently washed 2 times by 40 mL of 40% (v/v) methanol/water of -27.5 °C by means of vacuum filtration.

The difference in the sampling protocols was due to the improvement in the sampling technique over a period of time, by minimizing the requirement of quenching and washing solution. This was also necessary in order to increase the frequency of sampling to capture the dynamics after the perturbation of the chemostat.

Extraction and sample processing

Intracellular metabolites were extracted from the quenched mycelium samples by ethanol boiling in the presence of a U-^{13}C labeled internal standard mix, to allow correction for possible partial degradation of metabolites during extraction and ion suppression effects and machine drift during quantification with IDMS. The sample was further processed to obtain a final volume of 600 µL of extract. The details of the extraction and sample processing procedure have been described previously [38]. The extracts were frozen in liquid nitrogen and stored at -80 °C until analysis.

2.2.6 Rapid sampling for extracellular metabolite quantification

Approximately 1 mL of culture broth was withdrawn from the fermentor and was immediately quenched by rapid cooling to 0 °C over cold steel beads in a syringe [107] and immediately filtered over a 0.45 µm pore sized filter to remove the mycelium. An aliquot of 80 µL of this filtrate was mixed with 20 µL of U-^{13}C-labeled cell extract in a sample vial, to allow metabolite quantification with IDMS. The vials were frozen in liquid nitrogen and stored in -80 °C until further analysis.

2.2.7 Metabolite analysis

Intermediates and (by)products of the penicillin biosynthesis pathway were quantified with ion-pair reversed-phase liquid chromatography-isotope dilution electrospray ionization tandem mass spectrometry (IP–LC–ESI–ID–MS/MS) [151] using U-^{13}C-labeled cell extract as an internal standard mix [107,186]. The method for quantification of amino acid concentrations using GC-MS was adapted from de Jonge, et al. [37], In brief, 100 µL of intracellular sample was lyophilized and derivatized using 75 µL acetonitrile and 75 µL of N-methyl-N-(tertbutyldimethylsilyl) trifluoroacetamide (MTBSTFA, Thermo Scientific). After this derivatization step, the samples were analyzed by GC-MS. Also for amino acid quantification isotope dilution mass spectrometry (IDMS) was applied.

2.2.8 Cell dry weight and Total organic carbon determination

The biomass dry weight concentration was measured by filtration of three times 5 ml of culture broth on a pre-weighed glass fiber filter (type A/E, Pall Corporation, East Hills, NY; 47 mm diameter, 1 µm pore size) and drying to constant weight (24 h at 70 °C) as described elsewhere [37]. Part of the filtrate (± 5 mL) and culture broth (± 5 mL) were stored at -20 ºC and analyzed with a TOC analyzer (TOC-5050A, Shimadzu) for quantification of total organic carbon (TOC).

2.2.9 Experiment to verify non-spontaneous OPC formation

An experiment was performed to evaluate the kinetics of the conversion of α-AAA to OPC and to verify whether it is a spontaneous chemical reaction or an enzyme catalyzed reaction. This experiment was carried out using culture filtrate (supernatant) from a standard chemostat cultivation of *P. chrysogenum* (without any α-AAA added). Culture filtrate was obtained by removing the mycelium from the broth using glass fiber filters (type A/E, Pall Corporation, East Hills, NY; 47 mm diameter, 1 µm pore size; Pall, East Hills, NY, USA). In this experiment, fixed amounts of filtrate (10 mL) were introduced in two separate flasks, while the third flask contained 10 mL of water. To each flask, different amounts of a standard solution of DL-α-AAA (100 mM) were added to obtain different initial DL-α-AAA concentrations i.e. 200, 400 and 200 µM respectively. The flasks were shaken on an orbital shaker at a rotation speed of 200 rpm, at 25 °C for a period of 8 h. At regular time intervals, samples of 40 µL were taken from each flask to quantify the OPC and DL-α-AAA

concentrations with IP–LC–ESI–ID–MS/MS using U-^{13}C-labeled cell extract as an internal standard mix.

2.2.10 Model construction, parameter estimation and simulations

A kinetic model was constructed to describe the dynamics of α-AAA uptake in the presence of α-AAA in phase II. The kinetic parameters for the model were estimated by numerically solving sets of ordinary differential equations representing the mass balances of metabolites by non-linear weighted regression using least squares curve fit function in MATLAB.R2011b. (see Appendix I).

2.3 Results

To investigate whether the biosynthesis of L-α-AAA would be limiting for penicillin biosynthesis in the high producing industrial strain *P. chrysogenum* DS17690 a stimulus response experiment was performed. To this end, the strain was first cultivated under penicillin producing conditions in glucose-limited chemostat cultures without supplying external α-AAA. After approximately four residence times the medium feed of the chemostat was replaced by an identical feed containing 2 mM DL-α-AAA. At the same time a sterile concentrated DL-α-AAA solution was injected in the chemostat vessel, to instantaneously reach an DL-α-AAA concentration of 2 mM in the culture. Subsequently, the cultivation was continued for another 3 to 4 residence times. During the entire cultivation, samples were taken to investigate the effect of α-AAA addition on the culture behavior and penicillin biosynthesis. As a control, the measurements obtained from this step experiment were compared with measurements from two reference chemostats, carried out under identical conditions but without the addition of α-AAA.

2.3.1 Phase I: No α-AAA addition

All chemostat cultures reached a pseudo steady state with respect to the concentration of biomass dry weight, and rates of O_2 consumption and CO_2 production after approximately three residence times, as found previously [37,120,176]. A biomass dry weight concentration of 5.65 ± 0.12 g.L^{-1} was reached during phase I. No significant differences in metabolite levels and specific β-lactam production rate were observed between phase I (no α-AAA addition) of the step experiment and the corresponding cultivation period of the reference chemostats (supplementary data).

2.3.2 Phase II: α-AAA step experiment, short term metabolite response

The step change in DL-α-AAA concentration was carried out after 74 h of chemostat growth, at the point where the penicillin production rate was expected to have reached its maximum value, as was anticipated from the results from the reference chemostat cultivations. To determine the dynamics of the early response of the cells to the sudden increase of the extracellular α-AAA concentration, several samples were taken during the first hour after the step change. The measured time patterns of the intra and extracellular levels of α-AAA and related metabolites are shown in Figure 2.3.

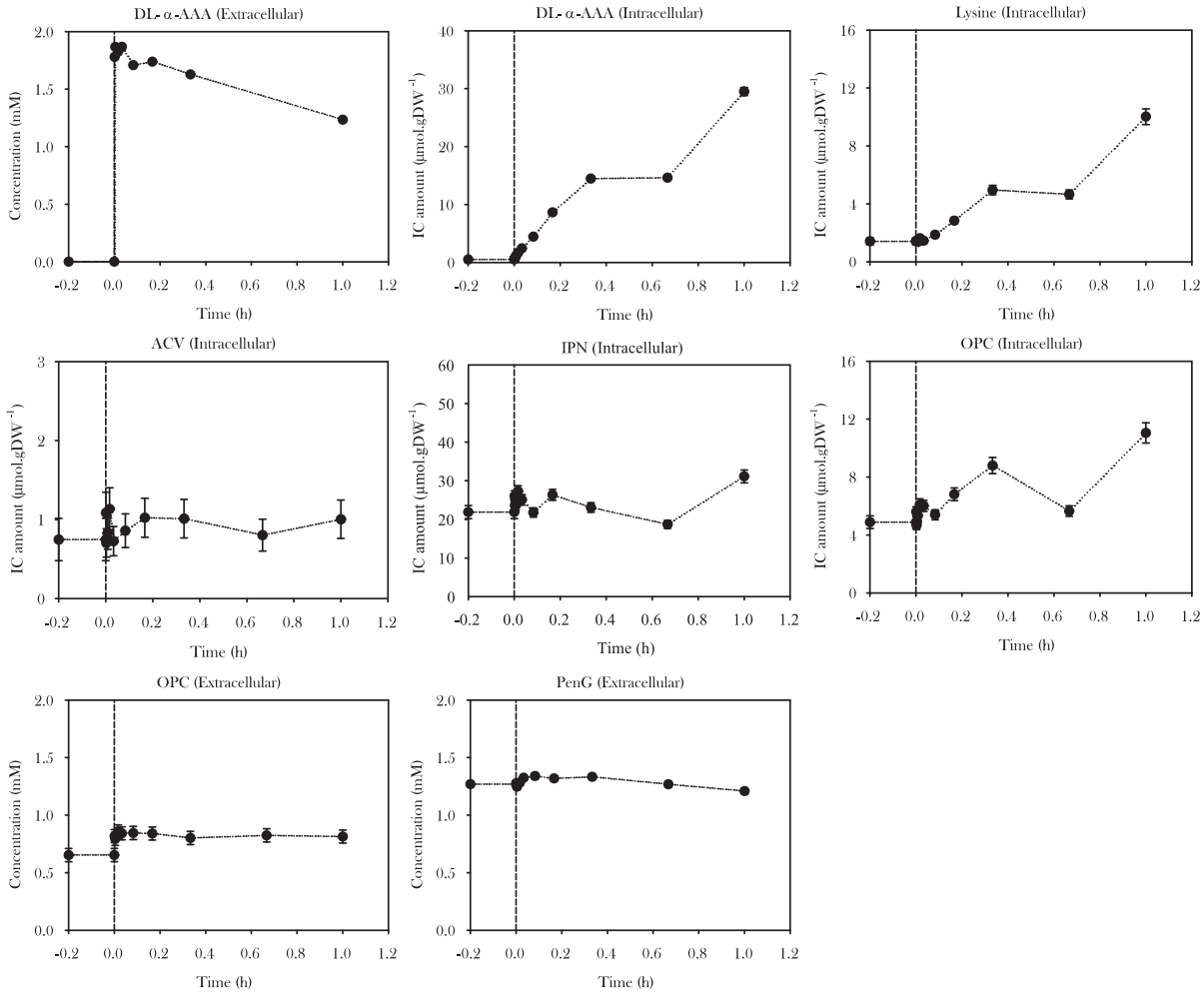

Figure 2.3: Dynamic response in intracellular amounts and extracellular concentrations of penicillin biosynthetic pathway metabolites after a step change in α-AAA concentration. Each data point represents a single sample and error bars give the standard deviation for replicate analysis.

The steady state extracellular concentration of α-AAA before the step was extremely low (1.1 μM). Directly after the step change, the extracellular concentration of α-AAA reached a value of approximately 1.8 mM. Subsequently, the extracellular α-AAA levels started to decrease and there was simultaneous fast increase of the intracellular level during the one hour period

after the step, which indicated that α-AAA was rapidly taken up by the cells. During this first hour, the intracellular α-AAA level increased 60 fold from 0.5 μmol.gDW^{-1} to 30 μmol. gDW^{-1}. Interestingly, the intracellular lysine level also increased significantly during this period, from 2 μmol.gDW^{-1} to 11 μmol.gDW^{-1}. This increase of the intracellular lysine level indicates that the α-AAA, which was taken up was assimilated by the cells into the lysine pathway. However, the strongly increased intracellular α-AAA level did not result in a significant change in the intracellular ACV level and levels of the other metabolites in the penicillin biosynthetic pathway, nor in the extracellular concentrations of the penicillin biosynthetic pathway metabolites.

2.3.3 Phase II: α-AAA step experiment, long term metabolite response

After the step change in α-AAA, a new steady state was reached and samples were taken for intracellular metabolite analysis during a period of 4-residence times. As shown in Figure 2.4, the high intracellular level of α-AAA, due to accumulation directly after the step, decreased within a few hours. In addition, the extracellular α-AAA concentration decreased and both the intracellular and extracellular levels reached pseudo steady state values at approx. 20 hours after the α-AAA step.

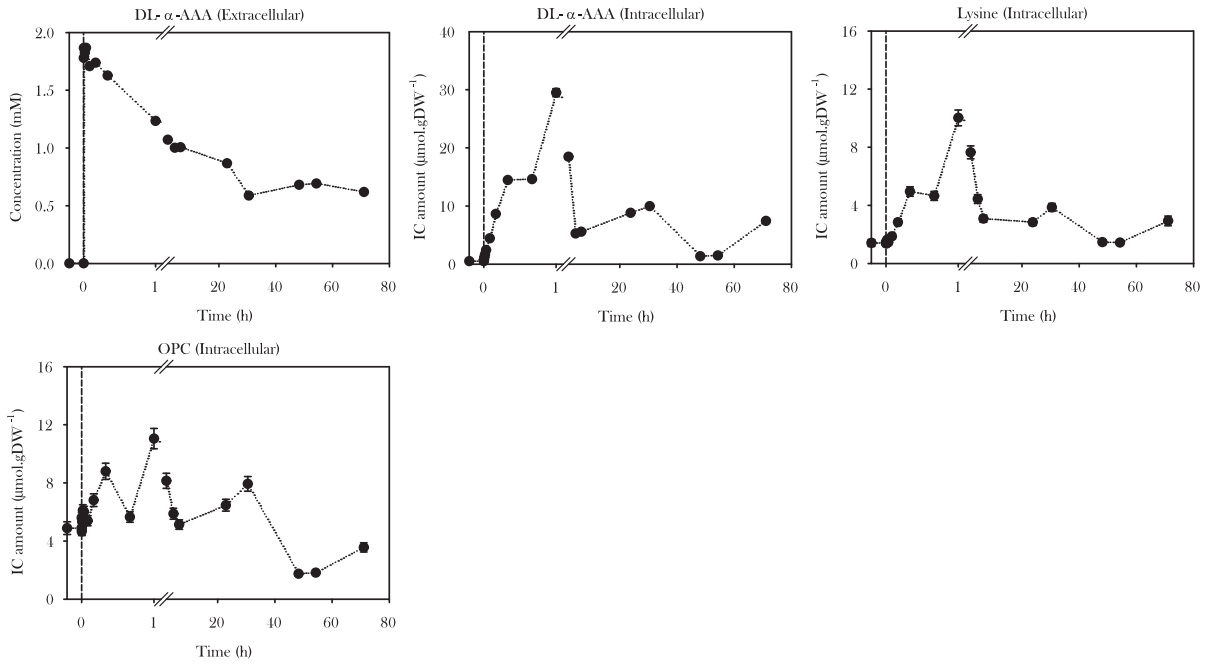

Figure 2.4: Long term response of intracellular amounts and extracellular concentrations of α-AAA related metabolites during phase II of the step experiment. Each data point represents a single sample and error bars give the standard deviation for replicate analysis.

The intracellular α-AAA remained at a significantly higher level than before the α-AAA step, probably due to the still high extracellular level. The intracellular levels of lysine and OPC reached approximately the pre-α-AAA step values in the new steady state. No lysine was found in the extracellular space and no increase in the penicillin biosynthetic pathway metabolites was observed after the new steady state was reached.

2.3.4 Metabolite patterns compared to the references

The intra- and extracellular levels of the metabolites of the β-lactam biosynthesis pathway measured during the step experiment are compared with the values of the reference chemostats in Figure 2.5. The comparison of concentrations in phase I and phase II indicate that there was no significant change in the penicillin pathway metabolite concentrations in the extracellular and intracellular spaces after the addition of α-AAA, and the concentrations just follow the pattern similar to that of the reference chemostat. Both the intra- and extracellular OPC levels in the step experiment were slightly elevated as compared to the reference chemostats, however there was no significant increase in phase II as compared to phase I. Thus, the increased intracellular α-AAA concentration, also at longer time scales, had no effect on the penicillin pathway kinetics.

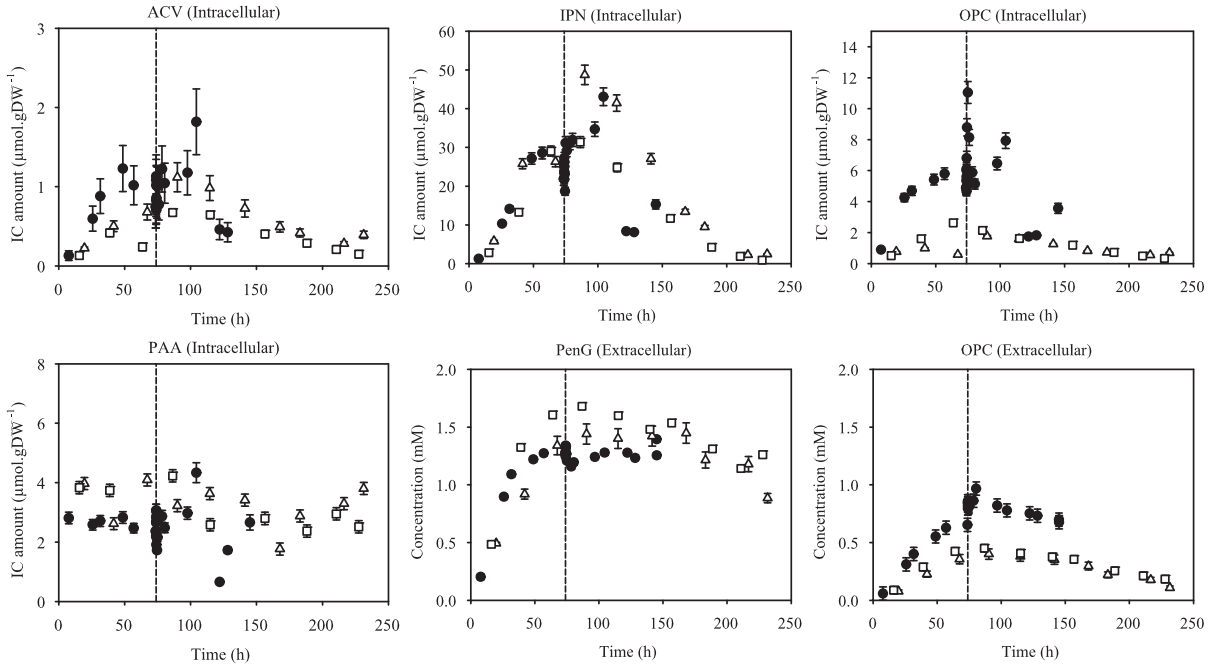

Figure 2.5: Intracellular amounts and extracellular concentrations of penicillin pathway metabolites over the entire fermentation of DL-α-AAA step experiment compared with reference chemostat cultures. The solid symbols represent the DL-α-AAA step experiment, while the open symbols represent the reference chemostats. The dotted line separates phase I and phase II in DL-α-AAA step experiment. Each data point represents a single sample and error bars give the standard deviation for replicate analysis.

2.3.5 ß-lactam production dynamics over the entire fermentation

The total biomass specific ß-lactam production rate was calculated from the measured IPN, 6APA, 8HPA and PenG concentrations in the effluent of the chemostat using the corresponding mass balance equations (see Appendix III). The time pattern of the ß-lactam production rate (see Figure 2.6) before the α-AAA step did not differ significantly from the corresponding time pattern observed for the reference chemostats. Also after the α-AAA step, there was no significant increase in ß-lactam production, which indicates that there was no effect of α-AAA on the penicillin biosynthetic pathway flux.

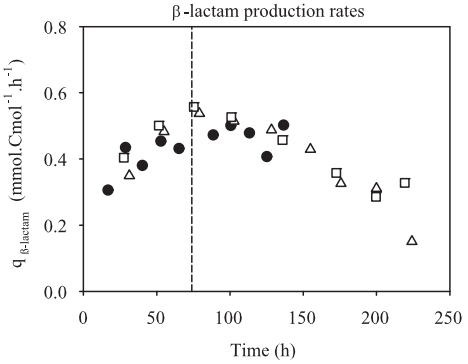

Figure 2.6: Comparison of the ß-lactam production rates for α-AAA step experiment and reference chemostats over the entire chemostat cultivation. The solid symbols represent the α-AAA step experiment and the open symbols represent reference chemostats.

The total ß-lactam production rate was maximal after a period of approximately 4-residence times, after which it decreased. This decrease of the ß-lactam production rate is due to degeneration of penicillin production and has been studied in detail by Douma et al. [42].

2.3.6 Biomass specific conversion rates in phase II

After the step increase in the DL-α-AAA concentration, termed as phase II, the average biomass concentration was 5.41 ± 0.11 g.L^{-1}, which is not significantly different from the biomass concentration during phase I. No differences were observed in the offgas concentrations of O_2/CO_2 before and after the step change (supplementary material). This is not surprising as the α-AAA uptake rate was, in terms of carbon consumption, only 0.6% of the glucose uptake rate. Also, there were no significant morphological differences observed under the microscope.

Table 2.1: Reconciled biomass specific conversion rates of penicillin pathway metabolites for phase II

Rates	*α-AAA step- Phase II*	*Reference*[*]
q_S	-20.49 ± 0.62	-19.69 ± 0.46
q_{PAA}	-0.400 ± 0.022	-0.455 ± 0.016
$q_{a\,AAA}$	-0.246 ± 0.042	0
q_{O_2}	-56.5 ± 2.5	-53.1 ± 1.6
q_{CO_2}	61.3 ± 2.6	57.8 ± 1.7
q_{biom}	50.2 ± 1.1	50.0 ± 1.0
q_{PenG}	0.324 ± 0.019	0.353 ± 0.022
q_{IPN}	0.0281 ± 0.0046	0.0187 ± 0.0047
$q_{6\,APA}$	0.077 ± 0.013	0.0535 ± 0.0015
q_{8HPA}	0.0187 ± 0.0038	0.0132 ± 0.0020
q_{oOHPAA}	0.0736 ± 0.0077	0.107 ± 0.022
q_{OPC}	0.199 ± 0.026	0.078 ± 0.012
$q_{byproducts}$	7.9 ± 1.1	6.18 ± 0.41

Specific rates of biomass growth and by-product formation are expressed mCmol.Cmol biomass^{-1}.h^{-1} other rates are expressed in mmol.Cmol biomass^{-1}.h^{-1}. For conversion of g biomass DW to Cmol, a Cmol weight of 28.05 g was used

*: Based on two chemostat cultivation

A comparison between the pseudo steady, state biomass specific conversion rates in phase II (80 h to 154h) and the reference chemostats (50h to 250h) are shown in Table 2.1. (using C-molar biomass weight of 28.05 gDW.Cmol^{-1}). No significant differences were found between the α-AAA step experiment and the reference chemostat with respect to the specific rates of glucose and PAA uptake, O_2 consumption, as well as CO_2, PenG and byproduct formation. Although there were differences in the OPC production rates between phase II of the step experiment and the reference chemostat, the OPC production rate during phase I of the step experiment (0.169 ± 0.015 mmol.Cmol^{-1}.h^{-1}) was not significantly different from the OPC production rate during phase II (see Table 2.1). Again, although there was a significant uptake rate of DL-α-AAA during phase II of about 0.246 ± 0.042 mmol.Cmol^{-1}.h^{-1}, this was not accompanied by any increase in ß-lactam production rates nor OPC production rate nor lysine secretion.

2.3.7 Flux analysis around the α-AAA node

To establish the flux distributions around the α-AAA node before and after the α-AAA step change, conventional steady state metabolic flux analysis was carried out using the stoichiometric model from van Gulik et al. [176], for growth and PenG production in *P. chrysogenum.* The fluxes around the α-AAA node in the lysine pathway leading to lysine, OPC and penicillin biosynthesis are shown in Figure 2.7. The flux analysis results for phase I, without α-AAA addition, shows that the *de novo* produced α-AAA (production rate: 0.440 mmol.Cmol^{-1}.h^{-1}) was consumed to produce lysine (56%), secreted OPC (38%) and secreted IPN (6%). Lysine was further consumed for biomass production (0.22 mmol.Cmol^{-1}.h^{-1}) and partly excreted in the form of proteins and/or peptides, as was observed previously [176].

After reaching a pseudo steady state in phase II, with α-AAA addition, the uptake rate of α-AAA was 0.246 mmol.Cmol^{-1}.h^{-1} (Table 2.1) which appeared to be similar as the biosynthesis rate of lysine calculated from the metabolic flux analysis. Considering this uptake rate, and assuming that there is no conversion of α-AAA to other unknown compounds during the steady state, the *de novo* biosynthesis of α-AAA should have decreased from a value of 0.440 mmol.Cmol^{-1}.h^{-1} during phase I to 0.228 mmol.Cmol^{-1}.h^{-1} during phase II. This implies that the increased level of intracellular α-AAA would have inhibited the *de-novo* synthesis.

After the step change in α-AAA, the uptake rate of α-AAA increased instantaneously from 0 to approx. 2.26 mmol.Cmol^{-1}.h^{-1} (calculated from a polynomial fit for the measured α-AAA concentrations as a function of time). This high initial uptake rate could be explained by the observed intracellular accumulation of α-AAA and lysine. Moreover, as the culture was a glucose limited chemostat, the growth rate was fixed so the fluxes from lysine towards biomass and peptides remained unaltered. Fluxes during the transient phase can be obtained from a kinetic model that takes into account the kinetics of the transporter, accumulation of intracellular α-AAA and of lysine.

Finally, it should also be kept in mind here that a racemic mixture of D+L- α-AAA has been supplied to the chemostat, while only the L-form of α-AAA can be used by the cells for lysine and β-lactam production. Remarkably, during phase II of the step experiment nearly 60% of the supplied α-AAA was consumed by the cells. Therefore, not only the L- but also the D-form of α-AAA must have been taken up. It has been reported, however, that in penicillin

fermentations OPC was found in both the L- and the D-form [24]. Conversion of D- α-AAA to D-OPC could explain that more than 50% of the supplied DL- α-AAA was taken up.

A) Phase I : pseudo steady state (at fermentation period - 73h)

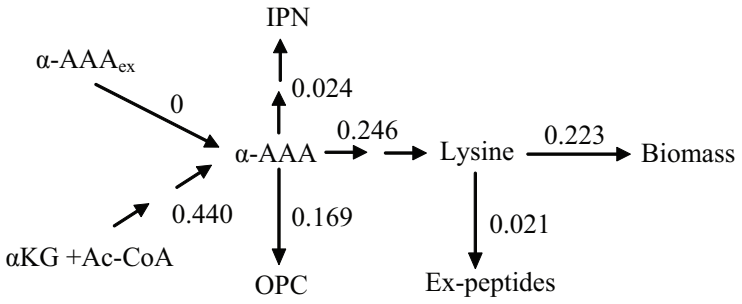

B) Phase II : pseudo steady state (fermentation period between 80h and 154h)

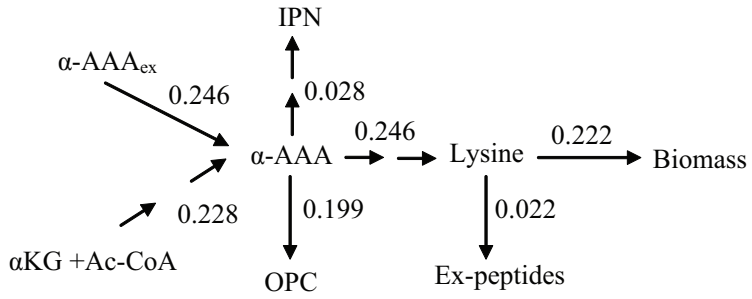

C) Calculated uptake rate of DL-α-AAA as function of time

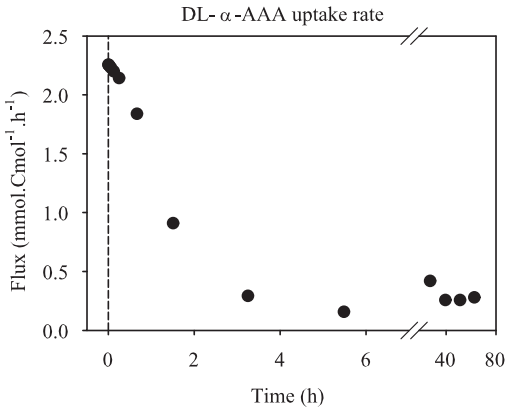

Figure 2.7: Metabolic flux analysis at α-AAA node in the lysine pathway leading to lysine, OPC and penicillin biosynthetic pathway. Lysine is further utilized for the production of biomass and peptides that are secreted. [A] Metabolic flux analysis in phase I without external α-AAA supply. [B] Metabolic flux analysis in phase II with external α-AAA supply. [C] Calculated uptake rate of DL-α-AAA from the polynomial fitting of the data points.

2.3.8 Kinetic model for α-AAA transport

It has been reported in literature that there are at least two transporters, the acidic and the general amino acid permeases, which could be responsible for the import of α-AAA into the cell [55,165]. It is known that these transporters are driven by the proton motive force through proton symport [71] and are only able to take up the L-form of α-AAA. However, our results indicate that both the L- and the D- form of α-AAA were taken up. This would imply that there might be more than two transporters taking part in the uptake of DL-α-AAA. With a *pKa* of 4.417 for α-AAA and for an extracellular pH of 6.5, while assuming a typical intracellular pH for filamentous fungi of 7.2 [100,101,134,145], the thermodynamic equilibrium ratio (in/out) of the total acid can be calculated to be 4.97 (see Appendix I). Figure 2.8 shows the experimentally determined IC/Ex ratio for DL-α-AAA after the step change in α-AAA. It shows that although the measurements are scattered, an equilibrium ratio of around five seems not in contradiction with the data.

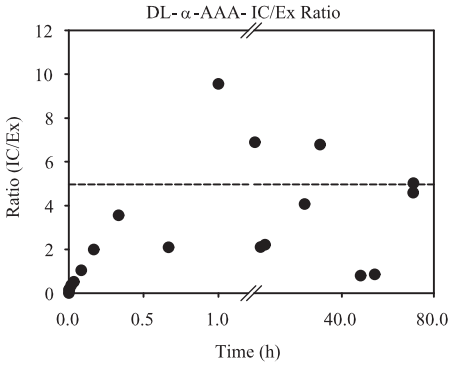

Figure 2.8: Intracellular to extracellular concentration ratio of DL-α-AAA in phase II. The horizontal dotted line represents the calculated equilibrium ratio of 4.97.

To estimate the capacity of the transporter, a kinetic model was constructed (see Appendix I). The transporter of α-AAA was assumed to be an H^+ symporter. The intracellular fluxes at the α-AAA node were obtained from the flux analysis at the end of Phase I. The *de novo* fluxes for α-AAA production and towards IPN and OPC formation are assumed to be constant. The flux towards lysine was assumed to be first order with respect to the intracellular α-AAA concentration. Furthermore, we assume that there are no changes in the enzyme levels and regulatory functions. The simulation results of the model shows (see Figure 2.9) that the model description for the step experiment was satisfactory for the first 20 min (0.33h) after the step change in extracellular α-AAA concentration. Thereafter, the model fit deviates from the experimental values due to changes in the regulation of the fluxes in the pathway because

of high intracellular α-AAA concentration or changes in the enzyme levels. The complete α-AAA kinetic model and its parameters are shown in Appendix I.

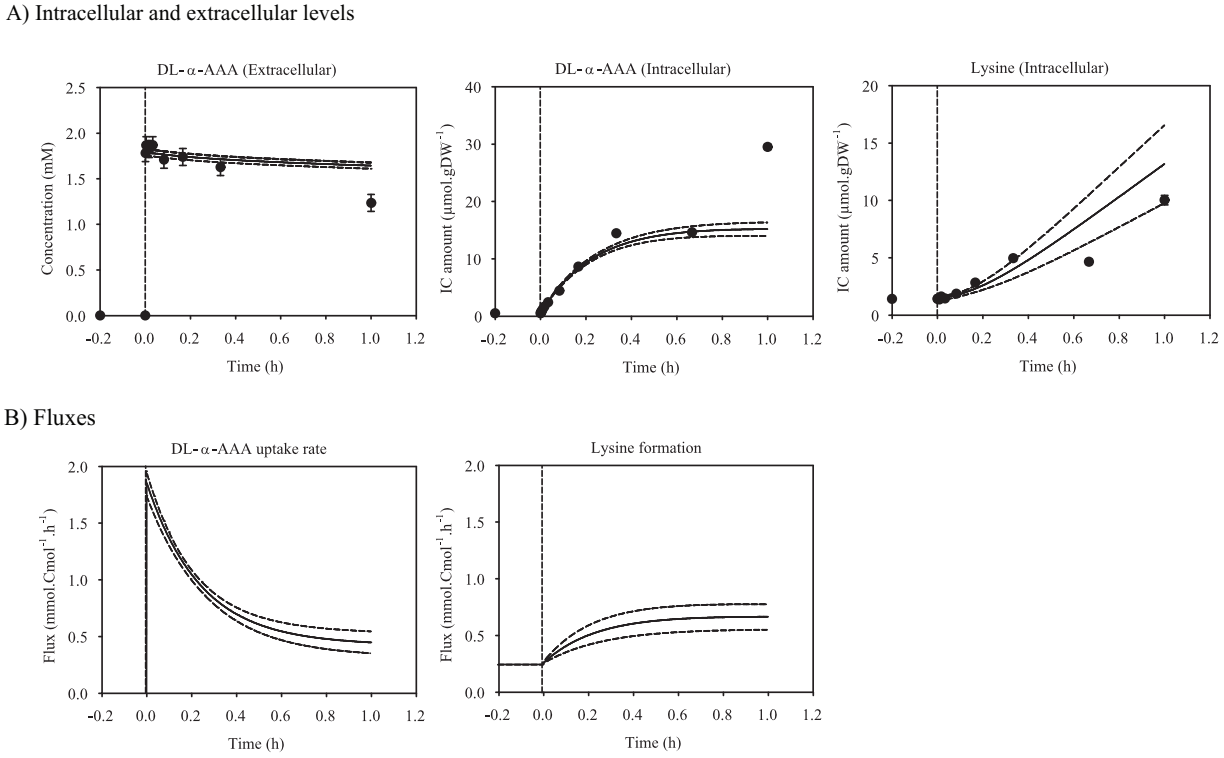

Figure 2.9: Model prediction during α-AAA step experiments: [A] concentrations [B] fluxes. Closed circles represent experimental data and error bars represent standard error. For extracellular data, errors are assumed to be 5% of maximum extracellular concentration. Solid line (-) represent the simulation values and dotted line (--) represent the region of the model error. The *de novo* α-AAA production flux is 0.44 mmol.Cmol^{-1}.h^{-1}. In addition to lysine formation, a constant flux flows towards OPC and IPN (0.193 mmol.Cmol^{-1}.h^{-1}).

2.3.9 OPC formation: An enzyme catalyzed reaction

During penicillin fermentations it has been observed that α-AAA is cyclized to OPC [70]. From our results it was seen that the formation of OPC was not proportional to the availability of α-AAA. This observation indicates that the cyclization of α-AAA is unlikely to be a chemical process, but probably a result of enzymatic conversion. We performed independent experiments to check the hypothesis that OPC formation is not a spontaneous chemical reaction. To this end, experiments were carried out wherein the spontaneous conversion of α-AAA to OPC in water and in culture supernatant was monitored. The results of these experiments are shown in Appendix II. The culture filtrate initially contained 470 ± 3 μM of OPC and 3.9 ± 0.3 μM of L-α-AAA. The addition of different amounts of a standard solution of DL-α-AAA in three different flasks resulted in initial DL-α-AAA concentrations of 194 ± 7, 416 ± 26 and 189 ± 5 μM respectively. According to the one-tailed t-test (p=0.025), there

was no significant change in concentrations of OPC or α-AAA and they remained constant over a period of 8 hours with experiments performed with supernatant. The experiments performed with water showed that there was hardly any conversion of α-AAA to OPC (1% over a period of 8 h). Given the large amount of OPC production in fermentations, where α-AAA concentrations are much lower, it can be concluded that OPC formation is not a spontaneous chemical reaction but must be an enzyme catalyzed reaction.

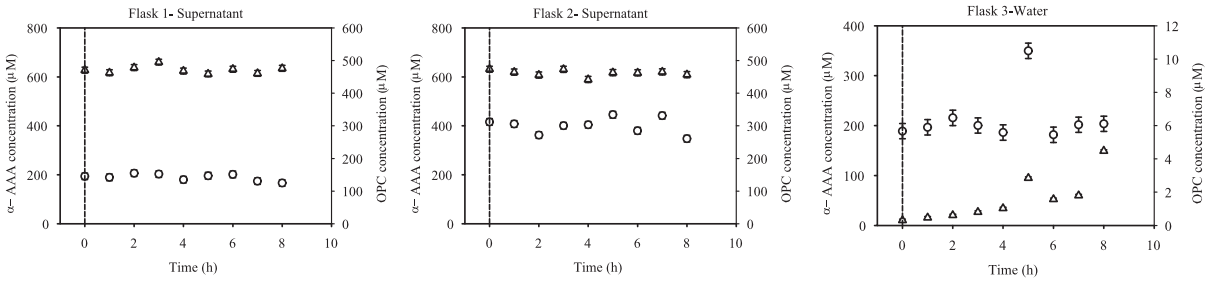

Figure 2.10: Experiments to verify non-spontaneous conversion of α-AAA to OPC in supernatant and water. Triangles represent OPC concentration and circles represent α-AAA concentration. Each data point represents a single sample and error bars give the standard error for replicate analysis. With one-tailed t-test (p=0.025), there was no significant change in concentrations of OPC or α-AAA with experiments performed in supernatant.

2.4 Discussion

Applying a stepwise increase from 0 to 2 mM DL-α-AAA to a PenG producing chemostat culture of *P. chrysogenum* resulted in a fast and very significant (~60 fold) increase of the intracellular α-AAA concentration. This indicated that α-AAA was rapidly taken up by the cells. If the endogenous biosynthesis of α-AAA would be rate-limiting for ACVS, the first enzyme of the penicillin biosynthesis pathway, an increased intracellular α-AAA concentration should lead to an increase in ACV production. Nevertheless, even a 60 times increased level of DL-α-AAA in the cell did not result in an increased flux through ACVS and no change in the fluxes and metabolite levels through the rest of the penicillin pathway was observed (both short and long term). While the penicillin production rate remained unchanged, L-α-AAA was assimilated in the lysine pathway, which was inferred from the observed 5 fold increase in intracellular level of L-lysine, shortly after the addition of α-AAA. These results clearly demonstrate that although α-AAA was consumed by the cells, the intracellular concentration was not rate limiting for ACVS in the high producing industrial strain *P. chrysogenum* DS17690. This would indicate that, due to random mutagenesis and selection during the classical strain improvement program, the strain can now produce sufficient intracellular L-α-AAA or might have altered the kinetic properties of ACVS or a combination of both.

Although penicillin production does not require net consumption of α-AAA, α-AAA is partly lost through excretion of the pathway intermediate IPN and conversion into its cyclic derivative OPC [79]. The loss of IPN can be eliminated by increasing the activities of the enzymes downstream, while OPC formation can be eliminated by identifying the cause of its formation and removing it. One of the hypotheses for formation of OPC is by spontaneous chemical reaction from α-AAA. In the α-AAA step experiment, it was seen that OPC formation increased by only 0.03 $mmol.Cmol^{-1}.h^{-1}$, which was approximately 7% of the incoming α-AAA through the medium. Spontaneous non-enzymatic ring closure to form OPC appeared therefore unlikely, which was verified by independent experiments, wherein, after incubation of α-AAA in either water or culture supernatant, no conversion to OPC was observed. Thus, it seems that there is an intracellular enzyme responsible for the conversion of intracellular α-AAA to OPC.

It was found that during phase II of the step experiment nearly 60% of the supplied α-AAA was consumed by the cells. The increased intracellular level of free lysine indicated that the consumed α-AAA was converted to lysine. It is known that the lysine pathway is tightly regulated. Increased lysine concentrations will cause feedback inhibition (K_i = 8 ± 2 μM) of homocitrate synthase [76,102] and of α-aminoadipate reductase (K_i = 260 μM) [2]. It is therefore likely that as a result of the increased intracellular lysine concentration, the *de novo* biosynthesis of L-α-AAA is inhibited while the L-α-AAA that is taken up is consumed for the production of lysine and subsequently biomass protein. Finally, the observed consumption of 60% of the fed DL-α-AAA implies that the D-α-AAA was also consumed. It is known that OPC can exist in both the isomer forms [24], which could explain the consumption of D-α-AAA.

Externally added α-AAA can be taken up by *P. chrysogenum* via the acidic amino acid permease (PcDip5) and the general amino acid permease (PcGap1) [165]. These permeases are known to be proton symporters and can transport α-AAA against the concentration gradient using the proton motive force [55,71,165]. As α-AAA carries one negative charge at pH 6.5 it has to be taken up against the negative membrane potential inside the cell. Thus, the most plausible mechanism for the uptake of α-AAA seems to be proton symport. To estimate the transporter capacity, the data obtained from stimulus responses experiments over a short time scale can be used [44], where the enzyme levels and the pathway regulation can be assumed to be constant. Therefore, a kinetic model for uptake of α-AAA was constructed

assuming a reversible H^+ symporter. The model simulation was capable of describing the intra- and extracellular concentrations of α-AAA over a period of 20 min, however, after that period the simulation deviates. This deviation of the model estimation might be due to tight control of the lysine biosynthesis pathway by the high intracellular level of lysine.

2.5 Conclusions

Supplying α-AAA through the medium increased the intracellular levels of α-AAA 60 fold, however, this did not result in increased levels of penicillin pathway intermediates nor increased penicillin production in the high producing *P. chrysogenum* DS17690 strain. This shows that this strain has lost its limitation to α-AAA for the penicillin-G production. As short term effect of the stepwise increase of the extracellular α-AAA concentration to 2 mM, the intracellular α-AAA and lysine levels increased temporarily, showing uptake and assimilation of externally supplied α-AAA. Furthermore, the pseudo steady state analysis indicates that the *de novo* production of α-AAA decreases two-fold with its external availability. The kinetic model confirms that the α-AAA anion is transported by H^+ symport.

2.6 Acknowledgements

We acknowledge the financial support from the Netherlands Organization for Scientific Research (NWO) via the IBOS (Integration of Biosynthesis and Organic Synthesis) programme of Advanced Chemical Technologies for Sustainability (ACTS) (project nr: IBOS 053.63.011) and was financially supported by DSM. This project was carried out within the research programme of the Kluyver Centre for Genomics of Industrial Fermentation, which is part of the Netherlands Genomics Initiative/ Netherlands Organization for Scientific Research. Authors thank L.P. de Jonge for providing data of one of the reference chemostats.

2.7 Appendix

2.7.1 Appendix I: Kinetic model for α-AAA transport and metabolism

A kinetic model was setup for α-AAA transport and metabolism. For the model setup all the concentrations were converted to $mmol.m^{-3}$ to have uniform units. The intracellular concentrations that were expressed in $\mu mol.gDW^{-1}$ were converted to $mmol \cdot m_{IC}^{-3}$ by using the specific cell volume V_x, which is 2.5 x 10^{-6} m_{IC}^3 cells.gDW^{-1} [131,160]. The intracellular fluxes obtained from flux analysis in $mmol.Cmol^{-1}.h^{-1}$ were first converted to $mmol.gDW^{-1}.h^{-1}$ by using C-molar biomass weight of 28.05 $gDW.Cmol^{-1}$ and then converted to

$\text{mmol.m}_{IC}^{-3}\text{.h}^{-1}$ using specific cell volume V_x. Cell dry weight C_x was expressed in gDW.m_{EC}^{-3} and the extracellular concentrations were expressed in mmol.m_{EC}^{-3}.

Transport Kinetics

The thermodynamic equilibrium ratio for the total acid for proton symport can be calculated as

$$K_{eq,AAA} = \left(\frac{C_{AAA,in}}{C_{AAA,ex}} \right)_{eq} = \left[\frac{1+10^{(pK-pH_{in})}}{1+10^{(pK-pH_{out})}} \right] \cdot 10^{(pH_{in}-pH_{out})} \quad \text{(A1)}$$

For an extracellular pH of 6.5, while assuming a typical intracellular pH for filamentous fungi of 7.2, with a *pKa* of 4.417 for α-AAA, the thermodynamic equilibrium ratio (in/out) of the total acid can be calculated as

$$K_{eq,AAA} = \left(\frac{C_{AAA,in}}{C_{AAA,ex}} \right)_{eq} = 4.97 \quad \text{(A2)}$$

Mass action kinetics was applied to describe the biomass specific uptake rate of α-AAA as

$$q_{up,AAA} = k_{up,AAA} \cdot C_{AAA,ex} \cdot \left(1 - \frac{C_{AAA,in}}{C_{AAA,ex} \cdot K_{eq,AAA}} \right) \quad \text{(A3)}$$

Flux towards lysine formation

With the increase in the intracellular α-AAA level, there was also increase in the intracellular lysine level. Thus, apart from the *de novo* flux from α-AAA towards lysine, additional flux was necessary to accommodate the accumulation of intracellular lysine. This was assumed proportional to the intracellular α-AAA concentration. Therefore, flux towards lysine formation can be written as,

$$v_{lys} = k_{lys} \cdot C_{AAA,in} + v_{denovo,lys} \quad \text{(A4)}$$

The balance for intracellular α-AAA follows as ($\text{mmol.m}_{IC}^{-3}\text{.h}^{-1}$)

$$\frac{dC_{AAA,in}}{dt} = v_{denovo,AAA} + q_{up,AAA} - v_{lys} - v_{denovo,IPN} - v_{denovo,OPC} - \mu \cdot C_{AAA,in} \quad \text{(A5)}$$

Here, the *de novo* fluxes towards IPN, OPC and μ are assumed to be constant for the period of first one hour and equal to the fluxes just before the step change in the extracellular α-AAA.

The balance for intracellular lysine follows as ($\mathrm{mmol.m_{IC}^{-3}.h^{-1}}$)

For the dynamic change in the intracellular lysine level

$$\frac{dC_{lys,in}}{dt} = v_{lys} - v_{denovo,consumption,lys} - \mu \cdot C_{lys,in} \qquad \text{(A6)}$$

The balance of extracellular AAA follows as ($\mathrm{mmol.m_{EC}^{-3}.h^{-1}}$)

$$\frac{dC_{AAA,ex}}{dt} = -q_{up,AAA} \cdot C_x \cdot V_x + \frac{\phi_{out}}{V} \cdot \left(C_{AAA,feedin} - C_{AAA,ex} \right) \qquad \text{(A7)}$$

Table 2.A1: Kinetic parameters of the model

Parameters	*Value*	*unit*	*Obtained from*
$k_{up,AAA}$	15.10 ± 0.89	$\mathrm{h^{-1}}$	model estimation
k_{lys}	0.99 ± 0.34	$\mathrm{h^{-1}}$	model estimation
$C_{AAA,in}(t=0)$	209 ± 17 (0.523 ± 0.043)[1]	$\mathrm{mmol.m_{IC}^{-3}}$	model estimation
$C_{lys,in}(t=0)$	610 ± 71 (1.53 ± 0.18)[1]	$\mathrm{mmol.m_{IC}^{-3}}$	model estimation
$C_{AAA,ex}(t=0)$	1792 ± 35	$\mathrm{mmol.m_{EC}^{-3}}$	model estimation
$C_{AAA,feedin}$	1691	$\mathrm{mmol.m_{EC}^{-3}}$	experimental value
C_x	5410	$\mathrm{gDW.m_{EC}^{-3}}$	experimental value
ϕ_{out}	200 x 10^{-6}	$\mathrm{m_{EC}^{3}.h^{-1}}$	experimental value
V	4 x 10^{-3}	$\mathrm{m_{EC}^{3}}$	experimental value
μ	0.05	$\mathrm{h^{-1}}$	experimental value
V_x	2.5 x 10^{-6}	$\mathrm{m_{IC}^{3}.gDW}$	[131,160]
$K_{eq,AAA}$	4.97	[-]	thermodynamic calculation
$v_{denovo,AAA}$	6275 (0.440)[2]	$\mathrm{mmol.m_{IC}^{-3}.h^{-1}}$	flux analysis
$v_{denovo,lys}$	3508 (0.246)[2]	$\mathrm{mmol.m_{IC}^{-3}.h^{-1}}$	flux analysis
$v_{denovo,consumption,lys}$	3508 (0.246)[2]	$\mathrm{mmol.m_{IC}^{-3}.h^{-1}}$	flux analysis
$v_{denovo,IPN}$	342 (0.024)[2]	$\mathrm{mmol.m_{IC}^{-3}.h^{-1}}$	flux analysis
$v_{denovo,OPC}$	2410 (0.169)[2]	$\mathrm{mmol.m_{IC}^{-3}.h^{-1}}$	flux analysis

[1] : The values in the brackets are intracelluar concentration in units $\mu\mathrm{mol.gDW^{-1}}$

[2] : The values in the brackets are intracellular fluxes in units $\mathrm{mmol.Cmol^{-1}.h^{-1}}$

The kinetic parameters of the model are given in Table 2.A1. For intracellular concentrations, the model estimates obtained in $mmol \cdot m_{IC}^{-3}$ are converted into μmol.gDW^{-1} by using the specific cell volume V_x, 2.5 x 10^{-6} m_{IC}^3 cells.gDW^{-1} [131,160]. For intracellular fluxes, the model estimates obtained in $mmol.m_{IC}^{-3}.h^{-1}$ are first converted to mmol.gDW^{-1}.h^{-1} using specific cell volume V_x 2.5 x 10^{-6} m_{IC}^3 cells.gDW^{-1} and then converted to mmol.Cmol^{-1}.h^{-1} by using C-molar biomass weight of 28.05 gDW.Cmol^{-1}. With these parameter values, the model description for the step experiment was satisfactory for the period of 20 min (0.33 h)

2.7.2 Appendix II: OPC formation from α-AAA

Experiments were carried out to study the spontaneous chemical conversion of α-AAA to OPC (Figure 2.10) in culture filtrate (supernatant) and in water. Over a period of 8 hours, there was no significant change in the concentrations of α-AAA and OPC.

2.7.3 Appendix III: Secretion rates, uptake rates and intracellular fluxes

Fluxes were calculated using the following balances (constant volume) :

For product :

$$\frac{dC_i}{dt} = q_{i,\text{sec}} \cdot C_x - \frac{\phi_{out}}{V} \cdot C_{i,out}$$

For substrate :

$$\frac{dC_i}{dt} = -q_{i,up} \cdot C_x + \frac{\phi_{in}}{V} \cdot C_{i,in} - \frac{\phi_{out}}{V} \cdot C_{i,out}$$

Intracellular balance :

$$\frac{dX_i}{dt} = v_{i,produced} - v_{i,consumed} - q_{i,\text{sec}} - \mu \cdot X_{i,out}$$

Where dC_i/dt stands for the change of extracellular concentration over time, q_i is the flux of i compound in mmol.Cmol^{-1}.h^{-1}, q_{sec} the secretion rate in mmol.Cmol^{-1}.h^{-1}, q_{up} the uptake rate in mmol.Cmol^{-1}.h^{-1}, C_x the biomasss concentration in Cmol.L^{-1}, D the dilution rate (0.05 h^{-1}), $C_{i,in}$ the concentration of the metabolite in the inflow in mmol.L^{-1}, and $C_{i,out}$ the concentration of the metabolite in the outflow/broth in mmol.L^{-1}. dX_i/dt stands for the change of intracellular amounts over time. v_i is the intracellular flux in mmol.Cmol^{-1}.h^{-1}.

2.8 Supplementary data:

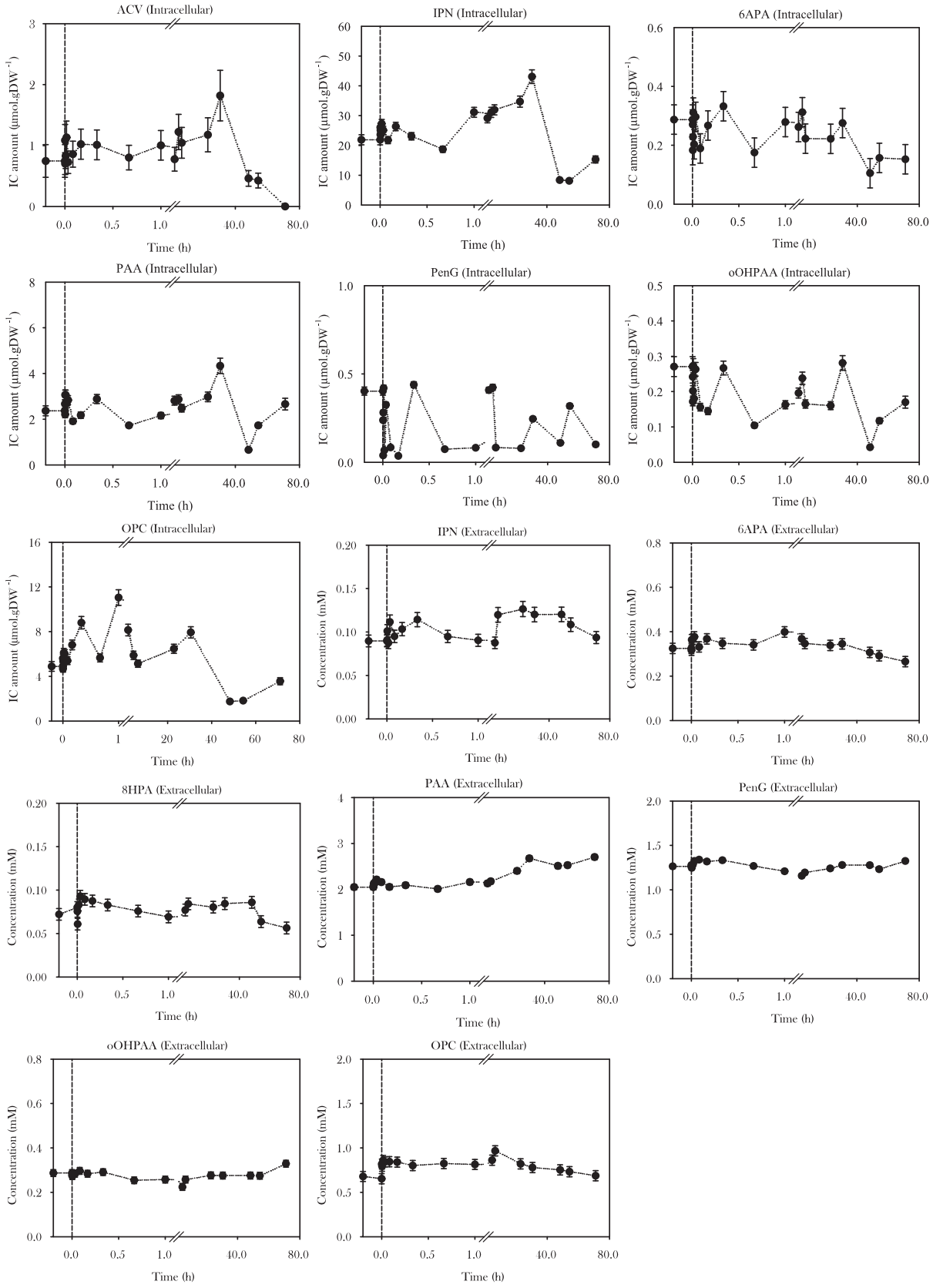

Figure 2.S1: Long term responses of the intra- and extracellular levels of α-AAA related metabolites during phase II of the step experiment.

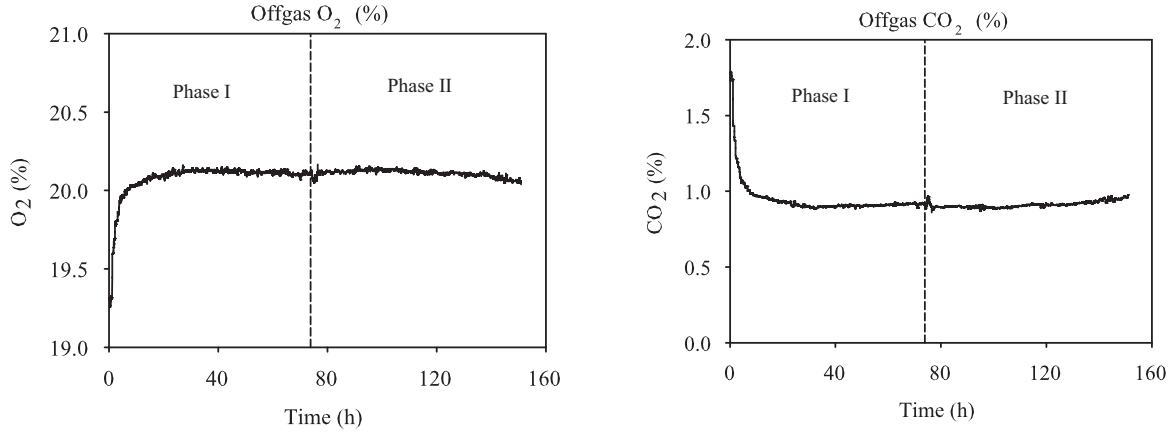

Figure 2.S2: Offgas O_2 and CO_2 measurements of the α-AAA step experiment.

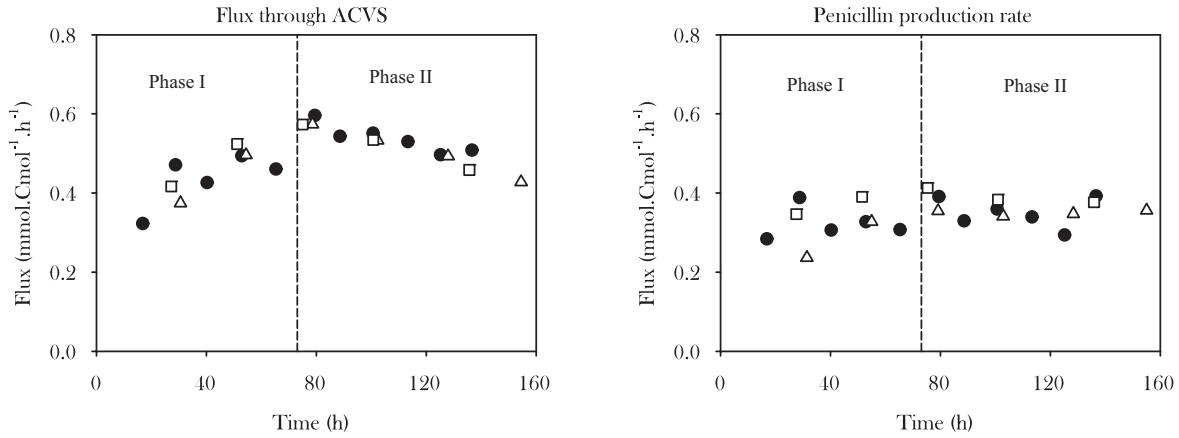

Figure 2.S3: Comparison of the fluxes through ACVS and PenG secretion rate for α-AAA step experiment and the reference chemostats over the entire chemostat cultivation. The solid symbols represent the α-AAA step experiment and the open symbols represent the reference chemostats. The dotted line separates the phase I and phase II in α-AAA step experiment.

Chapter 3

Novel insights in transport mechanisms and kinetics of phenylacetic acid and penicillin-G in *Penicillium chrysogenum*

Douma RD, Deshmukh AT, de Jonge LP, de Jong BW, Seifar RM, Heijnen JJ, van Gulik WM (2012). Novel insights in transport mechanisms and kinetics of phenylacetic acid and penicillin-G in *Penicillium chrysogenum*. Biotechnol Prog 28 (2):337-348.

Abstract

Although penicillin-G (PenG) production by the fungus *Penicillium chrysogenum* is a well-studied process, little is known about the mechanisms of transport of the precursor phenylacetic acid (PAA) and the product PenG over the cell membrane. To obtain more insight in the nature of these mechanisms, *in vivo* stimulus response experiments were performed with PAA and PenG in chemostat cultures of *P. chrysogenum* at time scales of seconds to minutes. The results indicated that PAA is able to enter the cell by passive diffusion of the undissociated acid at a high rate, but is at the same time actively excreted, possibly by an ABC transporter. This results in a futile cycle, dissipating a significant amount of metabolic energy, which was confirmed by increased rates of substrate and oxygen consumption, and carbon dioxide production. To estimate the kinetic properties of passive import and active export of PAA over the cell membrane, a dynamic mathematical model was constructed. With this model a good description of the dynamic data could be obtained. Also PenG was found to be rapidly taken up by the cells upon extracellular addition, indicating that PenG transport is reversible. The measured concentration gradient of PenG over the cell membrane corresponded well with facilitated transport. Also for PenG transport a dynamic model was constructed and validated with experimental data. The outcome of the model simulations were in agreement with the presence of a facilitated transport system for PenG.

Keywords:
Penicillium chrysogenum; penicillin; phenylacetic acid, membrane transport mechanisms

3.1 Introduction

Fermentation processes are increasingly used to produce fine and bulk chemicals. Improvement of these processes is often approached by genetically increasing the flux capacity from substrates to product within the producing microorganism. An important aspect for increasing production rates is the presence of suitable transport proteins, for importing the substrate(s) and exporting the product, with sufficient affinity and capacity. So far, relatively little research has been carried out on transport mechanisms for the import of substrates and the export of products of microbial cells. Published research on transport mechanisms has been reviewed for filamentous fungi [25] and *Saccharomyces cerevisiae* [174] amongst others.

Penicillin has been produced for more than 50 years via industrial fermentation and is a good example of a well-established fermentation process with an annual market of $5 billion in 1999 [40]. If the side-chain precursor phenylacetic acid (PAA) is supplied to the medium of *Penicillium chrysogenum,* it produces penicillin-G (PenG), which is excreted into the medium. Although penicillin production in *P. chrysogenum* is a well-studied process, there is still debate about the mechanisms behind the transport of PAA and PenG across the plasma membrane.

Hillenga et al. [72] concluded that the uptake of PAA occurs through passive diffusion of the undissociated acid over the cell membrane, which was supported by Eriksen et al. [48], who showed that passive diffusion is by far the predominant mechanism for PAA uptake. However, in an earlier study a specific protein mediated uptake mechanism for dissociated PAA was identified [52]. The latter claim was supported by a functional category analysis on the effect of PAA on genome wide expression levels in *P. chrysogenum* [65], which revealed that several transport-related genes were up regulated in the presence of PAA. In this study no distinction could be made, however, between uptake or secretion mechanisms. It was found that the yeast *S. cerevisiae* is able to actively excrete the anion form of PAA, using an ATP-binding cassette (ABC) transporter Pdr12p, as a detoxification mechanism [67]. The authors showed that, although also in the wild type strain the presence of PAA resulted in a decrease of the growth rate in batch culture, the growth rate of the null mutant *pdr12* was significantly lower under these conditions.

Measurement of the intracellular concentration of PAA of *P. chrysogenum* cells cultivated in the presence of the acid, revealed that the concentration was significantly lower than at thermodynamic equilibrium [42,43]. The cause of this could be a low membrane permeability coefficient in case of passive diffusion or the presence of a specific facilitated uptake system for PAA with a low capacity. Alternatively, there could be active export and simultaneous passive import (as shown in *S. cerevisiae*). This would result in an energy consuming futile cycle.

Although several groups have been studying the transport of antibiotics over the cell membrane, very little is known about the mechanism of penicillin export in *P. chrysogenum.* Nijland et al. [127] found that the expression of the *cefT* gene of *Acremonium chrysogenum* resulted in an increased cephalosporin secretion rate in *P. chrysogenum,* showing the implications of transport over the cell membrane for the productivity. Although no irrefutable evidence has been provided, secretion of PenG from the cell was linked to the presence of an ABC transporter [8,104,172].

To obtain more insights in the mechanisms, thermodynamics and kinetics of transport of PAA and PenG in whole cells of *P. chrysogenum*, different stimulus response experiments with glucose limited *P. chrysogenum* chemostat cultures were performed on different time scales using a recently developed rapid sampling and washing method [43]. Pulse experiments were performed in which PAA or PenG solutions were pulsed into *P. chrysogenum* chemostat cultures. During these experiments the dynamics of the intracellular levels of PAA and PenG and the oxygen consumption and carbon dioxide production were measured to obtain more insight in the mechanisms of transport. Mathematical models for PAA and PenG transport were constructed. The model parameters were estimated using the experimental results from these pulse experiments. Subsequently, the model structure was validated with ramp-up experiments in which the extracellular PAA and PenG concentrations were increased in a linear fashion within a period of tens of minutes and the intracellular concentration of PAA and PenG were monitored. Also the oxygen consumption was monitored to reveal the presence of a possible futile cycle in PAA transport.

3.2 Theoretical aspects

3.2.1 Kinetics of PAA transport

In an aqueous solution PAA attains a pH dependent equilibrium between the undissociated (HPAA) and dissociated (PAA^-) forms:

$$HPAA \rightleftarrows PAA^- + H^+ \quad (1)$$

With the dissociation equilibrium constant $K = \frac{C_{H^+} \cdot C_{PAA^-}}{C_{HPAA}}$ and the total phenylacetic acid concentration $C_{PAA} = C_{HPAA} + C_{PAA^-}$.

The pH dependent concentration of undissociated HPAA can be expressed as a function of the total acid (C_{PAA}):

$$C_{HPAA} = \frac{C_{PAA}}{1+10^{pH-pKa}} \quad (2)$$

The undissociated form of apolar weak acids, such as phenylacetic acid, (pKa = 4.31) can easily permeate through cell membranes [25,174], whereby the concentration gradient of the undissociated acid over the cell membrane is the driving force for passive import of PAA. Figure 3.1 shows two possible hypotheses for PAA transport. In hypothesis I there is only uptake by passive diffusion of the undissociated form of PAA [72].

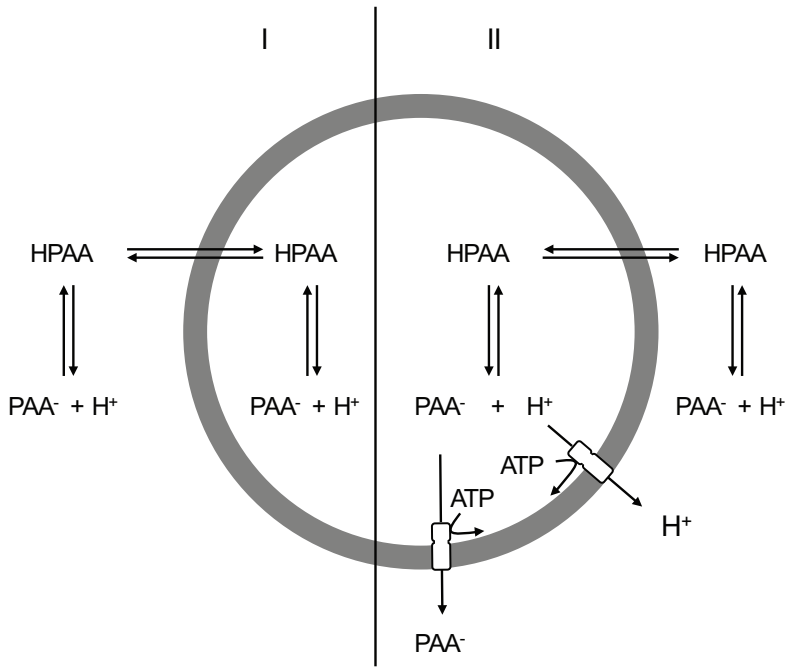

Figure 3.1: Different hypotheses for transport of PAA across the plasma membrane in *P. chrysogenum*.
(I) Passive diffusion alone and (II) passive diffusion in combination with active export by an ABC transporter.

For passive diffusion only, the net influx of PAA in mmol·CmolDW^{-1}·h^{-1} can be written as:

$$q_{diff,HPAA} = k_{perm,HPAA} \cdot A \cdot \left(\frac{C_{PAA,ex}}{1+10^{pH_{ex}-pKa}} - \frac{C_{PAA,in}}{1+10^{pH_{in}-pKa}} \right) \quad (3)$$

In which $k_{perm,HPAA}$ (m·h^{-1}) is the membrane permeability constant for PAA, A (m^2·CmolDW^{-1}) is the biomass specific membrane surface area and $C_{PAA,ex}$ and $C_{PAA,in}$ are the total phenylacetic acid concentrations outside and inside the cell. The specific area A can be calculated, assuming that the *P. chrysogenum* cell has a cylindrical shape and the top and bottom ends are not taken into account [131], as:

$$A = \frac{4}{d_{cell}} \cdot \mathrm{V_x} \quad (4)$$

Herein V_x is the specific cell volume, 7.0·10^{-5} m^3·CmolDW^{-1} [75,131], and d_{cell} is 5·10^{-6} m [131]. The total acid concentration ratio (in / ex) in thermodynamic equilibrium is given by the following equation:

$$\left(\frac{C_{PAA,in}}{C_{PAA,ex}} \right)^{eq} = \frac{1+10^{pH_{in}-pKa}}{1+10^{pH_{ex}-pKa}} \quad (5)$$

As shown by Douma et al. [43] the (in / ex) equilibrium ratio can be calculated to equal 5.0 for an extracellular pH of 6.5 and assuming an intracellular pH of 7.2, which is typical for filamentous fungi [100,101,134,145].

Hypothesis II combines uptake by passive diffusion of the undissociated form of PAA with active export of the anion by an ABC transporter, as is the case in *S. cerevisiae* [67], with simultaneous proton export through the plasma membrane H$^+$-ATPase, leading to an energy consuming futile cycle.

3.2.2 Kinetics of PenG transport

For a charged solute A^Z the Gibbs energy associated with facilitated export is:

$$\Delta G = RT \ln \left(\frac{C_{ex,A^Z}}{C_{in,A^Z}} \right) + Z \cdot F \cdot \Psi_{in} \quad (6)$$

with Z the charge of the transported species, F the Faraday constant of 96.5 kJ·V^{-1}·mol^{-1}, Ψ (V) the intracellular electrical potential and C the concentration. Figure 3.2 shows three possible mechanisms for the export of PenG (which is a negatively charged molecule, Z = 1) namely facilitated export, export by proton antiport and export with ATP hydrolysis using an

ABC transporter. The equilibrium constants for these three different mechanisms are respectively:

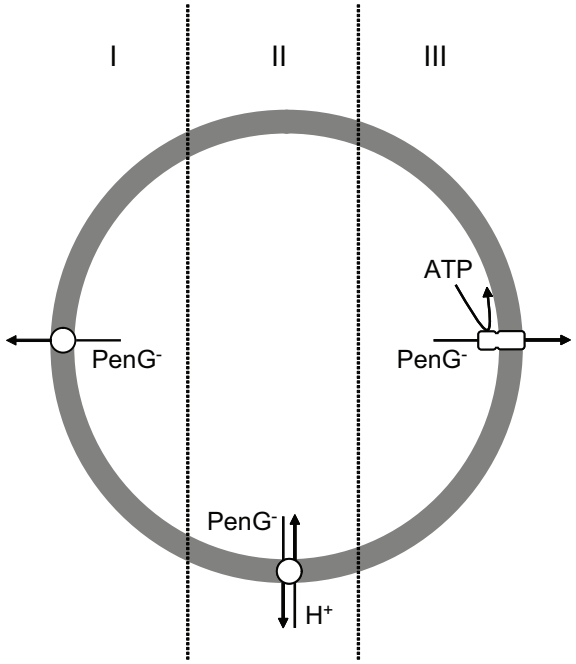

Figure 3.2: Different hypotheses for transport of PenG across the plasma membrane in *P. chrysogenum*.
(I) Facilitated diffusion of the anion of PenG driven by the membrane potential, (II) proton antiport of the anion of PenG, and (III) active export by an ABC transporter.

$$\left(K_{eq,penG}\right)_{fac} = \frac{C_{ex}}{C_{in}} = e^{\frac{+1\cdot F\cdot\Psi_{in}}{R\cdot T}} \tag{7}$$

$$\left(K_{eq,penG}\right)_{antip} = \frac{C_{ex}}{C_{in}} = \frac{C_{H^+,ex}}{C_{H^+,in}} e^{\frac{-2\cdot F\cdot\Psi_{in}}{R\cdot T}} = 10^{pH_{in}-pH_{ex}} \cdot e^{\frac{-2\cdot F\cdot\Psi_{in}}{R\cdot T}} \tag{8}$$

$$\left(K_{eq,penG}\right)_{ABC} = \frac{C_{ex}}{C_{in}} = e^{\frac{+1\cdot F\cdot\Psi_{in}+\Delta G_p}{R\cdot T}} \tag{9}$$

Under physiological conditions the energy gained from ATP hydrolysis (ΔG_p) is approximately -50 kJ·mol^{-1} [121].

As shown in Appendix I the kinetics of facilitated secretion of PenG (in mmol·CmolDW^{-1}·h^{-1}) can be described as:

$$q_{\mathrm{sec},PenG} = q_{\mathrm{sec},PenG}^{\max} \cdot \left(1 - \frac{C_{PenG,ex}}{C_{PenG,in}\cdot\left(K_{eq,penG}\right)_{fac}}\right) \tag{10}$$

3.3 Materials and methods

3.3.1 Strain

A high penicillin producing strain of *P. chrysogenum* (DS17690) was kindly donated by DSM Biotechnology Center (Delft, The Netherlands). This strain was used for all experiments.

3.3.2 Media

The cultivation medium was prepared according to Douma et al. [43], except that the PAA and PenG concentrations in the media used for the chemostat cultivations as well as for the ramp-up experiments were adapted as indicated in Table 3.1. PenG was added aseptically to the PenG ramp-up medium using a 0.2 μm filter (FP30/0.2 CA-S, Whatman, Maidstone, England).

Table 3.1: Cultivation medium composition was according to Douma et al. [43], with the exception of PAA and PenG concentration in the medium.

Medium	PAA concentration (mM)	PenG concentration (mM)
-PAA medium	0	0
+PAA medium	5	0
PAA-ramp medium	80	0
PenG-ramp medium	0	80

3.3.3 Chemostat cultivation

Aerobic, glucose limited chemostat cultivations were performed in 7 L turbine stirred bioreactors with a working volume of 4 L. All cultivations were performed at a dilution rate of 0.05 h^{-1}, a cultivation temperature of 25 °C, a pH of 6.50 ± 0.05 and 0.3 bar overpressure. Further details can be found in Nasution et al. [118]. The aeration rate in the PAA and PenG pulse experiments was 1 $L \cdot min^{-1}$ instead of 2 $L \cdot min^{-1}$ to obtain better resolution in the offgas data.

3.3.4 Perturbation experiments

A schematic representation of the perturbation experiments can be found in Figure 3.3. The pulse experiments were performed using chemostat cultivations without PAA in the feed medium (–PAA medium). After 5 residence times of chemostat cultivation the pulse experiments of PAA and PenG were initiated by rapidly injecting the described pulse

solution. Ramp-up experiments were performed in chemostats cultivated with PAA in the medium (+PAA medium) leading to the presence of about 2 mM of PAA and 2 mM of PenG in the culture broth during steady-state. After 5 residence times the medium supply was switched from chemostat feed medium to ramp-up medium (with the same feed rate of carbon source). During all perturbation experiments samples for intra- and extracellular PAA and PenG were taken.

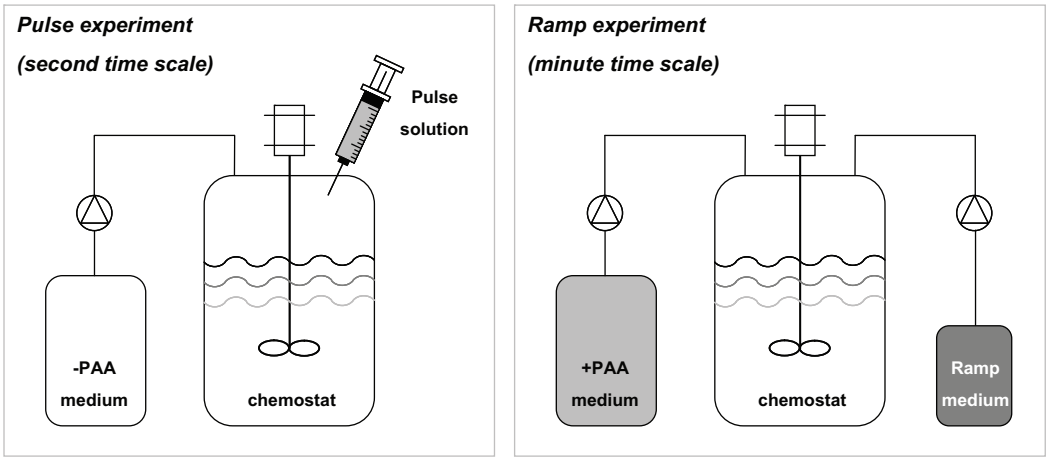

Figure 3.3: Schematic representations of the perturbation experiments. On the left, a pulse experiment (seconds time scale), which is started by adding a pulse solution to a chemostat. On the right, a ramp-up experiment (minutes time scale), which is started by switching from chemostat medium to ramp-up medium.

3.3.5 Pulse solutions

The solutions for the pulse experiments were prepared by dissolving 40 mmol of undissociated PAA (M_w = 136.15 g·mol^{-1}) in 20 mL of H_2O and dissolving 40 mmol of KPenG (M_w = 372.48 g·mol^{-1}) in 30 mL of H_2O. The pH of the PAA solution was set to 6.5 with KOH.

3.3.6 Rapid sampling for intracellular metabolites

Samples for intracellular metabolite determination were taken by rapid sampling. For the ramp-up experiments 10 mL broth samples were rapidly quenched in 50 mL of -40 °C 60% v/v aqueous methanol in a cold filtration unit, as described previously [43]. After filtration the filter cake was immediately washed 2 times with 50 mL of quenching solution. To facilitate sampling at second time scale during pulse experiments, the rapid sampling method of Lange et al. [98] was combined with the sample processing method of Douma et al.[43] as follows. Broth samples of 1 mL were quenched within one second in a tube containing 5 mL of cold aqueous quenching solution using the rapid sampling device as described by Lange et al. [98].

Immediately after sampling the content of the tube was transferred to a filtration unit containing 50 mL of quenching solution. The tube was rinsed twice with the quenching solution to ensure quantitative transfer of the cells to the filtration unit. After filtration the filter cake was immediately washed with 2 x 50 mL of quenching solution.

For accurate quantification with Isotope Dilution Mass Spectrometry (IDMS) [186], 100 µL of U-^{13}C labeled *P. chrysogenum* cell extract was added as internal standard to all filters containing the cold quenched biomass. Subsequently the filters containing the cell cakes were extracted using the boiling ethanol method and further processed towards MS-MS based quantification as described previously [43]. The complete procedure of sampling and subsequent sample processing until the boiling ethanol extraction took maximally one minute.

Samples of culture filtrate were taken using the cold steel beads method [107] as described earlier [43] for extracellular PAA and PenG analysis.

3.3.7 Validation experiment of the washing procedure

To investigate whether the applied filtration based washing method completely removed all extracellular metabolites, a validation experiment was performed. Therefore a 1 mL sample from a chemostat culture grown in the absence of PAA was rapidly withdrawn and immediately quenched in 5 mL -40 °C 60% v/v aqueous methanol solution containing ^{13}C labeled PAA and PenG (> 2mM each). This sample was further processed using the cold filtration method according to Douma et al.[43] and analyzed for its contents of ^{13}C labeled PAA and PenG.

3.3.8 Analytical procedures

Quantification of intracellular PAA and PenG was performed according to Seifar et al. using IDMS [151]. The extracellular concentrations of PAA and PenG were measured with HPLC-UV according to Christensen et al. [34]. Measurement of biomass concentration and offgas analysis were performed as described previously [176].

3.3.9 Parameter estimation

The kinetic parameters for the models for PAA and PenG transport were estimated by weighted nonlinear regression, using the least squares method in MATLAB 7.9.0,.

3.3.10 Simulations

All simulations of intracellular and extracellular PAA and PenG concentrations during perturbation experiments were performed by numerically solving the sets of ordinary differential equations representing the mass balances for intracellular and extracellular PAA and PenG (see Appendix II) using MATLAB 7.9.0.

3.4 Results and discussion

3.4.1 Chemostat cultivations

The chemostat cultivations used for the perturbation experiments in this study were replicates of the ones carried out by Douma et al. [43], showing similar measured macroscopic rates (growth rate, glucose consumption, PenG production etc.). The cultivations were very reproducible and the carbon and degree of reduction balances closed within 5% for each of the six cultivations which were carried out.

3.4.2 Validation experiment of the washing procedure

Culture broth from chemostat cultivations was sampled into a tube containing ^{13}C labeled PAA and PenG in concentrations higher than 2 mM in a -40 °C 60% v/v aqueous methanol solution. Samples were processed and analyzed as described in the section materials and methods to analyze whether extracellular ^{13}C labeled PAA and PenG would be found in the washed biomass. No labeled PAA and PenG could be detected in the cell extract, while the limits of detection were 0.0090 μmol·gDW^{-1} for PAA and 0.0016 μmol·gDW^{-1} for PenG. This proves the efficiency of the filtration method to remove extracellular metabolites. Furthermore, this clearly shows that extracellular PAA and PenG do not enter the cells during cold methanol quenching nor bind to the cell membrane of *P. chrysogenum*.

3.4.3 PAA transport

Two independent chemostat cultures without PAA in the feed medium were subjected to an instantaneous increase in the extracellular concentration of PAA from 0 to 10 mM. The biomass concentration at steady state was about 6 g/L. The results of the PAA pulse for these two independent experiments are shown in Figure 3.4. It can be seen from this figure that the sudden extracellular abundance of PAA resulted in a fast increase in the intracellular PAA level. The 10 mM PAA concentration proved to be non-toxic for the culture. Although the biomass concentration was reduced with 5 and 6% for chemostat 1 and 2 respectively after 24

hours, the culture could maintain the growth rate of 0.05 h^{-1} as imposed by the chemostat dilution rate.

Interestingly, the PAA pulse resulted in an overshoot of the intracellular PAA level, with a maximum around 30 seconds, corresponding with the sudden decrease of the culture pH after injection of the PAA solution. Although the pH of this solution had been set to 6.5 before, the pH was lower at the time of injection, possibly due to incompletely dissolved PAA. Furthermore, it can be seen from the results of the two independent experiments that the more pronounced decrease of the pH in experiment 1 coincides with a more pronounced overshoot of the intracellular PAA level. This observation indicates that PAA enters the cells via passive diffusion of the undissociated acid. If this is the only transport mechanism present and the rate of PAA consumption, e.g. for penicillin synthesis, is negligible compared to the rate of diffusion of PAA into the cells, the intracellular PAA level would reach its thermodynamic equilibrium. For a cultivation pH of 6.5, and assuming a cytosolic pH of 7.2, it can be calculated that the ratio of the intracellular to the extracellular concentration of PAA at thermodynamic equilibrium would equal to 5.0 [43]. However, approximately 50 seconds after the PAA pulse a stable ratio of about 0.5 was reached, which is one order of magnitude below the expected thermodynamic equilibrium. This would indicate that PAA is catabolized and/or consumed for penicillin-G synthesis and byproduct formation with such a rate that the diffusion into the cells is rate limiting.

The initial slope of the intracellular PAA concentration vs. time could be used to obtain a rough estimate of the membrane permeability constant for HPAA, $k_{perm,HPAA}$ (see Equation 3) assuming that PAA transport over the cell membrane occurs via passive diffusion alone. This gives a $k_{perm,HPAA}$ of $5 \cdot 10^{-6}$ $m \cdot s^{-1}$ and an initial PAA uptake rate of 50 $mmol \cdot CmolDW^{-1} \cdot h^{-1}$. Comparing this last figure with the maximum biomass specific penicillin production rate of *P. chrysogenum* DS17690 in glucose limited chemostat cultures, which was found to be 0.56 $mmol \cdot CmolDW^{-1} \cdot h^{-1}$ [176], shows that the rate of PAA consumption for PenG production is 2 orders of magnitude lower than the maximum uptake rate calculated from the pulse

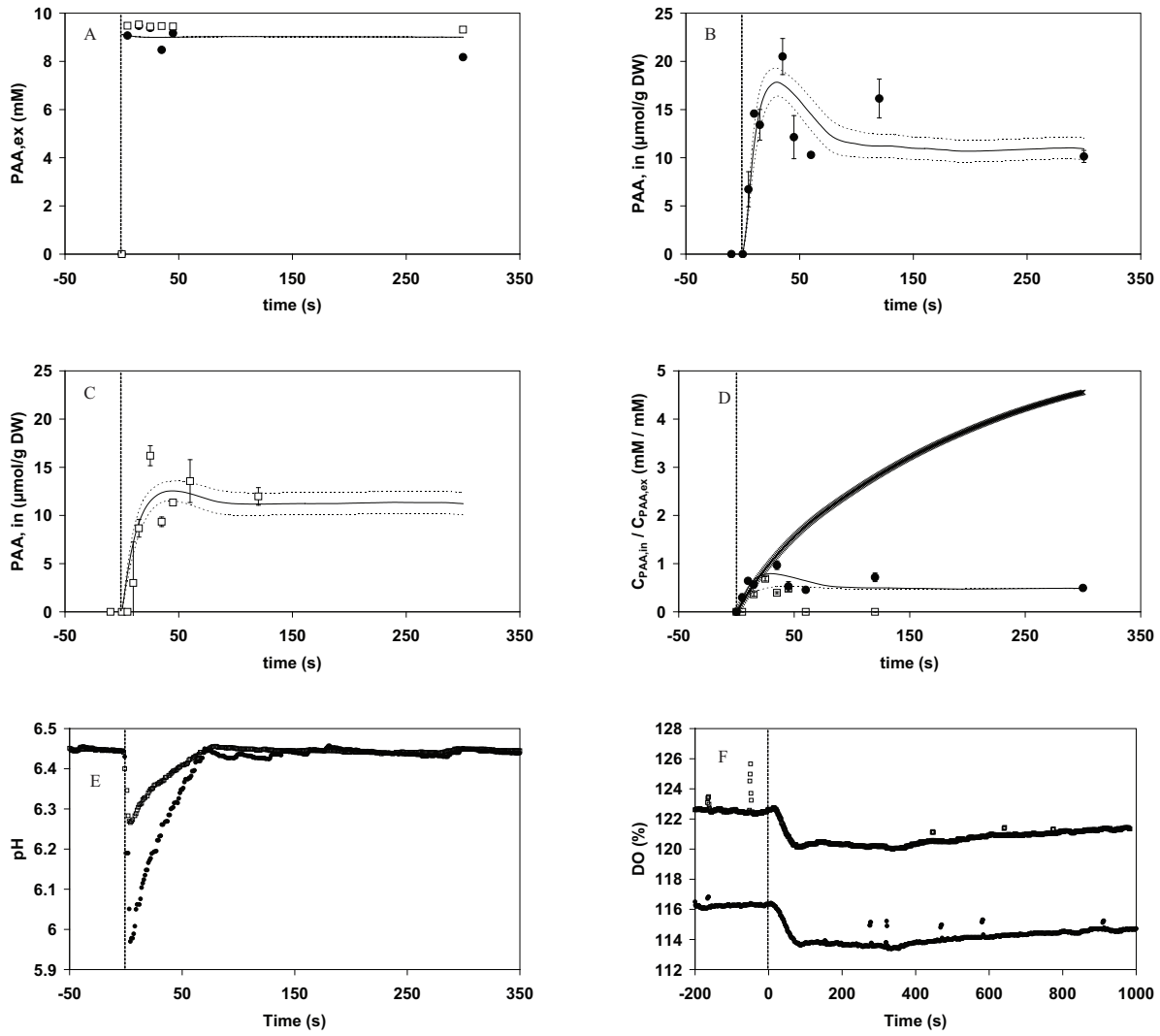

Figure 3.4: Results from the PAA pulse experiments, the pulse solution was injected into the reactor at t 5=0 s. A: Extracellular PAA concentration in PAA pulse 1 and 2. B: Intracellular PAA concentration in PAA pulse 1. C: Intracellular PAA concentration in PAA pulse 2. D: Ratio of intracellular to extracellular concentration in PAA pulse 1 and 2. E: pH in PAA pulse 1 and 2. F: Dissolved oxygen in PAA pulse 1 and 2. Experimental data of pulse experiment 1 (•) and pulse experiment 2 (□), model description of pulse experiment 1 (—) and pulse experiment 2 (– – –), and model based on passive diffusion alone at pHin = 7.2 and the measured pHex during PAA pulse 1 (xx). The dotted lines in panels A to F represent the error regions of the model descriptions.

experiment. This indicates that import of PAA is not likely to be limiting for PenG production. A similar conclusion was drawn by Hillenga et al. [72].

Directly after the addition of PAA to the chemostat, an immediate decrease in the dissolved oxygen concentration (DO) was observed (see Figure 3.4). This coincided with a decrease of the oxygen and an increase of the carbon dioxide concentration in the exhaust gas from the chemostat, indicating increased oxygen consumption and carbon dioxide production rates (results not shown). A possible explanation for this could be catabolism of the imported PAA. However, it has been reported that the industrial strain *P. chrysogenum* DS17690 is not

capable of using PAA as a carbon source, due to a point mutation in the *pahA* gene encoding phenylacetic acid hydroxylase [171]. Nevertheless, small amounts of oOHPAA are produced by this strain and excreted into the medium [176] . However, oOHPAA was not further catabolised in our strain, which was inferred from the complete recovery of PAA in Penicillin-G and oOHPAA (results not shown). This observation clearly shows the inability of our strain to use PAA as carbon source.

It has been reported that in the well-studied yeast *S. cerevisiae* the gene *PDR12* encodes for an ABC transporter involved in weak organic acid resistance, which is capable of exporting e.g. PAA and benzoic acid [67]. In cultivations of *S. cerevisiae* grown in the presence of benzoic acid, a higher respiration due to the ATP requirement for benzoic acid export was observed [96]. This is caused by passive diffusion of the undissociated form of benzoic acid into the cells and subsequent active export by the ABC transporter Pdr12p, creating an ATP consuming futile cycle. Our hypothesis (Figure 3.1, hypothesis II) is that, in a similar way, PAA is imported by passive diffusion in *P. chrysogenum* and simultaneously actively exported, possibly by an ABC transporter. This hypothesis is supported by both the observed increase of the oxygen consumption and carbon dioxide production rates upon PAA addition and the absence of thermodynamic equilibrium between intra- and extracellular PAA. Most remarkable is that the DO decreased almost instantaneously after PAA addition, indicating that the respiration rate of the cells increased immediately. This could indicate the presence of an active exporter with a broad substrate specificity, similar to Pdr12p in *S. cerevisiae* [67].

To test the hypothesis that also in *P. chrysogenum* PAA is actively exported from the cells, a model was constructed for uptake of PAA by passive diffusion of the undissociated acid and subsequent active export. The parameters of the model were estimated using the experimental data from the two pulse experiments. The obtained values of the model parameters are: $k_{perm,HPAA} = (5.2 \pm 1.2)\cdot 10^{-6}$ m·s^{-1}, $k_{export,PAA} = 0.054 \pm 0.016$ s^{-1}. The estimated permeability coefficient appears to be significantly lower than the value of $23\cdot 10^{-6}$ m·s^{-1} found by Hillenga et al. [72]. However, this value was obtained from transport studies with liposomes composed of *Escherichi. coli* lipids and egg yolk L-phosphatidylcholine, of which the permeability for PAA is most probably different than that of the plasma membrane of *P. chrysogenum*.

Similar stimulus response experiments were performed with *S. cerevisiae pdr12* with benzoic acid, which highly resembles the molecular structure of PAA, to measure the intracellular pH

[95]. Because the exporter was deleted, import and export of benzoic acid happened only by passive diffusion in *S. cerevisiae Pdr12Δ*, creating a thermodynamic equilibrium between the intra- and extracellular benzoic acid concentrations. The permeability constant for benzoic acid in *S. cerevisiae* was found to be $(9.2 \pm 7.4)\cdot10^{-6}$ m·s^{-1}, which is similar to our estimation of the permeability constant for PAA of $(5.2 \pm 1.2)\cdot10^{-6}$ m·s^{-1} for *P. chrysogenum*.

The rate of PAA export as function of the intracellular PAA concentration was first modeled with Michaelis-Menten kinetics. However, it was found that in our experiments the exporter was working in the linear range, as separate Michaelis-Menten parameters could not be estimated. Therefore the exporter was modeled by first order kinetics as:

$$q_{\mathrm{sec},PAA} = k_{\mathrm{export},PAA} \cdot C_{PAA} \qquad (11)$$

In which $k_{export,PAA}$ (h^{-1}) is the first order rate constant with $q_{\mathrm{sec},PAA}$ having units mmol·CmolDW^{-1}·h^{-1}.

The model description of the dynamics of the intracellular PAA concentration as well as the ratio between intracellular and extracellular PAA for the two pulse experiments are shown as solid lines in Figure 3.4. As mentioned, the sudden addition of the PAA solution caused a drop in the pH in the reactor, which was subsequently compensated for by NaOH addition by the pH control system. It took a few tens of seconds to return to the pH set point of 6.5 ± 0.05. Therefore the pH patterns, which were different for the two pulse experiments, were used as a model input. It can be seen from Figure 3.4 that the mathematical model shows a good description of the experimental data, which quantitatively supports the hypothesis of active export of PAA from the cells. The fluxes calculated from the model are presented in Figure 3.5, which shows the effect of the pH drop in the two pulse experiments. During the higher PAA influx caused by the increased concentration of undissociated PAA at decreased pH, also the rate of PAA export is increased to prevent accumulation. After the pH returned to the setpoint of 6.5, the calculated influx equaled the efflux to reach a steady state cycling rate of 59 ± 14 mmol·CmolDW^{-1}·h^{-1}.

The expected increase of the oxygen consumption rate, corresponding with the additional ATP dissipation for PAA export, was calculated by assuming that the active export of PAA requires one mol of ATP per mol of undissociated acid excreted. With each mole of PAA one

mole of protons has to be excreted, which requires an additional mole of ATP, as the stoichiometry of the yeast plasmalemma ATP-ase is one ATP per H^+.

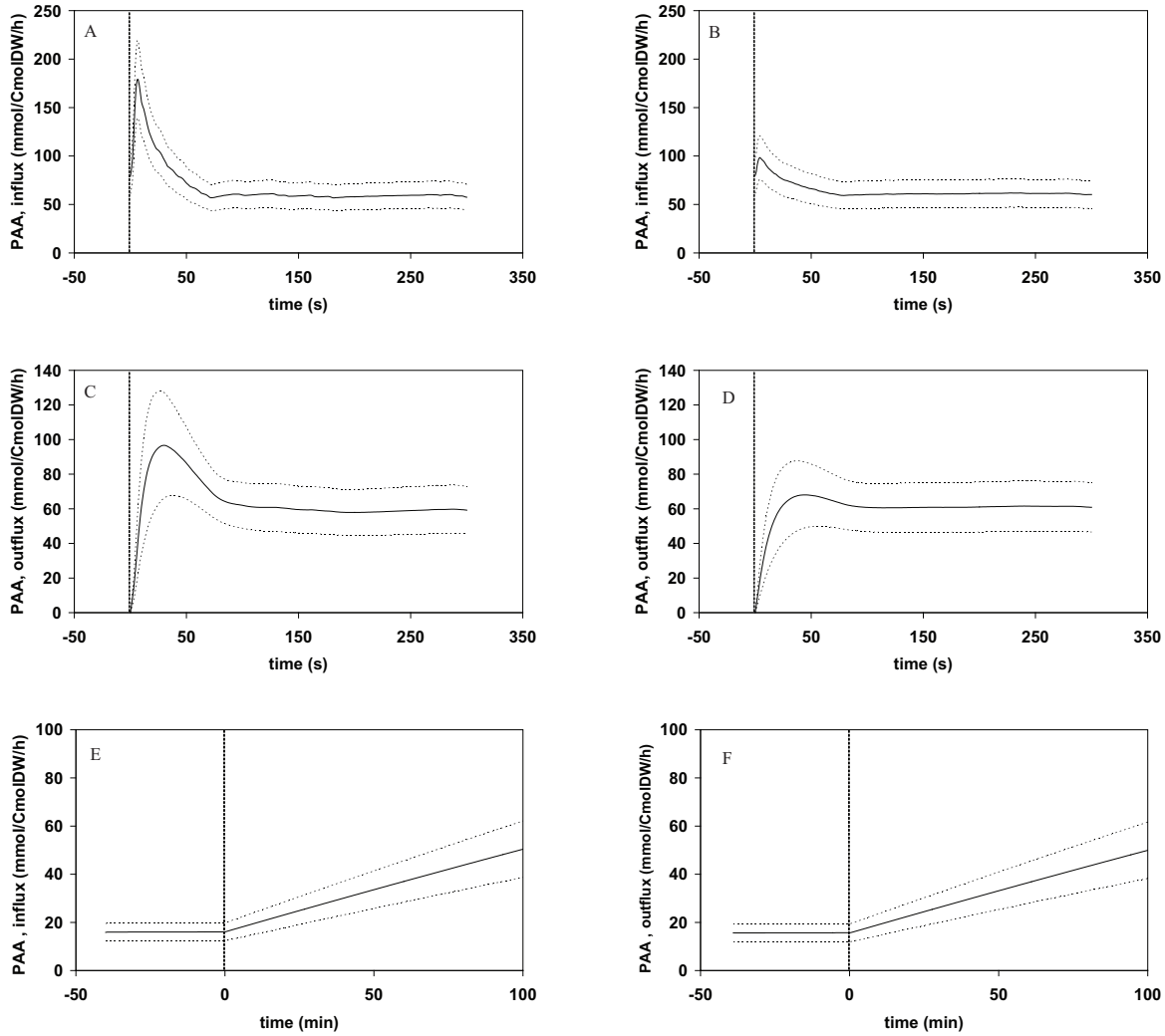

Figure 3.5: Model results for the PAA pulse and ramp-up experiments. [A]: PAA influx in PAA pulse 1. [B]: PAA influx in PAA pulse 2. [C]: PAA outflux in PAA pulse 1. [D]: PAA outflux in PAA pulse 2. [E]: Influx in PAA ramp-up. [F:] Outflux in PAA ramp-up. The pulse solution was added to the reactor at t = 0 s. The dotted lines represent the error regions of the model results.

The expected increase of the oxygen consumption rate, corresponding with the additional ATP dissipation for PAA export, was calculated by assuming that the active export of PAA requires one mol of ATP per mol of undissociated acid excreted. With each mole of PAA one mole of protons has to be excreted, which requires an additional mole of ATP, as the stoichiometry of the yeast plasmalemma ATP-ase is one ATP per H^+. To calculate the corresponding oxygen consumption, a value of the operational P/O ratio of 1.5 mol ATP per 0.5 mol O_2 was used, which was estimated from metabolic flux analysis using the stoichiometric model of van Gulik et al. [175] for the applied cultivation conditions (glucose

limited chemostats). Using the relation for $q_{sec,PAA}$ (equation 11) this leads to the following oxygen consumption rate (in mmol·CmolDW^{-1}·h^{-1}) due to PAA and H^+ export:

$$q_{O_2,PAA} = \frac{q_{\text{sec},PAA} + q_{\text{sec},H^+}}{2 \cdot (P/O)} \qquad (12)$$

Using Equation 12 the oxygen consumption associated with the above estimated PAA cycling rate is calculated to be $q_{O_2,PAA}$ = 32.1 ± 3.8 mmol·CmolDW^{-1}·h^{-1}. This value is significantly higher than the measured increase of the oxygen consumption rate after the PAA pulse, which was respectively 6.7 and 6.2 mmol·CmolDW^{-1}·h^{-1} for the two PAA pulse experiments. The reason for this is that the PAA pulses were given to glucose limited chemostat cultivations, which have a fixed glucose supply rate. This implies that the cells can only increase the glucose consumption for additional ATP generation by mobilization of storage carbohydrates (e.g. glycogen and trehalose) and temporary reduction of the growth rate. This results in a limited increase of the oxygen consumption rate. The appropriate way to obtain experimental data on the energetic consequences of the presence of PAA is to carry out steady state chemostat cultivations with and without supply of PAA in the feed medium. We have carried out such cultivations with the same high producing strain of *P. chrysogenum* under the same chemostat conditions (glucose limited, D=0.05 h^{-1}) of which the results have been published previously [120]. The addition of 4.85 mol.L^{-1} of PAA to the feed of the chemostat resulted in a steady state penicillin-G production rate of 0.35 mmol.CmolDW^{-1}.h^{-1} and increased biomass specific rates of glucose and oxygen consumption and carbon dioxide production (see Table 3.2). The steady state residual PAA concentration was approximately 2.75 mmol.L^{-1}. For these cultures no measurements of the intracellular PAA concentration were carried out. However, results of such measurements for identical chemostat cultures have been published by Douma et al. [43] They reported an intracellular PAA level of 2.97 ± 0.18 µmol.gDW^{-1} for glucose limited chemostat cultures of *P. chrysogenum* DS17690 carried out at D = 0.05 h^{-1} in the presence of PAA. Based on these data and our model for diffusion of undissociated PAA into the cells, the energetic consequences of PAA supply, in terms of increases in glucose and oxygen consumption and carbon dioxide production were calculated. The details of the calculations can be found in Appendix III. The results are compared with the experimental data from Nasution et al.[120], in Table 3.2. As can be seen from the results in table 3.2, the effect of PAA addition on glucose consumption and respiration has two contributions, a part associated with the biosynthesis of penicillin and a part associated with the export of PAA

and protons to counteract the influx of the undissociated form of the acid by diffusion. The good correspondence between the predicted and the measured values confirms the validity of our model for PAA cycling. Furthermore, these results show that a significant amount of metabolic energy, and thus a significant amount of supplied substrate, is lost by this futile cycle of passive influx and active export of PAA. The estimated rate of PAA export of 16.2 mmol.CmolDW^{-1}.h^{-1} for the PenG producing chemostat (Appendix III) leads to an additional consumption of 2 ATP per PAA exported, thus 32.4 mmol.CmolDW^{-1}.h^{-1}. Expressed per amount of PenG produced this yields a value of 32.4 / 0.35 = 93 mol ATP per mol of penicillin which corresponds with the value of 73 ± 20 mol/mol reported by van Gulik et al. [175]. This shows that the previously estimated additional ATP dissipation associated with PenG production can be completely attributed to active excretion of PAA.

Table 3.2: Measured and predicted increase in biomass specific oxygen consumption rate upon 10 mM PAA pulse. q_{O2}^{0} = 41.7 mmol·CmolDW^{-1}·h^{-1}.

	Experimental data		Model prediction
	PAA pulse 1 (mmol·CmolDW^{-1}·h^{-1})	PAA pulse 2 (mmol·CmolDW^{-1}·h^{-1})	(mmol·CmolDW^{-1}·h^{-1})
$q_{O2,PAA}$	6.7	6.2	16.3 ± 3.4

The obtained model was further challenged by testing its prediction of the intracellular PAA concentration upon a linearly increasing extracellular PAA concentration in the PAA-ramp-up experiments. In these experiments the extracellular PAA concentration was increased from the initial steady state value of 3 mM to 8 mM in a period of 90 minutes (see Figure 3.6A). Also in these experiments the oxygen consumption and carbon dioxide production increased (results not shown), while the DO level decreased (see Figure 3.6C) with increasing extracellular PAA concentration. Also in these experiments an increase of the extracellular PAA concentration coincided with an increase in the intracellular PAA concentration, as can be seen in Figure 3.6B. In this figure the solid line represents the model prediction. It can be seen that the model predictions for the intracellular concentrations are comparable to the experimental values during the steady state. But as the extracellular concentration was linearly increased, the model prediction started to deviate after approximately 1 h, whereby the predicted intracellular concentrations are higher than the experimental values. This could indicate that at increasing extracellular PAA concentrations the PAA exporter is upregulated. It has been observed that in *P. chrysogenum* several transport related genes are upregulated in

cultures grown in the presence of PAA. Amongst these is Pc22g14600 which belongs, similar to Pdr12 of *S. cerevisiae*, to the ABC-G transporter cluster [65].

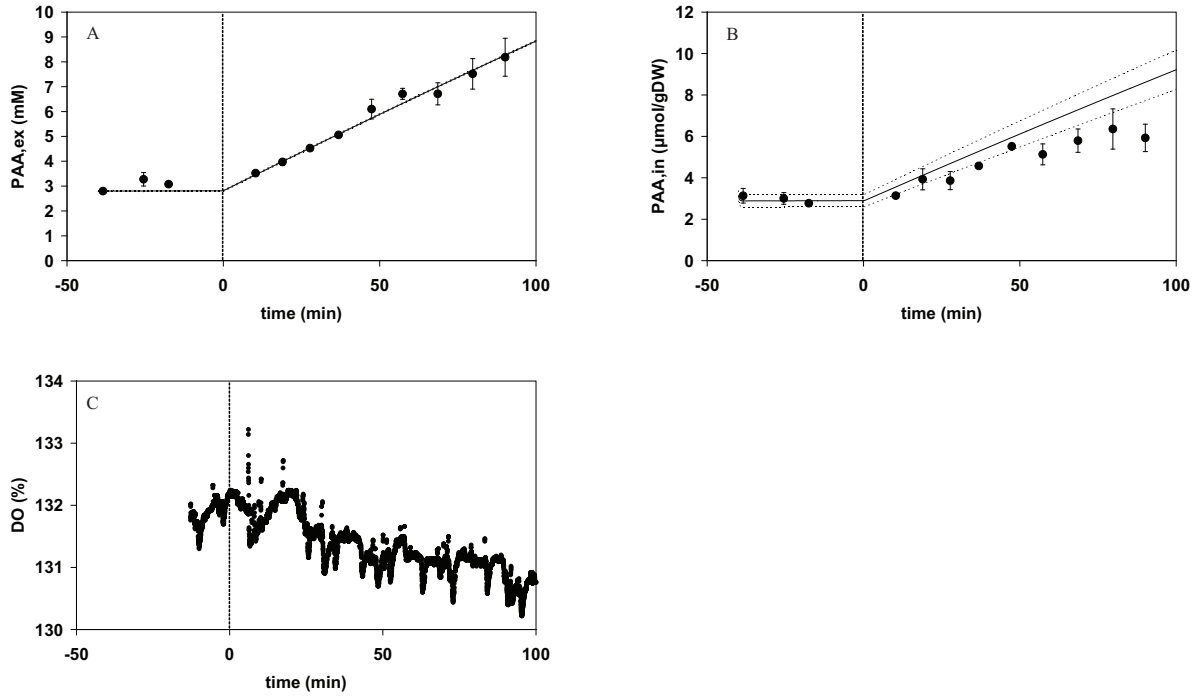

Figure 3.6: Results from the PAA-ramp-up experiment. [A]: Extracellular PAA concentration. [B: Intracellular PAA concentration. [C]: Dissolved oxygen. Experimental data (•) and model description (—). Addition of the ramp-up medium started at t = 0 min. The dotted lines in panels A and B represent the error regions of the model descriptions.

3.4.4 PenG transport

Similar to the PAA pulse experiments PenG pulse experiments were performed. The results of the PenG pulse experiment, in which the extracellular PenG concentration was increased instantaneously from 0 to 10 mM, are shown in Figure 3.7. Irrefutably very rapid intracellular accumulation of PenG was observed (see Figure 3.7B). Apparently PenG is not only excreted from the cells, but can also be taken up, making PenG transport not unidirectional. The ratio of the extracellular to the intracellular concentration ratio swiftly moved towards a value in the same order of magnitude as in PenG producing cultures (see Figure 3.7C), which was reported to be 71 ± 11 [43].

We considered three possible mechanisms for PenG transport, namely facilitated export (I), export by a proton antiport system (II) and export by an ABC transporter (III) (see Figure 3.2). Table 3.3 shows the predicted concentration ratios at thermodynamic equilibrium for these three possible mechanisms and for different values of the membrane potential $\Delta\Psi$. As

can be seen from Table 3.3, only the equilibrium ratio's for facilitated transport are in the same range as the measured concentration ratios, indicating that this is the most likely transport mechanism.

Table 3.3: Predicted extracellular to intracellular PenG concentration ratios for different transport modes for different values of $\Delta\Psi$.

Transport mode	$C_{p,ex} \cdot C_{p,in}^{-1}$ ($mM \cdot mM^{-1}$)		
	$\Delta\Psi$ = -80 mV	$\Delta\Psi$ = -100 mV	$\Delta\Psi$ = -130 mV
Facilitated transport	23	49	158
With proton antiport	$1.6 \cdot 10^3$	$7.6 \cdot 10^3$	$79 \cdot 10^3$
With ATP hydrolysis	$1.3 \cdot 10^{10}$	$2.8 \cdot 10^{10}$	$9.1 \cdot 10^{10}$

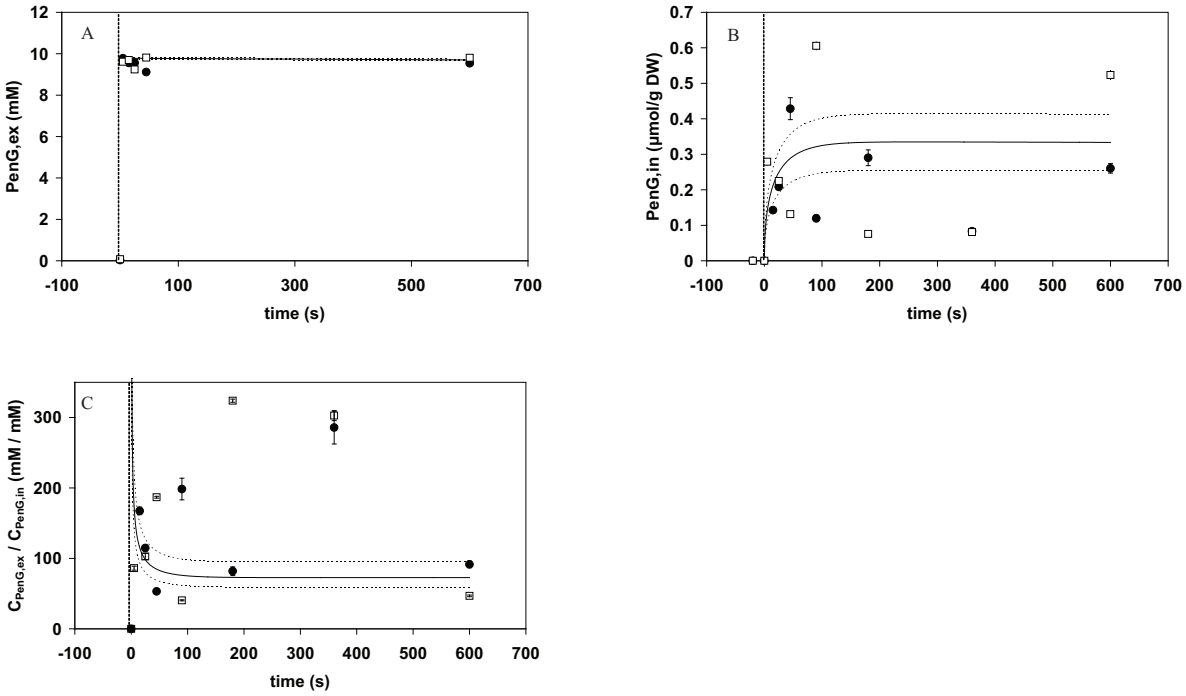

Figure 3.7: Results from the PenG pulse experiments. [A]: Extracellular PenG concentration. [B]: Intracellular PenG concentration. [C]: Ratio of intracellular to extracellular concentration. Experimental data of pulse experiment 1 (•), pulse experiment 2 (□) and model description (—). The pulse solution was added to the reactor at t = 0 s. The dotted lines represent the error regions of the model descriptions.

Subsequently an experiment was performed in which the extracellular PenG concentration was linearly increased from a steady state value of 1.8 mM to approx. 11 mM. Also in this PenG ramp-up experiment an increase of the extracellular PenG concentration coincided with an increase of the intracellular concentration. Hereby the intracellular concentration increased

proportional to the extracellular concentration, as can be inferred from the concentration ratio, which remained the same during the course of this experiment (see Figure 3.8C).

As can be seen from Figure 3.7, there is significant scattering in the data of the PenG-pulse experiment, complicating a proper estimation of the parameters of the dynamic model for facilitated PenG export (Equation 10). Therefore the parameters were estimated using the data obtained from the PenG-ramp-up experiment. Subsequently the model was validated using the data from the PenG-pulse experiment.

The fit of the model to the data from the PenG ramp-up experiment is shown as solid lines in Figure 3.8. The model parameters are the maximum capacity of the transporter protein, $q_{sec,PenG}^{max}$, with an estimated value of 0.83 ± 0.20 mmol·CmolDW^{-1}·h^{-1} and the equilibrium constant $(K_{eq})_{fac}$ with an estimated value of 73 ± 17. It should be noted that the estimated maximum transport capacity is only slightly higher than the maximal penicillin production rate of this strain of 0.56 mmol·CmolDW^{-1}·h^{-1} as has been reported by van Gulik et al. [176]. Product export could therefore be limiting for PenG production in *P. chrysogenum* DS17690.

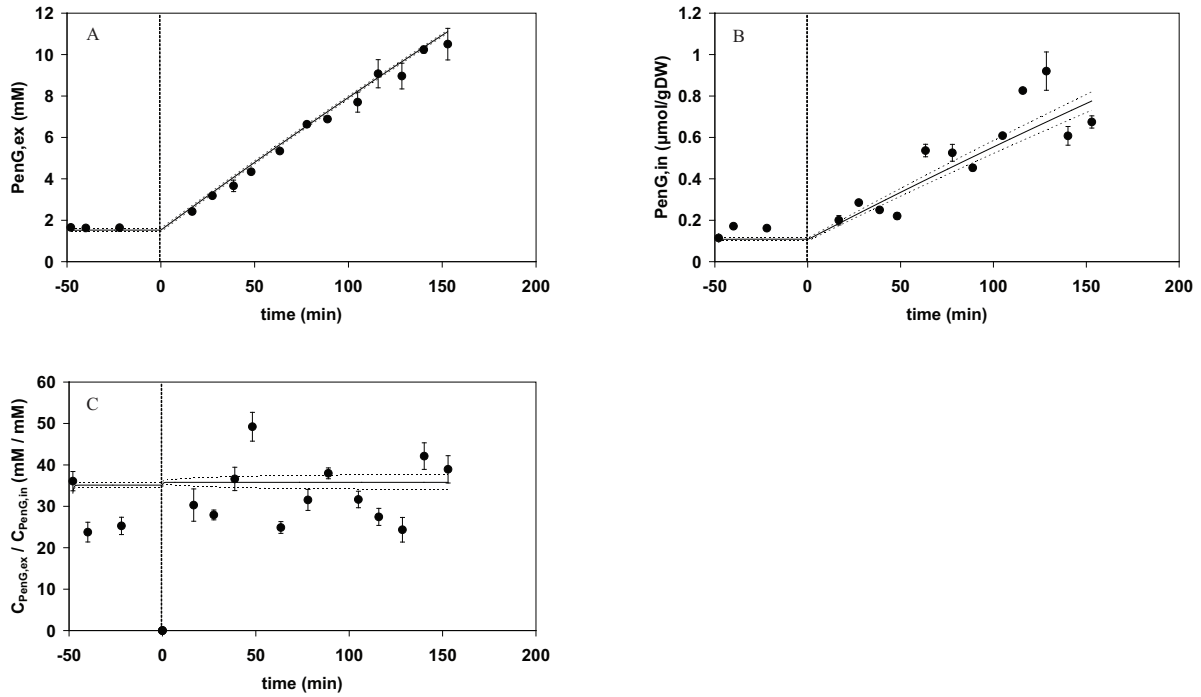

Figure 3.8: Results from the PenG-ramp-up experiment. [A]: Experimental data of the extracellular PenG concentration. [B]: Intracellular PenG concentration. [C]: Ratio of intracellular to extracellular concentration. Experimental data (•) and model description (—). Feeding of the ramp-up medium started at t = 0 min. The dotted lines represent the error regions of the model descriptions.

Moreover, the estimated value for $q_{sec,PenG}^{max}$ is dependent on the value for $(K_{eq})_{fac}$, which was found to vary from experiment to experiment (data not shown). Using the thus calibrated model the dynamics of the intracellular PenG concentration in the PenG pulse experiment was simulated (shown as solid lines in Figure 3.7). The model description of the fast and slow dynamics of the intracellular PenG in respectively the PenG-pulse and PenG-ramp-up experiments appeared to be satisfactory.

3.5 Conclusions

Perturbation experiments with PAA and PenG were performed in chemostat cultures of *P. chrysogenum* at two time scales. The results indicate that the undissociated form of PAA is transported into the cells by passive diffusion. As has been reported for *S. cerevisiae,* also *P. chrysogenum* seems to contain a weak acid exporter, which is capable of excreting PAA at the expense of ATP. A model for PAA transport, based on import by passive diffusion and active export showed a good description of the experimental data obtained from the perturbation experiments. The capacity of PAA import by passive diffusion was found to be 2 orders of magnitude higher than the maximal biomass specific consumption rate required for PenG production, showing that PAA import is unlikely to limit PenG production. From our study it appears that active export of PAA combined with passive diffusion of the undissociated acid into *P. chrysogenum* cells (PAA cycling) is responsible for an energy consuming futile cycle. We found that the additional energy requirement associated with PenG production can be fully explained by PAA cycling.

It was observed that transport of PenG across the cell membrane is reversible, because PenG was imported into the cell upon extracellular addition. The equilibrium ratio of extracellular to intracellular PenG strongly indicates that PenG is excreted from the cells by facilitated transport, whereby the negatively charged PenG molecule is pushed over the membrane by the negative membrane potential. This hypothesis is further supported by model predictions. The estimated model parameter values show that the export capacity is of the same order of magnitude as the maximum biomass specific PenG production rate, and could be limiting for PenG production in *P. chrysogenum* DS17690.

3.6 Acknowledgement

This project is financially supported by the Netherlands Ministry of Economic Affairs and the B-Basic partner organizations (www.b-basic.nl) through B-Basic, a public private NWO-ACTS programme (ACTS: Advanced Chemical Technologies for Sustainability). This project was carried out within the research programme of the Kluyver Centre for Genomics of Industrial Fermentation which is part of the Netherlands Genomics Initiative / Netherlands Organization for Scientific Research.

3.7 Appendix

3.7.1 Appendix I PenG secretion

Facilitated transport of negatively charged PenG, as depicted in Figure 3.2, can be described as follows:

$$T + PenG^-_{in} \rightleftarrows (TPenG)_{in} \quad \text{(AI-1)}$$

$$(TPenG)_{in} \rightleftarrows (TPenG)_{ex} \quad \text{(AI-2)}$$

$$(TPenG)_{ex} \underset{k_{up}}{\overset{k_{sec}}{\rightleftarrows}} T + PenG^-_{ex} \quad \text{(AI-3)}$$

In which T is a transporter protein with the following equilibrium constants:

$$K_1 = \frac{C_T \cdot C_{PenG,in}}{C_{TPenG,in}} \quad \text{(AI-4)}$$

$$K_2 = \frac{C_{TPenG,ex}}{C_{TPenG,in}} \quad \text{(AI-5)}$$

The secretion rate of PenG will then be:

$$q_{\text{sec},PenG} = k_{\text{sec}} \cdot C_{TPenG,ex} - k_{up} \cdot C_T \cdot C_{PenG,ex} \quad \text{(AI-6)}$$

The total permease species can be described as follows:

$$C_{T_O} = C_T + C_{TPenG,in} + C_{TPenG,ex} \quad \text{(AI-7)}$$

Substituting equations AI-4, AI-5 into AI-7:

$$C_T = \frac{C_{T_O}}{1 + \frac{C_{PenG,in}}{K_1} + \frac{K_2}{K_1} \cdot C_{PenG,in}} \quad \text{(AI-8)}$$

Substituting equations AI-5 and AI-7:

$$C_{TPenG,ex} = \frac{K_2}{K_1} \cdot C_{PenG,in} \cdot \frac{C_{T_O}}{1 + \frac{C_{PenG,in}}{K_1} + \frac{K_2}{K_1} \cdot C_{PenG,in}} \quad \text{(AI-9)}$$

The secretion rate can be rewritten by substituting AI-8 and AI-9 into AI-6:

$$q_{\sec,PenG} = \frac{k_{\sec} \cdot C_{T_O} \cdot \frac{K_2}{K_1}}{1 + \frac{C_{PenG,in}}{K_1} + \frac{K_2}{K_1} \cdot C_{PenG,in}} \cdot \left(C_{PenG,in} - \frac{C_{PenG,ex}}{\frac{K_2}{K_1} \cdot \frac{k_{\sec}}{k_{up}}} \right) \quad \text{(AI-10)}$$

When $C_{PenG,in} = 0$:

$$q_{\sec,PenG} = q_{\sec,PenG}^{\max} = -k_{up} \cdot C_{T_O} \cdot C_{PenG,ex} \quad \text{(AI-11)}$$

When $C_{PenG,ex} = 0$:

$$\left(q_{\sec,PenG}\right)_{PenG,ex=0} = \frac{k_{\sec} \cdot C_{T_O} \cdot \frac{K_2}{K_1} \cdot C_{PenG,in}}{1 + \frac{C_{PenG,in}}{K_1} + \frac{K_2}{K_1} \cdot C_{PenG,in}} \quad \text{(AI-12)}$$

At equilibrium, $q_{sec} = q_{up} = 0$ from AI-10:

$$\frac{C_{PenG,ex}}{C_{PenG,in}} = \frac{K_2}{K_1} \cdot \frac{k_{\sec}}{k_{up}} = \left(K_{eq,penG}\right)_{fac} \quad \text{(AI-13)}$$

From AI-10 we can write:

$$q_{\sec,PenG} = \frac{k_{\sec} \cdot C_{T_O} \cdot \frac{K_2}{K_1} \cdot C_{PenG,in}}{1 + \frac{C_{PenG,in}}{K_1} + \frac{K_2}{K_1} \cdot C_{PenG,in}} \cdot \left(1 - \frac{C_{PenG,ex}}{C_{PenG,in} \cdot \frac{K_2}{K_1} \cdot \frac{k_{\sec}}{k_{up}}} \right) \quad \text{(AI-14)}$$

At maximal secretion rate $K_2 >> K_1$, substituting AI-12 and AI-13 into AI-14:

$$q_{\sec,PenG} = q_{\sec,PenG}^{\max} \cdot \left(1 - \frac{C_{PenG,ex}}{C_{PenG,in} \cdot \left(K_{eq,penG}\right)_{fac}} \right) \quad \text{(AI-15)}$$

This simplified, one parameter version of the secretion rate cannot be simulated at initial $C_{PenG,in}$ equal to zero. For practical purposes this value is taken to be very small (1×10^{-15}) and is valid till (1×10^{-150}), which is a negligible concentration as compared to the intracellular concentrations of PenG.

3.7.2 Appendix II Simulations

To describe the system mass balances for intracellular PAA and PenG were constructed:

$$\frac{dC_{PAA,in}}{dt} = q_{diff,PAA} - q_{\sec,PAA} - q_p - \mu \cdot C_{PAA,in} \quad \text{(AII-1)}$$

$$\frac{dC_{PenG,in}}{dt} = -q_{\sec,PenG} + q_p - \mu \cdot C_{PenG,in} \quad \text{(AII-2)}$$

Furthermore extracellular PAA and PenG mass balances were constructed:

$$\frac{dC_{PAA,ex}}{dt} = -q_{diff,PAA} \cdot C_x + q_{\sec,PAA} \cdot C_x + D \cdot \left(C_{PAA,feedin} - C_{PAA,ex} \right) \quad \text{(AII-3)}$$

$$\frac{dC_{PenG,ex}}{dt} = q_{\sec,PenG} \cdot C_x + D \cdot \left(C_{PenG,feedin} - C_{PenG,ex} \right) \quad \text{(AII-4)}$$

The specific growth rate μ (h^{-1}) is included in the model to account for the dilution of the intracellular metabolites caused by growth of the cells, while D (h^{-1}) is included to account for the dilution of extracellular metabolites because of wash out. C_x ($CmolDW \cdot m^{-3}$) is the measured biomass dry weight.

3.7.3 Appendix III Calculation of the energy requirement for PenG biosynthesis and PAA cycling

PenG biosynthesis

If the yield of PenG on substrate, Y_{sp}, is known, the rate of substrate consumption for PenG biosynthesis, $q_{s,PenG}$, can be calculated from:

$$q_{s,PenG} = \frac{q_p}{Y_{sp}} \quad \text{(AIII-1)}$$

The corresponding oxygen consumption rate, $q_{O,}$ can be calculated from a generalized degree of reduction balance [34]:

$$q_o = \frac{1}{4}(\gamma_s \cdot q_{s,PenG} - \gamma_p \cdot q_p) \quad \text{(AIII-2)}$$

Wherein γ_s is the generalized degree of reduction of the substrate and γ_p is the generalized degree of reduction of the β-lactam moiety of the PenG molecule (note that for glucose γ_s = 24 and that γ_p = 38 for the β-lactam moiety of PenG).

The corresponding carbon dioxide production rate can be calculated from a carbon balance (note that one molecule of glucose contains 6 carbon atoms while the β-lactam moiety of PenG contains 8 carbon atoms):

$$q_c = 6q_s - 8q_p \quad \text{(AIII-3)}$$

Based on the known stoichiometry of the PenG biosynthesis pathway and the experimentally determined ATP stoichiometry of *P. chrysogenum* grown in carbon limited chemostats van Gulik et al. [175] calculated that the maximum theoretical yield of PenG on glucose is equal to 0.39 mol PenG per mol of glucose. For a specific PenG production rate of 0.35 $mmol.CmolDW^{-1}.h^{-1}$ it can be calculated that the corresponding glucose uptake rate equals

0.35 / 0.39 = 0.9 mmol.CmolDW^{-1}.h^{-1} and the corresponding oxygen consumption and carbon dioxide production rates equal 2.1 and 2.6 mmol.CmolDW^{-1}.h^{-1} respectively.

PAA cycling

From Eq. 11 with an estimated value of $k_{export,PAA}$ of 0.054 s^{-1} it can be calculated that for an intracellular PAA level of 2.97 μmol.gDW^{-1} the PAA excretion rate equals 16.2 mmol. CmolDW^{-1}.h^{-1}. Assuming that for each PAA^- exported a proton is excreted, the corresponding oxygen consumption rate can be calculated from Eq. 12 to be 11 mmol.CmolDW^{-1}.h^{-1} for P/O = 1.5. From the stoichiometry of aerobic glucose catabolism, i.e. 1 $C_6H_{12}O_6$ + 6 O_2 ➔ 6 CO_2 + 6 H_2O it follows that the corresponding rates of glucose uptake and carbon dioxide production equal 1.8 and 11 mmol.CmolDW^{-1}.h^{-1} respectively.

Chapter 4

In vivo kinetic analysis of the penicillin biosynthesis pathway using stimulus response experiments

Deshmukh AT, Maleki Seifar R, ten Pierick A, Heijnen JJ and van Gulik WM. *In vivo* kinetic analysis of the penicillin biosynthesis pathway using stimulus response experiments. *(Submitted for publication)*

Abstract

Rapid stimulus response experiments were carried out to obtain the *in vivo* kinetic properties of the enzymes and transport steps involved in the penicillin biosynthesis pathway of *Penicillium chrysogenum,* with the aim to identify possible bottlenecks. To specifically perturb the penicillin pathway, a high producing *P. chrysogenum strain* was grown in a glucose-limited chemostat in the absence of the side chain precursor for penicillin-G (PenG) formation, phenyl acetic acid (PAA). Subsequently, after a pseudo- steady state was reached, the culture was challenged by a step wise perturbation with 5 mM phenylacetic acid. The resulting transient response, in terms of the dynamics of the intra- and extra-cellular concentrations of all compounds related to the penicillin biosynthesis pathway, was monitored until a new steady state was reached.

We observed that within 10 seconds after the phenylacetic acid perturbation, intracellular penicillin-G could be detected, indicating that the complete biosynthetic pathway was already expressed during the preceding cultivation in the absence of PAA. Further, fluxes through the penicillin pathway were calculated for the chemostat cultivation in the absence and presence of PAA. The quantitative analysis of metabolome and fluxome responses showed that after the sudden availability of PAA and in the abundance of isopenicillin-N (IPN) and 6-aminopenicillanic acid (6APA), the ß-lactam flux is controlled by Isopenicillin-N Acyltransferase (IAT) but under normal PenG producing conditions, where intracellular IPN and 6APA are far lower, the fluxes were controlled by δ-[L-α-aminoadipyl]-L-cysteinyl-D-valine synthetase (ACVS) and/or Isopenicillin-N synthase (IPNS). Furthermore, from the measured ratios of extra-to intracellular concentrations, the thermodynamic feasibility of different secretion mechanisms of penicillin pathway metabolites was determined.

Keywords: *Penicillium chrysogenum*; penicillin biosynthesis pathway; stimulus response experiments; membrane transport.

4.1 Introduction

Although the discovery of penicillin took place in 1928, it still continues to dominate in the world of antibiotics with an annual production exceeding 60,000 tons. Nowadays most of the penicillin produced is converted into the intermediate 6-aminopenicillanic acid (6APA), which is used as starting material for the production of more effective semi synthetic penicillin's such as ampicillin and amoxicillin. As penicillin has a wide range of applications, to cope with its demand in a cost effective way, industries are striving to maximize productivities, yields and product titers [23,142]. Traditionally, high-producing strains have been developed through classical strain improvement by random mutagenesis and selection, which allowed the amplification of the penicillin biosynthesis pathway [164]. However, the currently available genetic engineering tools and known genome sequence [171], offers the possibility to use more rational approaches of metabolic engineering to increase the flux towards the desired products, and to genetically engineer the strain for the production of novel compounds [66]. Metabolic engineering deals with the analysis of metabolic fluxes and identifying the rate controlling step in the metabolic pathway [93]. The control of fluxes can either reside with the supply of precursors and/or cofactors from central carbon metabolism, with the enzyme levels in the pathway or with the transport of the metabolites across the cellular membrane. Metabolite transport across the cell membrane is an important factor, as insufficient transport capacity can severely limit the substrate and product fluxes. [44,62].

The penicillin biosynthetic pathway is well studied and characterized, both genetically and biochemically. However, complete understanding of the *in-vivo* pathway kinetics including the transport of metabolites across the cell membrane is still lacking. The complete penicillin biosynthesis pathway is encoded on a single gene cluster (*pcbAB-pcbC-penDE*) which consists of three enzymes, δ-[L-α-aminoadipyl]-L-cysteinyl-D-valine synthetase (ACVS), isopenicillinN synthase (IPNS) and acyltransferase (AT) [41]. AT has three activities, Isopenicillin-N Acyltransferase (IAT), Isopenicillin-N amidohydrolase (IAH) and Acyl-CoA: 6APA Acyltransferase (AAT) [4,5]. The activation of PAA to phenylacetyl-CoA (PA-CoA) takes place in the peroxisomes by phenylacetate–CoA ligase (PCL) [92] (see Chapter 1, Figure 1.2). Studies were performed to understand the kinetics of the enzymes of the penicillin biosynthetic pathway *in vitro* [5,27,92,161,189] and *in vivo* based on Michaelis-Menten mechanistic rate equations [125,135]. From various studies it was concluded that the control of the flux through the pathway was distributed over ACVS and IPNS and that IPNS

exerted the main control [45,124,125,159]. Other studies showed that, for high producing industrial strains, the flux through the pathway can be limited by the precursor supply from central carbon metabolism [79,120] or by the supply/regeneration of cofactors [89,176,191]. Some studies also suggested that the activity of IAT [182] or PCL can be limiting [126]. Transport of the penicillin pathway metabolites across the cell membrane so far received little attention and the transport mechanisms are still under debate [8,48,52,56,72]. However, recent *in vivo* studies on the transport of PAA and PenG showed that the supply of PAA and export of PenG may not be limiting the flux through the penicillin pathway [44].

In this study we developed a systematic procedure to identify possible bottlenecks in a product biosynthesis pathway by means of stimulus response experiments, and applied it to penicillin-G production in a high producing strain of *P. chrysogenum*. A key challenge is then to design a perturbation of the product pathway fluxes. To this end the strain was cultivated in a glucose limited chemostat in the absence of the penicillin-G side chain precursor PAA. Subsequently the culture was perturbed by a sudden supply of PAA and the short and long term responses of the intra- and extra- cellular concentrations of all compounds related to the penicillin biosynthesis pathway were measured. From the measured responses several candidate metabolic engineering targets for enhancement of the pathway flux were identified. Cultivation in the absence of PAA also allowed studying the metabolomics and fluxomics related to the production of 6APA, which is the precursor for the production of semi-synthetic ß-lactam antibiotics such as ampicillin and amoxicillin.

4.2 Materials and methods

4.2.1 Strain

A high-yielding strain, *P. chrysogenum* DS17690, was used for cultivation. This strain was kindly donated by DSM, Biotechnology center, Delft, The Netherlands. This strain has been extensively used for research on industrial penicillin production over the last decade [42,65,88,89,120,171]

4.2.2 Chemostat cultivations

Aerobic glucose-limited chemostat cultures of 4 L working volume were carried out in a 7 L turbine stirred bioreactor (Applikon, Schiedam, The Netherlands) at a dilution rate of 0.05 h^{-1}. The pH was controlled at 6.5 with 4M NaOH and the temperature at 25 ± 0.1 °C. The air flow

rate was set at 2 L/min (0.5 vvm), with 0.3 bar overpressure and the stirrer speed was set at 500 rpm. The dissolved oxygen tension was measured with a Mettler Toledo DOT sensor (Mettler-Toledo GmbH, Greinfensee, Switzerland) but not controlled, as it was known that under these fermentation conditions it does not drop below 80% of air saturation . Also the concentrations of O_2 and CO_2 (vol.%) in the offgas were monitored. Further details of the chemostat setup and operation have been described previously [37]. Four separate chemostat experiments were carried out, i.e. two PAA step experiments (chemostat 1 and chemostat 2) and two reference chemostat cultivations (reference 1 and reference 2), of which the feed medium contained PAA.

4.2.3 PAA step experiments

The strain *P. chrysogenum* DS17690 was first cultivated in an aerobic glucose-limited chemostat, without feeding the side chain precursor PAA (Figure 4.1). The part of the chemostat operation carried out without the addition of PAA is termed as Phase I. To perturb the steady state chemostat system a step change in the extracellular PAA concentration was given. This step change was accomplished by replacing the feed medium without PAA with a medium containing 5 mM PAA, while simultaneously injecting 25 mL of a sterile concentrated solution of PAA (800 mmol/L). This resulted in an instantaneous increase of the extracellular PAA concentration from 0 to 5 mM. The part after the step change in the PAA concentration is termed as Phase II (Figure 4.1). Phase I was carried out for a period of 10 residence times, after which the step change in the extracellular PAA was given. After the step change, phase II was continued until a steady state was reached.

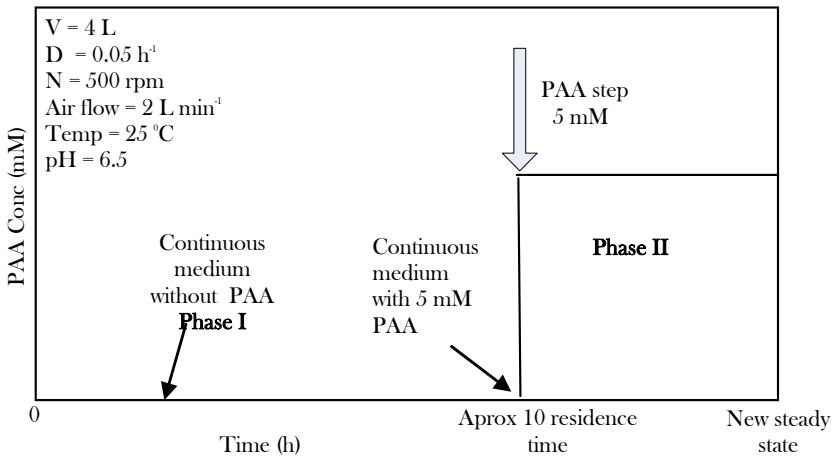

Figure 4.1: Schematic representation of the PAA step experiment.

4.2.4 Medium preparation

The composition of the chemostat medium was designed to support a steady state biomass concentration of 6 g/L dry weight and contained 0.5 Cmol/L of glucose (16.5 g/L glucose monohydrate), 5 g/L $(NH_4)_2SO_4$, 1 g/L KH_2PO_4, 0.5 g/L $MgSO_4 \cdot 7H_2O$, and 2 ml/L trace elements solution [43]. The same medium, without PAA, was used for the batch phase, preceding chemostat cultivation, as well as for phase I of the PAA step experiment. All medium components were dissolved in 50 L of demineralized water and the pH was set to 5.6 by adding KOH pellets. The medium was filter-sterilized (Supor DCF 0.2 μm filters, Pall Gelman Sciences, East Hills, NY) into a sterile medium vessel.

For phase II and for the reference chemostat cultivations the same medium was used, supplemented with 5 mmol/L of PAA. The required amount of PAA (250 mmol) was first dissolved in 4 L of demineralized water by continuous stirring while adding KOH pellets. After the PAA was completely dissolved, the pH of the solution was set to 5.6 by adding KOH pellets. This solution was autoclaved in a 50 L vessel for 40 min at 121ºC. The other medium components were dissolved in 46 L of demineralized water and the pH was set to 5.6. This solution was filter-sterilized (see above) and mixed with the PAA solution in the medium vessel. The pulse solutions for the PAA step experiments (20 mmol, pH: 6.5, volume: 25 mL) were also autoclaved for 40 min at 121ºC.

4.2.5 Rapid sampling and quenching for intracellular metabolite quantification

Cold filtration method

Chemostat 1**:** Approximately 10 g of sample was withdrawn within 2 s by means of a peristaltic pump into a cold filtration unit containing 50 mL 60% (v/v) methanol/water solution at -40 °C. This assured immediate quenching of all metabolic activity. After withdrawal of the cold liquid through vacuum filtration, the cells remaining on the filter were washed twice by pouring 50 mL of 60% (v/v) -40 °C methanol/water on the filter+cells and subsequent withdrawal. Further details have been described previously [43].

Chemostat 2: Rapid sampling and quenching was performed with a dedicated rapid sampling device [98]. Using this device approximately 1.2 g of sample was rapidly withdrawn from the fermentor and immediately quenched in 8 mL 40% (v/v) methanol/water solution, pre-cooled at -27.5 °C. This adaptation in the methanol concentration from 60% to 40% was done to

avoid leakage of the intracellular metabolites into the quenching solution [38]. With the lower concentration of methanol solution the temperature was also reduced from -40 °C to -27.5 °C to avoid freezing of the solution. The sample was then washed by filtration 3 times by 40 mL of 40% (v/v) -27.5 °C methanol/water solution by means of vacuum filtration.

Reference chemostats: Approximately 5 g of sample was withdrawn within 1 s by means of a peristaltic pump into a cold filtration unit containing 40 mL 40% (v/v) methanol/water solution at -27.5 °C. The sample was subsequently washed 2 times by 40 mL of 40% (v/v) methanol/water of -27.5 °C by means of vacuum filtration.

The difference in the sampling protocols was due to the improvement in the sampling technique over a period of time, by minimizing the requirement of quenching and washing solution. This was also necessary in order to increase the frequency of sampling to capture the dynamics after the perturbation of the chemostat. These different sampling protocols were validated, similar to that done by Douma et al. [43,44] to check the reproducibility of the concentrations of the penicillin pathway metabolites and the results did not show any difference in the metabolite concentrations (data not shown).

Extraction and sample processing

Intracellular metabolites were extracted from the quenched mycelium samples by ethanol boiling in the presence of a U-^{13}C labeled internal standard mix, to allow correction for possible partial degradation of metabolites during extraction and ion suppression effects and machine drift during quantification with IDMS. The sample was further processed to obtain a final volume of 600 µL of extract. The details of the extraction and sample processing procedure have been described previously [38]. The extracts were frozen in liquid nitrogen and stored at -80 °C until analysis.

4.2.6 Sampling and quenching for extracellular metabolite quantification

Approximately 1 mL of broth was rapidly withdrawn from a sample port in the bottom of the fermentor and was immediately quenched by rapid cooling to 0˚C over cold steel beads in a syringe [107]. The quenched sample was immediately filtered through a 0.45 µm pore sized filter to remove the mycelium. An aliquot of 80 µL of this filtrate was mixed with 20 µL of

U-^{13}C-labeled extract in a sample vial, to allow metabolite quantification with IDMS. The vials were immediately frozen in liquid nitrogen and stored at -80 °C until analysis.

4.2.7 Cell dry weight and Total organic carbon determination

The biomass dry weight concentration was measured by filtration of three times 5 ml of culture broth on pre-weighed glass fiber filters (type A/E, Pall Corporation, East Hills, NY; 47mm diameter, 1 μm pore size) and drying to constant weight (24 h at 70 °C) as described elsewhere [37]. Aliquots of the obtained filtrate (± 5 mL) and culture broth (± 5 mL) were stored at -20 ºC and analyzed with a TOC analyzer (TOC-5050A, Shimadzu) for measurement of total organic carbon (TOC) content.

4.2.8 Metabolite analysis

Intermediates and (by)products of the penicillin biosynthesis pathway were quantified with ion-pair reversed-phase liquid chromatography-isotope dilution electrospray ionization tandem mass spectrometry (IP–LC–ESI–ID–MS/MS) [151] using U-^{13}C-labeled cell extract as an internal standard mix [107,186]. For measurement of ACV and its symmetric disulfide bisACV, the analysis was first done without addition of a reducing agent. For quantification of the total amount of ACV, the analysis was carried out after the addition of the reducing agent, tris(2-carboxyethyl) phosphine hydrochloride (TCEP) [149]. This reducing agent effectively breaks all disulfide bonds between ACV and other thiol containing compounds to which it is bound.

Amino acid concentrations were quantified with GC-MS using a method adapted from de Jonge, et al. [37]. In brief, 100 μL of cell extract was lyophilized and derivatized using 75 μL acetonitrile and 75 μL of N-methyl-N-(tertbutyldimethylsilyl) trifluoroacetamide (MTBSTFA, Thermo Scientific). After this derivatization step, the samples were analyzed by GC-MS as described in de Jonge, et al. [37] . Also for amino acid quantification isotope dilution mass spectrometry (IDMS) was applied.

4.3 Results

To generate data for elucidating the *in vivo* kinetic properties of the penicillin biosynthesis pathway of *P. chrysogenum*, duplicate stimulus response experiments were carried out with the high producing industrial strain DS17690, whereby specifically the penicillin pathway was perturbed. This was done by initially cultivating the strain in a glucose-limited chemostat

at a dilution rate of 0.05 h^{-1} in the absence of the side chain precursor phenylacetic acid (PAA) and thus in the absence of penicillin-G (PenG) production. This first part of the experiment is designated as phase I. After approximately 200 hours of cultivation (10 residence times) in the absence of PAA, the feed of the chemostat was replaced by an identical feed containing 5 mM of PAA, while at the same time a concentrated PAA solution was injected in the chemostat vessel to instantaneously reach an extracellular PAA concentration of 5 mM. The chemostat operation after the PAA step is termed as phase II. As a control, the measurements obtained from two step experiments were compared with measurements from two reference chemostats, which were conventional carbon-limited chemostat cultivations carried out under the same conditions but in the presence of PAA.

4.3.1 General observations for phase I and phase II

The measured cell dry weight, and O_2 and CO_2 levels in the offgas of the chemostat as function of time are shown in Appendix I-Figure 4.A1. The average cell dry weight for phase I was 6.25 ± 0.28 gDW/L. However, within almost 200 h of chemostat cultivation, corresponding to 10 volume changes, no stable steady state was reached with respect to mycelium dry weight, and O_2 and CO_2 levels in the offgas. Shortly after the step increase in the PAA concentration from 0 to 5 mM, the cell dry weight reached a stable value of 5.43 ± 0.08 gDW/L, while also the O_2 and CO_2 levels in the offgas became stable. With the sudden availability of PAA, the production and secretion of PenG started immediately (see results section phase 2). No significant differences in cell morphology were observed under the microscope after the addition of PAA. For all chemostat experiments the carbon and degree of reduction balances closed between 94% and 106%.

4.3.2 Phase I: Chemostat cultivation in the absence of PAA

Metabolite concentrations

Figure 4.2 depicts a comparison between the measured intra- and extracellular concentrations of penicillin pathway metabolites in phase I (-PAA) and the reference chemostats (+PAA). For both conditions the intra and extracellular levels of the measured metabolites did not reach stable levels but showed dynamic patterns. The intracellular ACV concentration, analyzed after addition of the reducing agent TECP, increased during the first 90 h of phase I, in a similar fashion as for the reference chemostats. Thereafter it decreased steeply to a significantly lower level than for the reference chemostats. Similar to ACV, the intracellular

level of IPN initially steeply increased in the absence of PAA and reached a maximum value after about 50 hours of cultivation, followed by a gradual decline. Also in the reference chemostat the intracellular IPN level increased, although much less pronounced, and declined after 100 hours of cultivation. The intracellular level of 6APA fluctuated around 1 µmol/g DW in the absence of PAA while in the reference chemostats the level was below the detection limit (< 0.0010 µmol/g DW) [151]. The intracellular bisACV analyzed without addition of the reducing agent, TECP, was less than 0.08 µmol/g DW.

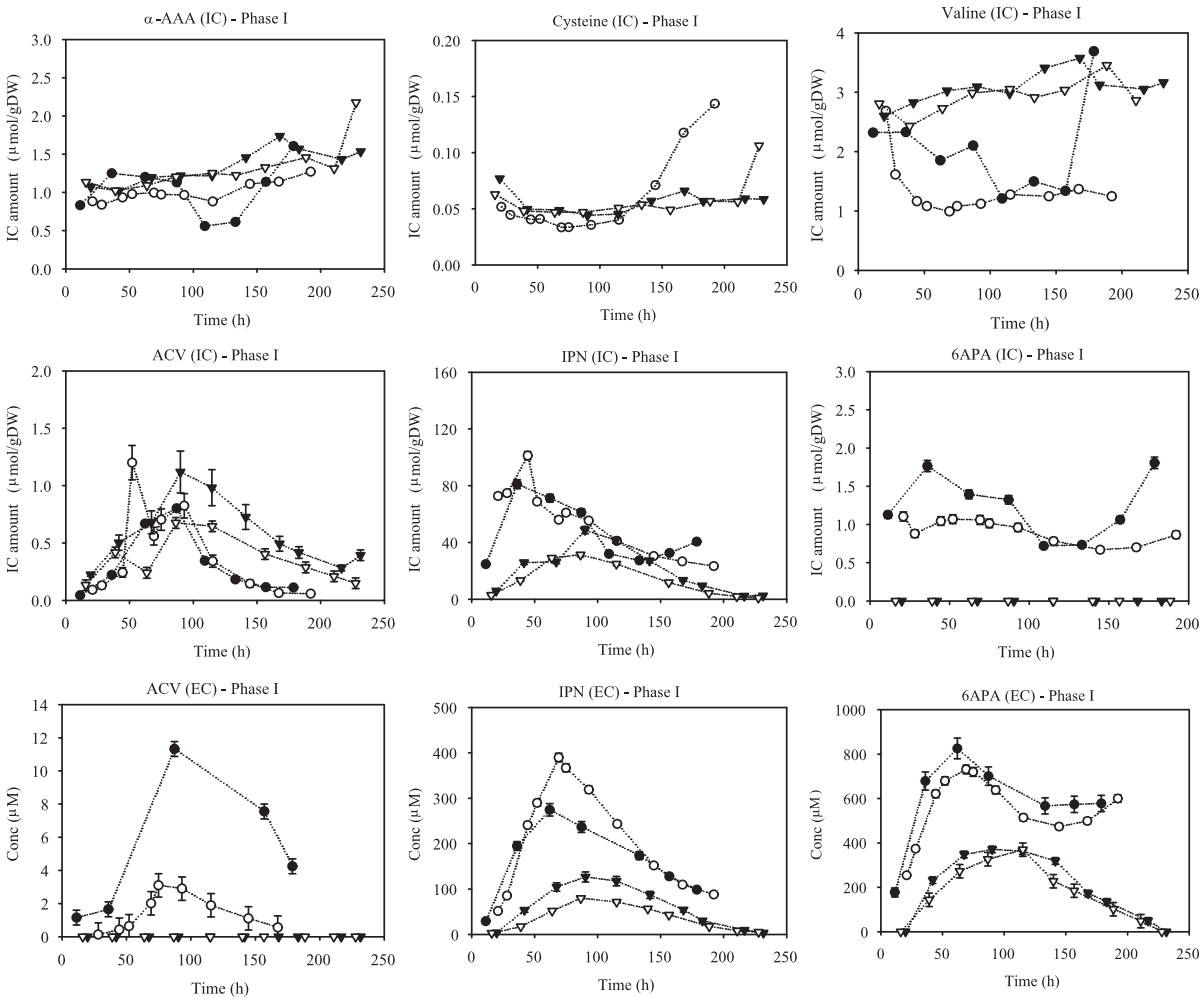

Figure 4.2: Measured intracellular and extracellular metabolite levels, plotted as a function of culture age for phase I (feed without PAA) in Chemostat 1(solid circles) and Chemostat 2 (open circles) and for the two reference chemostats (feed with PAA) (solid and open inverted triangles). Each data point represents a single sample and the error bars display the standard deviation for replicate analyses. Intracellular ACV is total ACV reduced by addition of TCEP.

In the absence of PAA supply, as PenG cannot be produced, IPN and 6APA were the main end products and both were excreted into the medium, while the concentration of ACV was negligible (< 10 µM) in the extracellular space. During the first 70 hours of chemostat cultivation, the extracellular concentrations of IPN and 6APA increased to values which were

almost a factor 2 higher as compared to the reference chemostats. The extracellular bisACV analyzed without addition of the reducing agent, TECP, was less than 1 μM.

The dynamic pattern of the penicillin pathway metabolites in phase I was different from the patterns of the three precursor amino acids L-α-AAA, L-cysteine and L-valine. The intracellular level of L-α-AAA increased slightly, very similar to what was observed for the reference chemostats. The L-cysteine level first remained stable, at the same level as observed for the reference chemostats, and increased towards the end of phase I. The intracellular level of L-valine decreased during phase I, but increased slowly in the reference chemostats. The patterns of none of the three precursor amino acids correlated with that of the tripeptide ACV, indicating that the observed pattern of the first metabolite in the penicillin pathway is not a result of changes in precursor availability.

Fluxes during phase I

A comparison of the dynamics of the secretion rates and intracellular fluxes during phase I with the reference chemostats is shown in Figure 4.3 and in Appendix VI-Figure 4.A5. The course of the biomass specific total ß-lactam production rate vs. time for phase I and for the reference chemostats was calculated from the measured intra- and extracellular levels of IPN, 6APA, 8HPA and PenG using the corresponding dynamic mass balance equations. The results show that the maximum ß-lactam secretion rate in the absence of PAA was approximately 50% of that of the reference chemostats (Figure 4.3A). In the absence of PAA the ß-lactam secretion rate reached a maximum after approximately 50 h of chemostat cultivation after which it decreased to a stable value of 0.2 mmol/Cmol.h. This initial increase and subsequent decrease in the production rate is also observed under PenG producing conditions [42] .

A comparison of the secretion rates of the end products, which is mainly 6APA in the absence of PAA (phase I), and PenG in the presence of PAA (reference chemostats) is shown in Figure 4.3B. Although the 6APA secretion rate in the absence of PAA is significantly smaller than the secretion rate of PenG in the presence of PAA (see Figure 4.3B), it is a factor 2 higher than in the reference chemostats (Appendix VI-Figure 4.A5). In accordance with the lower β-lactam secretion rate, the flux through ACVS in phase I (Figure 4.3C) was significantly lower as compared to the ACVS flux calculated for the reference chemostats. The ACVS flux in phase I reached a maximum of 0.38 mmol/Cmol.h at approx. 30 h of

cultivation time while for the reference chemostats the maximum flux through ACVS was 0.57 mmol/Cmol.h at approx 75 h.

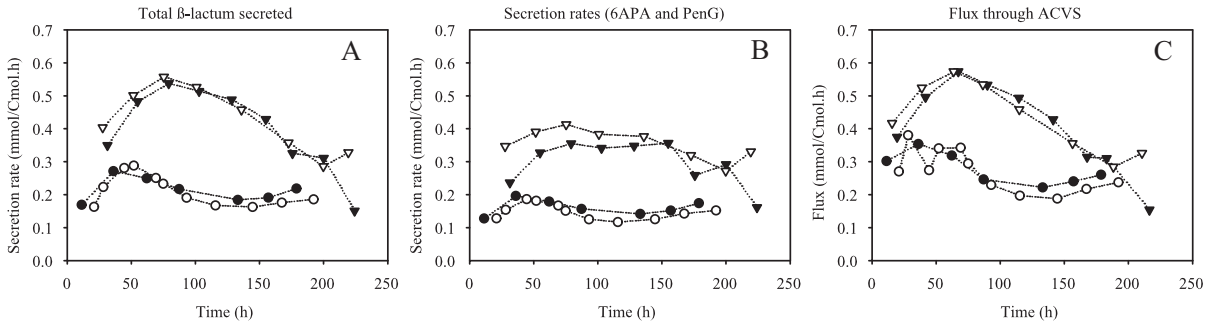

Figure 4.3: [A] Comparison of total ß-lactum secretion rate (IPN, 6APA and 8HPA) in phase I (- PAA) with ß-lactum secretion rates (IPN, 6APA, 8HPA and PenG) in the reference chemostats (+PAA). [B] Comparison of secretion rates of end products, 6APA in phase I (-PAA) and PenG in the reference chemostats (+ PAA). [C] Comparison of fluxes through ACVS in phase I (-PAA) and the reference chemostats (+ PAA). Results from Chemostat 1 and Chemostat 2 are represented by solid and open circles respectively and the reference chemostats are represented by solid and open inverted triangles.

4.3.3 Phase II: PAA step experiment

Short term metabolite responses

After approx. 200 h of chemostat cultivation in the absence of PAA, the feed of the chemostat was replaced by an identical feed containing 5 mM of PAA while at the same time a concentrated PAA solution was injected in the chemostat vessel to reach instantaneously an extracellular PAA concentration of 5 mM. To determine the short term dynamics of the penicillin pathway to the sudden availability of PAA, the first samples were taken within seconds and later on within minutes during the first hour after the step change. From the measured short term responses of the intra- and extracellular metabolite levels, i.e. within a time frame during which no changes in enzyme levels occur, the *in vivo* kinetic properties of the pathway enzymes/transporters can be obtained.

The sudden increase of extracellular PAA from 0 to 5 mM, resulted in an immediate increase (within 5 sec) in the intracellular level of PAA (Figure 4.4). Furthermore, there was immediate (< 5 sec) activation of PAA to PA-CoA after the PAA step, which is known to occur in the peroxisomes, through phenylacetyl CoA ligase (PCL). This confirms that PAA quickly reaches the cytoplasm and subsequently the peroxisomes. With the rapid availability of PA-CoA, the penicillin production was observed to start immediately (< 10 sec), with simultaneous decrease in the intracellular pools of IPN and 6APA. Furthermore, after the PAA step, it was observed that there was an increased demand for cysteine and valine, as their

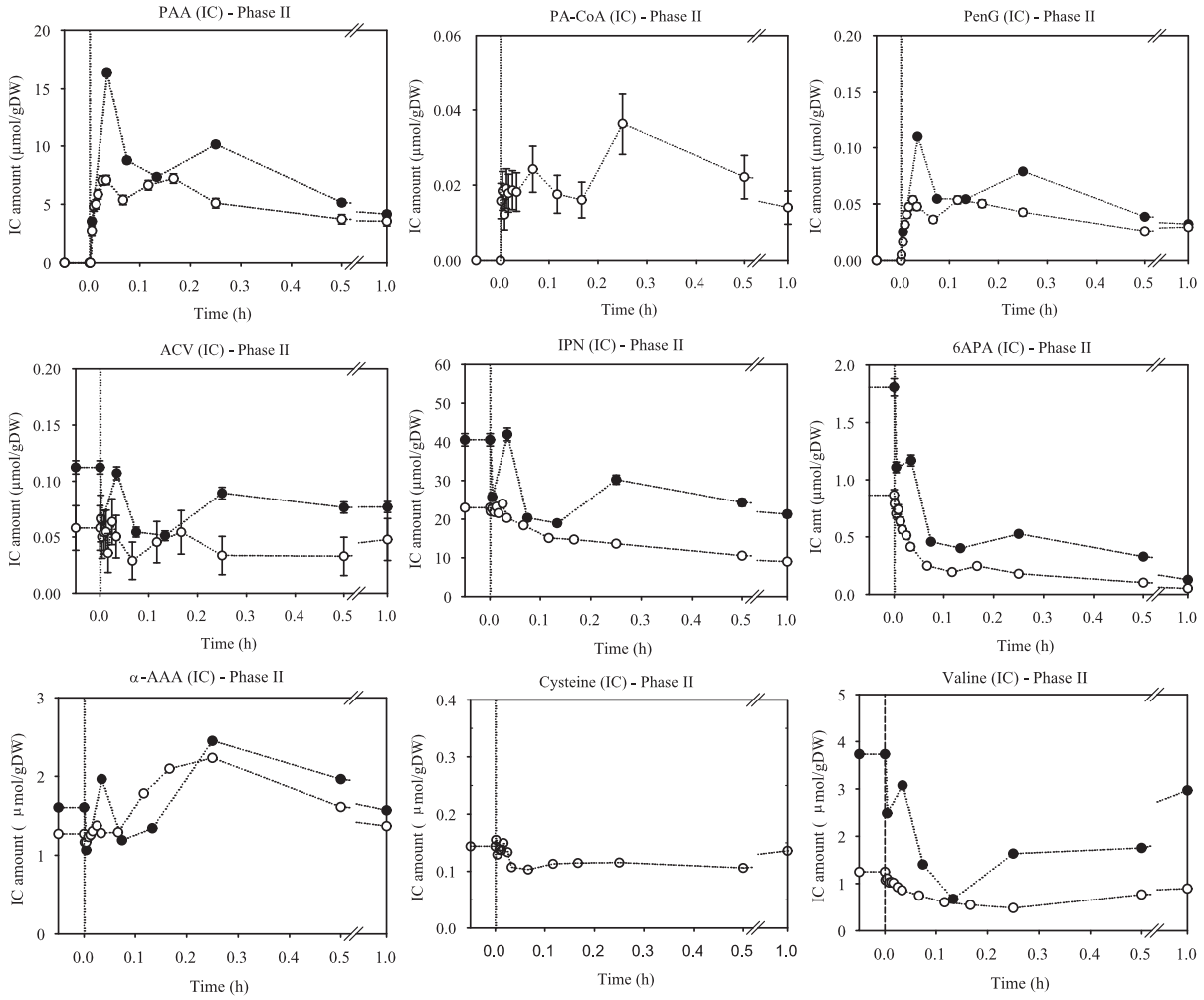

Figure 4.4: Intracellular response of penicillin pathway metabolites during the first 1 hour after the step change in PAA concentration in the extracellular space. Results from Chemostat 1 and Chemostat 2 are represented by solid and open circles respectively. Each data point represents a single sample and the error bars display the standard deviations for replicate analyses. Intracellular ACV is total ACV reduced by addition of TCEP.

levels decreased during the first few minutes after the step while α-AAA was accumulating, probably because it was released from IPN in exchange of PA-CoA to produce PenG. No significant changes in the extracellular levels of IPN, 6APA, 8HPA and OPC were observed compared to their steady state values before the PAA step (Appendix VI-Figure 4.A7), because of the large turnover time of the pool of extracellular metabolites, which is 20 h for a dilution rate of 0.05 h^{-1}.

Long term metabolite response in phase II

After the PAA step change, sampling for metabolite analysis was continued for a period of 8 residence times (165 h) until a steady state was reached (Figure 4.5). The extracellular PenG level reached a steady state value of 800 µM, however when compared with the levels observed for the reference chemostats, this value is a factor 2 lower. The intracellular IPN

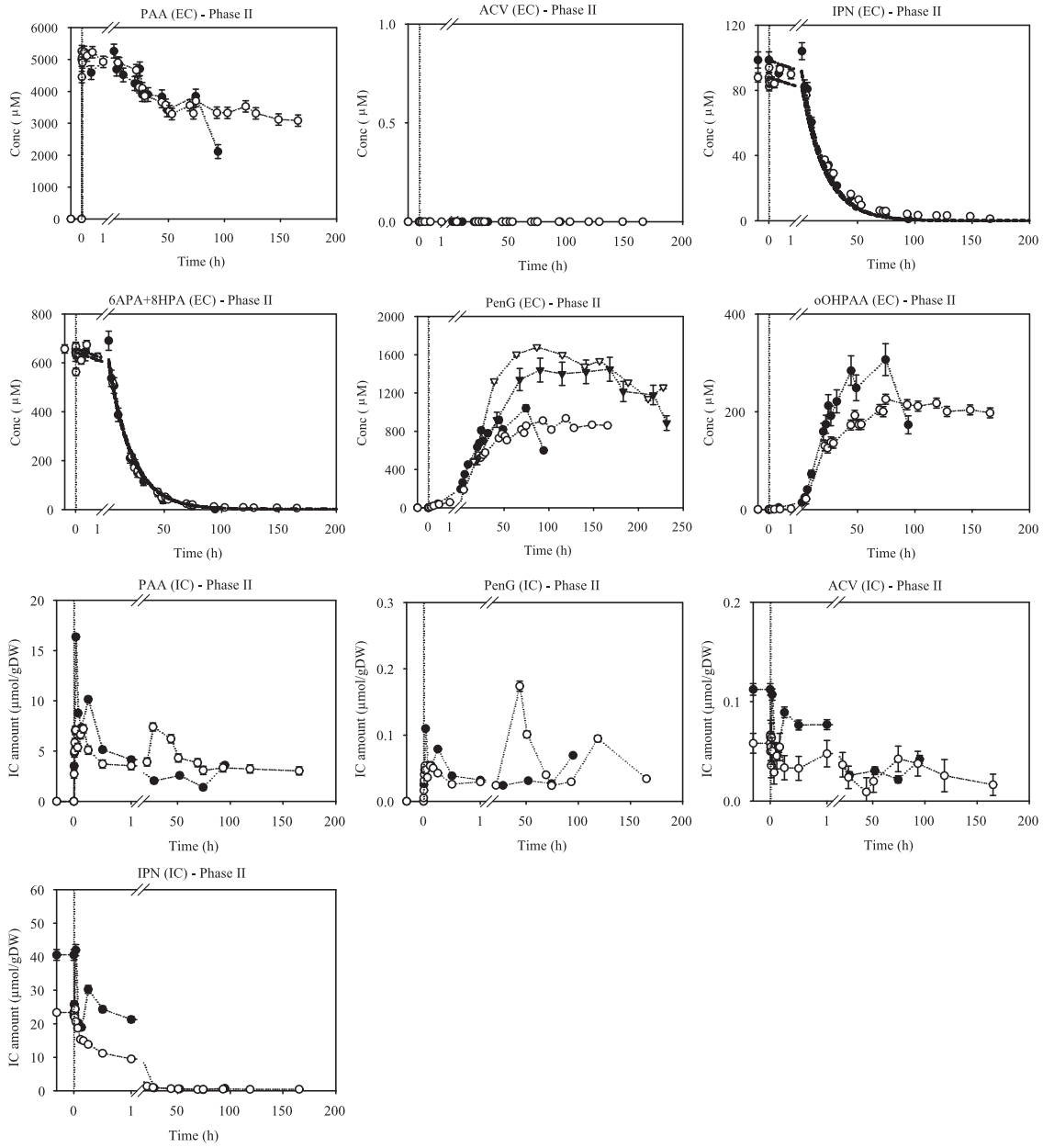

Figure 4.5: Measured intracellular and extracellular metabolites levels, plotted as a function of culture age for phase II (feed with PAA) in Chemostat 1(solid circles) and Chemostat 2 (open circles) and the two reference chemostats (solid and open inverted triangles). Each data point represents a single sample and the error bars display the standard deviation for replicate analysis. Intracellular ACV is total ACV reduced by addition of TCEP.

level was observed to drop to a low value of 0.44 µmol/gDW, while the extracellular concentration followed the chemostat washout curve. This indicates that after the PAA step the secretion rate of IPN decreased to a negligible value, probably due to the steep decrease in intracellular IPN. Furthermore, the intracellular levels of 6APA and 8HPA decreased to values below their detection limits (for 6APA: 0.0010 µmol/gDW and HPA: 0.0175 µmol/gDW) [151] after the first hour (Appendix VI-Figure 4.A6) The sum of extracellular 6APA and 8HPA also followed the washout curve, indicating that also the secretion of 6APA

was negligible and most probably the formation of 8HPA was from extracellular 6APA. Therefore, assuming that there was no 8HPA secretion in phase II, the rate constant for the production of 8HPA from 6APA in this phase was calculated as 0.0049 ± 0.0004 h^{-1} at a constant concentration of CO_2 in the gas phase (see Appendix V). It was also observed that there was a significant formation of ortho-hydroxyphenylacetic acid (oOHPAA) in the presence of PAA. It is known that PAA is converted to oOHPAA by phenylacetate hydroxylase (PAH), although its activity is far reduced compared to the earlier strains in the lineage. After the initial dynamic changes in the intracellular levels of the three precursor amino acids as response to the PAA step change, they reached a steady state level (see Appendix VI- Figure 4.A6).

Short term fluxome in phase II

Directly after the PAA step, the initial uptake rate of PAA was calculated to be ≈19 mmol/Cmol.h. With such a high influx of PAA (about 30 times higher than the maximum rate of PenG production of this strain) and immediate formation of PA-CoA, the production of PenG started immediately and reached a maximum value of 0.55 mmol/Cmol.h (see Figure 4.6). This value is significantly higher than the pathway flux (0.23 mmol/Cmol.h) in absence of PAA. The reason for this initial high flux was the presence of intracellular pools of IPN and 6APA accumulated during the cultivation in the absence of PAA. The sudden availability of PAA resulted in fast conversion of these accumulated intermediates to PenG via the IAT and AAT activities of AT.

After the depletion of the intracellular IPN and 6APA pools, the PenG production rate decreased to become equal to the value of the ACVS flux at the end of phase I. After the PAA step, an immediate 10% increase in the O_2 consumption and CO_2 production rates was observed as shown in Figure 4.6, which reached maximum values after approx. 30 min. The rapidity of the response can best be seen from the dissolved oxygen signal (DO), as the DO probe responded quicker (time delay of several seconds) than the offgas analysis system (time delay of several minutes).

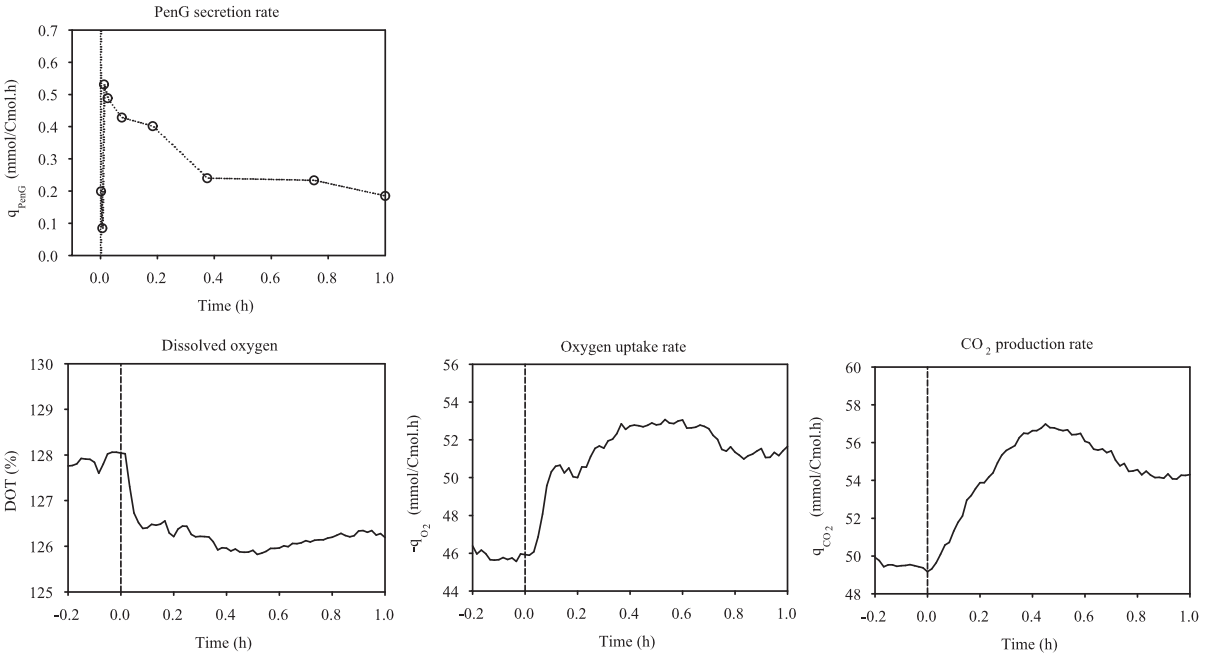

Figure 4.6: Upper panel: Penicillin secretion rate after the step change in PAA concentration for Chemostat 2. The open circles represent Chemostat 2, cultivated in presence of PAA. Lower panel: DOT, Oxygen consumption rate and CO_2 production rate response after giving a step change in PAA concentration for Chemostat 2.

Long term fluxome in phase II

After the initial dynamic changes in the fluxes induced by the PAA step, they reached pseudo steady state levels. Average biomass specific conversion rates were calculated for a time frame of 68h to 148h of phase II and the reconciled rates [178] are shown in Appendix II. As response to the PAA step, the secretion of by-products, which include IPN, 6APA, 8HPA and secreted peptides, decreased significantly as the fluxes were directed towards the production of PenG. The rate of PenG production remained at a value of about 0.23 mmol/Cmol.h, which is significantly lower than PenG production rate in case of reference chemostats which was 0.35 mmol/Cmol.h (Figure 4.7).

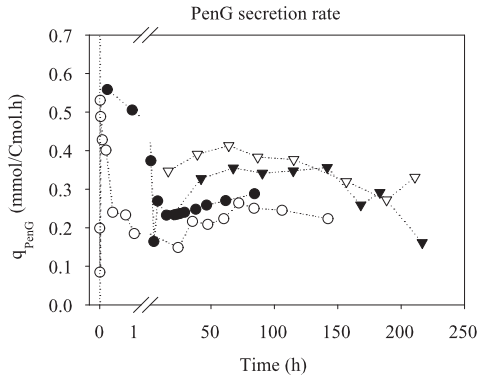

Figure 4.7: Penicillin secretion rate in steady state of phase II. The solid and open circles represent Chemostat 1 and Chemostat 2 respectively, cultivated in presence of PAA. The reference chemostats represented by solid and open inverted triangles are cultivated in presence of PAA.

The steady state rates of oxygen consumption, carbon dioxide production and glucose consumption in phase II were significantly higher than in phase I (see Table 4.A1). This indicates that the presence of PAA is responsible for a large amount of energy consumption due to PAA cycling over the cell membrane (passive import coupled to active export), as has been reported previously for this *P. chrysogenum* strain [44].

4.4 Discussion

The metabolomics data obtained from the glucose limited chemostats, in the absence and presence of the side chain precursor PAA, was used to obtain quantitative information on the *in vivo* kinetic properties of the pathway enzymes as well as the secretion mechanisms of intermediates and (by) products.

4.4.1 *In vivo* kinetics in absence of PAA (phase I)

ACVS, which condense the three precursor amino acids α-aminoadipic acid, cysteine and valine to the tripeptide ACV, is the node separating central carbon metabolism from the penicillin biosynthesis pathway. We observed a dynamic metabolite pattern associated only with the penicillin pathway metabolites, which specifically started from ACV and was subsequently extended to the other pathway metabolites. Comparatively the precursor amino acids were much more stable indicating that the central carbon metabolism remained in the pseudo steady state. This agrees with previous observations [120,176] that central carbon metabolism and the supply of the precursor amino acids is not limiting the penicillin pathway flux.

During the first 90 h of chemostat cultivation, an initial increase in the intracellular levels of the penicillin pathway metabolites was observed. This increase is generally associated with the induction of the penicillin pathway enzymes after the release of glucose repression which occurs in the batch phase [45,51,103]. For IPN and 6APA there was significant intracellular accumulation as compared to the reference chemostats, whereas the increase in ACV was typical and similar to that observed for the reference chemostats. The intracellular accumulation of ACV, IPN and 6APA, in absence of PAA, indicated that the capacities of the enzymes consuming these metabolites were insufficient and/or the capacities of their transporters were insufficient. Also, during the first 90 h of cultivation, in the absence of PAA, the extracellular levels of IPN and 6APA were two fold higher than for the reference

chemostats. Although, in general, the intra- and extra-cellular levels of ACV, IPN and for chemostat 2 6APA were higher as compared to the levels in the reference chemostats, the fluxes through the pathway during these initial stages of phase I were two fold lower than for the reference chemostats. This was because in the absence of PAA, 6APA becomes the final product instead of PenG. The observed accumulation of intracellular 6APA indicates that the secretion of 6APA is not as efficient as that of PenG resulting in less driving force to pull the flux through the pathway and possibly the higher intracellular concentration of 6APA inhibits the upstream pathway enzymes.

After the initial increase until ~90 h in phase I, the intracellular ACV level decreased. A very similar pattern was observed for both reference chemostats, although the decrease of the intracellular ACV level was more pronounced in the absence of PAA. Also the flux through the pathway (ACVS flux) decreased until it reached a value of approx. 0.23 mmol/Cmol.h. The intracellular ACV level depends on the supply of the precursor aminoacids, and the capacities of ACVS and IPNS. However, the observed time patterns of the intracellular levels of the precursor amino acids do not indicate a decrease in their supply, as the levels did not decrease after 90 h of cultivation. This would imply that either the capacity of ACVS has decreased (lower enzyme level) and/or the capacity of IPNS has increased. During this same time frame, however, the intracellular IPN and 6APA levels decreased, as well as the fluxes through IPNS and IAH. This indicates that IPNS capacity did not increase. Thus implies that the decrease in flux through ACVS and subsequently through the penicillin pathway must have been caused by a decrease of the capacity of ACVS and/or IPNS. It is known that under penicillin producing conditions the penicillin productivity degenerates over time, which is a detrimental factor for the continuous production of ß-lactam antibiotics. Douma et al, 2011 have studied this phenomenon in ethanol limited chemostat cultures and suggested that culture heterogeneity (the presence of low or non producing mutants in the stock cultures) could be responsible for the observed degeneration. Our results show that degeneration apparently also occurs in the absence of PAA. Remarkably, in the absence of PAA the flux through the pathway already started to decrease after 30 h of chemostat cultivation, while this occurred after 75 h of cultivation for both reference chemostats. This indicates that the degeneration is even enhanced in the absence of PAA, possibly because of high levels of pathway intermediates.

From the obtained results it can be inferred that the flux control solely resides in the penicillin biosynthesis pathway and is apparently not limited by the supply of the precursor amino acids by central metabolism. The initial accumulation of ACV and IPN indicate that the activity of IAH and/or secretion of 6APA is controlling the flux. However as fermentation progresses, due to degeneration of the pathway enzymes the fluxes are controlled by ACVS and/or IPNS. A kinetic model will help to distinguish between ACVS and IPNS as the flux controlling enzyme.

4.4.2 *In vivo* kinetics in presence of PAA

Short term metabolic response:

After the PAA step, which resulted in a sudden increase from 0 to 5 mM, the PAA was rapidly taken up by the cells with an initial flux of ~19 mmol/Cmol.h. In the studies of Douma et al. [44], the maximum uptake rate of PAA was nearly double (~50 mmol/Cmol.h) at double the extracellular PAA concentration (10 mM). This confirms the hypothesis that PAA passively diffuses through the cell membrane [44,72]. The observed rapid uptake of PAA and immediate activation of PAA to PA-CoA by PCL in the peroxisomes, demonstrates that PCL was already expressed during phase I in the absence of PAA and that PAA was rapidly transported from the cytosol into the peroxisomes. It has been reported that the peroxisomal membrane contain porins, which allow molecules with masses of approx. 300 Da to freely permeate while heavily restricting permeation of larger compounds, e.g. cofactors (NAD/H, NADP/H, CoA and its acylated derivatives) [9,60,163]. Because PAA is a relatively small molecule with a molecular mass of 136 Da, it is likely that it can pass freely though the peroxisomal porins.

With the rapid availability of PA-CoA the production of PenG started immediately, thereby halting the production of 6APA. The rate of penicillin production initially reached a value of 0.55 mmol/Cmol.h, which is similar to the maximum production rate reported by van Gulik et al (2000). The rapid onset of PenG production after the PAA step implies that all pathway enzymes ACVS, IPNS, IAT and PCL and transport proteins were fully functional during phase I in the absence of PAA. This is in agreement with transcript studies carried out by Harris et al. [65], which showed that the genes coding for the penicillin pathway enzymes are also expressed in the absence of PAA. The immediate secretion of PenG suggests that it is transported from peroxisomes to cytosol quickly. This is possible either by a high capacity

and high affinity peroxisomal transporter or free passage of PenG (molecular mass 334 Da) through the porins of the peroxisomes.

The high initial penicillin production rate during the first 20 min after the PAA step (being twice the pathway flux before the step), was accompanied by a rapid decrease in the intracellular levels of IPN and 6APA. This indicated that this high initial rate was supported by the conversion of intracellular pools of IPN and 6APA, which had accumulated during the absence of PAA.

In vitro experiments have shown that acyltransferase (AT) has two different activities for the production of PenG, namely Isopenicillin-N Acyltransferase (IAT) using IPN and PA-CoA, and Acyl-CoA: 6APA Acyltransferase (AAT), using 6APA and PA-CoA as substrates [5], see Chapter 1, Figure 1.2. To our best knowledge this is the first time that the simultaneous *in vivo* activities of IAT and AAT have been demonstrated. Thus in the abundant supply of the substrates IPN and 6APA, the possible bottleneck for PenG production can be narrowed down to the IAT and AAT capacities of AT and/or the transport capacity for secretion of PenG. Douma et al. [44] estimated a PenG transporter capacity of 0.83 ± 0.2 mmol/Cmol.h for this strain, which is only slightly higher than the secretion rate of 0.55 mmol/Cmol.h. However, as we did not observe any accumulation of intracellular PenG, it seems that the PenG secretion rate was not limiting. During the first 10 min after the PAA step the intracellular level of PA-CoA remained constant at a value of 7.1±1.2 μM, which is near the K_m value of PA-CoA for IAT and AAT of 6 μM [4]. Subsequently the PA-CoA level increased with less demand for PenG production. This suggests that the activity of IAT/AAT was limiting rather than the secretion of PenG and availability of PA-CoA. Furthermore, *in vitro* studies have shown that the ratio of AAT to IAT activity is more than 6 [5], which points out that the control of PenG production in the presence of PA-CoA and during the abundant availability of IPN and 6APA was residing with IAT.

Long term metabolic response

After the initial dynamic changes in metabolite levels and fluxes immediately after the PAA step, the intracellular levels of the precursor amino acids and of the pathway intermediates ACV, IPN or 6APA reached a pseudo steady state. The amino acid precursors reached values which were similar as during phase I. The ACV level decreased with a factor 2 compared with the end of phase I, and was 10 times lower than observed for the reference chemostats. The

IPN level decreased almost 50 fold, while 6APA decreased to a value below the detection limit. This decrease of the levels of the intermediates indicates that the combined capacities of IAT, AAT, and PenG secretion are higher in phase II than the combined capacities of IAH and 6APA secretion in phase I. The possible reason for the low capacity of IAH in phase I can be feedback inhibition by a high intracellular 6APA concentration and much higher K_m compared to IAT and AAT [5]

The steady state fluxes through the pathway reached after 165h in phase II were comparable with the fluxes through the pathway at the end of phase I. This suggests that during the entire phase II the pathway enzyme levels, specifically ACVS, IPNS and AT remained unchanged. This observation is in contrast with the results of degeneration studies carried out by Douma et al. [42], who reported that the penicillin production rate continuously decreased during prolonged chemostat cultivation. These degeneration studies were carried out for 700 h (21 residence times at dilution rate of 0.03 h^{-1}) the fluxes never reached steady state.
After an initial dynamic phase, also, the intracellular levels of the amino acid precursors reached stable values, which were similar as during phase I. Thus, in phase II with constant supply of precursor amino acids and unchanged fluxes similar to that the end of phase I, suggest that the pathway enzyme levels probably did not decrease in phase II.

With the depletion of the intracellular pools of IPN and 6APA, the PenG production decreased to a value comparable with the flux through the pathway at the end of phase I (0.23 mmol/Cmol.h). This depletion indicates that the control of fluxes through the penicillin biosynthetic pathway was shifted from IAT (in abundance of IPN and 6APA) to ACVS and/or IPNS. This observation is in agreement with previous studies where also ACVS and/or IPNS were identified as the rate limiting enzymes for the flux through the penicillin pathway [45,124].

In the presence of PAA there was formation of oOHPAA by phenylacetate hydroxylase (PAH). Although it has been reported that the industrial strain *P. chrysogenum* DS17690 is not capable of catabolising PAA due to a point mutation in the *pahA* gene encoding phenyl acetate hydroxylase [171], the activity of PAH is not completely absent. The transcriptome studies carried out by Harris et al. [65] also indicated that transcriptional regulation of *pahA* has been retained and an increase in transcript level was seen in the presence of PAA. Furthermore, in addition to the *pahA* gene there is possibly a second gene (Pc16g01770),

identical to *Aspergillus nidulans phacB,* responsible for oOHPAA production [65]. Thus reduction of *pahA* or homologues of *phacB* genes maybe considered as possible gene targets to avoid formation of oOHPAA.

4.4.3 Secretion of pathway metabolites

From accurate measurement of intracellular and extracellular metabolite concentrations, the possible mechanisms for their transport across the plasma membrane can be derived. This is relevant, because to achieve maximum penicillin production it is important that the intermediates are not secreted but directed towards the production of penicillin. Under PenG non-producing conditions (Phase I of the step experiment) IPN and 6APA are secreted at high rates while ACV secretion is negligible. Appendix VII–Figure 4.A8 gives the ratio of extra to intracellular concentrations (EC/IC) for the different penicillin pathway intermediates and (by)products. Intracellular concentrations were calculated from the measured intracellular amounts per g DW by assuming a specific cell volume of 2.5 mL/gDW [130].

IPN secretion mechanism

As can be seen from Appendix VII, the EC/IC ratio for IPN was found to be much smaller than one, indicating that the observed IPN secretion was not against the concentration gradient and thus does not require an energy consuming active transport mechanism. However, as IPN is an anion (with charge -1), it cannot diffuse across the cell membrane as such, so its transport over the cell membrane must occur via a specific transport protein. The possible mechanisms for IPN transport are in this case: H^+ symport (K_{eq}=0.2), uniport (K_{eq}=73), and H^+ antiport (K_{eq}=10^4). Furthermore, it is known that uptake of IPN from the medium does not take place [56] and the uptake is also not observed in the current experiment. Additionally, Ullán et al. [166] have identified the CefT protein which is responsible for IPN secretion and belongs to Family 3 of the Major Facilitator Superfamily (MFS) of membrane proteins as a Drug:H^+ antiporter [166]. Thus, comparing the K_{eq} of the three mechanisms with the measured EC/IC ratio (0.015) and observed absence of uptake, a probable transport mechanism for IPN is therefore irreversible secretion by proton antiport with an equilibrium constant of 10^4 (see Appendix IV).

6APA secretion mechanism

The mechanism of 6APA secretion has never been thoroughly investigated. From the literature it is known that 6APA is also efficiently taken up by the cells [56], indicating that an exporter might be reversible. In solution 6APA attains a pH dependent equilibrium between the zwitterion ($APA^{\pm}$), the negatively charged (APA^{-}) and the positively charged (APA^{+}) forms. Almost 99.5% of 6APA carries a negative charge at an intracellular pH of 7.2, while 0.5% of 6APA is a zwitterion. Also for the extracellular pH of 6.5, the anion form is the most abundant one (97.55%) and the zwitterion form of 6APA is 2.45% (see Appendix III). From the observed EC/IC ratio of 2 it can be inferred that proton symport of APA^{-} (K_{eq} of 0.2) or uniport of $APA^{\pm}$ (K_{eq} of 0.2) is not plausible.

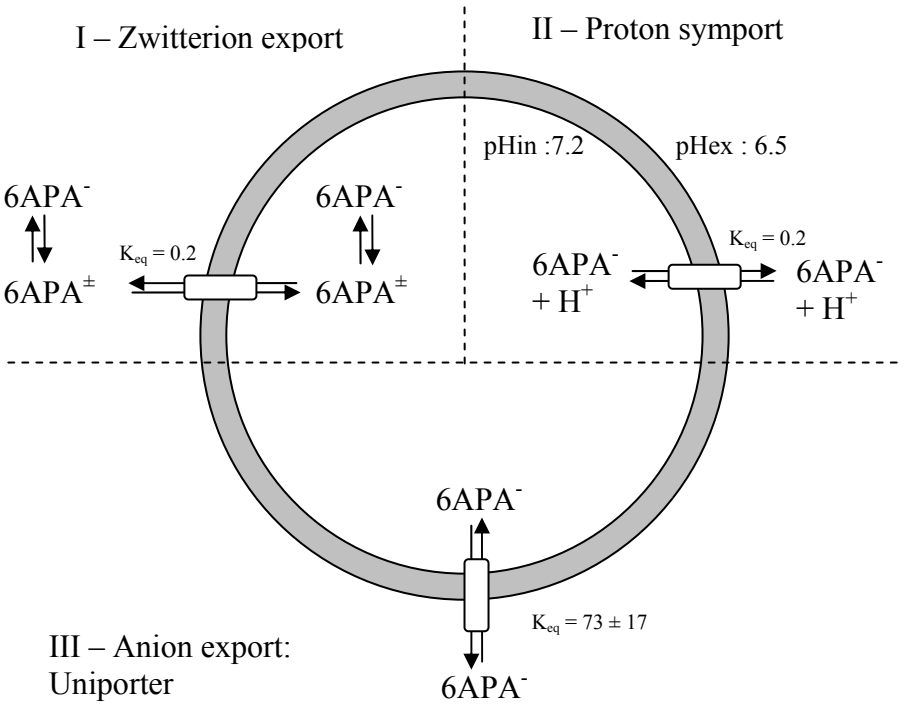

Figure 4.8: Possible mechanisms of 6APA transport.

The negatively charged form of 6APA can be secreted through a mechanism driven by the membrane potential difference. Douma et al. [43,44] calculated that for such a mechanism the EC/IC ratio for a negatively charged metabolite would by around 73±17 at thermodynamic equilibrium. The most probable mechanism is therefore secretion of the negatively charged form of 6APA with the membrane potential difference as driving force. However, the EC/IC ratio of 2 for 6APA is far away from thermodynamic equilibrium of 73, showing that the transport capacity is not extremely high.

8HPA secretion mechanism

8HPA, having a -2 charge, is produced by spontaneous carboxylation of 6APA and was found both in the intra- and extracellular spaces. In phase II, extracellular 8HPA is probably formed only from extracellular 6APA, as the sum of 6APA and 8HPA matches the washout curve (Figure 4.5). But this is not applicable to phase I, as the formation of extracellular 8HPA from extracellular 6APA with a rate constant of 0.0049 ± 0.004 h^{-1} does not match the experimental values. Therefore, there is probably transport of 8HPA across the plasma membrane. In phase I, the EC/IC ratio of 8HPA was found to hover around a value of 5, indicating that if secretion would occur, it would be against the concentration gradient. Alternatively, if there would be uptake of 8HPA, it would be down the concentration gradient. Since, 8HPA carries a -2 charge it is unlikely that it is taken up by the cell by a uniport mechanism, because it would occur against the negative membrane potential. Also an uptake with 2 protons, by a two proton symport mechanism is unlikely, as that would lead to an EC/IC ratio of 0.04. Thus the most probable transport mechanism for 8HPA is secretion against the concentration gradient via a uniport mechanism, driven by the membrane potential. The K_{eq} for 8HPA can then be calculated with $\psi = -0.110\ V$ and $Z = -2$ as, 5265. Such a large K_{eq} value suggests that the secretion will be highly irreversible but with a very low rate of secretion. It can therefore be assumed that the transporter is irreversible and secretes 8HPA with the help of the negative membrane potential.

OPC secretion mechanism

As shown in Appendix VII the measured EC/IC ratio of OPC was between 0.2 to 0.3 in phase I, however, in phase II in the presence of PAA the EC/IC ratio reaches a maximum value of 0.60 ± 0.15. Similarly, in the reference chemostats, in the presence of PAA, the EC/IC ratio reaches a value of 0.90 ± 0.10. These ratios are thus different in absence and presence of PAA. The transport mechanism, however, will have only one K_{eq} value. The EC/IC ratio less than one suggest that the secretion is not against the concentration gradient and therefore does not require energy. However, OPC carries a negative charge and thus passive diffusion over the plasma membrane is unlikely to occur. Our EC/IC ratio with a value more than 0.2 shows that proton symport of OPC^- (K_{eq} of 0.2) is not possible. A possible mechanism for OPC export could be a uniporter (K_{eq} of 73) or proton antiporter (K_{eq} of 10^4). Further distinction will need more detailed studies of the transporter.

PAA uptake and export mechanism

The undissociated form of phenyl acetic acid, can easily permeate through cell membranes [72], however, earlier studies suggested that there would be a specific uptake mechanism for dissociated PAA [52]. Douma et al. [44] showed that the experimental EC/IC ratio (3) is far from the thermodynamic equilibrium (0.2) for passive diffusion of the undissociated form of PAA. They explained this finding by the presence of an active secretion mechanism for PAA, consuming ATP (one mole of ATP for each PAA^- and one for the associated proton). While studying the genome wide gene expression responses to PAA, Harris et al. [65], have identified a possible PAA transporter gene (Pc2g14600) which belongs to the ABC-G transporter cluster [65]. The experimental EC/IC ratio of 3 observed in the current study and the significant increase in the respiration rate in the presence of PAA is thus in agreement with previous studies and indicative for active export of PAA from *P. chrysogenum* cells.

In phase II, after the PAA step the PAA accumulation in the cell started decreasing and reached a steady level within 30 min after the step which coincided with a significant increase of the oxygen uptake rate. This immediate response of the oxygen uptake rate indicates that the exporter was already present during the PAA step. Removing the PAA exporter gene can heavily decrease the energy burden on the cell.

PenG secretion mechanism

Very little work has been done to identify the penicillin transporters. Recent stimulus response experiments performed by Douma et al, 2011 showed that the transport of PenG is reversible and predicted that the secretion of negatively charged PenG is accomplished by facilitated export of $PenG^-$. The equilibrium ratio of extracellular to intracellular PenG of 73 (Appendix VII) in phase II after the PAA step and the measured EC/IC ratio being close to K_{eq} confirms the hypothesis that the secretion of PenG takes place by reversible facilitated transport driven by the membrane potential. The EC/IC ratio of PenG is near equilibrium and hence the transporter is having high capacity.

oOHPAA secretion mechanism

oOHPAA was measured in both intra and extracellular space. The EC/IC ratio of oOHPAA was approximately equal to 5 (see Appendix VII), which means that if there is secretion then it is against the concentration gradient. So, we initially hypothesized that the oxidation of PAA to oOHPAA could be done by a membrane bound mono-oxygenase in the extracellular

space. However, recent experiments carried out by Veiga et al. [177], with labeled phenyl alanine as nitrogen source, demonstrated that oOHPAA is formed in the cell and then secreted. Thus the secretion of oOHPAA is active against the concentration gradient, consuming energy in order to maintain potential gradient across the cell membrane. Also, there is a chance of undissociated oOHPAA diffusing back into the cell, and making a futile cycle consuming energy. Thus reduction of formation of oOHPAA is necessary to reduce the energy burden on the cell. For the measured EC/IC ratio of 5, a feasible mechanism for secretion of oOHPAA, which is negatively charged, could therefore be a uniport with a thermodynamic equilibrium of 73.

4.4.4 6APA production by fermentation route

6APA, which is produced by *P. chrysogenum* as one of the end products in the absence of PAA, is having a special importance in the pharmaceutical industry as it is used as precursor for the production of ampicillin and amoxicillin. Here we present quantitative data for the 6APA production in *P. chrysogenum* fermentations in the absence of PAA. As expected, in the absence of PAA the fluxes were directed towards production of 6APA. However, the activity of IAH (responsible for conversion of IPN to 6APA) and secretion of 6APA appear to be limiting for 6APA production. Thus in order to increase 6APA production, the activity of IAH should be increased, e.g. by increasing its protein concentration. Also, for a reversible 6APA transporter using membrane potential energy, the maximum thermodynamic equilibrium ratio of 73 ± 17 (see Appendix IV) can be obtained by identifying and overexpressing the 6APA transporter genes. Furthermore, the fluxes can be redirected towards 6APA production by decreasing IPN secretion. This can be achieved by deleting the genes which are responsible for the transporter proteins responsible for secretion of IPN. Ullán et al. [167], observed that hetrologous expression of the *A. chrysogenum cefT* gene in *P. chrysogenum* Wisconsin 54-1255 increased the secretion of IPN and reduced the secretion of PenG, demonstrating that the *cefT* gene encodes a hydrophilic ß-lactam transporter [167]. The CefT encodes a multidrug efflux pump belonging to the Major Facilitator Superfamily (MFS) of membrane proteins [166] which can act as an antiporter. The genome of *P. chrysogenum* contains at least 150 potential CefT homologs with similarities ranging from 37–84% [171], thus identification and deletion of those genes can significantly direct the flux towards 6APA production. One of the obstacles in the production of 6APA via fermentations is its carboxylation to 8HPA [69]. However, owing to its low carboxylation rate constant (0.0049 ±

0.0004 h^{-1}) (Appendix V) only 10% of the produced 6APA is converted to 8HPA. This spontaneous conversion can be avoided by using *in situ* product removal techniques. Thus our quantitative studies propose an alternate way to produce 6APA in fermentations rather than producing it enzymatically from PenG.

4.5 Conclusions

A successful specific perturbation of the penicillin pathway was carried out in order to understand the *in vivo* kinetics and elucidate rate limiting steps in the penicillin biosynthesis pathway. Chemostat cultivations of *P. chrysogenum* under glucose-limitation in the absence and presence of PAA were characterized by changing intracellular fluxes, metabolite and enzyme levels. Our quantitative analysis, in terms of metabolomics and fluxomics showed that for the industrial strain studied the penicillin pathway flux was not limited by the supply of the precursor amino acids and thus independent of central carbon metabolism. Further we also showed that under PenG producing conditions, with high concentrations of IPN and 6APA, the activity of IAT was limiting the maximum PenG production. However, at low concentrations of IPN and 6APA and due to the degeneration of enzymes, the control of the flux through the pathway shifted towards ACVS and/or IPNS.

In the absence of PAA, quantitative data for the production of 6APA was provided which is the starting material for antibiotics such as ampicillin and amoxillin. Also, the bottlenecks in the 6APA production were found to be the activity of IAH enzyme and/or secretion of 6APA. In the presence of PAA, the observed immediate formation and secretion of PenG implied that all the pathway enzymes and transporters were sufficiently expressed to produce PenG even in the absence of PAA. However, the presence of an active PAA exporter resulted in additional (≈10%) catabolism (futile cycling of PAA over membrane). Further with the measured EC/IC ratio the thermodynamic feasibility of secretion mechanisms of penicillin pathway metabolites was discussed. In conclusion, this experimental approach indentifies several metabolic engineering targets (enzymes/transporters) for directed genetic engineering to improve the flux towards the desired product (PenG/6APA).

4.6 Acknowledgements

We acknowledge the financial support from the Netherlands Organization for Scientific Research (NWO) via the IBOS (Integration of Biosynthesis and Organic Synthesis) programme of Advanced Chemical Technologies for Sustainability (ACTS) (project nr: IBOS 053.63.011) and also from DSM. This project was carried out within the research programme of the Kluyver Centre for Genomics of Industrial Fermentation, which is part of the Netherlands Genomics Initiative/ Netherlands Organization for Scientific Research. Authors thank L.P.de Jonge for providing data of one of the reference chemosats.

4.7 Appendix

4.7.1 Appendix I: Primary measurements

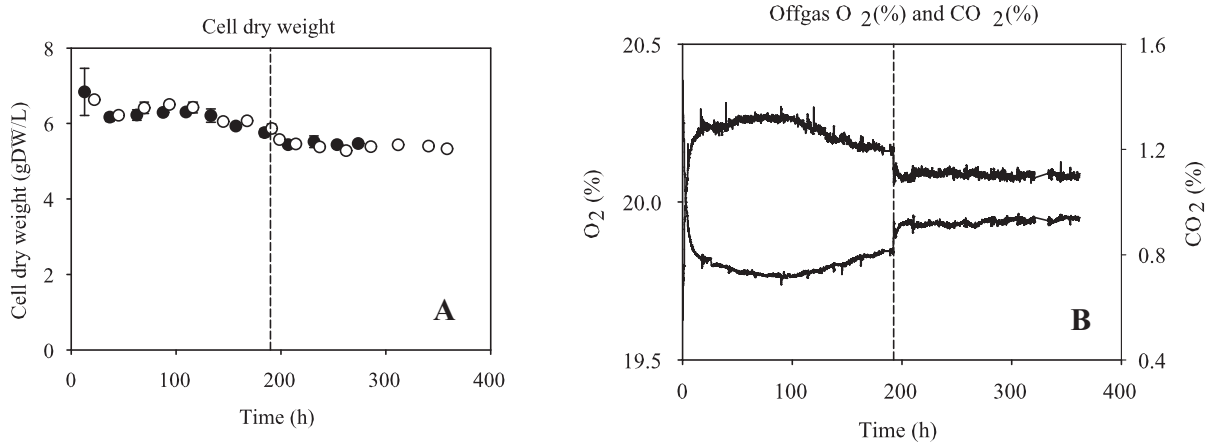

Figure 4.A1: [A] Cell Dry Weight (CDW) from a glucose-limited chemostat culture operated at a dilution rate of 0.05 h^{-1}. Results from Chemostat 1 and Chemostat 2 are represented by solid and open circles respectively. [B] The upper line represents offgas O_2 (%) and lower line represents offgas CO_2 (%) for Chemostat 2. The dotted line separates phase I and phase II. The x-axis time is for entire fermentation including phase I and phase II. Phase II starts at 192 h.

4.7.2 Appendix II: Reconciled biomass specific conversion rates

Table 4.A1 : Reconciled biomass specific conversion rates for different cultivation conditions.

Rate	***Absence of PAA[a]***	***Presence of PAA[b]***	***Reference[c]***
μ	49.4 ± 1.1	50.3 ± 1.3	50.0 ± 1.0
q_S	-18.93 ± 0.54	-20.44 ± 0.59	-19.69 ± 0.46
q_{O_2}	-46.7 ± 2.0	-57.4 ± 2.3	-53.1 ± 1.6
q_{CO_2}	51.0 ± 2.1	61.9 ± 2.4	57.8 ± 1.7
q_{PAA}	-	-0.284 ± 0.015	-0.455 ± 0.016
q_{PenG}	-	0.229 ± 0.014	0.350 ± 0.022
q_{oOHPAA}	-	0.0555 ± 0.0031	0.107 ± 0.022
q_{IPN}	0.0238 ± 0.0038	0.00108 ± 0.00037	0.0187 ± 0.0047
q_{6APA}	0.132 ± 0.018	0.0025 ± 0.0012	0.0535 ± 0.0015
q_{8HPA}	0.0124 ± 0.0021	0.00077 ± 0.00058	0.0132 ± 0.0020
q_{OPC}	0.0189 ± 0.0021	0.0227 ± 0.0013	0.078 ± 0.012
$q_{byproducts}$	5.22 ± 0.12	5.30 ± 0.14	6.18 ± 0.41

Specific rates of biomass growth and by-product formation are expressed mCmol/Cmol·h other rates are expressed in mmol/Cmol. h

a: Based on two chemostat cultivations within time frame of 167h to 192h of phase I

b: Based on two chemostat cultivations within time frame of 68h to 148h of phase II (260h to 340h – entire fermentation time)

c: Based on two reference chemostat cultivations

4.7.3 Appendix III: 6APA distribution w.r.t pH

In solution 6APA attains a pH dependent equilibrium between the zwitterion ($APA^{\pm}$), negatively charged (APA^{-}) and positively charged (APA^{+}) forms. Almost 99.5% of 6APA carries a negative charge at intracellular pH of 7.2, while 0.5% of 6APA is a zwitterion. For pH of 6.5, the anion form is 97.55%. and the zwitterion form of 6APA is 2.45%. With two pKa values for 6APA, $pK_{a1} = 2.5$ (Carboxyl) and $pK_{a2} = 4.9$ (amine), the distribution with respect to pH can be found out by the following equation

$$F_{6APA^{\pm}} = \frac{1}{1+10^{pk_{a1}-pH_{in}}+10^{pH_{in}-pK_{a2}}}$$

$$F_{6APA^{-}} = \frac{1}{1+10^{pk_{a2}-pH_{in}}+10^{(pK_{a2}\cdot pK_{a2})-(pH_{in})^2}}$$

The negatively charged 6APA can be secreted by membrane potential difference with the help of a membrane transporter. However, from the studies of Douma et al. [44], it was shown that at thermodynamic equilibrium EC/IC ratio for a negatively charged metabolite would by around 73±17. But the EC/IC ratio of 6APA was approximately 2 which lead us to hypothesis that maybe 0.5% of 6APA which is a zwitterion was being secreted. For experimental conditions for zwitterion export we can write,

$C_{6APA^{\pm},in} = 0.005 \times C_{6APA,in}$ and $C_{6APA^{\pm},ex} = 0.0245 \times C_{6APA,ex}$

At thermodynamic equilibrium, for the zwitterion, $C_{6APA^{\pm},in} = C_{6APA^{\pm},ex}$

$$\frac{C_{6APA,ex}}{C_{6APA,in}} = 0.2$$

Thus, the measured EC/IC ratio of 2 is far greater than the thermodynamic equilibrium of a zwitterion, indicating that the hypothesis of cell exporting zwitterion form of 6APA can be discarded.

Table 4.A2: Percentage (%) of 6APA in different forms at fermentation pH of 6.5 and intracellular pH of 7.2

pH	$F_{6APA\pm}$	F_{6APA-}	F_{6APA+}	***Sum***
6	7.36	92.64	0.03	100.03
6.5	2.45	97.55	0.01	100.01
7	0.79	99.21	0.00	100.00
7.2	0.50	99.50	0.00	100.00
8	0.08	99.92	0.00	100.0

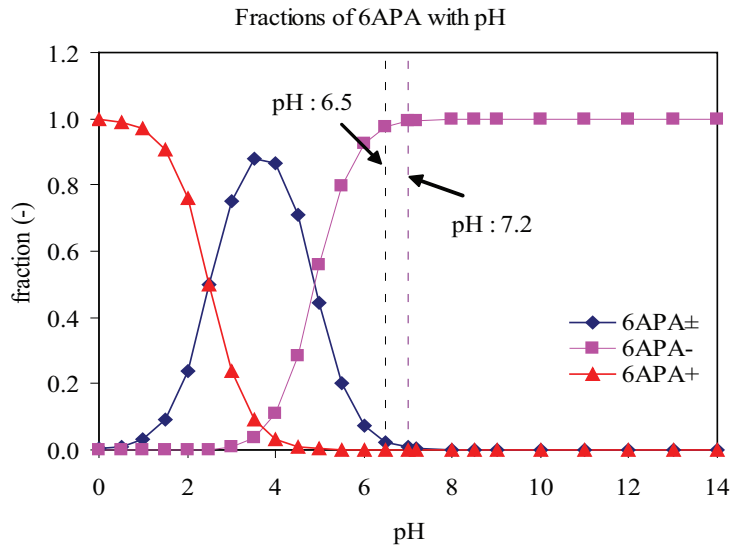

Figure 4.A2: Distribution of 6APA with respect to pH.

4.7.4 Appendix IV: Transport mechanisms

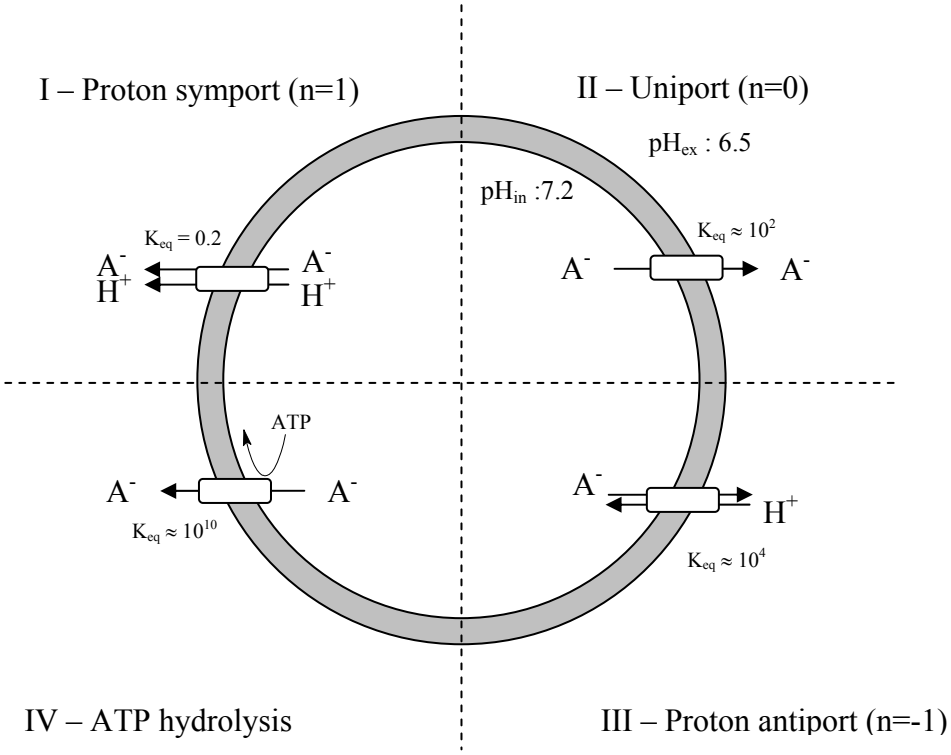

Figure 4.A3: Different types of transport mechanisms for proton coupled export of anions.

Gibbs energy associated with proton coupled export of an anion is as follows:

$$\Delta G_R = R \cdot T \cdot \ln\left(pH_{in} - pH_{ex}\right) + R \cdot T \cdot \ln\left(\frac{C_{ex,A^-}}{C_{in,A^-}}\right) + \left(1-n\right) \cdot F \cdot \Psi$$

At equilibrium, $\Delta G_R = 0$ gives,

$$\ln\left(\frac{C_{ex,A^-}}{C_{in,A^-}}\right) = \left(pH_{ex} - pH_{in}\right) \cdot n + \frac{\left(n-1\right) \cdot F \cdot \Psi}{R \cdot T}$$

With n is the number of protons transported, F is the Faraday constant of 96.5 $kJ \cdot V^{-1} \cdot mol^{-1}$, Ψ is the intracellular electrical potential (varying between -0.8V to -0.130V), pH_{in} = 7.2, pH_{ex} = 6.5, temperature, T = 298 K, R = 8.314 x 10^{-3} $kJ \cdot K^{-1} \cdot mol^{-1}$ and C is the concentration. Figure 4.A3 shows different possible mechanisms for the export of anions (which is a negatively charged molecule, Z = -1) namely facilitated export (n = 0), export by proton symport (n = 1), export by proton antiport (n = -1) and export with ATP hydrolysis using an ABC transporter. The equilibrium constants for these four different mechanisms are respectively:

$$K_{eq,uniport,(n=0)} = \frac{C_{ex}}{C_{in}} = e^{\frac{-1 \cdot F \cdot \Psi}{R \cdot T}} \approx 10^2$$

$$K_{eq,symport,(n=1)} = \frac{C_{ex}}{C_{in}} = 10^{pH_{ex}-pH_{in}} = 10^{6.5-7.2} = 0.2$$

$$K_{eq,antiport,(n=-1)} = \frac{C_{ex}}{C_{in}} = 10^{pH_{in}-pH_{ex}} \cdot e^{\frac{-2\cdot F\cdot \Psi}{R\cdot T}} \approx 10^{4}$$

$$K_{eq,ATP-hydrolyis,(n=0)} = \frac{C_{ex}}{C_{in}} = e^{\frac{-1\cdot F\cdot \Psi + \Delta G_p}{R\cdot T}} \approx 10^{10}$$

Under physiological conditions the energy gained from ATP hydrolysis (ΔG_p) is approximately -50 kJ·mol^{-1}.

4.7.5 Appendix V: Carboxylation of 6APA

6APA carboxylation kinetics to 8HPA has been found to be first order with respect to both 6APA concentration and to the dissolved CO_2 concentration [69]. In phase II, there is no secretion of 6APA and 8HPA, also the dissolved CO_2 concentration was constant during steady state. It is also known that pH has no effect on the carboxylation reaction because the dissolved CO_2 takes part in the reaction and not the bicarbonate. Thus the rate of 8HPA formation is written as

$$v_{8HPA,ex} = k_{8HPA,ex} \cdot C_{6APA,ex} \cdot C_{CO_2}$$

For constant CO_2 concentration we can write as

$$v_{8HPA,ex} = K_{8HPA} \cdot C_{6APA,ex}$$

Mass balance for extracellular 8HPA gives

$$\frac{dC_{8HPA,ex}}{dt} = v_{8HPA,ex} - D \cdot C_{8HPA,ex}$$

Thus rate constant is

$$K_{8HPA} = \frac{\frac{dC_{8HPA,ex}}{dt} + D \cdot C_{8HPA,ex}}{C_{6APA,ex}}$$

Thus, $K_{8HPA} = 0.00486 \pm 0.0043$ h^{-1}

4.7.6 Appendix VI: Intracellular and extracellular metabolite levels

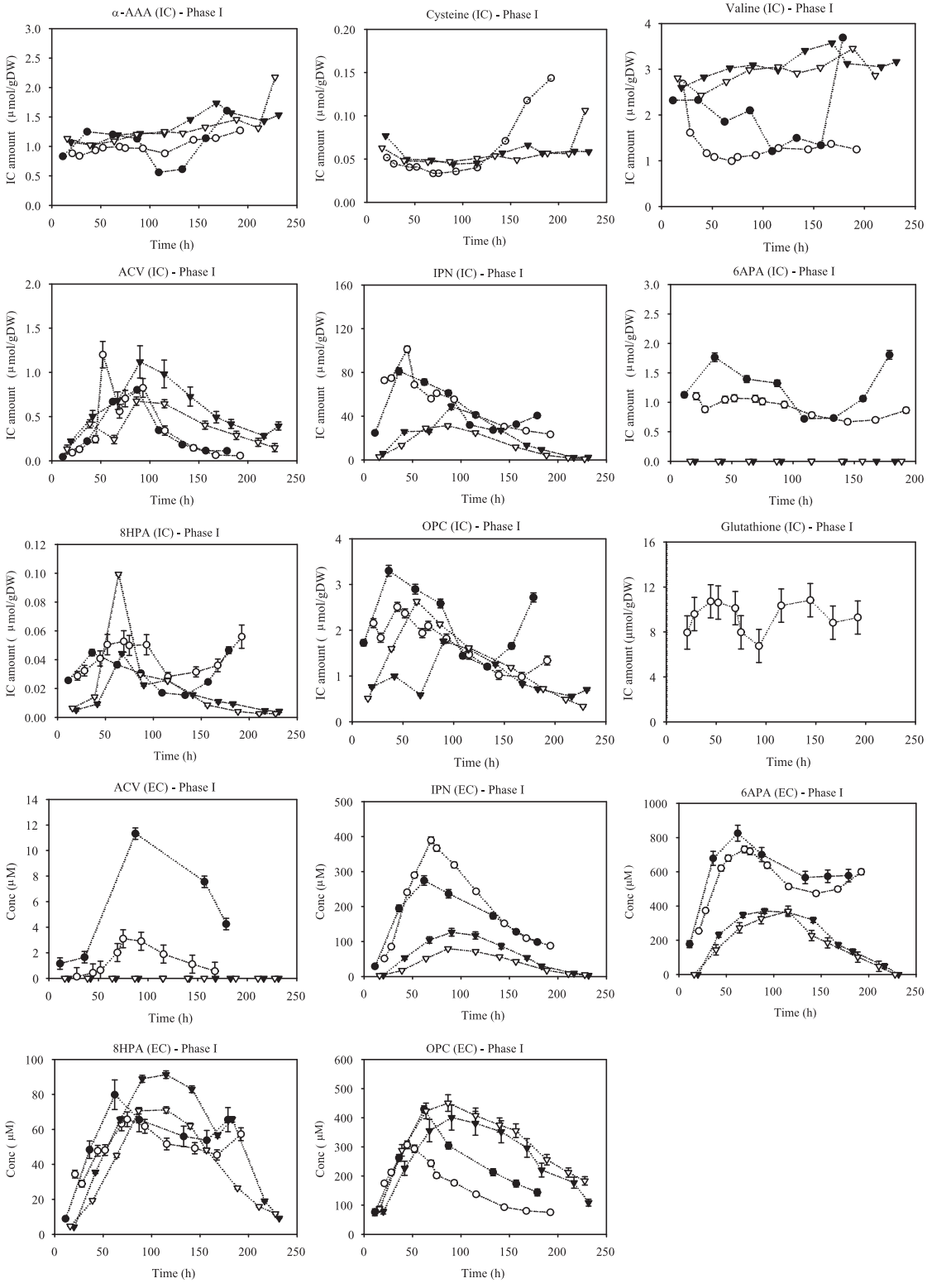

Figure 4.A4: Intracellular amounts and extracellular concentrations of metabolites as a function of culture age for phase I in Chemostat 1(solid circles) and Chemostat 2 (open circles) which are cultivated in absence of PAA. The reference chemostats (solid and open inverted triangles) are cultivated in presence of PAA. Each data point represents a single sample and the error bars gives the standard deviation for replicate analysis. Intracellular ACV is total ACV reduced by addition of TCEP. Extracellular ACV amounts were lower than 10µM. 6APA in the reference chemostats was below detection limit.

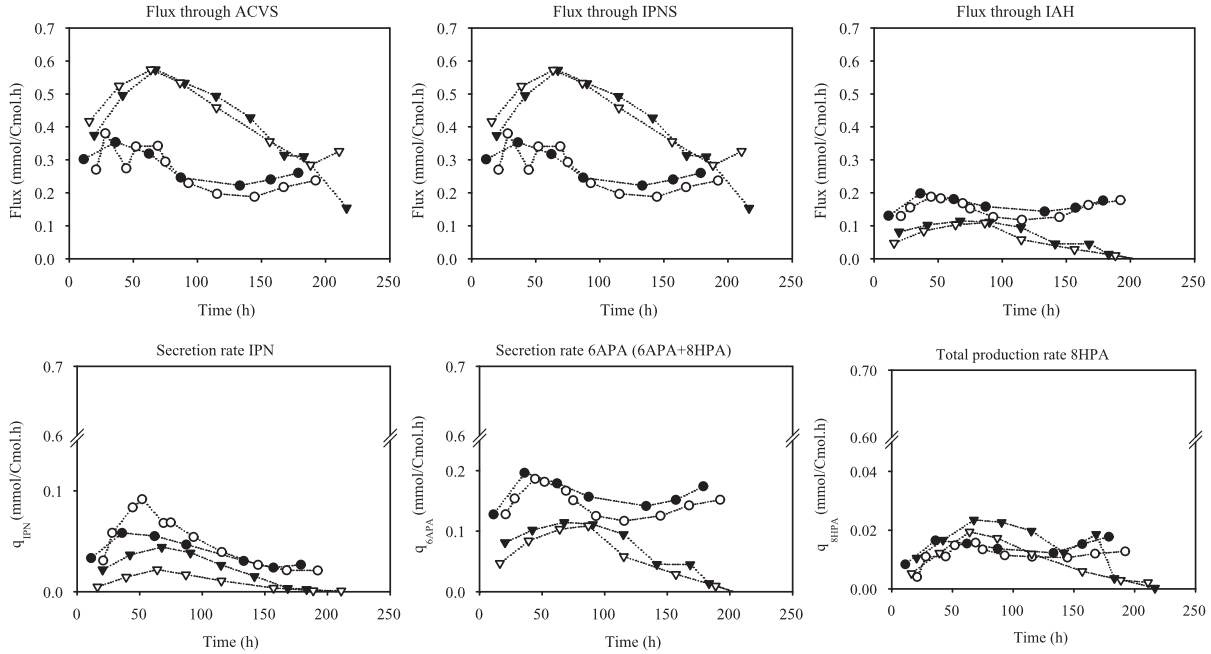

Figure 4.A5: Fluxes through the penicillin pathway and secretion rates of metabolites as a function of culture age for phase I in Chemostat 1 (solid circles) and Chemostat 2 (open circles) which are cultivated in absence of PAA. The reference chemostats (solid and open inverted triangles) are cultivated in presence of PAA.

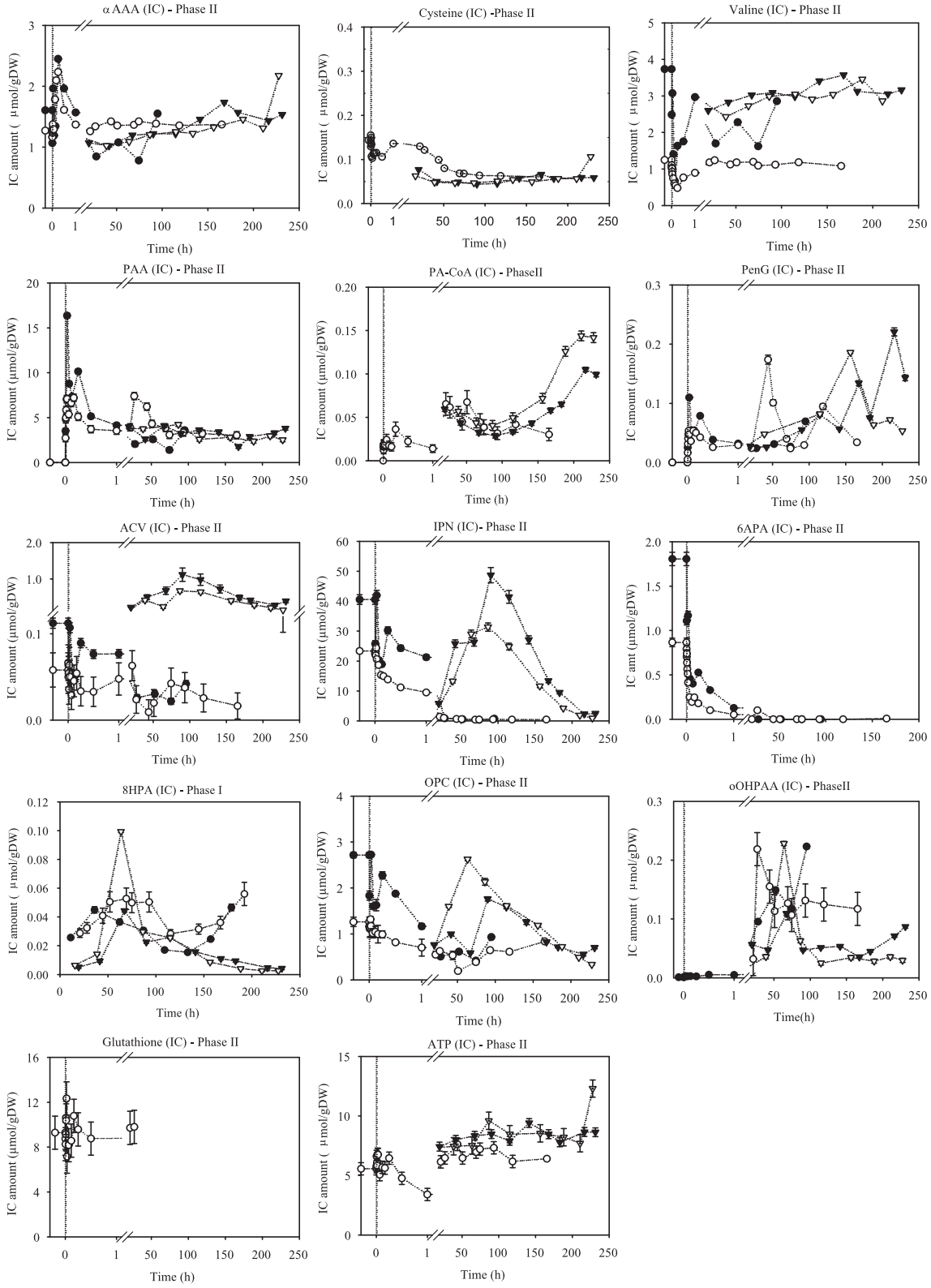

Figure 4.A6: Intracellular amounts of metabolites as a function of culture age for phase II in Chemostat 1(solid circles) and Chemostat 2 (open circles) which are cultivated in presence of PAA by a step change in extracellular PAA concentrations. The reference chemostats (solid and open inverted triangles) are cultivated in presence of PAA. Each data point represents a single sample and the error bars gives the standard deviation for replicate analysis. Intracellular ACV is total ACV reduced by addition of TCEP. Intracellular 6APA and 8HPA in chemostat 1 and chemostat 2 were below detection limit after first 1 h.

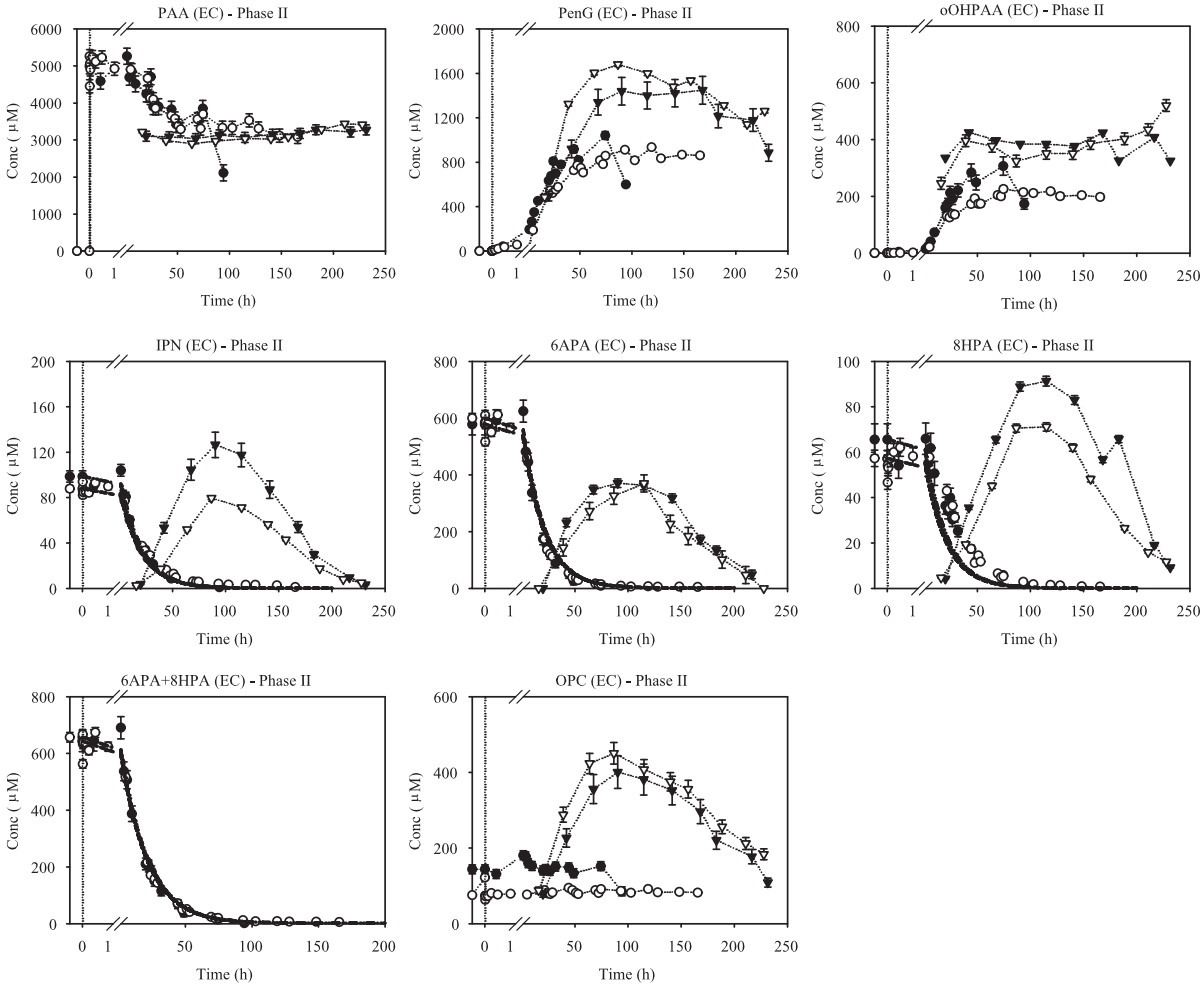

Figure 4.A7: Extracellular concentrations of metabolites as a function of culture age for phase II in Chemostat 1(solid circles) and Chemostat 2 (open circles) which are cultivated in presence of PAA by a step change in extracellular PAA concentrations. The reference chemostats (solid and open inverted triangles) are cultivated in presence of PAA. Each data point represents a single sample and the error bars gives the standard deviation for replicate analysis. Extracellular ACV amounts were below detection limit (0.1 µM).

4.7.7 Appendix VII: EC/IC ratios

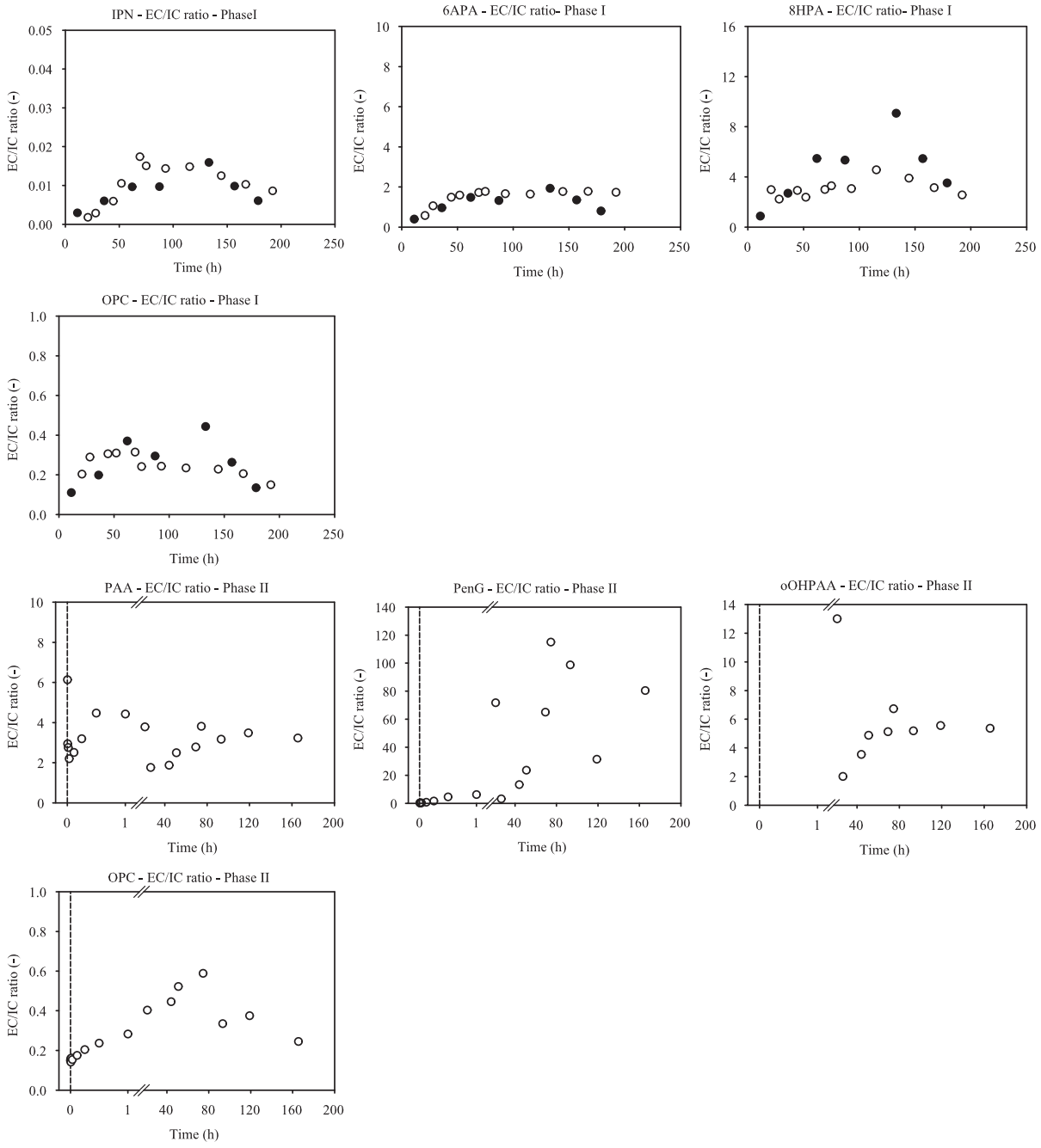

Figure 4.A8: Extracellular to intracellular ratios of concentrations of penicillin pathway metabolites as a function of culture age for phase I in Chemostat 1 (solid circles) and Chemostat 2 (open circles).

Table 4.A3: Possible transport mechanisms for different compounds.

Metabolite	***Feasible transport mechanism***	K_{eq}	***Average observed EC/IC ratio***	***Driving force***
IPN^{-1} secretion	Proton antiport	$\sim 10^4$	0.0154 ± 0.0014	Proton motive force
$6APA^{-1}$secretion	Uniport	73 ± 17	1.700 ± 0.016	Potential gradient
$PenG^{-1}$secretion	Uniport	73 ± 17	70 ± 33	Potential gradient
$8HPA^{-2}$ secretion	Uniport	5265	3.48 ± 0.73	Potential gradient
$oOHPAA^{-1}$secretion	Uniport	73 ± 17	5.47 ± 0.66	Potential gradient
OPC^{-1} secretion	Uniport/	73 ± 17	0.45 ± 0.10	Potential gradient
	Proton antiport	$\sim 10^4$		Proton motive force
HPAA uptake	Free diffusion	0.2 ~ 0.3	3.25 ± 0.49	Conc. gradient
$PAA^{-1} + H^+$ export	ATP hydrolysis	$\sim 10^{10}$	3.25 ± 0.49	ATP driven transport

Chapter 5

A complete *in vivo* kinetic model of the penicillin biosynthesis pathway in *Penicillium chrysogenum*

Deshmukh AT, Verheijen PJT, Heijnen JJ and van Gulik WM. A complete *in vivo* kinetic model of the penicillin biosynthesis pathway in *Penicillium chrysogenum*
(Submitted for publication)

Abstract

The aim of this study was to unravel the *in vivo* kinetic properties of enzymes and transporters and the identification of possible bottlenecks in the penicillin biosynthesis pathway of *Penicillium chrysogenum*. To this end a dynamic model of the pathway was constructed. The model included the formation of several byproducts as well as the transport of sidechain precursor phenyl acetic acid (PAA), pathway intermediates, and the product penicillin-G over the cytoplasmic membrane. To estimate the parameters of the model and changes in the enzyme levels under *in vivo* conditions, dynamic metabolite data were obtained at three different timescales (sec, min, hours) from glucose limited chemostat cultivation of *P. chrysogenum* perturbed by a step change in the extracellular PAA concentration. The model thus constructed is capable of describing the changes in the levels of intra- and extracellular metabolites, changes in the capacities of the penicillin pathway enzymes and estimating the fluxes through the pathway. Metabolic control analysis showed that both in the absence and presence of PAA, ACVS controls the flux through the penicillin biosynthesis pathway.

Keywords: *Penicillium chrysogenum*; kinetic modeling; penicillin biosynthetic pathway; stimulus response experiments; transport of metabolites.

5.1 Introduction

Since the discovery of penicillin, a large effort has been made to understand the *Penicillium chrysogenum* strain to improve the yields, product titers and productivities of the β-lactum antibiotics. High producing industrial strains were developed by repeated rounds of random mutagenesis and selection during the classical strain improvement program [164]. Based on advances in genetic engineering and with fully known genome sequence [171], a more rational approach of metabolic engineering can be applied to further improve the strain. In order to implement the metabolic engineering strategies, it is essential to understand the distribution of the fluxes through the metabolic pathways leading to the desired product and to identify the rate limiting step [123].

The penicillin pathway encoded in gene cluster (*pcbAB-pcbC-penDE*) consists of three enzymes, α-aminoadipyl-L-cysteinyl-D-valine synthetase (ACVS), isopenicillinN synthase (IPNS) and acyl-CoA: isopenicillin-N acyltransferase (AT) [41]. In addition, there is the necessity to activate the side chain precursor phenyl acetic acid (PAA) by phenylacetate–CoA ligase (PCL) [92]. Various studies have been conducted to find out the possible bottleneck for the production of penicillin in *P. chrysogenum* [80,120,124,126,135,159,176]. The limitations for the PenG production can be either residing in the central carbon metabolism (supply of precursor amino acids, ATP, NADPH) or the product pathway itself (secondary metabolism). Chemostat studies on high producing *P. chrysogenum* strains, supplied by different carbon sources (glucose, ethanol and acetate) and therefore having different flux distributions in central carbon metabolism, showed that there is no limitation for penicillin production with respect to the supply of precursor amino acids or the supply of cofactors [120,176]. As the central carbon metabolism is not limiting the flux towards penicillin production, thus the control of fluxes should reside somewhere in the penicillin biosynthesis pathway.

Nielsen and co-workers developed a kinetic model to identify possible bottlenecks in the penicillin product pathway. They estimated the enzyme capacities of the penicillin biosynthesis pathway, however all the affinity and inhibition parameters were obtained from literature. They showed that the flux control lies with ACVS and later shifts to IPNS in fed batch studies [125,135,159]. However, they did not include PCL in their study, which was also reported to be a limiting enzyme for the penicillin production [126]. Furthermore, the kinetic model developed by Nielsen and co-workers did not include transport of the precursor

PAA and of the product PenG across the cytoplasmic membrane of the cell. Insufficient transport of substrate and product across the membrane can severely limit the fluxes through the pathway. Thus, in order to identify possible bottlenecks in the penicillin biosynthesis pathway a complete model is essential that will include all the enzymes associated with the penicillin pathway and the transport proteins of precursors, products and by-products.

To estimate the parameters of a kinetic model under *in vivo* conditions, experimental data are required that vary in time over a wide range of concentrations. Such dynamic data can be obtained by applying a stimulus response strategy. Thereby a steady state culture is perturbed, whereafter the changes in the relevant pathway metabolites are quantified within a time frame during which no changes in enzyme levels are to be expected, i.e. seconds to minutes [108,119,128,140,162]. To specifically excite the penicillin pathway, a perturbation with the growth limiting substrate (e.g. glucose) would not provide enough changes in the concentrations of the penicillin pathway metabolites [119]. as the pathway is too far away from central metabolism. Therefore, a metabolite particular to the penicillin pathway should be used as a perturbation agent. The penicillin pathway intermediates ACV and IPN are not taken up by the cells [56] and therefore cannot be used as the external perturbing agents. Another metabolite in the pathway, 6APA, is taken up by the cell [56], but its ability to perturb the penicillin pathway fluxes is obscure as its transport mechanism and uptake rate are unknown. Another possibility would be the side chain precursor for PenG formation, PAA. If PAA is not supplied no PenG is formed, which is likely to result in the accumulation of pathway intermediates. Sudden supply of PAA would lead to the formation of PenG, which is known to be effectively exported. This should result in a suddenly increased pathway flux and thus dynamic changes in the associated metabolites. Import of PAA should not be the bottleneck, as it is known to be taken up rapidly by the cell by passive diffusion, that is 50-100 times faster than the export rate of PenG [44]. The dynamic data obtained from such a stimulus response experiment, i.e. fluxes and metabolite levels, can subsequently be used to estimate the in-vivo kinetic parameters of the pathway enzymes.

This study was aimed at constructing, a complete kinetic model for the penicillin biosynthesis pathway that not only includes all pathway enzymes (ACVS, IPNS, AT and PCL) but also the transport of PAA, PenG and the intermediates isopenicillinN (IPN), 6-aminopenicillanic acid (6APA), 8-hydroxypenillic acid (8HPA) and ortho-hydroxyphenylacetic acid (oOHPAA) across the cell membrane.

We applied the dataset obtained from the PAA step experiments described in chapter 4 to estimate the kinetic parameters of the model. The model is not only applied to describe the metabolite concentrations and fluxes in the pathway, but also to estimate *in vivo* changes of the enzyme levels of the pathway. Metabolic control analysis based on the developed model identified possible bottlenecks for the production of penicillin in the pathway. The model thus helped to get a deeper insight about the penicillin biosynthesis pathway.

5.2 Experimental set up: PAA step experiment

To perform a stimulus response experiment, the strain *P. chrysogenum* DS17690 was first cultivated in an aerobic glucose-limited chemostat (D = 0.05 h^{-1}) in the absence of external supply of PAA (Chapter 4, Figure 4.1). The part of the chemostat operation carried out without the addition of PAA is indicated as phase I. To perturb the steady state chemostat system a step change in PAA concentration was given. This step change was accomplished by replacing the feed medium without PAA with a medium containing 5 mM PAA and simultaneously injecting a solution of PAA. This resulted in an instantaneous increase of the extracellular PAA concentration from 0 to 5 mM. The part after the step change in the PAA concentration is indicated as phase II (Chapter 4, Figure 4.1). Phase I was carried out for 10 residence times where after the step change in extracellular PAA was given. After the step change, phase II was carried out till a new steady state was reached. Phase II is divided in short term periods (seconds and minutes scale) and a long term period (hours scale). The details of the PAA step experiment are discussed in details in Chapter 4.

5.3 Model structure

The general structure of the model includes the state vectors of all key metabolites involved in the penicillin biosynthesis pathway. A set of differential equations based on the compound balances for each metabolite is setup (Appendix II). The intracellular concentration and fluxes are based on per m^3 of intracellular volume of the cell. The extracellular concentration and fluxes are based per m^3 of the fermentor volume. In the model the intracellular compartments (e.g. mitochondria, peroxisomes) are not taken into account, as it is not possible to differentiate between the concentrations in the cytoplasm and the different organelles.

Figure 5.1 describes schematically the biosynthesis pathway for penicillin production in *P. chrysogenum*. The enzymes and metabolites that are present in the absence of PAA are shown

in the dotted box, whereas, in the presence of PAA, all the enzymes and metabolites in the figure are present. The penicillin biosynthesis pathway is described in details in chapter 4.

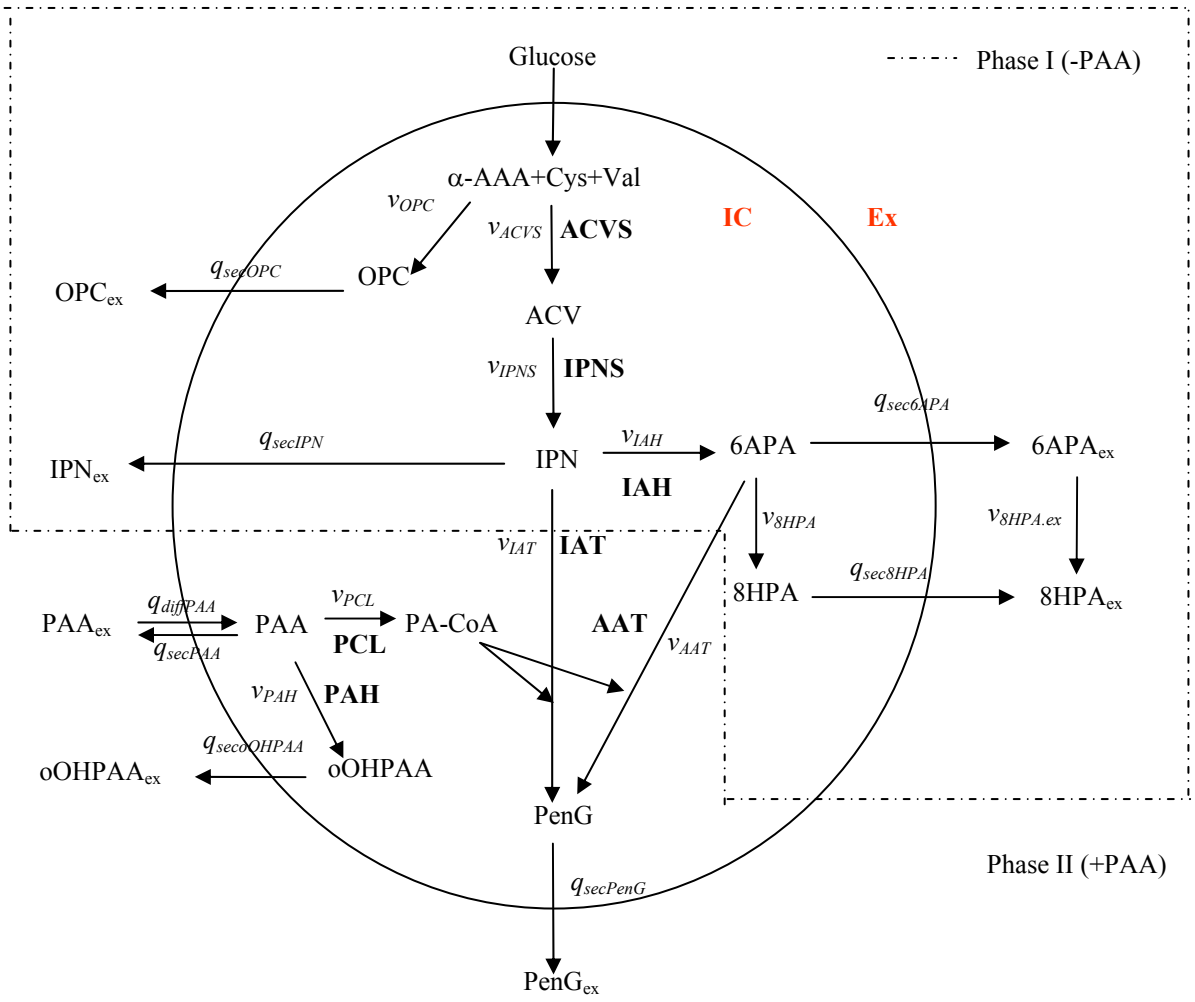

Figure 5.1: Structure of metabolic model for simulation dynamics for Pen pathway metabolites. Dotted box represents phase I (-PAA) and the whole model is for phase II (+PAA)

5.3.1 Kinetics of ACVS

δ-(L-α-Aminoadipyl)-L-cysteinyl-D-valine synthetase (ACVS) is the first enzyme in the pathway of penicillin biosynthesis. *In vitro* studies of purified ACVS of *P. chrysogenum* suggest that ACVS obeys Michaelis-Menten kinetics with respect to the precursor amino acids (α-AAA-K_m: 45 mmol/m^3, cysteine-K_m: 80 mmol/m^3, valine-K_m: 80 mmol/m^3) [161]. However, these *in vitro* K_m values for the respective amino acids differ for ACVS from different organisms [14,78,161,189]. Nielsen et al. [125] proposed a kinetic model for ACVS that was a function of rate constant, enzyme level, and concentrations of the three precursor amino acids. Further the rate constant was dependent on various effectors which include ATP,

Mg^{+2}, AMP, pyrophosphate, phosphate and CoA. The kinetic function also incorporated the feed back inhibition of ACVS by ACV. [125,135,190] and later was extended with an inhibition term by bisACV on the kinetics of ACVS [159]. Several studies have observed that the kinetics of ACVS is not limited by intracellular amounts of the precursor amino acids [120,176]. In other studies, it was observed that the penicillin pathway fluxes do not vary with external supply of α-AAA (chapter 3) and is also independent of intracellular cysteine levels [79]. In the PAA step experiment (chapter 4), it was also observed that the intracellular ACV flux changed significantly at short time scale whereas the concentration of the three precursor amino acids did hardly change. Therefore, it can be concluded that the *in vivo* kinetics of ACVS is not dependent on the availability of the precursor amino acids and the modified kinetic rate expression is assumed to have zero order kinetics with respect to the precursor amino acids. Furthermore, in *in vitro* studies it was observed that ACVS is inhibited by ACV and bisACV, having inhibition parameters as 540 mmol/m^3 and 1400 mmol/m^3 [161]. However, in the PAA step experiment, it was also observed that there was no formation of bisACV thus the inhibition term of bisACV is not included in the equation and only ACV product inhibition is applied,

$$v_{ACVS} = \frac{k_{ACVS}}{1 + C_{ACV} \cdot K_{i,ACV,ACVS}^{-1}} \qquad (1)$$

5.3.2 Kinetics of IPNS

Nielsen et al. [125] proposed that IPNS follows Michaelis-Menten type kinetics with respect to its substrate ACV. The *in vitro* $K_{m,ACV,IPNS}$ value for IPNS with respect to ACV was estimated to be 130 mmol/m^3 [137]. Bainbridge et al. [13] also observed that the dissolved oxygen has influence on the IPNS kinetics and found the kinetics to be of the first order in the concentration range of 0.07-0.18 mM. The PAA step experiment was designed to have no oxygen limitation and the dissolved oxygen (DO) was nearly constant and was more than 80% of the air saturation over the period of cultivation (chapter 4). Therefore, the oxygen term can be incorporated in the rate constant as the DO was never limiting. Nielsen et al. [125] also included inhibition of IPNS by glutathione in the kinetic function, with an *in vitro* inhibition constant of 8900 mmol/m^3 [137]. In our PAA step experiment, the intracellular glutathione level was near constant in time (4000-5000 mmol/m^3). Thus, to keep it simple the inhibition term by glutathione is absorbed in the rate constant term. In addition, it was observed in the PAA step experiment that there is a rapid decrease in the intracellular level of

6APA after the PAA step was given (chapter 4). Therefore, we assume that there is a possibility of 6APA inhibition on the activity of IPNS.

$$v_{IPNS} = \frac{k_{IPNS}}{1 + K_{m,ACV,IPNS} \cdot C_{ACV}^{-1}} \cdot \frac{1}{1 + C_{6APA} \cdot K_{i,6APA,IPNS}^{-1}} \quad (2)$$

5.3.3 Kinetics of Acetyl-CoA : lsopenicillin N Acyltransferase (AT)

The Acetyl-CoA : lsopenicillin N Acyltransferase is observed to have activities for isopenicillin-N amidohydrolase (IAH), isopenicillin-N acyltransferase (IAT), 6-aminopenicillanic acid acyltransferase (AAT) and penicillin amidase (PA) [5]. In the presence of PAA the production of PenG is assumed to take place by two different mechanisms, a one-step mechanism by IAT and a two-step mechanism in combination of IAH and AAT. In the absence of PAA and therewith PA-CoA, 6APA is produced by IAH. The experimental observations in the PAA step experiment showed that after the PAA step was given, accumulated intracellular levels of IPN and 6APA both decreased rapidly to produce PenG thus providing evidence of *in vivo* activities of IAT and AAT.

Acetyl-CoA: lsopenicillin N Acyltransferase (IAT)

In the one-step mechanism for PenG formation by IAT, the side chain of IPN, α-AAA, is directly replaced with the precursor PA-CoA by IAT. IAT needs two substrates, IPN (*in vitro* $K_{m,IPN,IAT}$: 23 mmol/m^3 and V_{max}: 1380 pkat/mg protein) and PA-CoA (*in vitro* $K_{m,PA\text{-}CoA,IAT}$: 6 mmol/m^3 and V_{max}: 9600 pKat/mg protein) [5]. IAT was proposed to follow two-substrate Michaelis-Menten type kinetics [135].

$$v_{IAT} = \frac{k_{IAT}}{1 + K_{m,IPN,IAT} \cdot C_{IPN}^{-1} + K_{m,PA-CoA,IAT} \cdot C_{PA-CoA}^{-1}} \quad (3)$$

lsopenicillin N Amidohydrolase (IAH)

In the two-step mechanism for PenG formation, the first step is the formation of 6APA and α-AAA from IPN (*in vitro* $K_{m,IPN,IAH}$: 4000 mmol/m^3 and V_{max}: 50 pkat/mg protein) by IAH activity [5]. Pissara et al. [135] proposed the reaction to follow Michaelis-Menten kinetics. In addition, a rapid decrease in the intracellular level of 6APA was observed in the PAA step experiment in the presence of PAA. Therefore, we assume that there is a possibility of 6APA inhibition on the activity of IAH.

$$v_{IAH} = \frac{k_{IAH}}{1 + K_{m,IPN,IAH} \cdot C_{IPN}^{-1}} \cdot \frac{1}{1 + C_{6APA} \cdot K_{i,6APA,IAH}^{-1}} \quad (4)$$

Acyl-CoA: 6APA Acyltransferase (AAT)

In the two step mechanism, in the presence of PA-CoA, the 6APA produced by IAH activity is converted to PenG. The AAT activity needs two substrates; 6APA (*in vitro* $K_{m,:6APA,AAT}$ 9.3 mmol/m^3 and V_{max}*:* 7400 pkat/mg protein) and PA-CoA (*in vitro* $K_{m,PA\text{-}CoA,AAT}$: 6 mmol/m^3 and V_{max}*:* 9600 pkat/mg protein) [5]. IAH was proposed to follow two-substrate Michaelis-Menten kinetics [5,135].

$$v_{AAT} = \frac{k_{AAT}}{1 + K_{m,6APA,AAT} \cdot C_{6APA}^{-1} + K_{m,PA-CoA,AAT} \cdot C_{PA-CoA}^{-1}} \quad (5)$$

Penicillin amidase (PA)

AT has been identified to also have penicillin amidase activity [5]. Penicillin amidase uses penicillin as a substrate, cleaves the amide bond between the side chain PAA and the 6APA nucleus, and releases PAA and 6APA [5]. In the PAA step experiment, however, there was no evidence of any activity of penicillin amidase, as there was no production of 6APA from PenG in phase II (+PAA). Therefore, the PA activity contribution is neglected in the model development.

Activity ratios of IAH : IAT : AAT

Considering the *in vitro* activities as measured by Alvarez et al. [5], we can find the ratios of the three activities. The IAH activity with respect to its substrate was found to be V_{max}*:* 50 pkat/mg protein. The maximum IAT activity of its two substrates (IPN and PA-CoA) was with respect to IPN (V_{max}*:* 1380 pkat/mg protein). The maximum AAT activity of its two substrates (6APA and PA-CoA) was for 6APA (V_{max}*:* 7400 pkat/mg protein). Thus, the ratio of IAH:IAT:AAT can be calculated as 0.04 : 1 : 5.36.

5.3.4 Kinetics of phenylacetyl-CoA ligase (PCL) for formation of PA-CoA

In the PAA step experiment, with rapid uptake of PAA it was observed that there was immediate activation of PAA to PA-CoA by PCL. Koetsier et al. [92] determined *in vitro* apparent K_m for PCL of 6100 mmol/m^3 for PAA. This K_m value was 3 times higher than the intracellular PAA levels. This suggests that the formation of PA-CoA can be described by

first order kinetics in PAA. In addition, due to rapid changes in the intracellular concentration of PA-CoA there is a possibility of feedback inhibition of PA-CoA on PCL.

$$v_{PCL} = k_{PCL} \cdot C_{PAA} \cdot \frac{1}{1 + C_{PA-CoA} \cdot K_{i,PA-CoA,PCL}^{-1}} \quad (6)$$

5.3.5 Kinetics of formation of 8HPA

The kinetics of carboxylation of 6APA to 8HPA has been found to be a first order with respect to both 6APA concentration and to the dissolved CO_2 concentration [69]. In the PAA step experiment, 8HPA was detected in the intra- and extracellular space. Henriksen et al. [69] found that pH has no effect on the carboxylation reaction because it was dissolved CO_2 that takes part in the reaction and not the bicarbonate. For the PAA step experiment, the dissolved CO_2 level was nearly constant and therefore the CO_2 concentration term can be incorporated in the rate constant.

$$v_{8HPA,in} = k_{8HPA} \cdot C_{6APA,in} \quad (7)$$

$$v_{8HPA,ex} = k_{8HPA} \cdot C_{6APA,ex} \quad (8)$$

5.3.6 Kinetics of phenyl acetate hydroxylase for formation of oOHPAA

The oxidation of PAA to oOHPAA is reported to be enzymatically catalyzed by phenylacetate hydroxylase (PAH) [65,141]. In the strain *P. chrysogenum* DS17690, an increased level of transcripts for PAH are observed in the presence of PAA [171]. Although the location of PAH was uncertain, oOHPAA has been observed to form inside the cell and then secreted [177]. We assume here that PAH is present in the cell and follows Michaelis-Menten kinetics with the enzyme capacity increasing over the period of cultivation in the presence of PAA as observed in the transcriptome studies performed by van den Berg et al. [171]. Thus, PAH capacity is expressed by an exponential time function

$$v_{PAH} = \frac{k_{PAH}}{1 + K_{m,PAA,PAH} \cdot C_{PAA}^{-1}}, \text{ where } k_{PAH} = k_{PAH,1} + k_{PAH,2} \cdot \left(1 - e^{\frac{-t}{\tau_{PAH}}}\right) \quad (9)$$

5.3.7 Kinetics of formation of 6-oxo-piperidine-2-carboxylic acid (OPC)

Another by-product that is formed during fermentation is 6-oxo-piperidine-2-carboxylic acid (OPC). This is formed by cyclization of α-AAA. A spontaneous, non-enzymatic ring closure is far too slow at 25 ^{o}C, and therefore it is assumed to be an enzymatic reaction [70,79]. The

formation of OPC is assumed to be in the linear range of Michaelis-Menten equation and thus follows first order kinetics with respect to the intracellular level of α-AAA.

$$v_{OPC} = k_{OPC} \cdot C_{\alpha-AAA} \quad (10)$$

5.3.8 Kinetics of transport processes

Transport processes across the plasma membrane are important to maintain an appropriate level of the nutrients, substrates and products in the cell for the desired pathway to work optimally. A detailed description about the secretion mechanisms of the metabolites in the penicillin pathway is described in chapter 4 of this thesis and by Douma et al. [44].

For the production of PenG, the side chain precursor PAA is added externally and a sufficient amount of PAA should be maintained in the cell for PenG production. Douma et al. [44] showed through their stimulus response experiments that PAA is very rapidly taken up by the cell by passive diffusion with a membrane permeability coefficient of (5.2 ± 1.2) x 10^{-6} m/s. The uptake of PAA for the reversible passive diffusion is given be the equation,

$$q_{diff,PAA} = k_{diff,PAA} \cdot A \cdot \left(\frac{C_{PAA,ex}}{1+10^{pH_{ex}-pK_a}} - \frac{C_{PAA}}{1+10^{pH_{in}-pK_a}} \right) \quad (11)$$

Where, $A = 4/d_{cell}$, is in m^2 of membrane per m^3 of cellular volume. Furthermore, Douma et al. [44] also showed the presence of an active secretion mechanism for PAA, consuming ATP. In the model development thus for the irreversible active export of PAA an equation similar to that developed by Douma et al. [44] is used. However, by observing the data over the longer period of time in phase II, the model equation was extended to accommodate the PAA exporter capacity to increase with time. This increase was supported from the transcriptome studies, where the transcript level of certain ABC transporters were upregulated in the presence of PAA [171,181] and therefore the active export of PAA is described by an exponential time function given by the following equation,

$$q_{sec,PAA} = k_{sec,PAA} \cdot C_{PAA} \quad \text{, where, } k_{sec,PAA} = k_{sec,PAA1} + k_{sec,PAA2} \cdot \left(1 - e^{\frac{-t}{\tau_{PAA}}} \right) \quad (12)$$

Douma et al. [44], also derived the mechanism for a reversible secretion of negatively charged ions such as $PenG^-$. For such a reversible transport a two parameter model was derived and the parameters, maximum transporter capacity of 0.83 ± 0.20 mmol/Cmol.h and K_{eq} of 73 ± 17, were estimated. However, the equation used by Douma et al., [44] was not able to

describe the situation when the starting intracellular concentration of PenG is zero because the intracellular PenG concentration term was in denominator in the equation. Therefore, the equation was modified to accommodate such a situation given by the equation,

$$q_{sec,PenG} = k_{sec,PenG} \cdot \left(C_{PenG} - \frac{C_{PenG,ex}}{K_{eq,secPenG}} \right) \qquad (13)$$

For the other pathway metabolites such as IPN^-, $6APA^-$, $8HPA^{-2}$, $oOHPAA^-$, OPC^- the secretion mechanism are explained in thesis chapter 4 and equations similar to the reversible transport of negatively charged $PenG^-$ will be used to describe the transport of the other anionic pathway metabolites. The type of transport mechanism and the resulting K_{eq} values used for the model are given in Appendix IV. It should be noted that the rate parameters in the kinetic function are proportional to enzyme level and are time dependant, whereas affinity and inhibition parameters are time independent.

5.4 Parameter estimation

The data obtained from the PAA step experiment was used to estimate the kinetic model parameters. The phase I data consisted of metabolite levels, which changed significantly but slowly, whereas after the PAA step in phase II, there were initially rapid changes in the metabolite levels that subsequently reached steady state levels. Thus, to specifically describe the two different behaviors of the metabolite levels in the two phases the parameter estimation routine was also divided in two parts and then combined with an overall optimization routine thus preserving the unity of the model for the entire cultivation period including phase I and phase II. The parameter estimation algorithm is sketched in Figure 5.2.

Phase I (0 to 192 h), which was performed in the absence of external PAA, consisted of metabolites ACV, IPN, 6APA, 8HPA, and OPC. Ten different reactions were taken along: eqs. 1, 2, 4, 7, 8, 10 and eq.13 (adapted for the secretion of IPN, 6APA, 8HPA and OPC). Levels of the mentioned metabolites varied slowly during this period, therefore they were assumed to be in pseudo steady-state. However, the variations indicated that the levels of the pathway enzymes changed over the cultivation period, stabilized after ~150 h and remained constant during phase II. The rate parameters for the pathway enzymes and transporters involved were estimated by data reconciliation performed for each data point in phase I as per the routine described by Verheijen [178]. The total number of parameters estimated in phase I

were 72 using 81 data points and 10 kinetic equations. For this estimation problem the affinity parameters were kept constant.

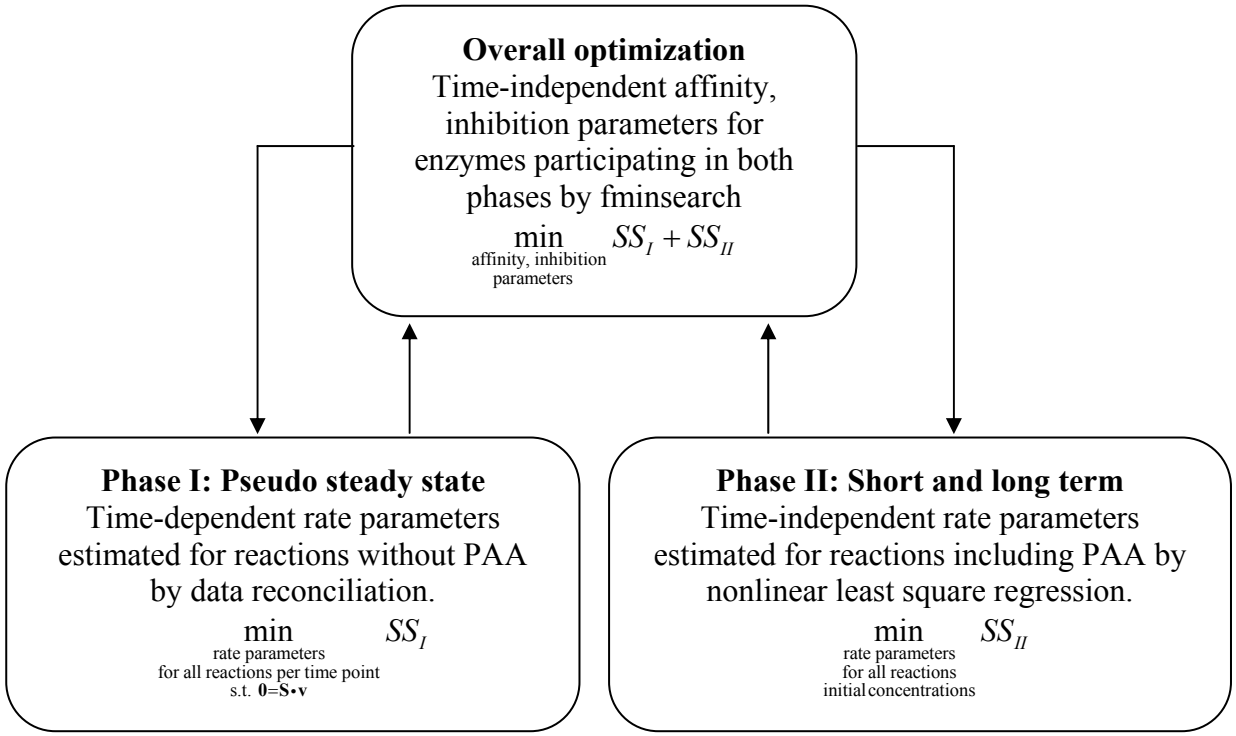

Figure 5.2: Algorithm to find the parameters in the two phases, where SS is the sum of squares of residuals, the difference between data and model weighted by the experimental error.

For phase II, the dynamic data obtained after the PAA step were used. Metabolites, whose concentrations dropped below their detection limits, were assumed to have a concentration value of zero with an error equal to that of the lowest concentration. The metabolites that took part in phase II in addition to those in phase I were PAA, PA-CoA, PenG, and oOHPAA. The model in phase II was described by 16 dynamic mass balances that contained 18 reaction rates. An ODE-solver calculated the concentration profile to be compared with the dynamic data. For each reaction a constant rate parameter was taken except those of PAH and PAA exporter which are given by eqs. 9 and 12. These parameters, together with the initial concentrations at the start of the PAA step, were estimated by non-linear weighted regression using the least squares curve fit function in MATLAB. The total parameters estimated in phase II were 28 using 398 data points and 18 kinetic equations.

In both phases the affinity and inhibition parameters were kept the same for the solution of the individual estimation problems. In order to estimate these affinity and inhibition parameters

for the enzymes that are participating in both the phases, the sum of squares obtained from both phases were combined and minimized. These parameters were estimated by unconstrained nonlinear optimization using the fminsearch algorithm in MATLAB. The final result consisted of the time independent affinity and inhibition parameters, the time dependent rate parameters for each time point in phase I, the time independent rate parameters for phase II.

5.5 Results

5.5.1 Phase I: Absence of PAA

In phase I, assuming pseudo steady state condition, data reconciliation was performed on each data point. Some of the affinity and inhibition parameters were found to be collinear during parameter estimation and therefore could not be estimated. In these cases parameters were obtained from literature (see Table 5.A1). Some of the affinity and inhibition parameters were estimated to be out of their respective concentration ranges, therefore they could not be well determined (see Table 5.A3). All other affinity and inhibition parameters were estimated by the overall optimization routine (see Table 5.A2).

The model estimations of the concentrations fit well to the experimental data within the errors of the model (Figure 5.3). The model estimation of the rate parameters for each data point is shown in Figure 5.4A and the corresponding fold change in the enzyme levels (using the time period of PAA addition as reference) is shown in Figure 5.4B. After the end of the batch phase, the enzyme levels of ACVS and IAH showed typical behavior of induction after the end of batch phase and increased up to 75h, thereafter they decreased and reached a pseudo steady state level after 150h. The estimation of IPNS enzyme level had relatively large errors, however, within the error range IPNS level was stable over the cultivation period. From Table 5.A4, we see that the estimated enzyme capacity of IPNS is 2-10 times higher than the capacity of ACVS, whereas IAH capacity is more than 100 times higher than ACVS capacity. The transporter rate constants for secretion of IPN and 6APA also increased after the batch phase until 75 h, thereafter they remained constant, whereas the transporter rate constants of 8HPA and OPC remained stable over the period of phase I cultivation.

Figure 5.5 shows fluxes through the pathway enzymes ACVS, IPNS, and IAH and the secretion fluxes of the pathway metabolites. The flux through ACVS increased as there was induction of ACVS, however, it further dropped as the enzyme level decreased. The flux

through IPNS was the same as that of flux through ACVS as it is assumed that there is no secretion of ACV. The capacities of IPNS and IAH were much higher as compared to the flux flowing through the pathway. In the absence of PAA, there was a significant secretion of IPN and 6APA. The formation of 8HPA was of the same order of magnitude intra and extracellularly. Only 0.05% of the total flux flowing through the pathway goes towards the formation of intracellular 8HPA.

A) Intracellular level of the penicillin pathway metabolites based on per m^3 of the cell volume for phase I and phase II

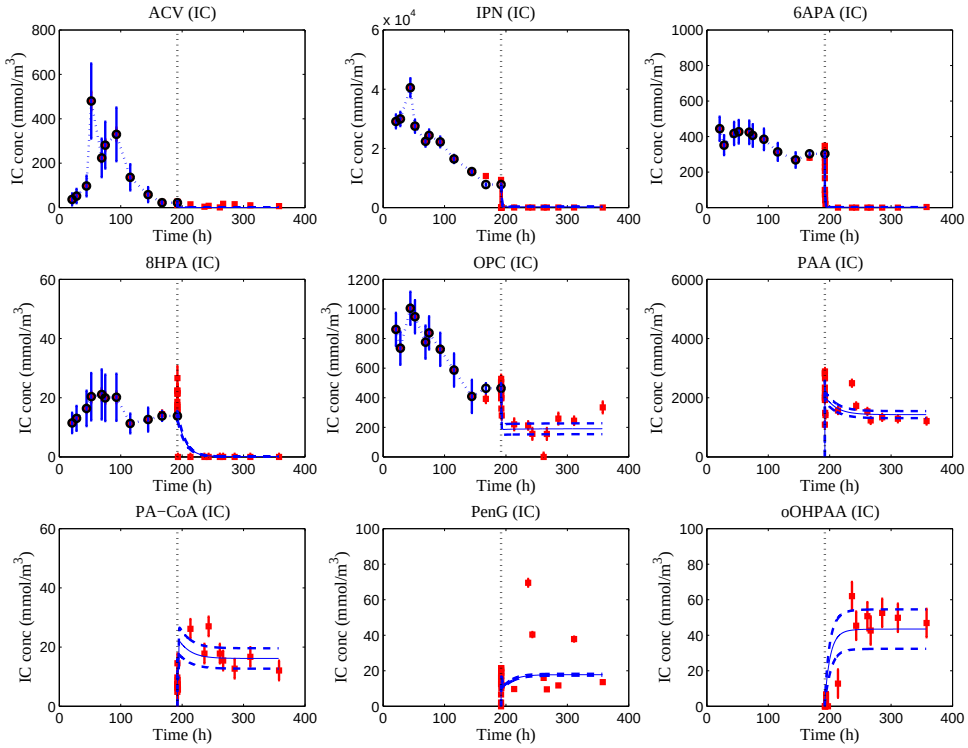

B) Extracellular level of the penicillin pathway metabolites based on per m^3 of the fermentor volume for phase I and phase II

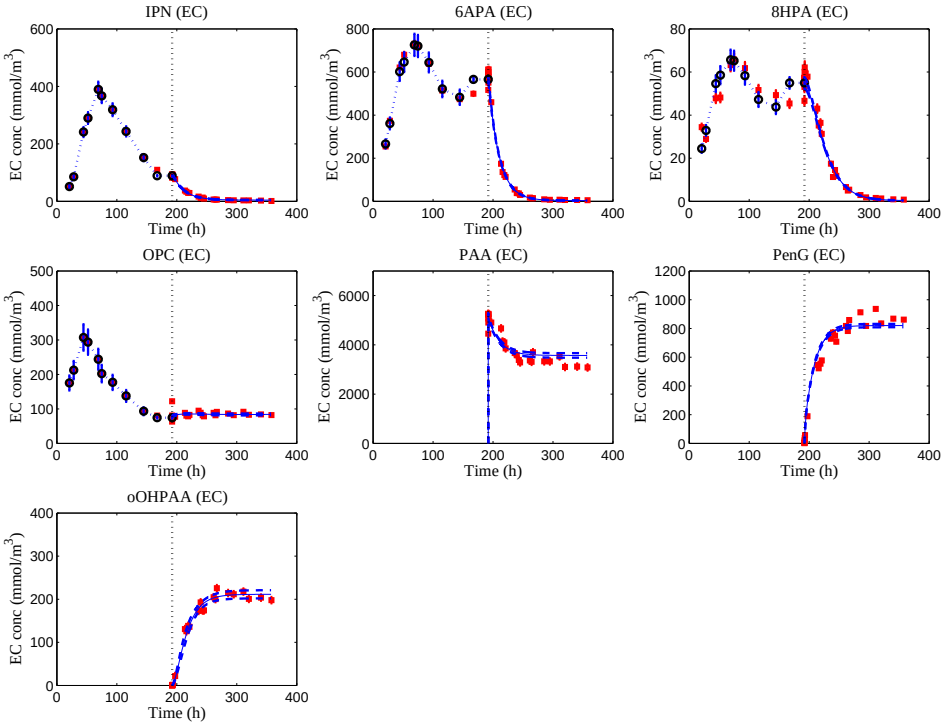

Figure 5.3: [A] Model estimation of intracellular metabolite levels [B] Model estimation of extracellular metabolite levels. For phase I, the metabolite levels are obtained by data reconciliation, represented by blue circles connected by dotted line at each data point. For phase II, solid line (-) represent the model estimation of metabolite levels and the dotted line (--) represent the error region of the model. Open red squares represent the experimental values. The vertical dotted line separates phase I and phase II.

A) Enzyme capacities based on per m^3 of the cell volume and rate constants

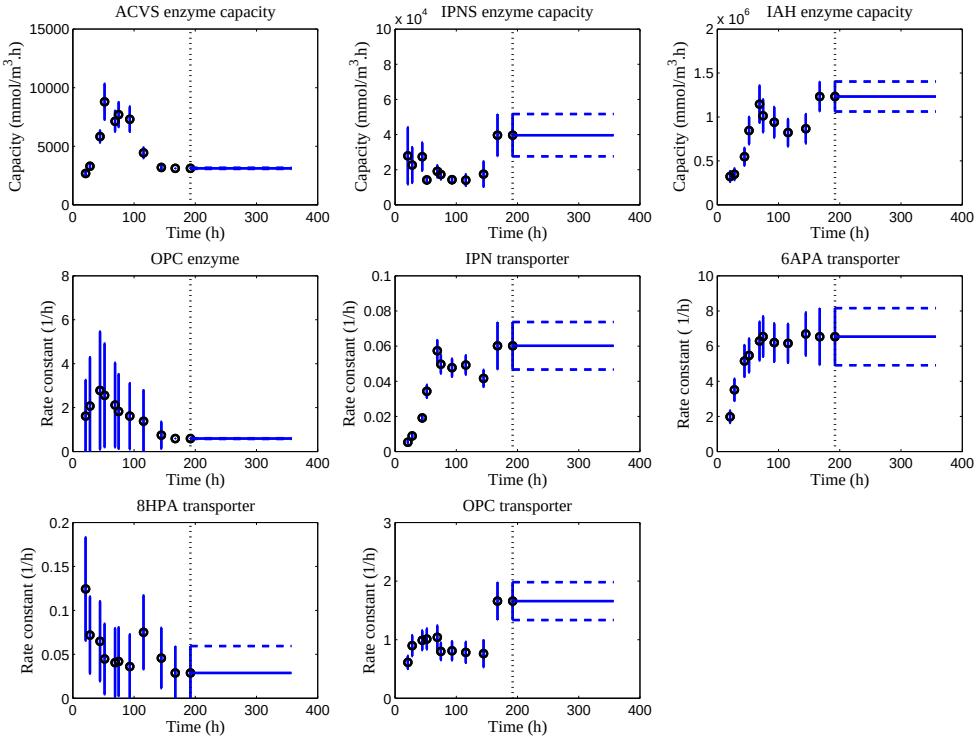

B) Fold change in enzyme levels and rate constants

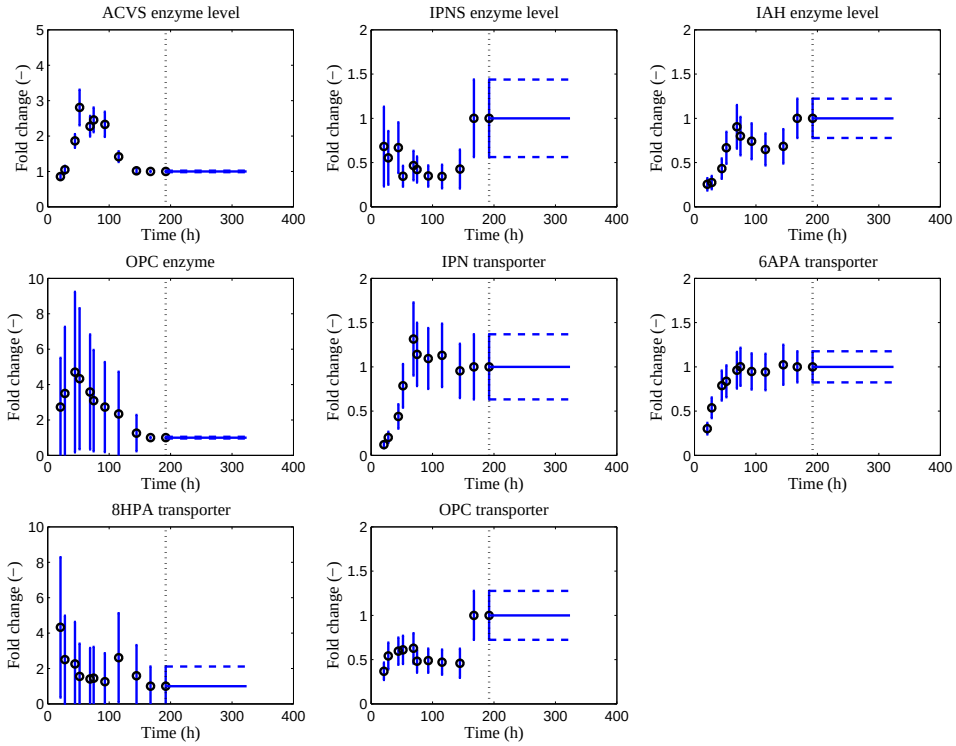

Figure 5.4: [A] Model estimation of enzyme capacities by data reconciliation in phase I, represented by blue circles at each data point. For phase II, enzyme capacities are assumed to be constant with a value as estimated at the start of phase II. [B] The fold changes in the enzyme levels by considering that the level reaches 1 at the end of phase I. The vertical dotted line separates phase I and phase II

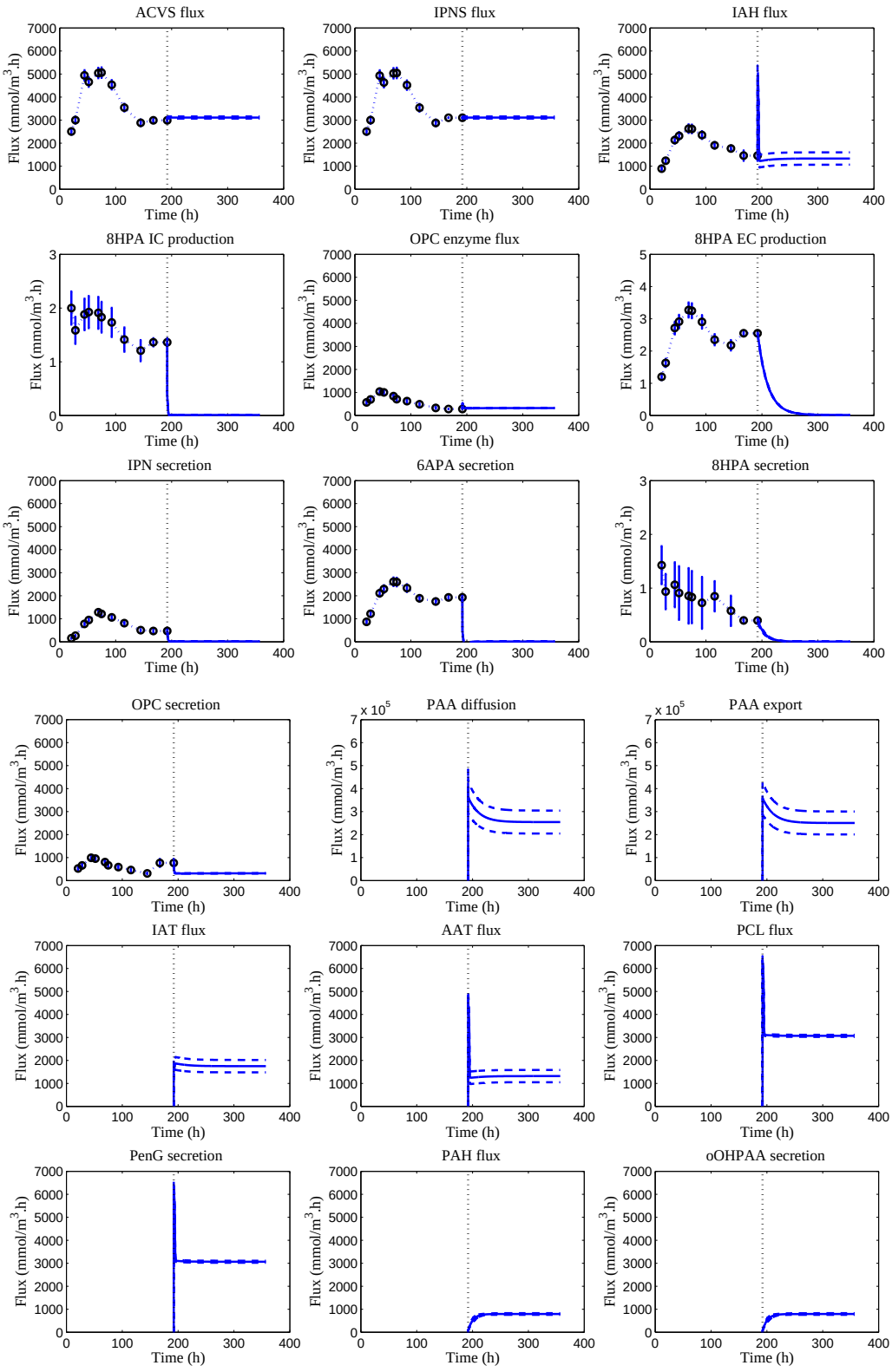

Figure 5.5: Model estimation of fluxes through the penicillin biosynthesis pathway. Phase I fluxes represented by blue circles are estimated by data reconciliation at each data point. For phase II, solid line (-) represent the model estimation of the fluxes and the dotted line (--) represent the error region of the model. All the fluxes are based on per m^3 of the cell volume, except for 8HPA EC production where the production rate is based on per m^3 of the fermentor volume. The vertical dotted line separates phase I and phase II.

5.5.2 Phase II: Short term response after PAA step

In phase II, the estimation of the parameters was performed for a time frame of 1 h. The discrete measurements of cell dry weight and intracellular α-AAA, used as input to the model, were made continuous by fitting them with an exponential and Gaussian function respectively. The concentration patterns estimated by the model matched well with the measurements and the model was able to estimate the rapid dynamics through the penicillin pathway (Figure 5.6A). As there was no evidence for changing enzyme levels for most of the penicillin pathway enzymes in phase II, they were kept at constant levels in the model (Figure 5.4), except the change in PAA exporter capacity and PAH capacity that catalyzes oOHPAA. These two enzymes were assumed to increase (by induction) in the presence of PAA. From the dynamics in the offgas O_2 measurements after the PAA step, the time constant for the PAA exporter was estimated as 0.21 h. Here we assume that the energy consumed by the PAA exporter in the form of ATP, is represented by the observed increase in oxygen uptake rate in the PAA step experiment. The time constant for PAH was estimated to be 8.4 ± 3.3 h by parameter estimation routine for phase II.

The fluxes estimated for the first 1h after the PAA step, are depicted in Figure 5.6B. After the PAA step, the model calculated an initial uptake flux of 4 x 10^5 mmol/m^3.h for PAA by considering passive diffusion, with a membrane permeability coefficient of 0.0162 ± 0.0032 m/h ((4.50 ± 0.88) x 10^{-6} m/s). With this high uptake rate there was also immediate active export of PAA starting from zero and reaching almost the same export rate as that of the uptake rate of PAA, excluding the small PAA consumption for PenG and oOHPAA production. With the availability of intracellular PAA the intracellular flux through PCL to produce PA-CoA increased to ~6500 mmol/m^3.h. With the availability of PA-CoA, IAT and AAT simultaneously started producing PenG. The PenG flux through IAT immediately increased from 0 to 1870 ± 280 mmol/m^3.h and the PenG flux through AAT from 0 to 4630 ± 390 mmol/m^3.h. The flux through PCL was equivalent to the flux that was handled combined by IAT and AAT to produce PenG. Thus, the total PenG production is the summation of the fluxes through IAT and AAT. The secretion rate of PenG equals the intracellular PenG production rate because the intracellular accumulation of PenG was very small.

A) Concentration estimation for first 1 h in phase II

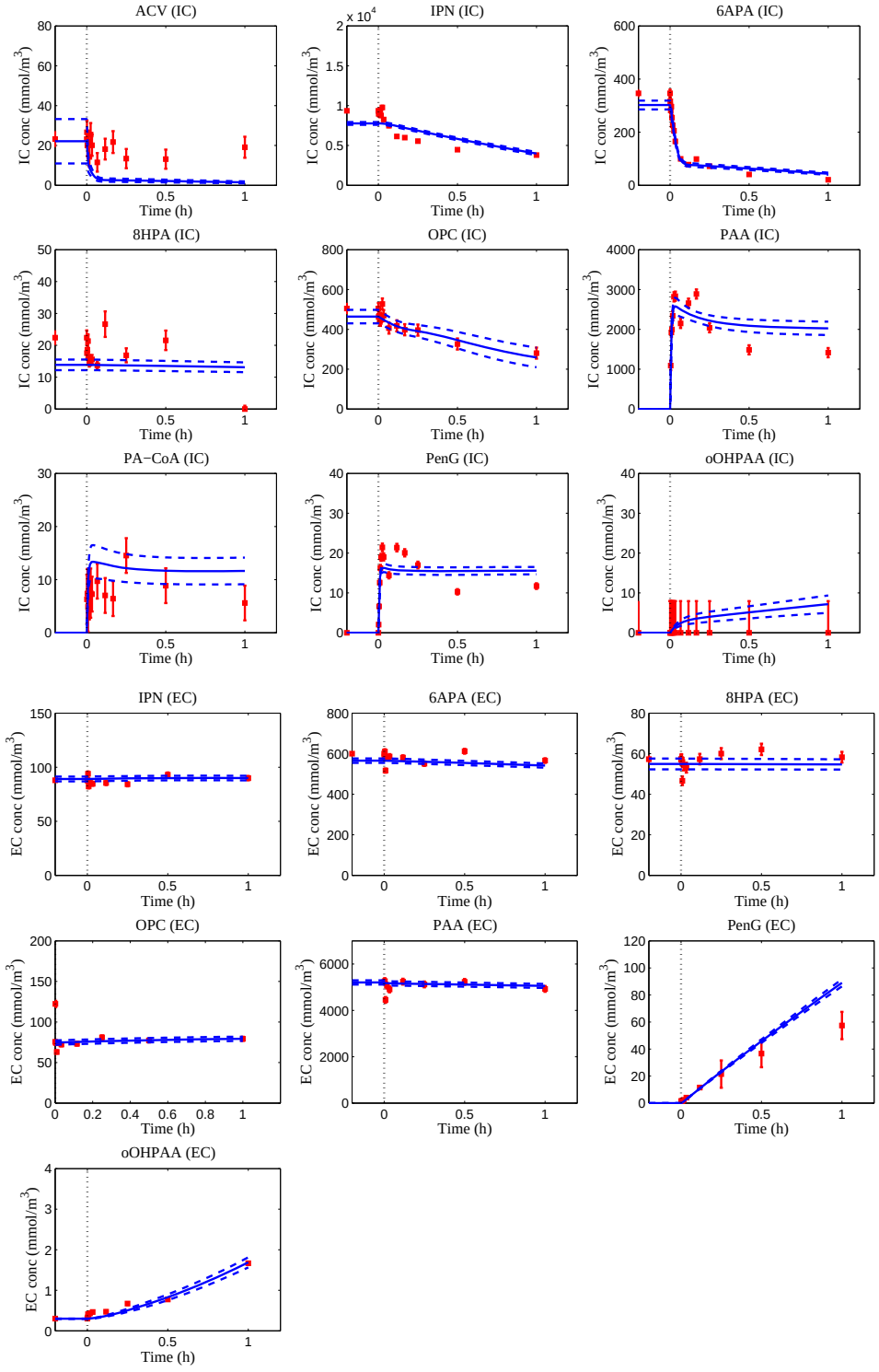

Figure 5.6: [A] Model estimation of metabolite concentrations for first 1 h after the PAA step. Open squares represent experimental data and error bars represent standard error. Solid line (-) represent the model estimation of the concentration and the dotted line (--) represent the error region of the model.

B) Flux estimation for first 1 h in phase II

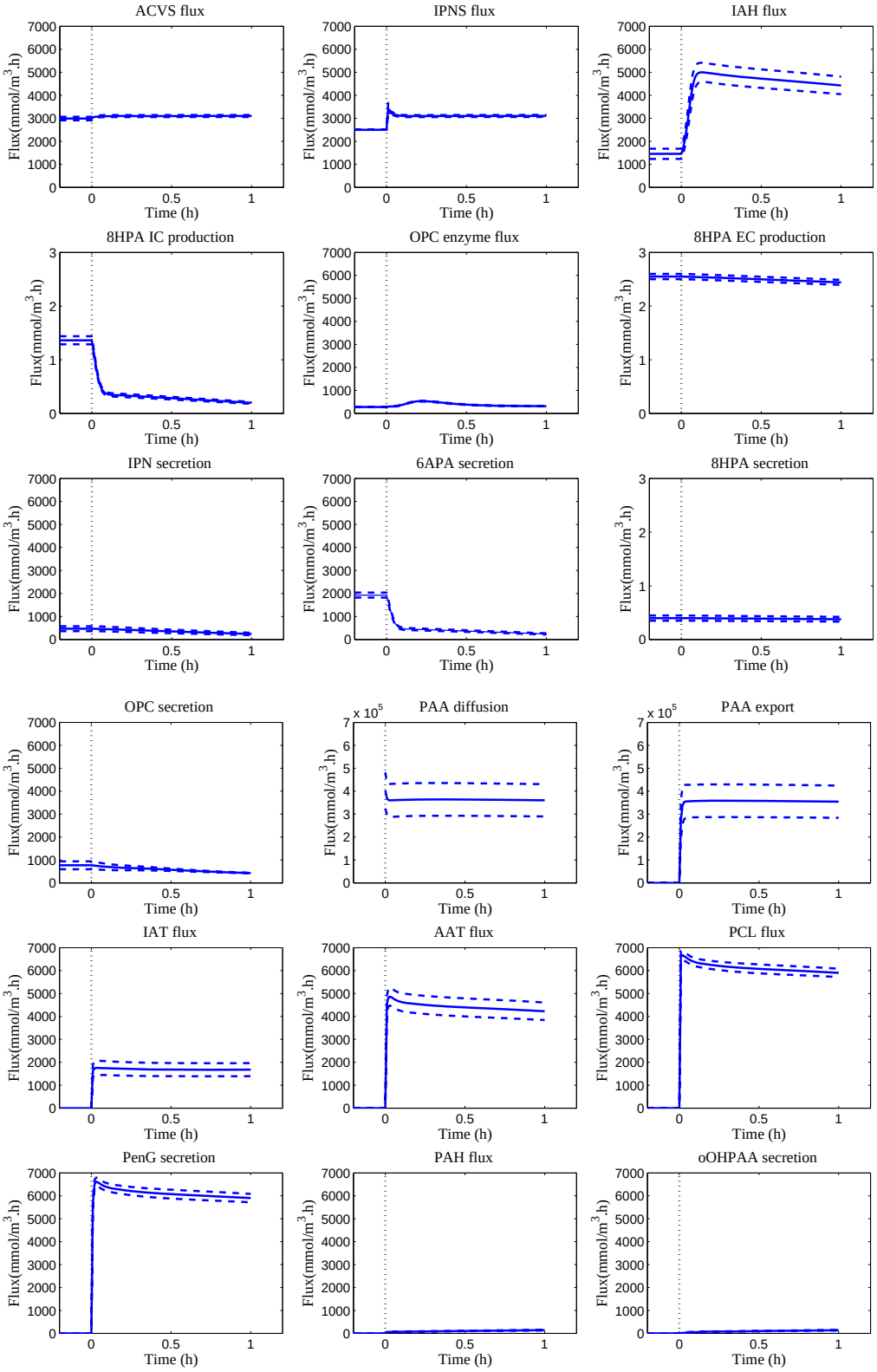

Figure 5.6: [B] Model estimation of fluxes through the penicillin biosynthesis pathway for first 1 h after the PAA step. Solid line (-) represents the model estimation of the fluxes and the dotted line (--) represents the error region of the model. All fluxes are based on per m^3 of the cell volume, except for 8HPA EC production where the production rate is based on per m^3 of the fermentor volume.

The flux through AAT eventually started decreasing as its substrate 6APA depleted, while the flux through IAT sustained. The capacity of IAT was ~3 to 4 times less than the capacity of AAT. With decrease in the 6APA level to values lower than the inhibiting concentration of 10 μM 6APA for IAH, the flux through IAH increased rapidly from 1460 ± 220 mmol/m^3.h at the end of phase I to 4950 ± 410 mmol/m^3.h consuming IPN and producing 6APA. However, as its substrate IPN depleted, the flux through IAH also decreased. Although the PenG production increased upto 6375 ± 170 mmol/m^3.h the flux through ACVS and IPNS remained with the error region and hence unchanged (2990 ± 80 mmol/m^3.h). Therefore, the high initial PenG production rate was achieved only because of accumulated pools of IPN and 6APA. ACV feedback inhibition does not play any role in phase II as the estimated inhibition constant is almost 50 times larger than the intracellular ACV concentration.

5.5.3 Phase II: Long term response in the presence of PAA

As the model estimation of the metabolite concentrations fits well to the experimental data and they reach steady state, this confirms the assumption that the pathway enzyme capacities remain constant over phase II of the cultivation period. With the depletion of accumulated intracellular IPN and 6APA (Figure 5.3) , the PenG production decreased (Figure 5.5) and reached a steady state rate of 3070 ± 40 mmol/m^3.h, similar to the flux through ACVS at the end of phase I. This additionally confirms our hypothesis that the pathway enzyme capacities do not change in phase II. With drop in intracellular IPN levels below the K_m value of IAH, the flux through IAH decreased. The most remarkable thing to note is that after reaching the steady state, there is still a considerable flux through IAH-AAT pathway (1330 ± 270 mmol/m^3.h) compared to the flux through IAT pathway (1750 ± 270 mmol/m^3.h) for PenG production. This was even when the 6APA concentration decreased below the detection limit (0.4 mmol/m^3). This indicates that both the pathways are important for the production of PenG. With the depletion of intracellular IPN, the secretion rate of IPN decreased to a very low level (16 ± 3 mmol/m^3.h). The secretion rate of 6APA also decreased significantly and after 2.5 h of the PAA step there was even a small amount of 6APA uptake (uptake rate of 25 ± 3 mmol/m^3.h) from the extracellular space. However, this uptake was only for a short period and in the steady state 6APA is secreted in small amount (14 ± 3 mmol/m^3.h). With the increasing PAH level in phase II, the production/secretion of oOHPAA also increased significantly and reached a steady state value of 790 ± 35 mmol/m^3.h. The OPC production and secretion rates were in steady state (315 ± 10 mmol/m^3.h).

5.5.4 Flux control coefficients

In order to identify possible bottlenecks in the penicillin biosynthesis pathway, it is important to understand how the flux is controlled by the individual enzymes and/or transporters in the pathway. This can be achieved by determining the flux control coefficients that represents the sensitivity of the pathway flux to the changes in the enzyme level in a pathway and thus allows identifying those enzymes/transporters which are targets for genetic modification of the flux controlling enzyme [50,81,82,135]. The flux control coefficient are calculated as

$$C_i^J = \frac{\Delta J / J}{\Delta e_i / e_i} \qquad (14)$$

where ΔJ is the change in the flux, which in this case can be taken as change in the secretion rate of important products (6APA in phase I and secretion rate of PenG phase II), because of fractional change in enzyme or transporter levels Δe_i in the network described by the model shown in Figure 5.1.

Flux control for 6APA in phase I

As 6APA is the most important byproduct of phase I, flux control coefficients with respect to 6APA secretion rate (Figure 5.7) were obtained with the help of the developed kinetic model. For the first 50 h, ACVS was the dominating enzyme as it has a control of 50% on the 6APA secretion rate. For the cultivation period from 50 h to ~ 115 h, the control shifted from ACVS to 6APA transport (~45%). However, from 115 h onwards, ACVS controlled the 6APA secretion rate and increased upto 70% by the end of phase I. It is also interesting to note that during the first 50 h a significant amount of flux was associated with the growth associated dilution term $\mu.C_{IPN}$ due to high accumulation of IPN in the cell, where μ is specific growth rate of the biomass.

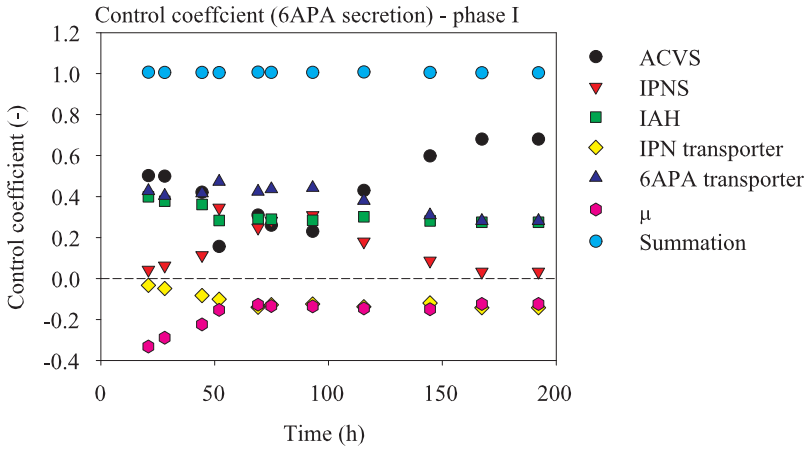

Figure 5.7: Flux control coefficient with respect to 6APA secretion in phase I.

Flux control for PenG in phase II

In phase II, PenG is the relevant product and in the presence of PAA, the rate of 6APA secretion drops to zero and the fluxes are directed towards PenG production. Therefore, flux control coefficients are calculated with respect to the PenG secretion rate when the system reaches steady state after 100 h after the PAA step. Control coefficients thus obtained with the help of the developed kinetic model indicates that 94% of the PenG secretion rate was controlled by ACVS in the steady state. IPNS controlled 3.5% flux, wheras IAT controlled 2% flux, The control of flux by all the other enzymes/transporters was less than 1% and therefore not playing any role for controlling the flux through the penicillin biosynthesis pathway.

5.6 Discussion

In the quest to understand the *in vivo* enzyme kinetics and to investigate possible bottlenecks in the penicillin biosynthesis pathway, a kinetic model was constructed. The kinetic model describes the mechanisms of the penicillin pathway enzymes and the transporter proteins of the precursor (PAA) and (by)-products. The data obtained from thesis chapter 4 were used to estimate kinetic parameters of the enzymes of the penicillin biosynthesis pathway.

5.6.1 Phase I: Absence of PAA

The model simulations for the penicillin biosynthesis pathway, for the high producing *P. chrysogenum* strain cultivated in the absence of PAA, were able to describe the changing pattern of metabolite levels by allowing changes in enzyme capacities. The increase in enzyme capacities of ACVS and IAH represents the typical behavior of induction of enzymes after the end of the batch phase in accordance to the earlier assumption that the gene encoding these enzymes are repressed at high glucose concentrations [51,63]. After reaching a maximum β-lactam flux capacity of ~8800 mmol/m^3.h, the capacity of ACVS decreased almost 2-3 fold within 192 h (Figure 5.4B), a phenomenon described as degeneration [35,42]. The estimated decrease in the ACVS enzyme capacity was similar to the measured decrease in ACVS enzyme capacity as observed by Douma et al. [42] in their studies for degeneration. The estimated IPNS enzyme capacity pattern was, however, different than their IPNS enzyme measurements. This can be due to difference in the experimental conditions. They cultivated the strain in presence of PAA, whereas the phase I of the PAA step experiment was conducted in the absence of PAA. Under these conditions, the IPN produced in the cell is not effectively consumed and therefore might lead to a different induction of IPNS. The estimated IPNS

capacity in the absence of PAA remains stable within the errors over the cultivation period. For each data point in phase I, the estimated capacity of IPNS and IAH are always higher than the capacity of ACVS; therefore these will never control the flux through the pathway. When flux control coefficients were calculated with respect to the 6APA secretion rate, it confirmed that ACVS controls the flux during the first 50 h and again after 100 h of the cultivation period. For a short period, the 6APA secretion rate was controlled by the 6APA transporter. By the end of phase I, 70% of the flux was controlled by ACVS. This is in agreement with the outcome of the metabolic control analysis carried out by Pissara et al. [135] from their fed batch studies for PenV production. They estimated that in the absence of feedback inhibition of ACV on ACVS, the pathway flux was controlled by ACVS [135]. Thus, improvement in the capacity of ACVS is again identified as the primary metabolic engineering target for improvement of the fluxes through the pathway.

In the absence of PAA, there was significant 6APA production. The maximum flux through IAH for 6APA production was about 2630 ± 185 mmol/m^3.h, which was 50% of the maximum PenG production (5000 mmol/m^3.h) under similar chemostat cultivation conditions in the presence of PAA [37,120]. This shows that the activity of IAH is significant and not just only a residual activity of AT as observed by Alvarez et al. [5] in their *in vitro* studies. Their observation may be different because they did not take into account the feedback inhibition of IAH by the product 6APA. We estimated a feedback inhibition parameter of 6APA for IAH of about 10 μM. Alvarez et al. (1993) observed in *in vitro* studies that IAH was able to produce 30 μg of 6APA/mL, which is equivalent to 139 μM. This 6APA concentration is 14 times higher than our estimated inhibition parameter. Therefore, the activity of IAH might have been significantly reduced in their *in vitro* assay. The estimated $K_{m,\ IPN}$ value (< 2 x 10^5 mmol/m^3) for IAH with respect to intracellular IPN was not similar to the *in vitro* value (4000 mmol/m^3) observed by Alvarez et al. [5].

Our studies thus indicate that if the intracellular level of 6APA is kept below its inhibiting concentration for IAH by efficiently and irreversibly secreting 6APA, then in the absence of PAA, IAH will be able to produce a large amount of 6APA. This indicates that 6APA, which is the starting material for the production of semi-synthetic antibiotics such as ampicillin and amoxillin, and is currently obtained from the hydrolysis of penicillin-G, can be in principle produced directly from fermentation, however, an effective exporter is needed to keep a non-inhibiting level of intracellular 6APA.

5.6.2 Phase II : Short and long term response in the presence of PAA

In phase II, all the enzyme capacities and rate constants were kept constant except for the PAA exporter capacity and PAH capacity. These two enzymes were assumed to increase with time. This is in agreement with the transcript studies performed by Harris et al. [65] that in the presence of PAA, the PAH and several ABC transporters are up-regulated. For all the other enzymes and the transporters the rate constants were kept constant for the first 1 h and also up to new steady state in the presence of PAA.

After the PAA step, with the availability of PA-CoA the formation of PenG starts immediately by using the accumulated intracellular IPN and 6APA. This formation takes place by IAT and AAT, the two activities of AT. AT is one enzyme complex and is known to have three activities of IAH, IAT and AAT. *In vitro* studies have shown that the V_{max} ratio of IAH : IAT : AAT was 0.04 : 1 : 5.4 [5]. Another study by Pissara et al. [135] estimated capacities of IAH, IAT and AAT by their kinetic model. Nonetheless, they did not fix the ratio of the V_{max} of the three activities of AT as obtained by *in vitro* studies by Alvarez et al. [5] and estimated the ratios as 0.3 : 1 : 0.14 for IAH : IAT : AAT [135]. These ratios obtained by Pissara et al. [135] were completely different than those obtained by the *in vitro* studies. In both cases the inhibition by 6APA of IAH was not considered. Therefore, in order to estimate the capacities of the three activities of AT, we investigated both conditions by imposing the two sets of ratios as constants, but no satisfactory fit could be obtained. The best fit was obtained only when the capacities of three activities of the AT were estimated by considering the inhibition by 6APA for IAH and by not fixing the ratio of IAH : IAT : AAT. The ratio of the estimated capacities was 700 : 1 : 3 (Figure 5.4A). Thus, our estimation with respect to the ratio of IAT:AAT is much closer to that obtained by the *in vitro* studies by Alvarez et al. [5]. The main reason that our estimation of the IAH capacity is much higher than the *in vitro* studies is because we included the inhibition of IAH by 6APA.

In phase II after the PAA step change, the model estimated the fluxes in the penicillin biosynthesis pathway (Figure 5.5). The undissociated form of PAA enters the cell by passive diffusion with a flux of 4 x 10^5 mmol/m^3.h with membrane permeability close to that found by Douma et al. [44]. The uptake rate of PAA was 100 times higher than the maximum production rate of PenG (~6400 mmol/m^3.h). Therefore the uptake of PAA was not limiting the production of PenG. This confirms the outcome proposed by Douma et al. [44] during their studies for the PAA transport. Furthermore, we also incorporated the PAA exporter in

the model to obtain proper fit for the intra- and extracellular PAA levels, in confirmation of the model proposed by Douma et al. [44]. This indicates that due to the high PAA uptake rate, cells immediately start exporting PAA in order to avoid the acidification of the intracellular space because of the dissociation of PAA at intracellular pH of 7.2. This futile cycling, which consumes significant amount of energy, can be avoided if the PAA exporter is identified and deleted.

With the intracellular availability of PAA, there was immediate formation of PA-CoA by PCL with the flux increasing to a maximum of ~ 6500 mmol/m^3. h. This fast production of PA-CoA by PCL is proposed in the model by a first order kinetic function with respect to the intracellular PAA but is affected by the product feedback inhibition. Alternatively, Michaelis-Menten equation type rate equation was tested with the *in vitro* $K_{m,PAA,PCL}$ value of 6100 mmol/m^3 for PAA [92]. However, with such a high K_m value the model could not estimate the rapid formation of PA-CoA. When the model was allowed to estimate the k_{PCL} and $K_{m,PAA,PCL,}$, a correlation was observed between them, and therefore individual values could not be estimated. Another rate equation was tested based on first order function in PAA without the inhibition term. However, without the feedback inhibition term, the model was not able to describe the long term trends in the intracellular PA-CoA in the presence of PAA. Ultimately, the assumption of the first order function and with product inhibition gave good fit for the intracellular PA-CoA.

With the availability of PA-CoA, IPN and 6APA, the production of PenG started immediately, reaching a flux of ~6400 mmol/m^3.h and a similar secretion rate. This indicated that the PenG secretion rate was not limiting under the current experimental conditions. This agrees with the conclusion reached by Douma et al. [44]. The PenG production takes place by two routes: IAH-AAT route and IAT route. As the capacity of IAH-AAT route is much higher but having a large $K_{m,IPN,IAH}$ (< 2x 10^5 mmol/m^3), this route is the high capacity but low affinity route. Whereas, PenG production by IAT route having lower $K_{m,IPN,IAT}$ of 23 mmol/m^3 as compared to $K_{m,IPN,IAH}$ (< 2x 10^5 mmol/m^3) is the low capacity and high affinity route.

In the end the flux control coefficients were calculated in order to identify the enzyme that is a bottleneck for increasing the production of PenG. The flux control coefficients point out that ACVS controls 94% of the flux through the penicillin biosynthesis pathway. Therefore,

modifying ACVS through genetic engineering or constructing a synthetic enzyme could provide a solution.

5.6.3 Affinity and inhibition parameters: Comparison between *in vivo* and *in vitro*

The model could not estimate affinity parameters such as $K_{m,ACV,IPNS}$, $K_{m,IPN,IAT}$, $K_{m,PA\text{-}CoA,IAT}$ $K_{m,6APA,AAT}$, $K_{m,PA\text{-}CoA,AAT}$ and inhibition parameter $K_{i,ACV,ACVS}$, however, the model fit was good even with the parameters obtained from the literature (Table 5.A1). However, this was not the case for affinity parameters $K_{m,IPN,IAH}$ (4000 mmol/m^3), where it did not provide satisfactory fit to the data. The model estimation of this parameter was, however, outside the concentration range of the available data and therefore were not determined (see Table 5.A3).

5.7 Conclusions

To understand the *in vivo* enzyme kinetic properties of the penicillin biosynthetic pathway in *P. chrysogenum,* a dynamic model of the pathway, was constructed. In this model the formation of several byproducts as well as the transport of precursor (PAA), intermediates/by-products (IPN, 6APA, 8HPA, oOHPAA and OPC), and the product penicillin-G over the cytoplasmic membrane were included. The proposed model estimates the pseudo steady state and time-dependent metabolic states of *P. chrysogenum* cells under *in vivo* conditions during the long term chemostat in absence and presence of PAA. The model is capable of describing the flux through the biosynthetic pathway and predicting changes in the levels of intra- and extracellular metabolites. Additionally, one of the important contributions of the model was its capability to estimate changing rate parameters, which reflects the changing levels for enzymes/transporters in the penicillin biosynthesis pathway.

The estimated enzyme capacities in the phase I showed induction and degeneration of the enzymes in the pathway in agreement with previous direct experimental measurements of these enzymes. Furthermore, the capacity of the three different activities of AT were estimated. In phase II, with the availability of PA-CoA, PenG is produced by two routes: IAH-AAT and IAT, both routes contributing significant flux for PenG production. The flux control coefficient points out that in phase I, control of 6APA production shifts from ACVS to 6APA transporter and back to ACVS which controls 70% of the flux by the end of phase I, whereas in phase II, 94% of PenG production rate is controlled by ACVS.

5.8 . Acknowledgements

We acknowledge the financial support from the Netherlands Organization for Scientific Research (NWO) via the IBOS (Integration of Biosynthesis and Organic Synthesis) programme of Advanced Chemical Technologies for Sustainability (ACTS) (project nr: IBOS 053.63.011) and was also financially supported by DSM. This project was carried out within the research programme of the Kluyver Centre for Genomics of Industrial Fermentation, which is part of the Netherlands Genomics Initiative/ Netherlands Organization for Scientific Research.

5.9 . Appendix

5.9.1 Appendix I

The following observations/assumptions were taken into account while setting up the model equations.

A) Kinetic assumptions

ACVS: eq. 1

ACVS is independent of precursor amino acids.

Feedback inhibition of ACVS by intracellular ACV with $K_{i,ACV}$: 540 mmol/m^3.

As intracellular bisACV is absent, inhibition term by bisACV is absent.

IPNS: eq. 2

Inhibition of IPNS by intracellular 6APA.

Inhibition by GSH is coupled in the IPNS enzyme capacity term (k_{IPNS}).

The dissolved oxygen concentration term is coupled in the IPNS enzyme capacity (k_{IPNS}) .

IAH: eq. 4 - Inhibition of IAH by intracellular 6APA.

PA activity is not considered.

PCL: eq. 6 - Inhibition of PCL by intracellular PA-CoA.

B) Assumptions with respect to enzyme and transporter levels

In phase I, ACVS, IPNS, IAH, and OPC enzyme levels change with time.

In phase I, the transporter levels for IPN, 6APA, 8HPA and OPC change with time.

In phase II, except PAH enzyme level and PAA exporter level all other enzyme levels are kept constant.

PAH enzyme level (eq. 8) and PAA exporter level (eq. 11) changes with time in phase II defined by an exponential increase.

C) Assumptions with respect to transport mechanisms

IPN is irreversibly secreted by proton antiport.

6APA, 8HPA, oOHPAA, OPC, PenG are reversibly secreted using membrane potential as driving force using uniport mechanism.

PAA diffuses passively through the plasma membrane and is actively irreversibly exported using ABC transporter.

D) Observations from PAA step experiment

ACV secretion is negligible.

Intracellular bisACV is not formed.

Intracellular glutathione concentration is constant.

Dissolved O_2 and CO_2 levels are constant.

oOHPAA is formed inside the cell and secreted.

Penicillin amidase activity is not observed.

5.9.2 Appendix II

Balance equations for intracellular metabolites

$$\frac{dC_{ACV}}{dt} = v_{ACVS} - v_{IPNS} - \mu \cdot C_{ACV}$$

$$\frac{dC_{IPN}}{dt} = v_{IPNS} - v_{IAH} - v_{IAT} - q_{\mathrm{sec},IPN} - \mu \cdot C_{IPN}$$

$$\frac{dC_{6APA}}{dt} = v_{IAH} - v_{AAT} - v_{8HPA} - q_{sec,6APA} - \mu \cdot C_{6APA}$$

$$\frac{dC_{PenG}}{dt} = v_{IAT} + v_{AAT} - q_{sec,PenG} - \mu \cdot C_{PenG}$$

$$\frac{dC_{8HPA}}{dt} = v_{8HPA} - q_{sec,8HPA} - \mu \cdot C_{8HPA}$$

$$\frac{dC_{PAA}}{dt} = q_{diff,PAA} - v_{PCL} - v_{PAH} - q_{sec,PAA} - \mu \cdot C_{PAA}$$

$$\frac{dC_{oOHPPA}}{dt} = v_{PAH} - q_{sec,oOHPAA} - \mu \cdot C_{oOHPAA}$$

$$\frac{dC_{OPC}}{dt} = v_{OPC} - q_{sec,OPC} - \mu \cdot C_{OPC}$$

Balance equations for extracellular metabolites

$$\frac{dC_{IPN,ex}}{dt} = \left(q_{sec,IPN} \cdot C_x \cdot V_x\right) - D \cdot C_{IPN,ex}$$

$$\frac{dC_{6APA,ex}}{dt} = \left(q_{sec,6APA} \cdot C_x \cdot V_x\right) - v_{8HPA,ex} - D \cdot C_{6APA,ex}$$

$$\frac{dC_{PenG,ex}}{dt} = \left(q_{sec,PenG} \cdot C_x \cdot V_x\right) - D \cdot C_{PenG,ex}$$

$$\frac{dC_{8HPA,ex}}{dt} = \left(q_{sec,8HPA} \cdot C_x \cdot V_x\right) + v_{8HPA,ex} - D \cdot C_{8HPA,ex}$$

$$\frac{dC_{PAA,ex}}{dt} = q_{\mathrm{sec},PAA} \cdot C_x \cdot V_x - q_{diff,PAA} \cdot C_x \cdot V_x + D \cdot \left(C_{PAA,feedin} - C_{PAA,ex}\right)$$

$$\frac{dC_{oOHPPA,ex}}{dt} = \left(q_{sec,oOHPAA} \cdot C_x \cdot V_x\right) - D \cdot C_{oOHPAA,ex}$$

$$\frac{dC_{OPC,ex}}{dt} = \left(q_{secOPC} \cdot C_x \cdot V_x\right) - D \cdot C_{OPC,ex}$$

The specific growth rate μ (= 0.05h^{-1}) is included in the balances for the intracellular compounds to account for the dilution of the intracellular metabolites caused by growth of the cells. While D (= 0.05h^{-1}) is included in the balances for extracellular metabolites to account for the wash-out of extracellular metabolites. Please note that all the intracellular concentrations (C_i), intracellular fluxes (v_i) and secretion rates (q_i) are based on per m^3 of cell volume. All the extracellular concentrations ($C_{i,ex}$), and extracellular flux ($v_{8HPA,ex}$) are based on per m^3 of fermentor volume V_x is the m^3 intracellular fluid per gram biomass dry weight

5.9.3 Appendix III

Table 5.A1: Affinity and other model parameters obtained from literature

Parameter	*Value*	*Units*	*Reference*
$K_{m,ACV,IPNS}$	130	mmol/m^3	[137]
$K_{i,ACV,ACVS}$	540	mmol/m^3	[159]
$K_{m,IPN,IAT}$	23	mmol/m^3	[4]
$K_{m,PACoA,IAT}$	6	mmol/m^3	[4]
$K_{m,PACoA,AAT}$	6	mmol/m^3	[4]
$K_{m,6APA,AAT}$	9.3	mmol/m^3	[4]
V_x	2.5 x 10^{-6}	m^3/g DW	[131,160],
d_{cell}	5 x 10^{-6}	m	[131]
pH_{ex}	6.5	-	Experimental condition
pH_{in}	7.2	-	[100,101]
pK_a	4.23	-	-

Table 5.A2: Kinetic parameters estimated from overall optimization using data from both phases

Parameter	*Value*	*Units*
$K_{i,6APA,IPNS}$	< 600	mmol/m^3
$K_{i,6APA,IAH}$	< 10	mmol/m^3
$k_{8HPA,ex/in}$	(4.51 ± 0.18) x 10^{-3}	1/h
$K_{eq,secAPA}$, $K_{eq,secPenG}$, $K_{eq,secoOHPAA}$, $K_{eq,secOPC}$	80.1 ± 9.5	[-]

Table 5.A3: Kinetic parameters with low sensitivity

Parameter	*Value*	*Units*
$K_{i,PA-CoA,PCL}$	1	mmol/m^3
$K_{m,IPN,IAH}$	2 x 10^5	mmol/m^3
$K_{m,PAA,PAH}$	1	mmol/m^3

Some of the parameters estimated were out of the concentration range of the metabolites and therefore could not be well determined.

Table 5.A4: Rate parameters estimated from phase II optimization based on per m^3 of cell volume

Parameter	*Value*	*Units*
k_{ACVS}	3115 ± 45	mmol/m^3.h
k_{IPNS}	(4.0 ± 1.2) x 10^4	mmol/m^3.h
k_{IAH}	(1.23 ± 0.20) x 10^6	mmol/m^3.h
k_{IAT}	(2.55 ± 0.40) x 10^3	mmol/m^3.h
k_{AAT}	(7.30 ± 0.90) x 10^3	mmol/m^3.h
k_{PCL}	38 ± 8	1/h
$k_{PAH,1}$	61 ± 16	mmol/m^3.h
$k_{PAH,2}$	733 ± 34	mmol/m^3.h
τ_{PAH}	8.4 ± 3.3	h
k_{OPC}	0.591 ± 0.019	1/h
$k_{diff,PAA}$	0.0162 ± 0.0032	m/h
$k_{sec,PAA1}$	130 ± 35	1/h
$k_{sec,PAA2}$	45 ± 24	1/h
τ_{PAA}^{*}	0.212 ± 0.014	h
$k_{sec,PenG}$	410 ± 25	1/h
$k_{\mathrm{sec},IPN}$	0.060 ± 0.014	1/h
$k_{sec,6APA}$	6.5 ± 1.6	1/h
$k_{sec,8HPA}$	0.029 ± 0.030	1/h
$k_{sec,oOHPAA}$	19.4 ± 5.3	1/h
$k_{sec,OPC}$	1.66 ± 0.32	1/h

τ_{PAA}^{*} : Estimated by fitting offgas O_2 data for the first hour after PAA step using exponential decay function.

Table 5.A5: Thermodynamic equilibrium values for transporters

Parameter	*Value*	*Obtained from*
$K_{eq,\mathrm{sec}\,IPN}$	10^4	Thermodynamic calculation
$K_{eq,\mathrm{sec}\,HPA}$	5265	Thermodynamic calculation

Table 5.A6: Estimated initial concentrations for phase II based on per m^3 of cell volume for intracellular concentration and based on per m^3 of fermentor volume for extracellular concentrations

Parameter	*Value*	*Units*
ACV_{SS}	22 ± 11	mmol/m^3
IPN_{ss}	7765 ± 175	mmol/m^3
$6APA_{SS}$	300 ± 17	mmol/m^3
$8HPA_{SS}$	13.9 ± 1.7	mmol/m^3
OPC_{SS}	464 ± 34	mmol/m^3
$IPN_{ex,ss}$	89.5 ± 2.2	mmol/m^3
$6APA_{ex,SS}$	565 ± 11	mmol/m^3
$8HPA_{ex,SS}$	54.9 ± 2.7	mmol/m^3
$OPC_{ex,SS}$	74.6 ± 2.7	mmol/m^3
$C_{PAA,feedin}$	4620 ± 90	mmol/m^3
$PAA_{ex,ss}$	5210 ± 90	mmol/m^3

5.9.4 Appendix IV

Table 5.A7: Transport mechanisms assumed for different compounds (from thesis chapter 4)

Metabolite	***Feasible transport mechanism***	K_{eq}	***Direction***	***Driving force***
IPN^{-1} secretion	Proton antiport	~ 10^4	Irreversible	Proton motive force
$6APA^{-1}$secretion	Uniport	73 ± 17	Reversible	Potential gradient
$PenG^{-1}$secretion	Uniport	73 ± 17	Reversible	Potential gradient
$8HPA^{-2}$ secretion	Uniport	5265	Reversible	Potential gradient
$oOHPAA^{-1}$secretion	Uniport	73 ± 17	Reversible	Potential gradient
OPC^{-1}secretion	Uniport	73 ± 17	Reversible	Potential gradient
HPAA uptake	Free diffusion	0.2 ~ 0.3	Reversible	Concentration gradient
PAA^{-1} + H^+ export	ATP hydrolysis	~ 10^{10}	Irreversible	ATP driven transport

Chapter 6

Determination of L-α-aminoadipyl-L-cysteinyl-D-valine in cell extracts of *Penicillium chrysogenum* using Ion Pair-RP-UPLC-MS/MS

Seifar RM*, Deshmukh AT*, Heijnen JJ, van Gulik WM (2012). Determination of δ-[L-α-aminoadipyl]-L-cysteinyl-D-valine in cell extracts of *Penicillium chrysogenum* using ion pair-RP-UPLC-MS/MS. Journal of Separation Science 35 (2):225-230.

*: *These authors contributed equally*

Abstract

L-α-aminoadipyl-L-cysteinyl-D-valine (ACV) is a key intermediate in the biosynthesis pathway of penicillins and cephalosporins. Therefore the accurate quantification of ACV is relevant, e.g. for kinetic studies on the production of these β-lactam antibiotics. However, accurate quantification of ACV is a challenge, because it is an active thiol compound which, upon exposure to air, can easily react with other thiol compounds to form oxidized disulfides. We have found that, during exposure to air, the oxidation of ACV occurs both in aqueous standard solutions as well as in biological samples. Qualitative and quantitative determinations of ACV and the oxidized dimer bisACV have been carried out using ion pair reversed phase ultra high performance liquid chromatography, hyphenated with tandem mass spectrometry, (IP-RP-UPLC-MS/MS) as analytical platform. We show that by application of tris(2-carboxy-ethyl)phosphine hydrochloride (TCEP) as reducing reagent, the total amount of ACV can be determined, while using maleimide as derivatizing reagent enables to quantify the free reduced form only.

Keywords: cell extract, maleimide, TCEP, thiols, *Penicillium chrysogenum*

6.1 Introduction

Penicillins and cephalosporins are sulfur-containing ß-lactam antibiotics, which are industrially produced in large scale fermentations, e.g. of the fungi *Penicillium chrysogenum* and *Cephalosporium acremonium*. The first essential step in their biosynthesis is the formation of the tripeptide ACV by the non-ribosomal α-aminoadipyl-L-cysteinyl-D-valine (ACV) synthetase from its constituent precursor amino acids [14,161,189]. ACV possesses a reactive free thiol moiety in its molecular structure. In general, thiol containing metabolites are the most reactive reducing species operating at the physiological pH of living cells [29]. The reactivity of thiols is caused by the large dipole moment and nucleophilicity [153]. In biological samples thiols can either be found in their free reduced form, or as oxidized disulfides [36]. bisACV is one of the oxidized disulfide forms of ACV [36,161], see Figure 6.1.

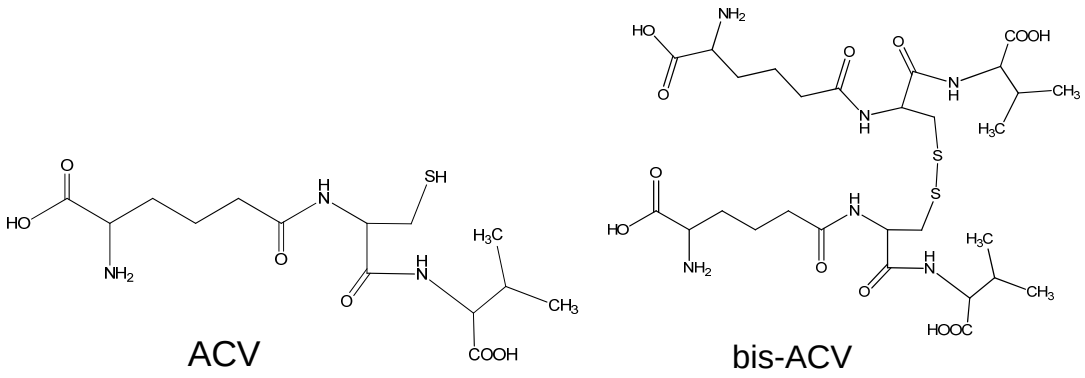

Figure 6.1:. Chemical structures of ACV and its corresponding oxidized disulfide bisACV.

In the intracellular environment the oxidized disulfide forms of ACV can be reduced back into ACV by means of the thioredoxin reductase (TR) system [36,161]. In order to study the kinetics of ACV synthetase, e.g. determine the maximum capacity and affinity constants [125,135] or the secretion mechanism, which requires measurement of the concentration gradient over the cell membrane, it is essential to have accurate measurements of the intra and extra-cellular ACV levels[96,183]. As ACV is spontaneously oxidized by attachment to other thiol containing metabolites, accurate quantification can only be performed if the free reduced form is protected at the time of sampling, and further oxidation during sample processing is prevented.

The choice of the method for the quantification of ACV depends on the biological question, that is, whether the total ACV (sum of free ACV, bisACV and ACV bound to other thiol containing compounds) should be measured or only the free reduced form. Quantification of the total ACV present in a sample requires the reduction of the disulfide bonds between ACV and the thiol containing compounds to which it is bound. Many reducing reagents, such as dithioerythritol [157], dithiothreitol [111], mercaptoethanl [85], $NaBH_4$ [157], tris-(2-carboxyethyl)-phosphine, TCEP [152], have been applied to reduce disulfide bonds. In the present study TCEP has been chosen because of its water solubility and stability in aqueous solutions and because it has been reported as most efficient in reducing disulphide compounds [6]

To determine only the free reduced form of ACV at the time of sampling, the thiol groups should be rapidly protected, e.g. by application of derivatizing reagents. It has been shown that thiol groups can be protected using derivatizing reagents such as 5, 5'-dithiobis (2-nitrobenzoic acid), (Ellman's reagent) [61] varieties of N-substituted maleimide [11,152,156], and 4-fluoro-7-sulfamoybenzofurazan [192]. Maleimides have been extensively used for derivatizing thiols in biological samples, because of their rapid reaction with thiols at physiological pH values [152]. Figure 6.2 shows the typical reaction of maleimide with a thiol containing compound. Here we report, for the first time to our knowledge, the application of TCEP and maleimide, as reducing and derivatizing reagents respectively, in cell extract samples from *P. chrysogenum,* prior to analysis with ion pair reversed phase ultra high performance liquid chromatography hyphenated with tandem mass spectrometry, IP-RP-UPLC-MS/MS.

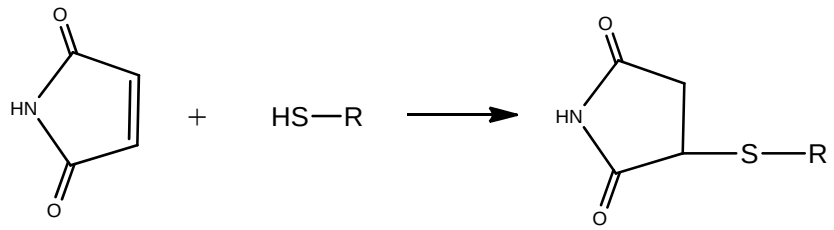

Figure 6.2: Derivatization of a typical thiol compound with maleimide.

6.2 Materials and Methods

6.2.1 Materials and reagents

Dibutylammonium acetate, DBAA, concentrate 0.5M, Tris(2-carboxy-ethyl)phosphine hydrochloride (Fluka), TCEP and ACV were purchased from Sigma-Aldrich(Steinheim - Germany). bisACV was kindly provided by DSM (Delft, The Netherlands).
Fermentation broth and cell extracts were obtained from glucose limited chemostat cultures of *P. chrysogenum* [43]. Culture filtrate was obtained by removing biomass from the broth using glass fiber filters (type A/E; 47mm diameter, 1 µm pore size, Pall Corporation, East Hills, NY).

The labeled internal standard was prepared as published previously [109,150,151,186,188]. Briefly, a U-^{13}C-cell extract, containing U-^{13}C-labeled ACV, was obtained from a *P. chrysogenum* fed-batch culture, grown on 100% U-^{13}C-labeled glucose.

6.2.2 Liquid chromatography

The IP-RP-UPLC runs were performed with an Acquity™ UPLC system (Waters, Milford, MA, USA). The temperature of the autosampler was set at 4°C and the column temperature was kept at room temperature 25°C. The injection volume was 5µl in all runs. All chromatographic runs were performed on a reversed phase column (Acquity™ UPLC® BEH C18, 1.7µm, 100 × 1mm i.d., Waters, Ireland). A guard column (BEH C18, 1.7µm, 10 × 1mm i.d., Waters, Ireland) was employed to protect the analytical column from particles. The flow rate was set at 0.2ml/min. All sample solutions contained 10mM DBAA. Reduced or derivatized samples contained 10mM TCEP or maleimide respectively. A fixed amount of ^{13}C-labeled ACV containing cell extract was added as internal standard to all sample solutions and standard calibration mixtures [109,150,151,186,188]. Linear gradient elution was used in all runs. Mobile phase A was composed of 2mM DBAA and 5% (v/v) acetonitrile and mobile phase B consisted of 2mM DBAA and 84% (v/v) acetonitrile. The pH of the 2mM DBAA solution (without any organic solvent) was about 6.7. The elution started with a ratio of 5% mobile phase B. Then, mobile phase B was increased by a linear gradient to 40% in a period of 8 min followed by a second linear gradient in which mobile phase B was increased to 100% within a period of 0.5min and thereafter kept constant for 1.5min. Subsequently the column was re-equilibrated with the initial mobile phase composition for another 2min. The

effluent from the analytical column was mixed with a flow of 0.1ml/min of 50% (v/v) acetonitrile solution provided by a Waters 515 high-performance liquid chromatography (HPLC) pump before entering the ion source of the MS system.

6.2.3 Mass spectrometry

A Waters Quattro Premier XE, (Micromass MS Technologies-Waters) equipped with an Electrospray ion source was used throughout this study. The ESI was operated in negative mode. Data were processed using Masslynx 4.1 software (Waters). Metabolite detection was performed in multiple reaction monitoring MRM, mode. The general settings were as follows: the ESI Capillary voltage was 2.8kV in negative ionization mode, the extractor voltage was 5V, the RF lens voltage 0.5V. The desolvation gas flow (nitrogen) was 700 l/hr with the temperature set at 360°C, the cone gas flow (nitrogen) was 50 l/hr and the source block temperature was 120°C.

MRM transitions and corresponding instrument settings yielding the highest signal to noise ratios were separately found for ACV and bisACV by infusing standard solutions (10µM) in acetonitrile/water (1:1 v/v) at a flow rate of 10µl/min using an integrated syringe pump. Selected reaction monitoring (SRM) transition with highest signal to noise ratio for each compound was chosen for quantification purpose. The dwell time was 0.05s and the inter-channel delay and inter-scan delays were 0.05s. The cone voltage for ACV and ACV-maleimide was set to 25V and for bisACV to 50V and the collision energy for all compounds was set to 20eV. For labeled ACV the same instrument settings were used as for the corresponding unlabeled standard metabolite. The *m/z* values for ^{13}C-labeled ACV were simply obtained by adding the number of the carbon atoms to the *m/z* value of unlabeled ACV. Table 6.1 shows the obtained *m/z* values of precursor and fragmentation ions of ACV, bisACV and derivatized ACV.

Table 6.1: *m/z* values for determination of ACV, bis-ACV and maleimide derivatized ACV.

Compound	*Precursor ion*	*Fragment ion*	*Labeled precursor ion*	*Labeled fragment ion*
ACV	362	185	376.5	193.3
*bis-ACV	723	362	-	-
ACV-maleimide	459	362	473	376.5

*no ^{13}C-precursor could be found for bis-ACV.

6.3 Results and discussion

6.3.1 Oxidation of ACV to disulfides

As ACV is a thiol containing metabolite, it is a labile molecule and can easily be oxidized to mixed or symmetrical disulfides [152]. Even in an aqueous standard solution of ACV traces of bisACV (the oxidized disulfide) can be detected after a few hours, as the result of oxidation. Figure 6.3 shows SRM chromatograms of an aqueous standard solution of ACV after a couple of hours exposure to air at room temperature. As can be seen from this figure traces of bisACV could be found, while in the freshly prepared standard solution of ACV, no bisACV could be detected. It should be emphasized that in this case bisACV is the only oxidation product, because no other thiol containing compounds were present in the aqueous solution. To study the oxidation of ACV under conditions when also other thiol compounds are present, as is the case for biological samples, shake flask experiments were carried out using culture filtrate from a chemostat cultivation of *P. chrysogenum*. In this experiment fixed amounts of filtrate (5ml) were introduced in three separate flasks. The filtrate initially contained approx. 53µM of bisACV and an approx. 8µM of ACV. To each flask different amounts of a standard solution of ACV (10mM) were added to obtain different initial ACV concentrations, i.e. 32, 56 and 100µM. The flasks were incubated at 25 °C in an orbital shaker at a rotation speed of 150rpm for a period of 28hours. At regular time intervals, samples of 40µl were taken from each flask to quantify the ACV and bisACV concentrations. Figure 6.4 presents the results for the oxidation of ACV showing a continuous decrease of the ACV and a slight increase of the bisACV concentration in time. According to a one tailed t-test ($p=0.025$) this increase of bisACV was only significant for flasks B and C which contained higher initial ACV concentrations. It should be noted that the amounts of produced bisACV were significantly smaller than the amounts of consumed ACV. This clearly indicates that there must be other thiol-containing compounds present in the filtrate, to which ACV attaches itself. The yields of bisACV on ACV (calculated as 2 times the amount of bisACV produced / the amount of ACV converted) for these experiments are given in Table 6.2. As for the lowest initial ACV concentration (flask A) the increase of the bisACV concentration was not significant, the yield was not calculated. From the obtained results for flasks B and C it can be seen that the yield of bisACV on ACV increases at increasing initial ACV concentration. This might be explained by depletion of the other thiol compounds (apart from ACV) present in the supernatant.

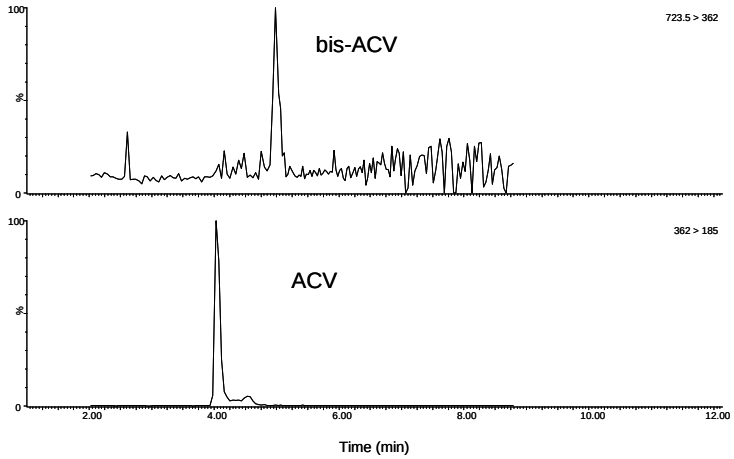

Figure 6.3:. SRM transitions of a standard aqueous solution of 10µM ACV. Upper SRM transition is for bisACV and lower SRM transition is for ACV.

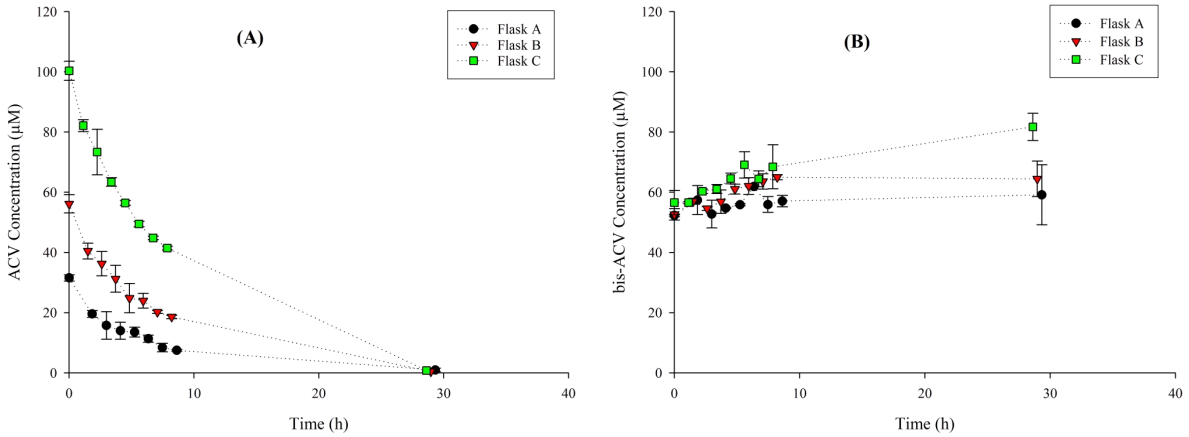

Figure 6.4: Determination of ACV and bisACV in culture filtrate obtained from a glucose limited chemostat of *P. chrysogenum*. (A) Time course of oxidation of ACV. (B) Time course of formation of bisACV. Error bars represent standard errors.

Table 6.2: The observed results for the oxidation of ACV and the yield of produced bis-ACV on ACV in a shake flask experiment at 25°C and 150rpm.

Flasks	Initial concentration of ACV (µM)	Yield of bis-ACV on ACV (%)*
A	31.6 ± 1.1	-
B	56.2 ± 3.0	28 ± 18
C	100.4 ± 3.2	50.1 ± 8.6

*Yield: (2 × mol of bis-ACV produced) / (mol of ACV disappeared)

6.3.2 Comparison of the effects of the application of TCEP and maleimide

It is known that TCEP is able to reduce disulfides rapidly (in less than 5 min) and completely in aqueous solutions [26,97,147] while maleimide immediately and selectively stabilizes thiol containing compounds by derivatizing the thiol groups. In a simple experiment an aqueous standard solution containing both ACV and bisACV was divided into two identical parts. Then to one part TCEP and to the other one maleimide was added. The final concentration of each additive in these solutions was 10mM. As shown in Figure 6.5 only ACV could be detected in the presence of TCEP while no bisACV could be found. The addition of maleimide at this point was not necessary because the presence of TCEP was enough to avoid the oxidation of thiol groups. In the presence of maleimide both the ACV-maleimide complex and bisACV could be detected. The results of this experiment thus show the selective quantification of total and free ACV using TCEP and maleimide, as reducing and derivatizing agents respectively.

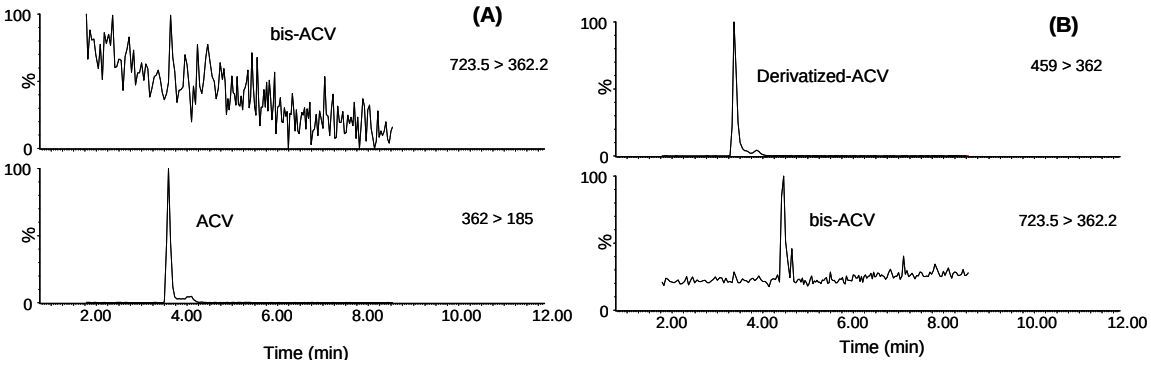

Figure 6.5: SRM transitions observed for standard aqueous solutions containing ACV and bisACV. (A) Standard solution treated with TCEP. (B) Standard solution containing maleimide.

6.3.3 Comparison of calibration curves in the presence and absence of TCEP or maleimide

To investigate the effect of TCEP and maleimide on the quality of the calibration curve for ACV, three equal sets of aqueous standard calibration mixtures of ACV were prepared. The standard calibration mixtures of the first set contained 10mM of TCEP while the second set of standard calibration mixtures contained 10mM of maleimide. TCEP and maleimide were added to the standard solutions about one hour prior to analysis. The third set contained no additive and served as the control. The results are displayed in Figure 6.6. It can be seen from this figure, that similar calibration curves, with high linearity, could be obtained in the presence of TCEP and maleimide. However, for standards containing no additives, the ACV

signals were at noise levels up to 40µM. In this case the non-linear calibration curve could easily be converted to the linear one by addition of TCEP, which shows the reductive recovery of ACV. Similar results were obtained for calibration curves for glutathione (results not shown) which is a thiol compound with similar characteristics as ACV.

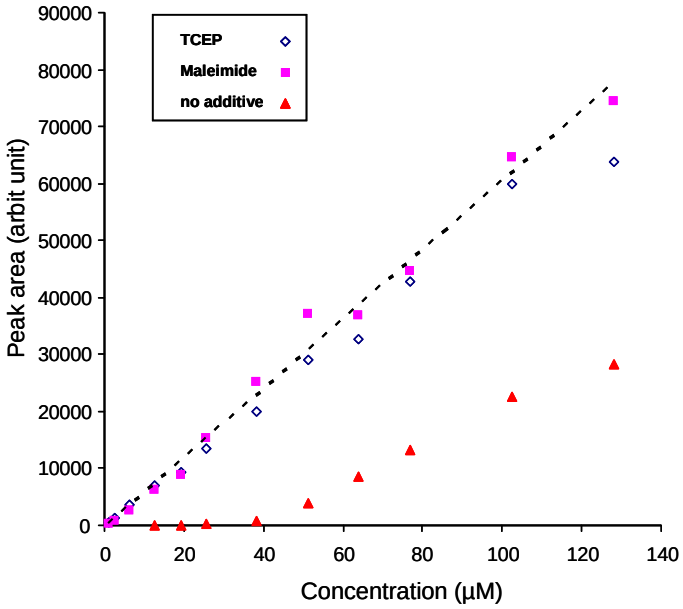

Figure 6.6: The effect of either TCEP or maleimide on the observed linearity of the calibration curves of ACV.

6.3.4 Proof of concept: Determination of free and total ACV in cell extracts of *P. chrysogenum*

To prove the applicability of this method to biological samples, the free and total amounts of ACV in cell extracts of *P. chrysogenum* [118] were determined using maleimide and TCEP as additives. With this purpose four broth samples were taken rapidly (within 20s) from a steady state glucose limited chemostat of *P. chrysogenum*. The samples were processed according to the procedure described by Douma et al. [43]. For determination of the free reduced form of ACV, maleimide was added to the first two samples immediately after the cell harvesting and washing procedure and before the metabolite extraction step. The other two samples were processed without using any additive. Subsequently, ACV was quantified in all 4 samples. The results are presented in table 6.3. In the two samples to which maleimide was added ACV could be detected and quantified, while in the samples without maleimide ACV could not be detected. To quantify the total amount of ACV in these samples, the reducing reagent TCEP was added. After addition of TCEP it was possible to measure ACV, as result of the effective reduction of all symmetrical and unsymmetrical oxidized disulfides. As expected the total

amount of ACV in the samples analyzed in the presence of TCEP was higher compared to the samples containing maleimide.

Table 6.3: The obtained results of the quantification of ACV in cell extract in the presence of the reducing reagent TCEP, and the derivatizing reagent maleimide.

Type of added reagent	*Amount measured (µmol/ g DW)*
*No additive	not detected
TCEP	0.63 ± 0.06
Maleimide	0.40 ± 0.06

*neither TCEP nor maleimide was added. The observed peak for ACV was at noise level

6.4 Concluding remarks

The effect of application of either TCEP as reducing reagent or maleimide as derivatizing reagent on quantification of the thiol containing tripeptide, ACV, has been studied. Shake flask experiments carried out using filtrate from a chemostat culture of *P. chrysogenum* showed that ACV gradually disappears, partly (50% or less) as a result of oxidation to the symmetrical disulfide (bisACV). The remaining part reacts most probably with other sulfides present in the filtrate and is oxidized to mixed asymmetrical disulfides. It was also demonstrated that oxidation of ACV to bisACV occurs even in an, initially pure, aqueous standard solution. It was shown that for a meaningful quantification of ACV in sample solutions the presence of either a reducing reagent such as TCEP or a thiol derivatizing reagent such as maleimide is needed. The total ACV amount (the sum of free and oxidized forms) can be quantified by addition of TCEP to the sample solutions. Maleimide effectively derivatizes the thiol moiety of the free ACV molecules present at the time of addition, enabling quantification of the free form only. Therefore, higher concentrations of ACV should be expected in the presence of TCEP in samples compared to maleimide. To prevent further oxidation of the reduced form of ACV during sample processing, maleimide should be added to the sample as soon as possible, while the moment of the addition of TCEP is less critical. Both the quantification of the free reduced form of ACV as well as the total amount of ACV (bound and free forms) are highly relevant. With accurate determination of free intracellular ACV it is possible to study enzyme kinetics in which the free reduced form of ACV is used as substrate, such as ACV synthetase and membrane transporters for ACV secretion. For determination of the total ACV biosynthesis rate quantification of the total amount of produced ACV is required.

Chapter 7

Production of δ-[L-α-aminoadipyl]-L-cysteinyl-D-valine as a model non ribosomal peptide in *P. chrysogenum*

Deshmukh AT, de Reus PE, Maleki Seifar R, Pieterse M, Pinkse MWH, Verhaert PDEM, Verheijen PJT, van der Klei IJ, Heijnen JJ and van Gulik WM. Production of δ-[L-α-aminoadipyl]-L-cysteinyl-D-valine as a model non ribosomal peptide in *P. chrysogenum*
(Ssubmitted for publication)

Abstract

Due to potential pharmaceutical and food applications of peptides synthesized by non-ribosomal peptide synthetases, there is a growing need for their efficient and sustainable synthesis. Here we have studied the production of a non-ribosomal peptide using *P. chrysogenum* as host organism. As a model system, δ-[L-α-aminoadipyl]-L-cysteinyl-D-valine synthetase (ACVS), the first enzyme of the penicillin biosynthesis pathway, was used to produce the peptide δ-[L-α-aminoadipyl]-L-cysteinyl-D-valine (ACV) in *P. chrysogenum*. For this purpose, the native ACVS gene was expressed in a high producing *P. chrysogenum* strain from which all copies of the penicillin gene cluster were removed. This strain was used to study the production of ACV and its secretion mechanism in a glucose-limited chemostat. We observed that a significant amount of ACV was produced and secreted, but that the production decreased significantly over the cultivation period due to a fivefold decrease of the ACVS enzyme level. A large part of the ACV produced was further oxidized to disulfides such as bisACV. Accurate quantification of the total and free forms of ACV and glutathione (GSH) was achieved by using the reducing agent tris (2-carboxyethyl) phosphine hydrochloride (TCEP) and the derivatizing agent, ethyl maleimide, respectively. A kinetic model was constructed that describes the kinetics of formation of ACV and bisACV and their secretion mechanisms. Metabolic control analysis showed that more than 80% of the flux for ACV production is controlled initially by the ACV transporter, however, after 210 h the flux is controlled by ACVS. Furthermore, the increase in the ratio of glutathione to glutathione disulfide showed that the redox state of the cell became more reduced over the cultivation period.

Keywords: *Penicillium chrysogenum*; non-ribosomal peptide; ACVS; transport of metabolites, thiol quantification.

7.1 Introduction

The fungal kingdom has many unusual metabolic pathways that are optimized by evolution to produce several pharmacological important secondary metabolites. A class of such bioactive natural products is synthesized by multifunctional Non-Ribosomal Peptide Synthetases (NRPS) to produce Non-Ribosomal Peptides (NRP). The NRPs contain not only the common amino acids but also nonproteinogenic amino acids, D-amino acids, heterocyclic elements, and glycosylated as well as N-methylated residues in contrast to ribosomal peptides [148,154]. NRPs are known to act as antibiotic, immunomodulatory, cytostatic, surfactant, siderophore or antifungal agents [90,112].

The synthesis of non-ribosomal peptides takes place by a thiotemplate mechanism, which consists of so-called 'modules' of initiation, elongation and termination. The modules consist of several 'domains' (see Figure 7.1). In the initiation module, which lacks the condensation 'C-domain', the adenylation 'A-domain' selects the first amino acid substrate and activates it as an aminoacyl adenylate [99]. The thiolation domain or peptidyl carrier protein 'PCP' covalently binds the formed adenylate as a thioester. In each elongation module, the condensation 'C-domain' then forms the peptide bond with the next substrate molecule [133]. The number of elongation modules determines the size and complexity of the produced NRP, as each module by definition incorporates one specific amino acid or other substrate monomer [27,180].

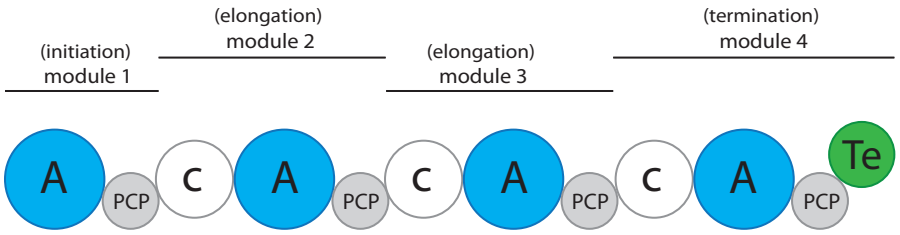

Figure 7.1: The general structure of a non-ribosomal peptide synthetase includes an adenylation 'A' domain, peptidyl carrier protein 'PCP', condensation 'C' domain and a thioesterase 'Te' domain for termination. Each module is responsible for incorporation of one substrate.

Once each module has incorporated a monomer, the release of the synthesized NRP requires an additional C-terminal thioesterase 'TE-domain' [154] Modifications to amino acid precursors such as epimerization and N-methylation can be made at different points during synthesis [99,180]. As, in principle, a large variety of modules can be incorporated into a

NRPS through genetic engineering, it has opened the search for bioactive compounds widely present in various bacteria and fungi. In order to identify relevant gene clusters from the sequenced microbial genomes, tools such as antiSMASH (antibiotics & Secondary Metabolite Analysis Shell) have been developed [110]. This facilitates the discovery and engineering of novel antibiotics, cytostatics, antitumor drugs and other beneficial non-ribosomal peptides.

7.1.1 Production of ACV as a model NRP in *Penicillium chrysogenum*

Efficient production of known NRPs as well as studying novel NRPs calls for a suitable biological production process. In order to produce a significant quantity of the NRP of interest, understanding the relation between NRP-production cellular energetics, redox metabolism and supply of precursors through central carbon metabolism is essential. In addition, understanding of secretion mechanisms of NRPs is necessary, as an insufficient secretion rate leads to intracellular product accumulation, which is likely to have inhibiting effects, resulting in lower production rates.

The non-ribosomal tripeptide δ-(L-α-aminoadipyl)-L-cysteine-D-valine (ACV) is the precursor of all penicillin and cephalosporin compounds and therefore the mechanism of ACV formation has been studied extensively for different organisms [27,78,83,161,189]. This makes ACV a suitable model compound for metabolic engineering studies aimed at designing a cell factory for the production of NRPs. *P. chrysogenum,* the most widely used organism for the production of β-lactams, naturally expresses ACVS. It has desirable large scale fermentation characteristics; it is robust and high-yielding strains have been developed through random mutagenesis [40,77,138,139]. Besides ACVS, over 9 other non-ribosomal peptide synthetases have been found in *P. chrysogenum* [170]. Most of them are expressed at low levels, but their expression opens up possibilities for further research into non-ribosomal peptide synthetases of *P. chrysogenum* beyond ACVS.

7.1.2 Mechanism and kinetics of ACV Synthetase

ACV Synthetase (ACVS) is a large and extremely unstable enzyme, responsible for linking three L-amino acids during the biosynthesis of ACV [189]. In 1993, ACVS was successfully isolated from *Acremonium chrysogenum* [3] and later from *P. chrysogenum* [161] and characterized. The enzyme is found to be located in the cytosol of *P. chrysogenum* [106,168]. By thiol-template mechanisms, the three precursor amino acid constituents are bound to thiol

groups of the enzyme after activation. The dipeptide δ-(L-α-aminoadipyl)-L-cysteine (LL-AC) is then formed by a reaction of the α-amino group of L-cysteine with the δ-carboxyl group of L- α-aminoadipate [105]. Figure 7.2 shows the initiation, elongation and termination of ACV by ACVS.

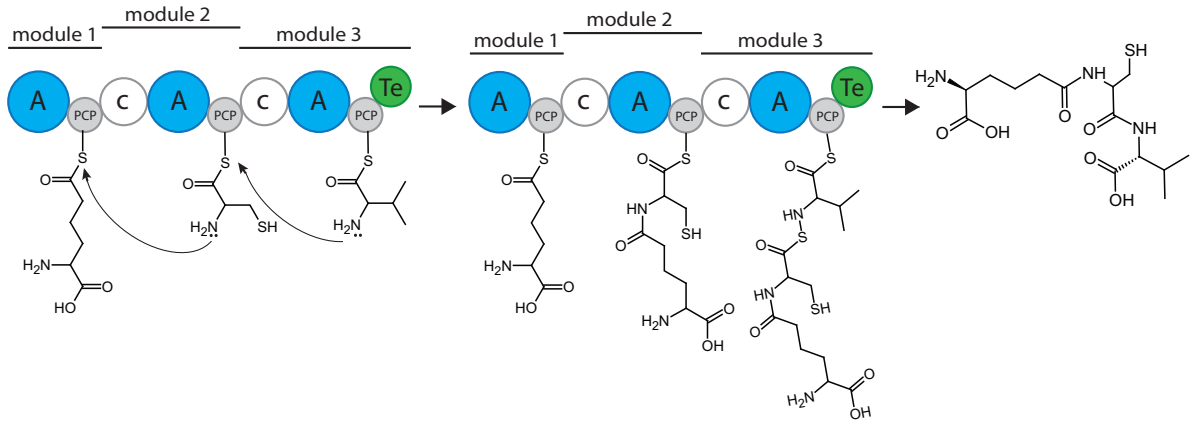

Figure 7.2: Schematic overview of the formation of LLD-ACV by ACV Synthetase. First, δ-(L-α-aminoadipyl)-L-cysteine (LL-AC) is formed by reaction of the α-amino group of L-cysteine with the δ-carboxyl group of L- α-aminoadipate. Before completion of the tripeptide, L-valine is converted to D-valine [86,180].

Figure 7.3 shows the first step of the penicillin synthesis pathway: the formation of ACV from its three amino acid constituents, L-α-aminoadipate (α-AAA), L-cysteine and L-valine. From *in vitro* studies it was found that ACVS exhibits Michaelis-Menten kinetics with respect to L-α-aminoadipate (K_m: 0.045 mM), L-cysteine (K_m: 0.080 mM) and L-valine (K_m: 0.080 mM) in *P. chrysogenum* [161,189]. Both ACV and its dimer form bisACV can inhibit ACVS. The inhibition parameter of bisACV was estimated *in vitro* to be 1.4 mM, and for ACV as 0.54 mM [159,161]

Figure 7.4 shows the formation of bisACV, the disulphide resulting from the oxidization of the thiol groups of two molecules of ACV. The Gibbs free energy change associated with this spontaneous and irreversible oxidization is favorable: $\Delta G'^{\circ} = -172$ kJ/mol [159]. Formation of bisACV can occur both inside the cell, and after ACV secretion outside the cell. It is unknown whether bisACV is also secreted. An intracellular thioredoxin/thioredoxin reductase (TR) system acts to reduce ACV dimers back into ACV using NADPH [36]. This cyclic oxidation/reduction clearly leads to an energy waste where 2H from NADPH is oxidized with $1/2O_2$ to H_2O.

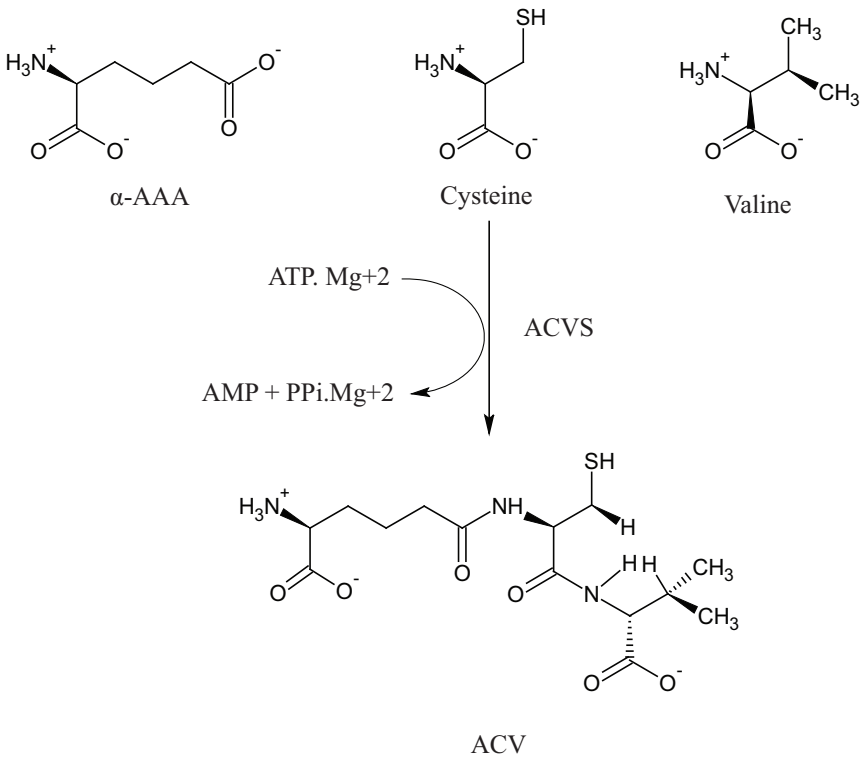

Figure 7.3: ACV is formed by ACV Synthetase from its three constituent amino acids L-α-aminoadipate acid, L-cysteine and L-valine.

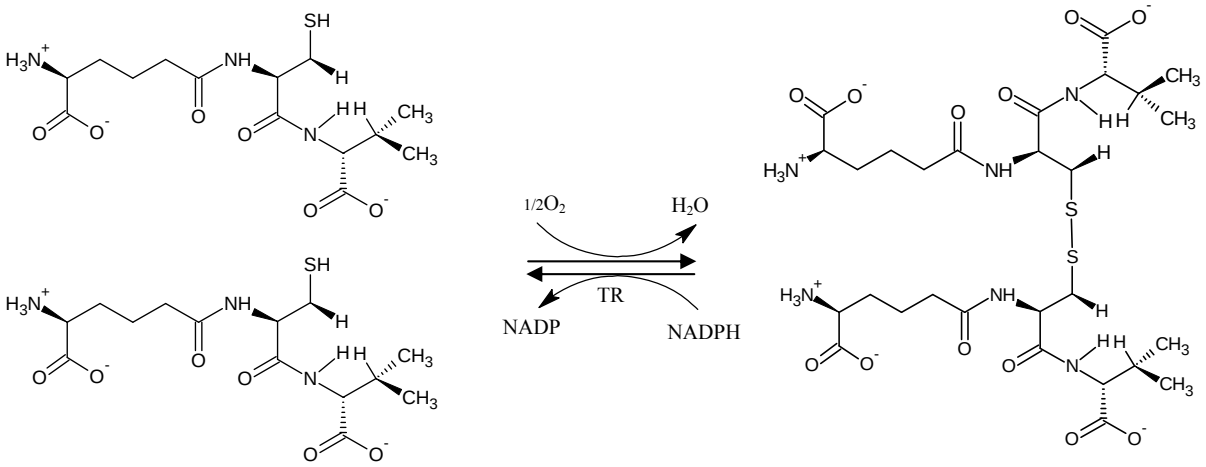

Figure 7.4: Spontaneous oxidation of ACV to its dimer bisACV and intracellular reduction back to ACV by thioredoxin/ thioredoxin reductase system (TR) [36]

Here we have studied the production and transmembrane transport of ACV in a *P. chrysogenum* strain synthesizing this non ribosomal peptide as sole product. For this purpose a non-producing *P. chrysogenum* strain, which was obtained previously by removing all copies of the penicillin gene cluster from the high producing industrial strain DS17690, was transformed with the gene encoding the native ACV synthase (ACVS) gene under control of the IPNS promoter. The rate of ACV secretion and fluxes through ACVS were experimentally

determined in glucose limited chemostat cultures under conditions known to favor penicillin-G production in the penicillin producing strain and were compared with the penicillin-G (PenG) producing parental strain DS17690, cultivated under the same conditions. Accurate quantification of intracellular and extracellular ACV and bisACV was performed to obtain more insight in the secretion mechanisms of these compounds and their kinetic properties. In addition, the kinetics of bisACV formation from ACV was studied.

Another important byproduct during the fermentation of *P. chrysogenum* is 6-oxopiperidine-2-carboxylic acid (OPC), a cyclized product of the amino acid precursor α-aminoadipate. Formation of OPC is undesirable, as it competes with ACVS for the substrate α-aminoadipate. The mechanism of formation of this unwanted byproduct has therefore been much debated in literature. It has been proposed that spontaneous cyclization of α-aminoadipate into OPC is too slow to account for the observed OPC levels [70,79], thus enzymatic activity is thought to be involved. It has therefore been suggested that OPC is formed in a side-reaction of one of the enzymatic steps in penicillin biosynthesis [79]. Other studies have indicated that there may be a distinct enzyme, other than the penicillin pathway enzymes, responsible for OPC formation [70]. We therefore also quantified OPC formation in the ACV producing mutant strain.

7.2 Materials and Methods

7.2.1 Strain development

Strains and growth conditions

The *Penicillium chrysogenum* strains used in this study are listed in Table 7.1. For strain construction purposes, YGG medium was used, as described by Bartoszewska et al. [16]. For biochemical analyses, *P. chrysogenum* strains were cultivated on penicillin production medium (PPM) of which the composition has been described previously [129]. Regeneration of transformed *P. chrysogenum* protoplasts was performed on phleomycin selection agar with a composition as described by Opaliński Ł et al. [129]. To induce conidiospore formation, R-agar was used [16]. *Escherichia coli* DH5α (Stratagene) and DB3.1 (Invitrogen) were used for cloning purposes. *E. coli* strains were grown at 37 ºC in LB medium as described by Opaliński Ł et al. [129]

Molecular techniques

Oligonucleotides and plasmids used in this study are listed in Supplementary Tables 7.S1 and S2, respectively. Standard recombinant DNA manipulations were carried out according to Sambrook et al. [144]. For preparation of *P. chrysogenum* protoplasts, mycelia were cultured on YGG medium. Protoplasting and transformation were performed using established protocols [30]. Restriction enzymes and other DNA modifying enzymes were used according to the instructions of the suppliers (Fermentas, Roche). Polymerase chain reactions (PCR) were performed with Phusion polymerase (Fermentas) for cloning purposes and with Phire polymerase (Fermentas) for colony PCR on *P. chrysogenum* transformants. DNA recombination reactions were performed according to the instructions of the multisite Gateway three-fragment vector construction kit (Invitrogen).

Plasmid constructions

Construction of plasmids and strains can be found in Supplementary Material.

Biochemical techniques

Crude extracts of *Penicillium chrysogenum* cells were prepared as described previously [88]. Protein concentrations were determined using the RC/DC Protein Assay (Bio-Rad) using bovine serum albumin as a standard. SDS-polyacrylamide gel electrophoresis and western blotting were performed in accordance with established protocols using specific polyclonal antibodies against ACVS.

Table 7.1: *P. chrysogenum* strains used in this study.

Strain	*description*	*reference*
DS17690	High Penicillin-producing parental strain	[65]
DS55153	strain lacking all penicillin biosynthesis gene clusters; derivative of DS50652; Amds+	DSM lab collection [65,126]
DS62824	DS55153 with integrated P_{pcbC}-*pcbAB*-T_{penDE} expression cassette; #1-17; $Amds^{+}$, $Phleo^{R}$	This study

Key: $Amds^{+}$, capable of utilizing acetamide as sole nitrogen source; $Phleo^{R}$, phleomycin resistant.

7.2.2 Chemostat cultivation

Chemostat cultivations were carried out under glucose-limited aerobic conditions in a 7 L turbine stirred bioreactor (Applikon, Schiedam, The Netherlands) with 4 L of working volume and a dilution rate of 0.05 h^{-1}. The pH was controlled at 6.5 with 4M NaOH and the temperature was controlled at 25 ± 0.1 °C. The air flow rate was set at 2 L/min (0.5 vvm), with 0.3 bar overpressure and the stirrer speed was set at 500 rpm. The dissolved oxygen tension was measured with a Mettler Toledo DOT sensor (Mettler-Toledo GmbH, Greinfensee, Switzerland) but not controlled, as under these fermentation conditions dissolved O_2 concentration does not drop below 80% of air saturation. Offgas was passed through a condenser at 4 °C, and an offgas analyzer (NGA2000, Rosemount, USA) was used to measure offgas CO_2 and O_2. Further details of the chemostat setup and operation have been described previously [37].

The composition of the chemostat medium was designed to support a biomass concentration of 6 g/L dry weight. This medium contained 0.5 Cmol/L of glucose (16.5 g/L glucose monohydrate), 5 g/L $(NH_4)_2SO_4$, 1 g/L KH_2PO_4, 0.5 g/L $MgSO_4 \cdot 7H_2O$, and 10 ml/L trace elements solution. The trace element solution contained 15 g/L Na_2-EDTA$\cdot 2H_2O$, 0.5 g/L $CuSO_4 \cdot 5H_2O$, 2 g/L $ZnSO_4$ $7H_2O$, 2 g/L $MnSO_4 \cdot H_2O$, 4 g/L $FeSO_4 \cdot 7H_2O$ and 0.5 g/L $CaCl_2$ $2H_2O$. All medium components were dissolved in 50 L of demineralized water and the pH was set to 5.6 by adding KOH pellets. The medium was filter-sterilized (Supor DCF 0.2 μm filters, Pall Gelman Sciences, East Hills, NY) into a sterile medium vessel.

Rapid sampling, quenching and washing by cold filtration for intracellular metabolite quantification

Rapid sampling was carried out with a dedicated rapid sampling device [98]. Using this device approximately 1.2 g of sample was rapidly withdrawn (in less than 1 s) from the bioreactor. The sample was directly injected in 8 mL 40% (v/v) methanol/water solution at -27.5 °C for immediate quenching of all metabolic activity. For this quenching procedure it has been reported that metabolite leakage was minimal in *P. chrysogenum* [38]. Subsequently, using a cold filtration method (using PALL 0.8 μm, 47 mm membrane filters), each sample was washed 3 times with 30 ml of 40% (v/v) methanol/water at -27.5 °C [43] to effectively remove extracellular metabolites. The choice of 40% methanol was to avoid leakage of the intracellular metabolites into the solution [38].

Metabolite extraction

Extraction of the intracellular metabolites from the quenched and washed mycelium was performed with the boiling ethanol method, whereby the filter paper with the mycelium was submerged in 30 mL of 75% (v/v) ethanol/water at 73 °C, and at the same time 120 µL of U-^{13}C-extract was added as internal standard. Subsequently, the tube containing the filter paper in ethanol/water was incubated for 3 min in a waterbath at 95 °C [59,98] then chilled on ice and stored at -80 ºC until further processing.

For further processing the ethanol extract was thawed, centrifuged at 4700 rpm at 4 °C for 7 min and filtered using 0.2 µm Whatman filters (FP30/0.2 CA-S) to remove the filter paper and biomass. Subsequently, the extract was concentrated in a rapid vaporization setup (RapidVAP, Labconco Corporation, Kansas City, Missouri, USA) to a volume of approximately 200 µl was reached. This resulted in the complete removal of the ethanol from the extract. The thus obtained watery extracts were adjusted to 600 µl using milli-Q water and centrifuged at 20,000 rpm at 4 °C for 10 min. The supernatant was transferred to filtering eppendorfs (Millipore Durapore PVDF 0.22 µm) and centrifuged at 5000 G for 15 min. The remaining volume in each eppendorf was split into two cryovials and frozen in liquid nitrogen and stored at -80 °C. One vial was used for analysis of intracellular ACV, bisACV, glutathione (GSH), glutathione disulphide (GSSG) and OPC [149]. The other vial was used for the quantification of free intracellular amino acids.

Rapid sampling for extracellular metabolite quantification

Approximately 1 mL of broth was withdrawn from the fermentor into a syringe containing cold (-20 °C) stainless steel beads for immediate quenching by rapid cooling to ± 1 °C, directly followed by filtration through a 0.45 µm pore size filter (Whatman FP20/45 CA-S) [107] and. An aliquot of 80 µL of the thus obtained filtrate was mixed with 20 µL of U-^{13}C-extract, frozen in liquid nitrogen and stored at –80 °C until further analysis

7.2.3 Metabolite quantification

Thiol compounds and OPC

ACV, bisACV, GSH, GSSG and OPC were quantified with ion-pair reversed-phase liquid chromatography-isotope dilution electrospray ionization tandem mass spectrometry (IP–LC–

ESI–ID–MS/MS) [151] using U-^{13}C-labeled cell extract as an internal standard mix [107,186].

For quantification of the total amount of ACV and GSH, the analysis was carried out after reducing all oxidized forms, i.e. bisACV, GSSG as well as ACV and GSH bound to other thiol compounds present in the sample. This was accomplished by the addition of tris(2-carboxyethyl) phosphine hydrochloride (TCEP) to the sample prior to the analysis (5 µL of TCEP for 100 µL of sample) [149]

For proper quantification of the free, non-oxidized forms of ACV and GSH, they were derivatized in the moment of sampling with ethyl maleimide (EM), thereby converting the free ACV and GSH into their complex forms ACV-EM and GSH-EM and preventing them from being oxidized during further sample processing. For intracellular samples, EM was added along with 120 µL of U-^{13}C-extract just before the ethanol boiling step, such that the final concentration of EM in the sample was 2 mM (24 µl of 100 mM EM stock in water for 1.2 ml sample). Similarly, for extracellular samples EM was added such that the final concentration in the sample was 2 mM [149].

In order to quantify these compounds, calibration curves of ACV-EM and GSH-EM were used. Although the quantification was based on IP–LC–ESI–ID–MS/MS, for the ACV-EM and GSH-EM, the amounts of the labeled internal standards U-^{13}C-ACV-EM and U-^{13}C-GSH-EM were not sufficient for quantification, so U-^{13}C-OPC was used as an internal standard.

Amino acids:

Free amino acids were quantified with GC-MS using a method adapted from de Jonge, et al. [37]. In brief, 100 µL of cell extract was lyophilized and derivatized using 75 µL acetonitrile and 75 µL of N-methyl-N-(tertbutyldimethylsilyl) trifluoroacetamide (MTBSTFA, Thermo Scientific). After this derivatization step, the samples were analyzed by GC-MS. Also for the amino acid quantification isotope dilution mass spectrometry (IDMS) was applied using U-^{13}C-labeled cell extract as an internal standard mix [107,186]

7.2.4 Cell dry weight and total organic carbon determination of broth and filtrate

The biomass dry weight concentration was measured by filtration of three times 5 ml of culture broth on a pre-weighed glass fiber filter (PALL A/E glass fiber filter 47mm) and dried for 24 h at 70 °C. For TOC analysis ± 5 mL of broth and filtrate were stored at -20 °C and analyzed with a TOC analyzer (TOC-5050A, Shimadzu).

7.2.5 Quantification of ACVS

Four samples of 40 ml of fermentation broth were taken after approximately 75 h, 150 h, 300 h and 450 h of chemostat cultivation and centrifuged (6 min, 4700 rpm, 4 °C). The obtained pellet was washed by resuspending it in 40 mL, 10 mM potassium phosphate buffer with 2 mM EDTA (pH 7.5) and again centrifuged (same conditions as described above). The pellet thus obtained was resuspended in 10 mL potassium phosphate buffer and stored at -20 °C until further processing [43,64].

For ACVS protein quantification 2.5 mL of the stored biomass at -20 °C was thawed and ground to a fine powder in liquid nitrogen. Following, sonication was performed to increase cell disruption. After pelleting of cellular debris, the proteins were extracted from the supernatant by cold TCA/acetone precipitation. For each time point, 0.5 mg of total protein was redissolved in 50 mM triethyl ammonium bicarbonate, with 25% MeOH and 2 mM dithiotreitol to reduce protein disulfide bonds. After alkylation of the free thiol groups with 5 mM iodoacetamide, the proteins were digested with sequencing grade trypsin. Relative quantitative proteomics was done by trypsin-catalyzed O^{18} labeling, essentially as described by Bezarosti et al. [18]. The mixtures of O^{16} and O^{18} labeled peptides were analyzed by nanoflow LC-MS/MS using a nanoAcquity (Waters) and an LTQ-Orbitrap Velos (Thermo Fisher). Database searches were done using Mascot (www.matrixscience.com) in the Uniprot protein database, using *Penicillium chrysogenum* as taxonomy restrain. Protein quantification of ACVS was done using MSQuant [113].

7.2.6 Model construction, parameter estimation and simulations

A kinetic model was constructed to describe the formation and secretion of ACV and bisACV. The kinetic parameters for the model were estimated by weighted nonlinear regression, using the least-squares method in MATLAB R2012b. All simulations of intracellular and extracellular concentrations were performed by numerically solving the sets

of ordinary differential equations representing the mass balances for intracellular and extracellular metabolites using MATLAB R2012b (see Appendix II).

7.3 Results

7.3.1 Strain construction

ACV producing strains of *P. chrysogenum* were obtained by transforming protoplasts of *P. chrysogenum* DS55153, a strain lacking all penicillin biosynthesis gene clusters [65,126] with plasmid pDest43_phleo.Ppcbc.pcbAB.TpenDE containing markers amdS+, phleoR (see supplementary material). The obtained transformants were genetically checked for the presence of *pcbAB* that expresses the ACVS enzyme. The expression of ACVS was determined by Western blot analysis, of which the results are shown in Figure 7.5.

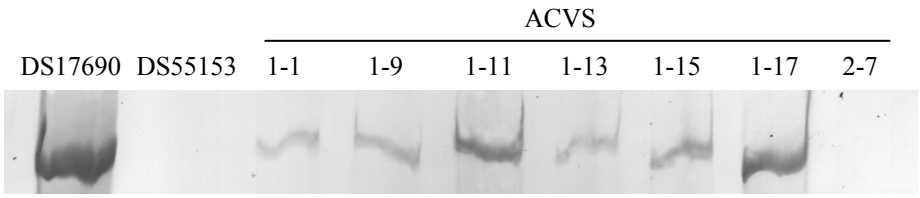

Figure 7.5: A comparison of the Western blot analysis for various *P. chrysogenum* strains expressing ACVS. The control strains are, a high producing *P. chrysogenum* DS17690 and a clusterfree strain of *P. chrysogenum* DS55153.

The expression level was compared (Figure 7.5) to the high producing wild type strain of *P. chrysogenum* DS17690 and the clusterfree strain *P. chrysogenum* DS55153. As the clusterfree strain does not contain the penicillin biosynthesis genes, it shows no expression of ACVS. The DS17690, which is a high producing strain, had the highest expression level of ACVS. Several transformants that were prepared showed variable intensities of ACVS expression. ACVS 1-17, coded as DS62824, was used for the further evaluation of ACV production and secretion in glucose limited chemostat cultivations.

7.3.2 Chemostat cultivations of the ACV producing strain DS62824

Biomass and Offgas measurements

A comparison of measured cell dry weight and O_2 and CO_2 levels in the offgas for the duplicate chemostat cultivations 1 and 2 of the ACVS producing mutant strain (ACVS 1-17) are shown in Figure 7.6. The two chemostats were reproducible with respect to measured cell dry weight and O_2 and CO_2 levels in the offgas. The mycelium dry weight concentration

steadily decreased during the course of the fermentations. The offgas oxygen and CO_2 levels were in a pseudo steady state during a period of 30 h to 150 h that was followed by a change to reach a second pseudo steady state during the period of 250 h to 400 h. The dissolved oxygen did not drop below 85% of the air saturation.

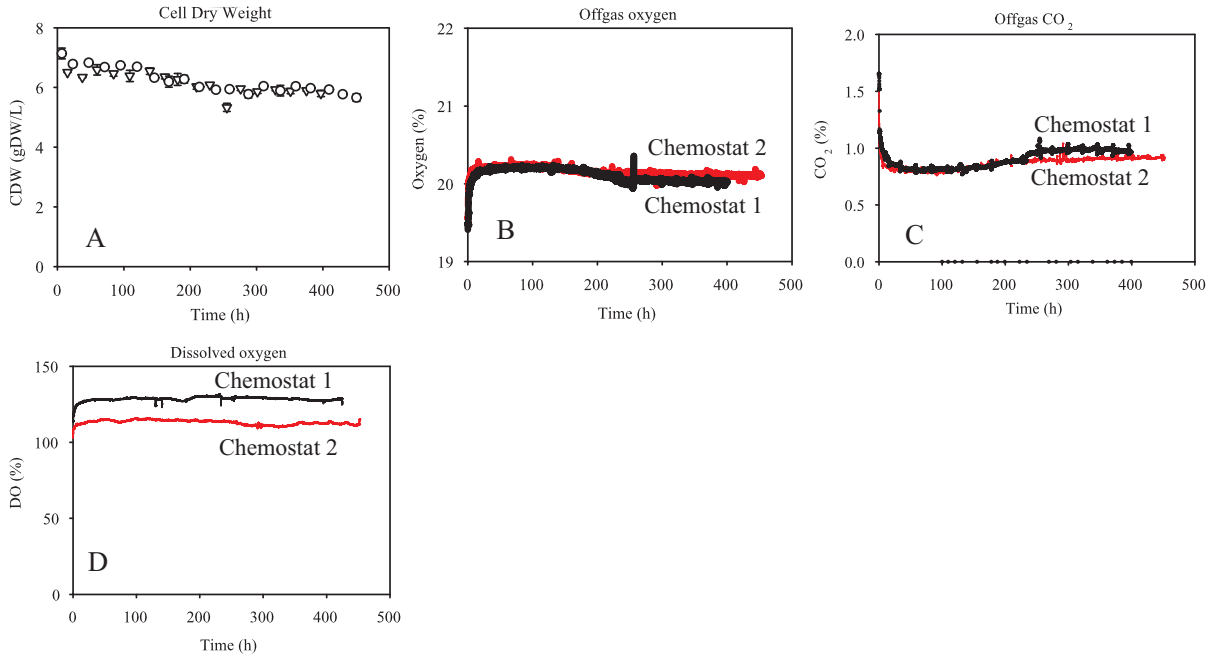

Figure 7.6: [A] Cell dry weight for chemostat 1 (open circles) and chemostat 2 (open triangles) [B] oxygen level in offgas for chemostat 1 (black) and chemostat 2 (red) [C] CO_2 level in offgas for chemostat 1 (black) and chemostat 2 (red) [D] Dissolved oxygen level for chemostat 1 (black) and chemostat 2 (red).

Intracellular free and total ACV levels

Quantification of measured total intracellular ACV was performed only for chemostat 1 by using TCEP (Figure 7.7A). For chemostat 2 as shown in Figure 7.7B, the oxidation of ACV was stopped by addition of EM at the time of sampling leading to the formation of the complex ACV-ethyl maleimide (ACV-EM) representing the free ACV present at the time of sampling. Due to the prevention of further oxidation of ACV by the addition of EM, accurate quantification of bisACV was also possible.

For chemostat 2, the total intracellular ACV level was calculated by the summation method, whereby free ACV (ACV-EM complex) was added to two times the concentration of bisACV, an approach used by Theilgaard et al. [160]. The intracellular total ACV level obtained by the two methods: measured total ACV (after complete reduction by the addition of TCEP in chemostat 1) and calculated total ACV (summation method in chemostat 2) showed nearly the same results and the same time behavior (Figure 7.7A and 7.7B). This

would indicate that the amount of ACV bound to other thiol compounds, which is not included if the summation method is applied, is relatively small.

Analysis of samples of which the oxidation of ACV was not prevented by the addition of EM showed a low level of free ACV (Appendix V), indicating that significant oxidation of ACV occurs during sample processing.

In the absence of IPNS, which converts ACV to IPN in the penicillin biosynthesis pathway, we observed, as expected, that there was a significant intracellular accumulation of ACV. During the first 100 h of chemostat cultivation, there was an increase in the intracellular level of ACV up to ~80 µmol/gDW, after which the level decreased to ~30 µmol/gDW and remained in that range up to 400 h. In addition, there was formation of bisACV, showing a similar time profile as that of free ACV (ACV-EM). The maximum intracellular level of bisACV occurred between 50 h and 100 h of fermentation. The amount of bisACV formed was approximately 10%-20% of that of free ACV, which showed that nearly all intracellular ACV was present in a reduced state.

A) Chemostat 1 - addition of TCEP

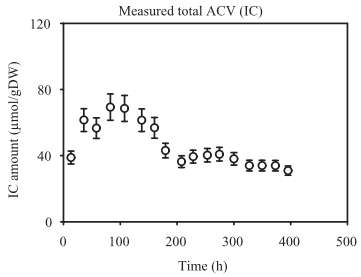

B) Chemostat 2 - addition of EM

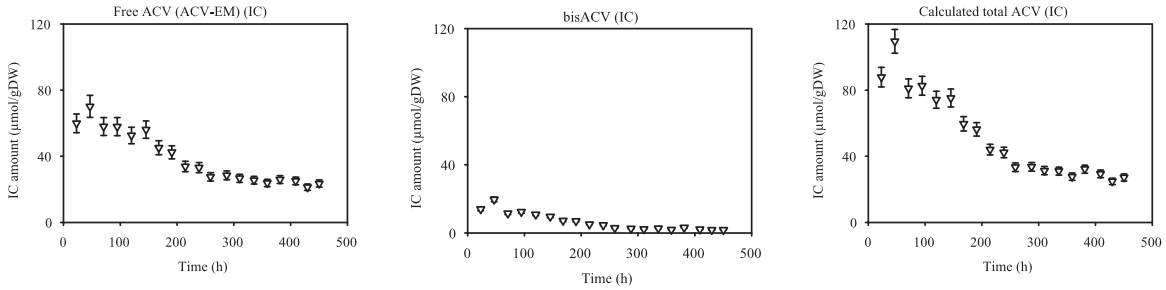

Figure 7.7: [A] Measured intracellular total ACV as determined by addition of TCEP for chemostat 1 (o). [B] For chemostat 2 (∇), intracellular ACV as determined by addition of EM, intracellular bisACV level and calculated intracellular total ACV by summation method (ACV-EM + 2 x bisACV). Each data point represents a single sample and the error bars gives the standard deviation for replicate analysis.

Extracellular free and total ACV levels

For both chemostat experiments the total extracellular ACV level was quantified after addition of TCEP. The results were very comparable for both chemostats (Figure 7.8A). During the first 100 h of chemostat cultivation the extracellular total ACV level increased to a value of 550 µM and then decreased to 200 µM, a trend similar to what was observed of the intracellular total ACV level.

With the addition of EM to the extracellular samples in chemostat 2, extracellular free ACV in the form of the ACV-EM complex and bisACV were quantified (Figure 7.8B). The extracellular free ACV followed a similar trend as that of intracellular free ACV and reached a maximum concentration of 80 µM during the initial stage of the chemostat 2, where after it decreased to a low level of ~3 µM in the later stage of the chemostat cultivation. In the extracellular space, there was significant formation of bisACV, up to approximately 70 µM.

A) Chemostat 1 and Chemostat 2 - addition of TCEP

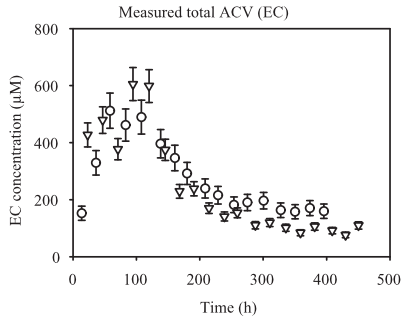

B) Chemostat 2 - addition of EM

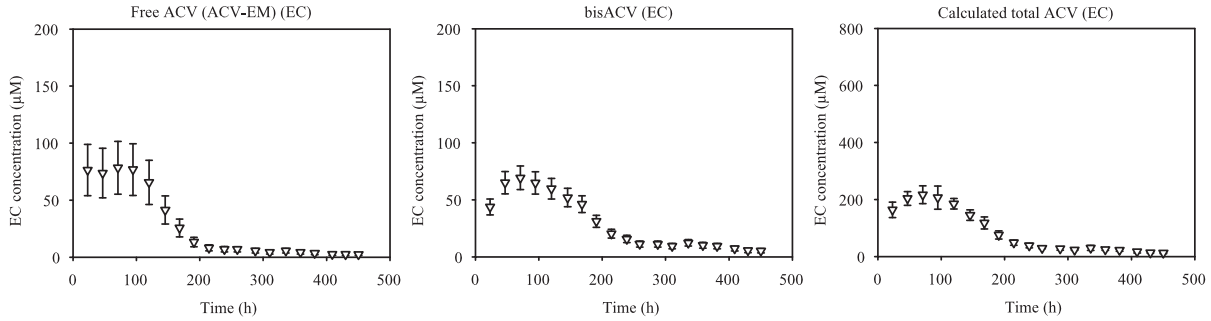

Figure 7.8: [A] A comparison of extracellular total ACV for chemostat 1(o) and chemostat 2 (∇), as determined by addition of TCEP. [B] For chemostat 2, extracellular free ACV as determined by addition of EM, extracellular bisACV level and calculated extracellular total ACV by summation method. Each data point represents a single sample and the error bars gives the standard deviation for replicate analysis.

For chemostat 2, the measured extracellular total ACV level obtained by addition of TCEP was much higher than the calculated extracellular total ACV level obtained by the summation

method (Figure 7.8A and Figure 7.8B). The difference in the levels obtained by these two methods shows that there was significant reaction of extracellular ACV with other extracellular thiol compounds, which is not taken into account in the summation method.

Precursor amino acid and ATP/ADP levels

As the formation of ACV depends on the supply of the three precursor amino acids α-AAA, cysteine and valine and ATP, it is important to understand the impact of their supply on the dynamics in the production of ACV. The dynamics observed in the intracellular level of ACV were, however, very different from the intracellular level of the precursor amino acids (see Figure 7.9). The amino acid levels hardly changed over the cultivation period in both fermentations. The intracellular ATP and ADP levels also remained more or less constant over the period of cultivation as shown in Figure 7.9. This indicates that the changes in the ACV level are not related to changes in the ACV precursors and/or ATP/ADP levels.

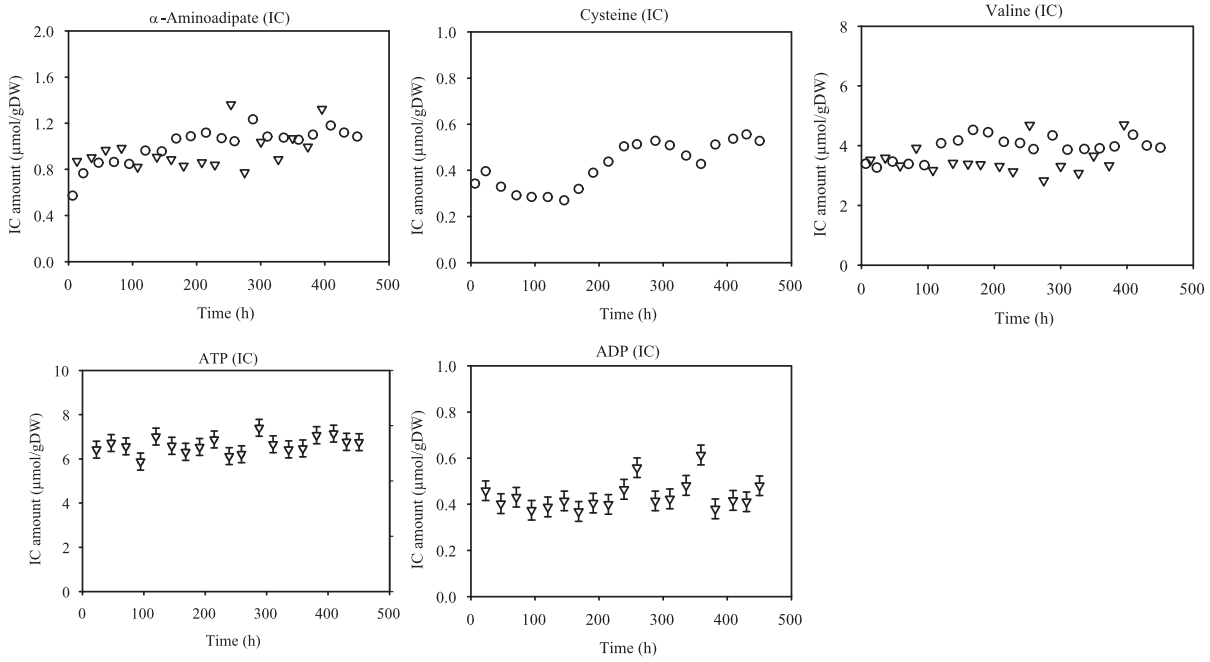

Figure 7.9: Intracellular levels of the precursor amino acids: α-aminoadipate, cysteine and valine and ATP/ADP levels in chemostat 1 (o) and chemostat 2 (∇).

ACV synthesis and secretion

The ACV secretion rate and the ACVS flux were calculated as a function of culture age using the mass balance equations given in Appendix III. The secretion rate of ACV was calculated from the measured total extracellular ACV as determined by TCEP. The maximum secretion rate (see Figure 7.10A) was observed after approx. 100 h of chemostat cultivation and reached

a value of 0.125 mmol/Cmol.h. The secretion rate decreased 6 fold to around 0.04 mmol/Cmol.h towards the end of the fermentation.

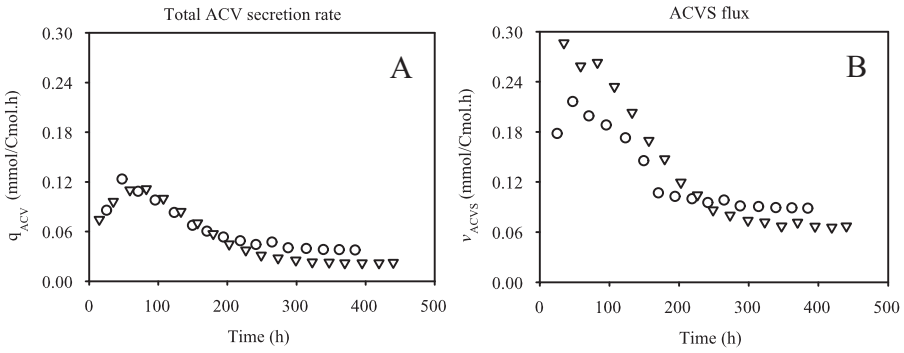

Figure 7.10: [A] ACV secretion rate calculated using the total extracellular ACV as determined through TCEP addition [B] flux through ACVS for chemostat 1 (o) and chemostat 2 (∇).

In order to calculate the flux through ACVS, the measured extracellular total ACV as well as the accumulated intracellular total ACV must be taken into account. Because a significant amount of ACV was present inside the cells, expressed per L of total broth roughly the same as outside, the calculated flux through ACVS reached a maximum value in the range of 0.19 – 0.27 mol/Cmol.h, which is two times higher than the secretion rate of ACV into the medium (Figure 7.10B). Subsequently, the ACVS flux decreased 3 fold to a value of about 0.08 mmol/Cmol.h as the fermentation progressed.

OPC formation

The intracellular α-AAA is partly converted to the by-product 6-oxopiperidine-2-carboxylic acid (OPC), which is excreted. The intra- and extracellular levels of OPC for both chemostats are shown in Figure 7.11. The intracellular OPC concentration followed closely the dynamics of intracellular ACV, reached a maximum level of ~0.8 µmol/gDW at 100 h and subsequently dropped to 0.2 µmol/gDW. The extracellular OPC level followed a similar trend as the intracellular level and both decreased approximately 6 fold during the 400 hours of chemostat cultivation.

From these results, it was calculated that the secretion rate of OPC decreased from 0.012 mmol/Cmol.h to 0.004 mmol/Cmol.h (Figure 7.11). The rate of OPC synthesis is very similar to the OPC secretion rate, because the intracellular amount of OPC is small compared to the extracellular amount.

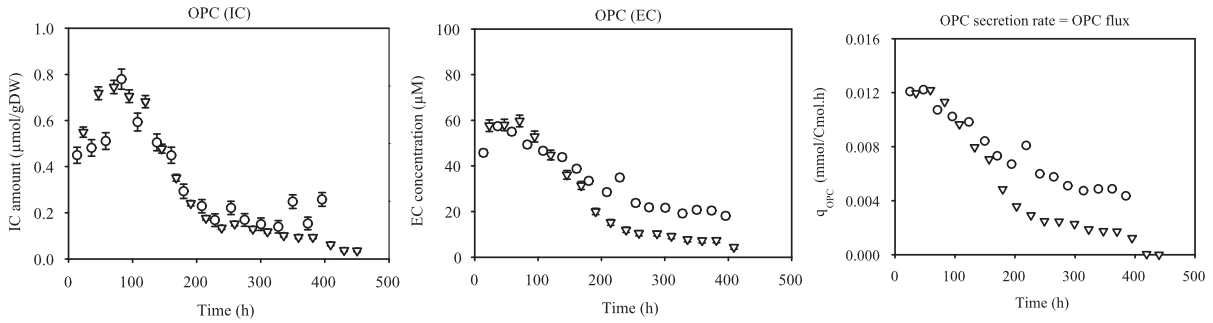

Figure 7.11: Intra- and extracellular level of OPC and OPC secretion rate in chemostat 1 (o) and chemostat 2 (∇). Each data point represents a single sample and the error bars gives the standard deviation for replicate analysis.

7.3.3 Flux analysis of the central metabolism

The biomass-specific net conversion rates, i.e., growth rate, glucose and oxygen consumption rates, and the production rates of carbon dioxide, ACV, bisACV, OPC and byproducts during the two states of chemostat 1 were calculated from their steady-state mole balances (see Appendix III). The experimentally set gas and liquid inflow rates and the measured concentrations of compounds, including their experimental errors, were used as input data for these calculations. Because with the available set of measurements an over determined system was obtained, data reconciliation and gross error detection could be applied. Under the constraint that the elemental conservation relations should be satisfied, standard data reconciliation techniques were used to obtain the best estimates of the net conversion rates with their standard errors, according to Verheijen [178]. The results are shown in Table 7.A3 (Appendix IV). It was observed that between state 1 and state 2 the ACV flux decreased in the range of 55% to 70% for chemostat 1 and chemostat 2 respectively. In addition, there was increase in glucose uptake rate, O_2 uptake rate and CO_2 production rate in state 2. Applying essentially the same data reconciliation procedure, conventional metabolic flux analysis was carried out using a previously published stoichiometric model [176]. The model was modified by eliminating the penicillin pathway reactions after ACV towards penicillin. The obtained flux distribution for both chemostats is shown in Figure 7.12. The fluxes during maximum production of ACV (state 1) and during minimum production of ACV (state 2), are shown separated by "/". Also, the flux towards the production of ACV is shown in Figure 7.13.

The analysis showed (Figure 7.12 and 7.13) that with a decrease in ACV production there was less demand for the precursor amino acids, that is, their biosynthesis fluxes were decreased during state 2. The decrease in the fluxes was by 25%~35%, 45%~60% and 15%~20% for α-AAA , cysteine and valine respectively. It is known that the formation of ACV by ACVS

requires 3 moles of ATP per mole of ACV produced. Although the production rate of ACV was lower during state 2, the glucose uptake had increased significantly in state 2 (Figure 7.12). Accordingly, the glycolytic and TCA cycle fluxes were higher during state 2 than during state 1. From the flux analysis it was calculated that the rate of ATP production was 37%~28% higher during state 2 as compared to state 1, which can also be seen from the increased oxygen consumption rate in state 2 (Table 7.A3) . This increase in ATP production is surprising, considering the lower production of ACV during state 2.

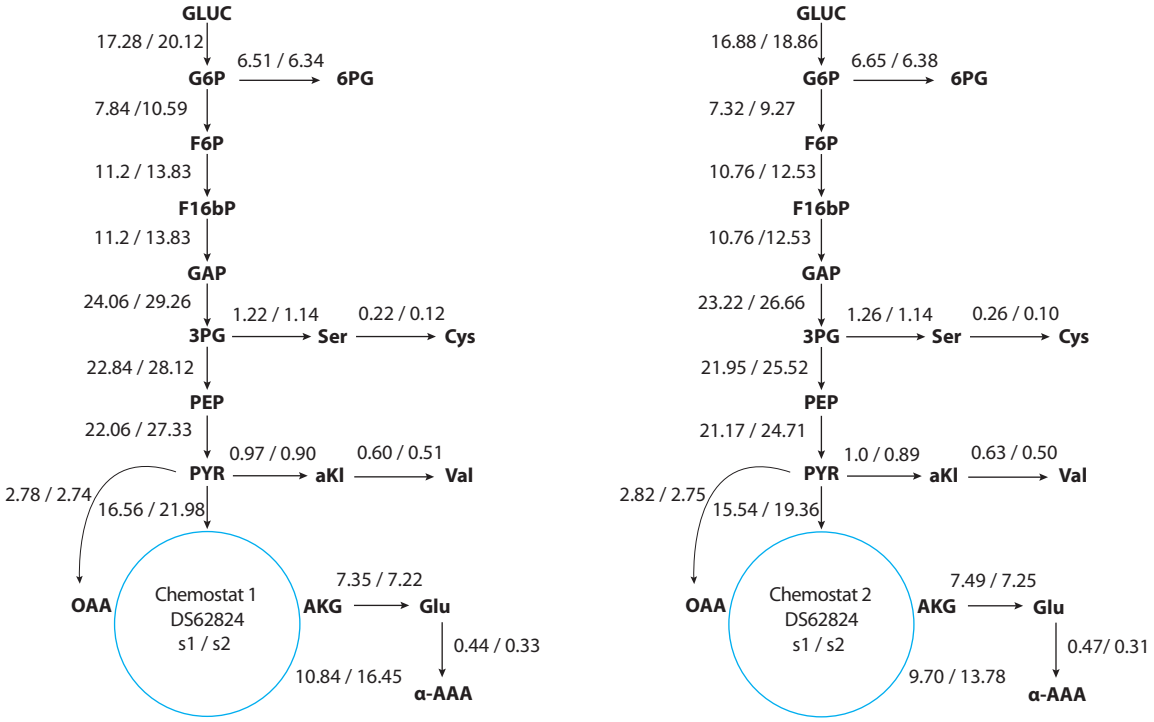

Figure 7.12: Calculated flux distribution (chemostat 1 and chemostat 2) through central carbon metabolism and TCA cycle for *P. chrysogenum* DS62824 expressing only ACVS assuming steady state (state 1 and 2, are separated by a "/"). State 1 (s1) represents the maximum ACV production (chemostat 1, t = 58 h to 107 h and chemostat 2, , t = 23 h to 120 h) and state 2 (s2) represents minimum ACV production (chemostat 1, 327 h to 395 h and chemostat 2, , t = 310 h to 381 h). Fluxes are expressed in the unit mmol/Cmol.h.

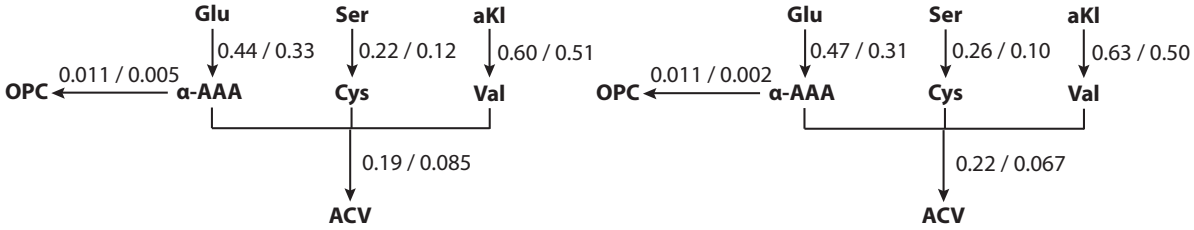

Figure 7.13: Fluxes towards ACV and OPC formation for the state 1 and state 2 two for *P. chrysogenum* DS62824 expressing only ACVS assuming steady state. The flux towards ACV is the total flux including the secretion and accumulation of total ACV. Fluxes are expressed in the unit mmol/Cmol.h.

ACV production also requires reducing equivalents in the form of NADPH (mainly for sulphate reduction to synthesize cysteine). The decrease in flux through the pentose phosphate pathway, which produces the major part of NADPH, is only 3%. Thus, the decrease in the ACV flux was probably not caused by a limitation in the supply of the precursor amino acids neither by ATP or NADPH availability, similar as was observed for the penicillin producing parent strain. During state 2 of the fermentation the rate of OPC formation was also significantly lower (82%).

7.3.4 ACVS protein level

To investigate whether the drop in the intracellular ACV level and ACVS flux could have been the result of a decreasing ACVS enzyme level, mass spectrometry was applied to quantify ACVS in the mycelium samples taken from chemostat 2. The results depicted in Figure 7.14A revealed that AVCS indeed decreased fivefold during almost 500 hours of chemostat cultivation. A plot of the ACVS flux against the ACVS level shows that the ACVS flux is proportional to the ACVS enzyme level (Figure 7.14B).

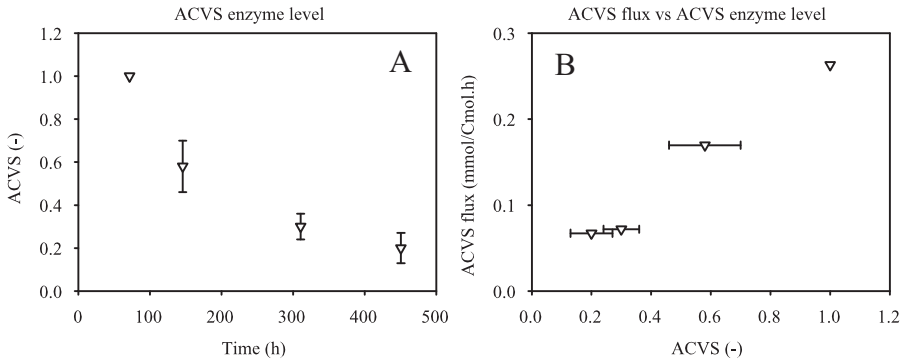

Figure 7.14: [A] ACVS enzyme level as a function of culture age for chemostat 2 (∇). The enzyme levels are expressed relative to the measured level at a culture age of 75 h. [B] ACVS flux plotted against the ACVS protein level for chemostat 2 (∇). The error bars represent the standard deviations of replicate analyses.

7.3.5 Secretion kinetics of ACV, bisACV and OPC

Understanding the secretion mechanism and its rate is essential for developing a profitable production process for any non-ribosomal peptide. Elucidating the secretion mechanism of ACV was therefore one of the key aspects of this investigation. At an intracellular pH of 7.2 in *P. chrysogenum* [100,101,134,145,173], intracellular ACV carries one negative charge, because the carboxylic acid group is present in the dissociated form. This implicates that ACV cannot pass the membrane as such and therefore its transport over the cell membrane must

occur via a specific transport protein. Possible mechanisms for this could be proton symport (K_{eq}=0.2), uniport (K_{eq}=73), or proton antiport (K_{eq}=10^4) (see Appendix I), where K_{eq} is the extracellular to intracellular (EC/IC) concentration ratio at equilibrium. The measured ratio of extracellular to intracellular free ACV was 0.0035 at its highest intracellular level (after 80 hours of cultivation), after which it decreased and stabilized to a value of approximately 0.0002 (Figure 7.15). The measured EC/IC ratio for ACV appeared to be far less than all the three K_{eq} ratios for the three different mechanisms (Appendix I). This implies that, in principle, all three secretion mechanisms are possible. In addition, from literature it is known that ACV is not detectably taken up from the medium by *P. chrysogenum* cells [56], which means that the secretion is practically irreversible. Therefore, a possible mechanism for the irreversible transport of ACV^{-1} can be proton antiport.

In the extracellular space we also observed bisACV, so it was essential to know whether bisACV is also secreted, or formed only from the spontaneous oxidation of extracellular ACV. Assuming that the rate constant of spontaneous bisACV formation is similar in the intra- and extracellular space, the rate of bisACV formation should depend in a similar way on the concentration of ACV. Nevertheless we observed that, although the extracellular free ACV concentration is much lower than the intracellular free ACV concentration, the extracellular bisACV concentration is much more higher than the intracellular bisACV concentration (Figure 7.7 and 7.8). Therefore, we assume that bisACV is also secreted and this hypothesis is also validated with the model. The EC/IC ratio of bisACV shown in Figure 7.15 was in the range of 0.011 ± 0.003 over the period of chemostat cultivation. As bisACV carries a double negative charge, the K_{eq} of a diprotic acid for (double) proton symport would be 0.04, for a uniporter the K_{eq} would be 5265 and for an antiporter the K_{eq} would be in the range of ~ 10^8. Thus, again all three mechanisms are possible for the export of bisACV.

With respect to the secretion mechanism of OPC, as it carries one negative charge therefore passive diffusion over the plasma membrane is unlikely to occur. The steady ratio of extracellular to intracellular OPC was slightly higher than 0.2, showing that proton symport of OPC^- (K_{eq} of 0.2) is not possible. A possible mechanism for OPC^- secretion could be a uniporter (K_{eq} of 73) or proton antiporter (K_{eq} of 10^4).

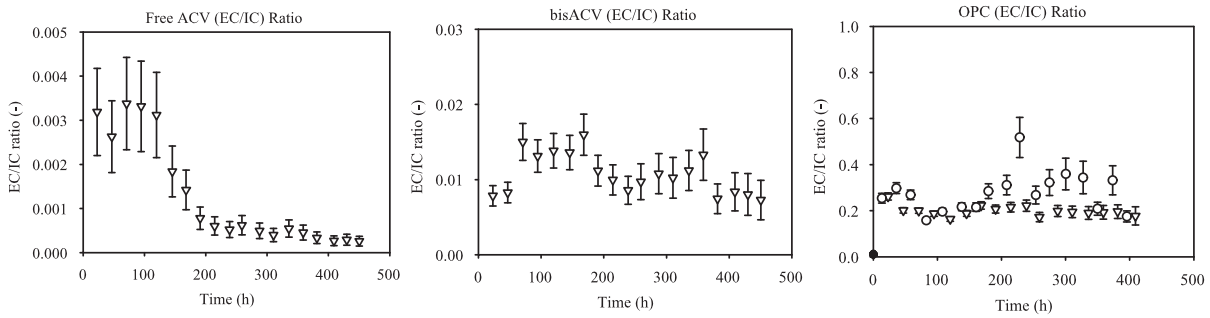

Figure 7.15: Ratios of extra- to intracellular (EC/IC) ACV-EM complex which represents the free ACV^{-}, EC/IC ratio of $bisACV^{-2}$ and EC/IC ratio of OPC^{-} for chemostat 1 (o) and chemostat 2 (∇).

7.3.6 Kinetic model for ACV production and secretion

To understand the kinetics of ACV and bisACV formation and to validate their transport mechanism across the plasma membrane, a kinetic model was developed (see Appendix II). The structure of the kinetic model is as shown in Figure 7.16. The decrease of the ACVS enzyme level during chemostat cultivation was described with an exponential decay function. The rate equation for ACVS included inhibition by both intracellular free ACV and intracellular bisACV.

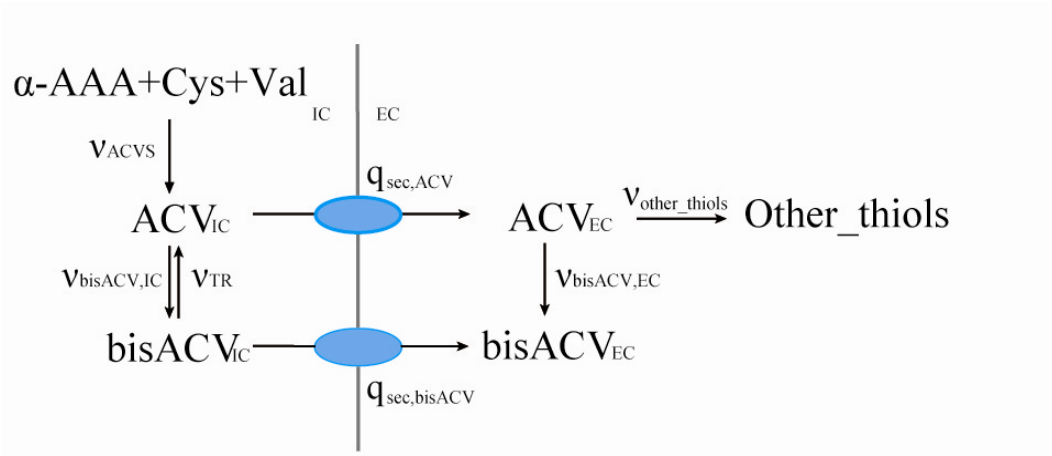

Figure 7.16: Structure of the kinetic model.

The rate of formation of bisACV, a spontaneous chemical reaction, was assumed to be a function of both the ACV concentration and the dissolved oxygen concentration. The dissolved oxygen concentration term can be incorporated into the rate constant term, being constant in time and equal in and out of the cell. There was no sufficient independent information to estimate the flux from intracellular bisACV towards intracellular ACV by the TR system. Therefore a net flux towards the formation of intracellular bisACV was assumed. Furthermore, as argued before, it was necessary to incorporate the secretion of bisACV in the model. The model was also tested by assuming that there was no bisACV secretion. However,

without bisACV secretion the model could not satisfactorily estimate the extracellular time profiles of ACV and bisACV.

The transport mechanism for ACV^- was assumed to be an irreversible antiporter and mechanism for $bisACV^{-2}$ secretion was described by the most simple irreversible mass action kinetics. In the extracellular space, as there was reaction of ACV with other extracellular thiol compounds, the kinetics of the formation of these other thiols compounds is assumed to follow a hyperbolic function of free ACV. The description of complete kinetic model and estimated parameters (Table 7.A2) are shown in Appendix II.

As the enzymes only recognize free ACV, the measured concentrations from chemostat 2 were used for parameter estimation and simulations. For this purpose, the data available after 70 h of cultivation was used, as prior to that information regarding the ACVS enzyme level was not available. Figure 7.17 shows the simulation results with respect to the concentrations (Figure 7.17A) and fluxes (Figure 7.17B). The model was able to describe the dynamics in the intra- and extracellular metabolite levels. The flux through ACVS starts at a high value of 0.21 mmol/Cmol.h and exponentially decreases to a value of 0.05 mmol/Cmol.h at the end of chemostat after 400 h. The free ACV secretion rate was ~ 25% of the ACVS flux. The model also describes the extracellular formation of other thiol compounds from ACV, being in total 50% of the free ACV secretion rate. Please note that the secretion rate of free ACV is far less than the secretion rate considering measured extracellular total ACV. The sum of the free ACV secretion rate, two times the bisACV secretion rate, and formation rate of other thiol compounds equaled the total ACV secretion rate calculated from the measured total ACV concentration in the effluent of the chemostat (see Figure 7.17B).

The inhibition parameters of ACV and bisACV could not be determined well but their lower bounds were obtained. The lower limit of inhibition parameter for both ACV and bisACV was 10 mM. Compared to the measured intracellular concentrations these inhibition constants are large, which would imply that inhibition of ACVS by bisACV is absent and that the inhibition by free ACV is very limited.

A) Concentrations

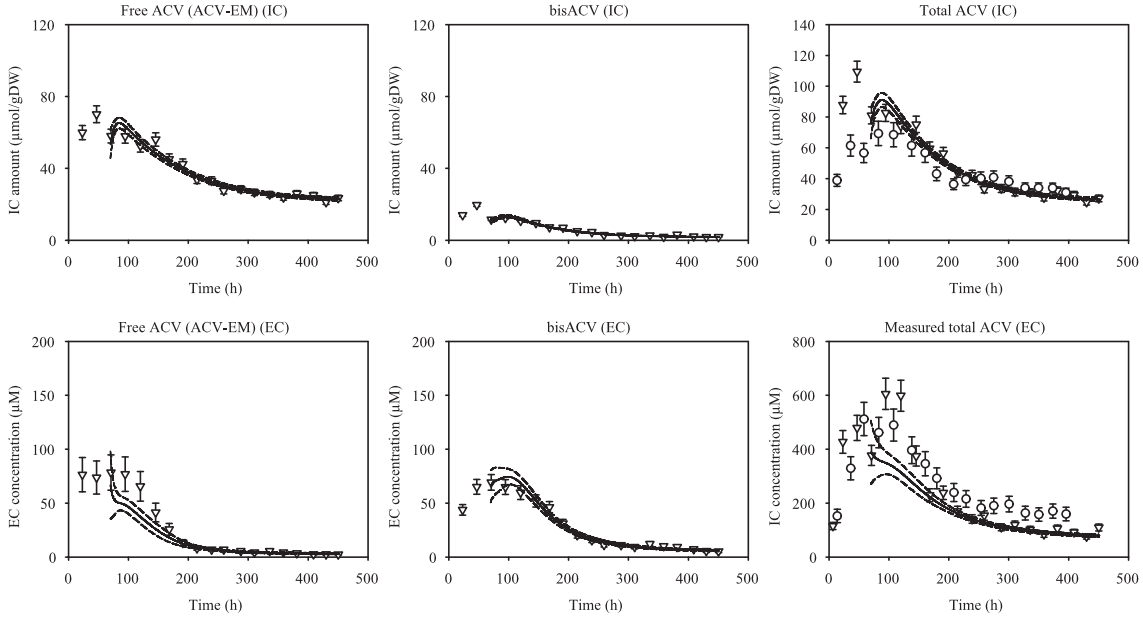

B) Fluxes

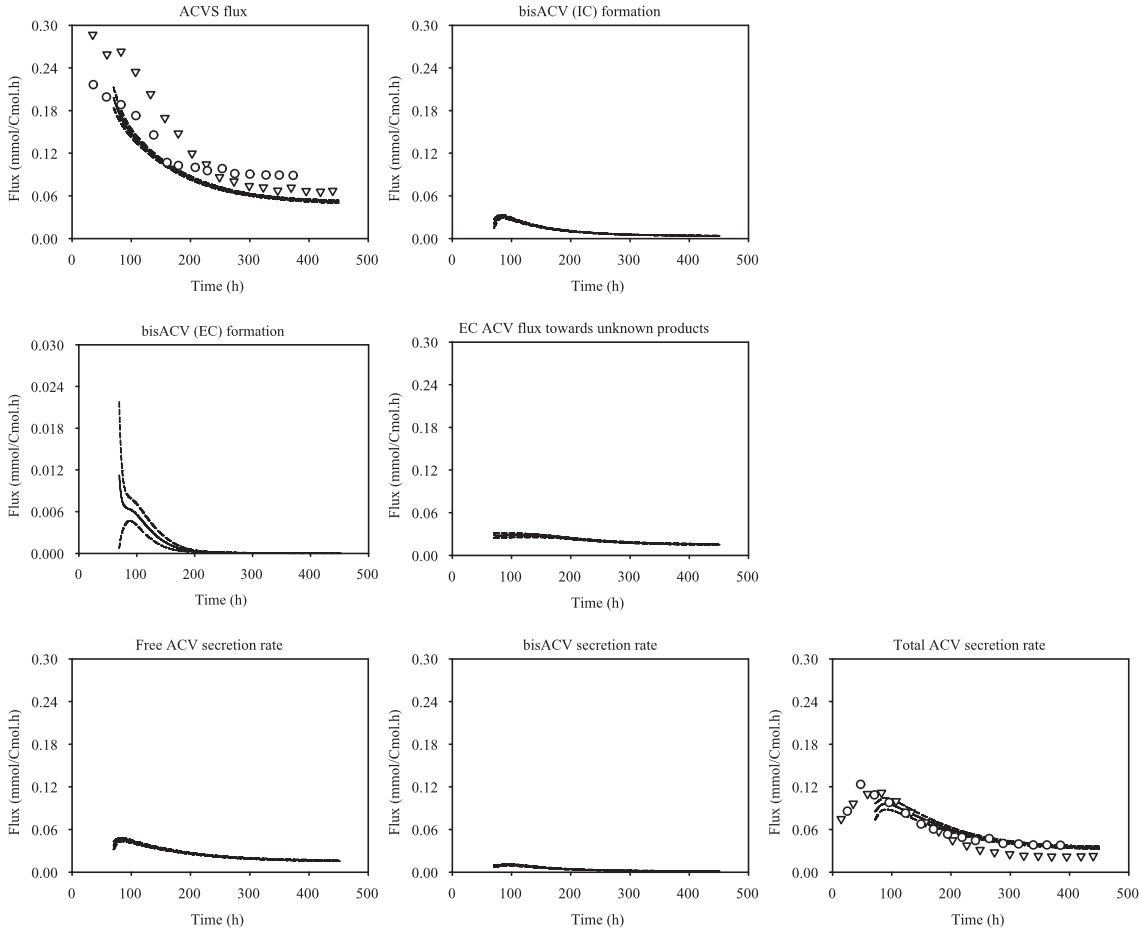

Figure 7.17: Model description for the production of ACV and related compounds [A] intra- and extracellular concentrations compared with data for chemostat 1 (o) and chemostat 2 (∇). [B] Intracellular fluxes and secretion rates ACVS flux and total ACV secretion rate are compared with the measured secretion rate for chemostat 1 (o) and chemostat 2 (∇). Solid line (—) represent the estimated values and dotted line (--) represent the error region of the model description.

7.3.7 Metabolic control analysis

To identify potential bottlenecks for the production of ACV, it is important to find out to which extent a particular enzyme influences the overall flux through a metabolic network. This can be achieved by determining the flux control coefficients of the enzymes of the network [50,81,82,135]. We applied the kinetic model for ACV production and secretion to obtain the flux control coefficients by determining the effects of changes in the enzyme and transporter levels on the rate of ACV production.

After 100 h of the fermentation time, 80% of the flux was controlled by ACV exporter. After approximately ~210 h the flux control shifts towards ACVS. At the end of the fermentation at 450 h, 84% of the flux for ACV production was controlled by ACVS. The results of the metabolic control analysis thus indicate that the main bottleneck during initial period for ACV production is the ACV exporter but due to degeneration of ACVS, the control shifts towards ACVS after 10 residence time.

7.3.8 Redox state of the cell

The redox state of the cell is relevant when products are thiol compounds. This state can be described by the ratio of a redox couple such as NADPH:NADP. This ratio can be determined by measuring the ratios of concentrations of the oxidized and reduced metabolites of suitable equilibrium reactions such as glutathione reductase for the redox couple of GSH:GSSG and TR for the redox couple of ACV:bisACV. However, this requires methods for accurate quantification of free GSH, free ACV, GSSG and bisACV, as well as immediate stabilization of the reduced forms during sampling, which was achieved by immediate addition of EM.

Figure 18A shows the measured intracellular free GSH in the form of the GSH-EM complex, intracellular GSSG and measured intra- and extracellular total GSH (as determined by addition of TCEP). The measured intracellular level of total GSH was stable throughout the fermentation and remained in the range of 8-10 μmol/gDW. The measured total extracellular GSH concentration was less than 4 μM, which suggest that there was very limited secretion of GSH by this strain of *P. chrysogenum.* Intracellular formation of GSSG was observed, whereby the level initially decreased and later on stabilized during the cultivation. No extracellular GSSG was detected.

Figure 7.18B shows the ratio of free GSH (GSH-EM): GSSG and free ACV (ACV-EM):bisACV. These ratios can be considered as indicators of the redox state of the cells (red/ox) The ratio of free GSH:GSSG was calculated to increase from 10 to 30 after 100 h of chemostat cultivation. A similar trend, although more gradual, was observed for the ratio of free ACV:bisACV which increased from 5 to 12. The increase in the ratios of free GSH:GSSG and free ACV:bisACV indicates that the redox state of the cells became more reduced during prolonged chemostat cultivation.

A)

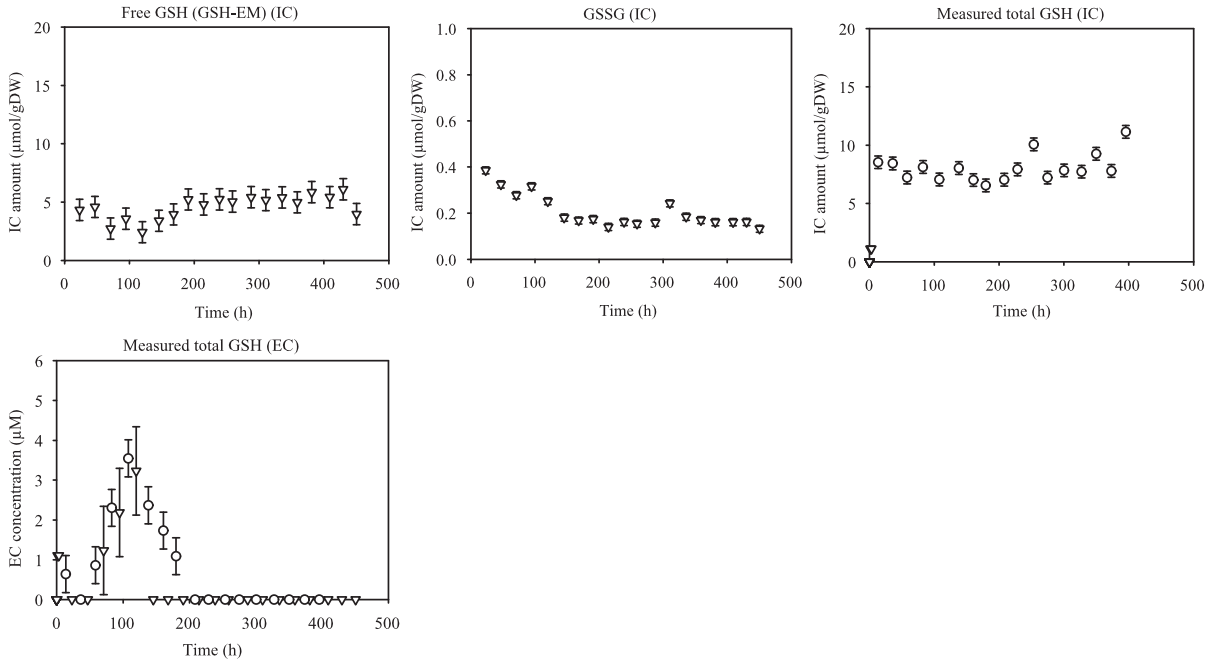

B)

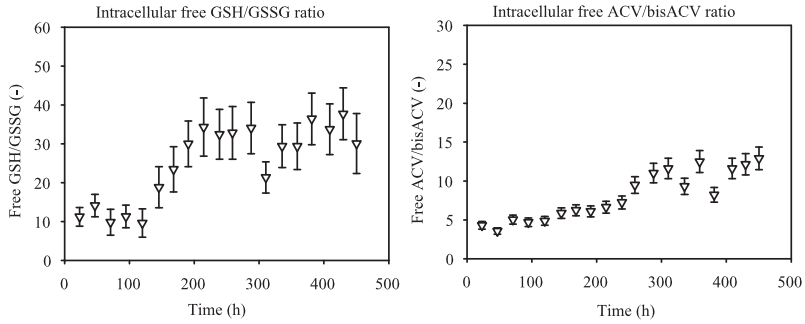

Figure 7.18: [A] Intra and extracellular levels of free GSH (GSH-EM), GSSG and measured total GSH for chemostat 1 (o) and chemostat 2 (∇). [B] Ratio of intracellular free GSH:GSSG and ratio of intracellular free ACV:bisACV

7.4 Discussion

This study was carried out to demonstrate the concept of a cell factory for the production of non-ribosomal peptides, using *P. chrysogenum* as a production host. This was achieved by constructing a *P. chrysogenum* strain that synthesizes an NRP (ACV) as the main product. Subsequently the metabolism of the strain was studied by cultivating it in a glucose-limited chemostat.

The two glucose-limited chemostat cultivations carried out appeared reproducible and showed that the constructed strain, DS62824, could produce and secrete ACV in significant amounts. After the batch phase, which was carried out under glucose excess conditions, the culture was operated as a chemostat, whereby glucose was the growth limiting nutrient. Directly after the start of the chemostat phase an increase in the intracellular level of total ACV was observed, which reached a maximum value after approx. 100 hours of glucose limited growth. The observed increase of the intracellular ACV level is in accordance to earlier findings, that IPNS promoter used in this strain for the gene encoding ACVS is repressed at high glucose concentrations [51,63]. The maximum free intracellular ACV level reached in our strain was almost 80 times higher than the maximum ACV level (~ 1 μmol/gDW) measured in the parent strain [37] cultivated under the same conditions. However, because in the parent strain the produced intracellular ACV is immediately converted to IPN and, in the presence of phenylacetic acid (PAA) further to PenG, no significant intracellular accumulation of ACV occurs.

During glucose limited chemostat cultivation, the ACV producing strain also excreted ACV. The time pattern of the extracellular ACV concentration was similar to the one of intercellular ACV, whereby a maximum total extracellular ACV concentration of 550 μM was reached. This was in contrast to the penicillin-G producing parent strain where the total extracellular ACV concentration remained below 10 μM (thesis chapter 4). Clearly, the extracellular ACV concentration, and in a chemostat culture thus also the secretion rate because ACV is continuously removed via the effluent, was higher at higher intracellular concentrations. The calculated flux through ACVS for the DS62824 strain reached a maximum in the range of 0.19 to 0.27 mmol/Cmol.h between 20 h and 60 h of chemostat cultivation. This flux was significantly lower than the maximum ACVS flux of 0.57 mmol/Cmol.h and 0.38 mmol/Cmol.h in the wild type strain (DS17690) cultivated in the presence and absence of

PAA respectively (thesis chapter 4). This was expected because the expression level of ACVS was lower in the DS62824 strain as compared to the ACVS expression level in the wild type strain, as observed from Western blot analysis (Figure 7.5). The total ACV secretion rate calculated from the measured extracellular total ACV level (using TCEP) was in the range of 0.10 to 0.12 mmol/Cmol.h at its maximum, which occurred after about 100 h of cultivation. This secretion rate was around three times lower than the secretion rate of PenG under similar chemostat conditions in the parent strain (DS17690) in the presence of PAA [37,120].

During chemostat cultivation, the production of ACV did not sustain, and started to decrease after 100 h of glucose limited chemostat growth. A possible factor that may have limited ACV production was allosteric inhibition of ACVS by ACV and bisACV. The published values of the inhibition constants of ACV and bisACV are 0.54 mM and 1.4 mM respectively, and were obtained from *in vitro* enzyme studies [159,161]. The intracellular concentrations of free ACV and bisACV measured in chemostat 2 were significantly higher than the published inhibition constants. Together, the accumulated levels of intracellular ACV and bisACV could therefore have lowered the *in vivo* capacity of ACVS. However, the inhibition parameters obtained from the kinetic model in this study were significantly higher (> 10 mM) than those obtained the *in vitro* studies of Theilgaard et al. [159,161]. The inhibition parameter of ACV from our *in vivo* study, is very similar to the value ($K_{i,ACV}$: 12.5 mM) estimated by Nielsen et al. [124] who used a kinetic model for a different *P. chrysogenum* strain. This points out that inhibition parameters determined under *in vivo* conditions may be significantly different from the corresponding parameters determined *in vitro*. This could be well caused by the applied conditions in the *in vitro* assay, which deviate from the intracellular conditions. This absence of inhibition of ACVS by ACV and/or bisACV was also confirmed by the plot of the ACVS flux vs. the ACVS enzyme level (Figure 7.14B), which showed that the ACVS flux is proportional to the enzyme level. This finding also indicates that, the high intracellular ACV and bisACV levels, which also changed significantly during the chemostat cultivations, do not affect the kinetics of ACVS.

Other factors which could affect the ACVS flux may arise from central carbon metabolism, namely the availability of the precursor amino acids and ATP. However, we observed that the intracellular levels of the amino acid precursor hardly changed throughout the cultivations (Figure 7.9). Even at their minimum levels, the measured intracellular concentrations of α-

AAA (0.24 mM), cysteine (0.11 mM) and valine (1.2 mM) were far above the reported *in vitro* K_m values of 0.045 mM, 0.08 mM and 0.08 mM respectively [161]. In addition, the intracellular ATP and ADP levels did not change significantly over the cultivation period (Figure 7.9). Together, these observations suggest that there was no limitation posed by the central carbon metabolism (precursors, ATP, NADPH) of *P. chrysogenum* DS62824 to ACV production. This agrees with similar findings for the wild type strain for the PenG production [176].

From the results of the metabolic flux analysis of the two states (Figures 7.12 and 7.13), it can be seen that the rate of ACV biosynthesis had decreased significantly 55%-to 70% during the second state of the chemostat cultivation. Surprisingly,, this decrease coincided with an increased flux through the glycolysis and through the TCA cycle, resulting in a 28% to 37% higher rate of ATP production. This showed that more and more energy was used during the cultivation, possibly a futile cycle of the redox reaction of GSH and ACV and other unknown phenomena.

According to our results, the most plausible cause of the observed decrease of the rate of ACV biosynthesis during prolonged chemostat cultivation appeared to be a decreasing ACVS enzyme level. The observed proportionality of the ACVS flux with the enzyme level (Figure 7.14B) suggests that except the enzyme level no other factor affects the flux through ACVS. Douma et al. [42] also reported that a decreasing penicillin production in a chemostat, termed degeneration, was caused by decreasing enzyme levels in the penicillin pathway, including ACVS.

The simulation results of the developed kinetic model matched reasonably to the experimental data (Figure 7.17A). The model also described the fluxes through ACVS and the secretion rates of ACV and bisACV. According to the model simulations, the maximum ACV secretion rate was 0.06 mmol/Cmol.h. There was also significant secretion of bisACV (0.03 mmol/Cmol.h) and a significant flux towards the formation of other extracellular thiol compounds (0.03 mmol/Cmol.h). Therefore, the production rate of free ACV was much lower than the total ACV secretion rate (Figure 7.17B), which included the free ACV secretion rate, twice the bisACV formation/secretion rate and the rate of dimer formation of ACV with other

extracellular thiol compounds (Figure 7.17B). Metabolic control analysis showed that the secretion rate of ACV was the limiting factor for ACV production, rather than the flux through ACVS or the availability of intracellular free ACV. Therefore, identifying and overexpressing the transporter responsible for ACV secretion is another metabolic engineering target. Possible transporters playing a role in ACV secretion could be (homologues of) GSH or IPN transporters that include the CefT transporter of the MFS family having H^+ antiporter mechanism of transport [106], high affinity GSH transporters Hgt1p or Pgt1 of the OPT family [20] or the MRPI protein of the ABC transporter family [46].

The addition of EM to the samples allowed the accurate quantification of thiol compounds such as ACV and GSH, and the ratio of their free to dimerized forms was determined. Glutathione is an important molecule in protecting cells against oxidative stress and it has been reported that increasing oxidative stress results in a decrease of GSH alongside an increase in GSSG [47]. The ratio of intracellular GSH to GSSG increased throughout the fermentation, stabilizing around 30, which is in accordance with values stated for *E. coli* [136] and values determined for several *P. chrysogenum* mutants cultivated under different conditions [47,160]. The ACV:bisACV ratio stabilized around a values of 12 at the end of the cultivation period, which is in contradiction to values published by Theilgaard et al.,[160] which were close to unity. It cannot be excluded that this has been caused by oxidation/dimerization of ACV during sample processing, because the authors did not mention the use of derivatizing agents to protect the highly reactive thiol group. The increase in the free GSH:GSSG ratio and in the free ACV:bisACV ratio (Figure 7.18B) during the chemostat cultures indicates that the redox state of the cell becomes more reduced as the cultivation progresses.

The intracellular bisACV produced from ACV is converted back to reduced ACV by an intracellular TR system [36]. However, compared to what has been measured under normal PenG producing conditions for the parent strain, a significant amount of intracellular bisACV accumulated during chemostat cultivation of the ACV producing strain, indicating that the capacity of the TR system may not have been sufficient for the accumulated level of bisACV. A capacity limitation of the thioredoxin system has not been previously reported in literature;

instead, the thioredoxin capacity was found to be sufficient, albeit at a far lower intracellular ACV concentration of 11.8 mM [160].

The intracellular OPC concentration in the chemostats showed the same dynamic pattern as seen for ACV. Because spontaneous cyclization of α-aminoadipate has not been observed to occur (thesis chapter 4) it must be an enzyme-catalyzed conversion. This suggests that OPC formation may be a side activity of ACVS. However, because the flux towards OPC in this strain (DS62824) was 10 times lower than the flux towards OPC in the wild type (DS17690) strain [37], it is likely that enzymes other than ACVS of the penicillin pathway also play a role in OPC formation in the wild type strain (DS17690). Activated α-AAA can be released from ACVS as well as from AT. Thus in the DS62824 strain, where AT is absent, the 10 fold lower OPC synthesis rate indicates that AT might be responsible for the major part of the observed OPC formation.

7.5 Conclusions

This study addresses various important aspects in the development of a cell factory for the sustainable production of a non-ribosomal model peptide (ACV), which includes precursor, redox and energy supply, stability of pathway enzymes, conversion of precursors and end product to unwanted compounds and product export. For this purpose, a strain of *P. chrysogenum* only expressing ACVS of the penicillin pathway enzymes was constructed. The issue of accurate quantification of thiol compounds was solved by adding Ethyl-maleimide for derivatizing the reactive sulfhydryl bond in ACV at the time of sampling. The strain was able to produce a total maximum in the range of 0.19-0.27 mmol/Cmol.h and secrete total ACV at a rate of 0.125 mmol/Cmol.h, which is a significant amount and represents about 35% of the penicillin production in the wild type strain.

Flux analysis showed that the requirement of the precursor amino acids, ATP and NADPH are not limiting the ACV production. The decrease in the ACV synthesis was attributed to degeneration phenomena also seen in the *P. chrysogenum* DS17690 fermentation leading to decreasing ACVS enzyme level. The secretion mechanism of ACV^{-}, $bisACV^{-2}$ and OPC^{-} were hypothesized based on measured EC/IC ratio. A kinetic model was developed and parameters were estimated for the ACVS enzyme capacity, for the free ACV and bisACV secretion capacities and for the spontaneous oxidation of ACV. Metabolic control analysis showed that

in DS62824 strain, ACV transporter controls more than 80% of the flux for ACV production during the initial stages of the fermentation and later the control shifts towards ACVS. Therefore, identifying and over-expressing transporters of ACV to increase the secretion rate is one of the first metabolic engineering targets. Accurate quantification of GSH and GSSG gave insight about the redox state of the cell that became more reduced over the period of cultivation. In addition, OPC formation in DS62824 was attributed to the side activity of ACVS, whereas in the wild type strain AT was identified as the major contributor.

In conclusion, the production of ACV in *P. chrysogenum* was found to be a promising system for the production of non-ribosomal peptides.

7.6 Acknowledgements

We acknowledge the financial support from the Netherlands Organization for Scientific Research (NWO) via the IBOS (Integration of Biosynthesis and Organic Synthesis) programme of Advanced Chemical Technologies for Sustainability (ACTS) (project nr: IBOS 053.63.011) and was also financially supported by DSM. This project was carried out within the research programme of the Kluyver Centre for Genomics of Industrial Fermentation, which is part of the Netherlands Genomics Initiative/ Netherlands Organization for Scientific Research. The authors also thank Jan A.K.W. Kiel and Annemarie Kralt for the construction of the strain.

7.7 Appendix

7.7.1 Appendix I: Different transport mechanisms

Gibbs energy associated with proton coupled export of an anion with charge -1is as follows:

$$\Delta G_R = R \cdot T \cdot \ln\left(pH_{in} - pH_{ex}\right) + R \cdot T \cdot \ln\left(\frac{C_{ex,A^-}}{C_{in,A^-}}\right) + \left(1-n\right) \cdot F \cdot \Psi \qquad \text{(A1)}$$

At equilibrium, $\Delta G_R = 0$ gives,

$$\ln\left(\frac{C_{ex,A^-}}{C_{in,A^-}}\right) = \left(pH_{ex} - pH_{in}\right) \cdot n + \frac{\left(n-1\right) \cdot F \cdot \Psi}{R \cdot T} \qquad \text{(A2)}$$

With n is the number of protons symported, F is the Faraday constant of 96.5 $kJ \cdot V^{-1} \cdot mol^{-1}$, Ψ is the intracellular electrical potential (varying between -0.08V to -0.130V), pH_{in} = 7.2, pH_{ex}=6.5, temperature, T=298 K, R= 8.314 x 10^{-3} $kJ \cdot K^{-1} \cdot mol^{-1}$ and C is the concentration.

Figure 7.A1 shows different possible mechanisms for the export of anions (Z=-1) : facilitated export (n = 0), export by proton symport (n=1), export by proton antiport (n = -1) and export with ATP hydrolysis using an ABC transporter.

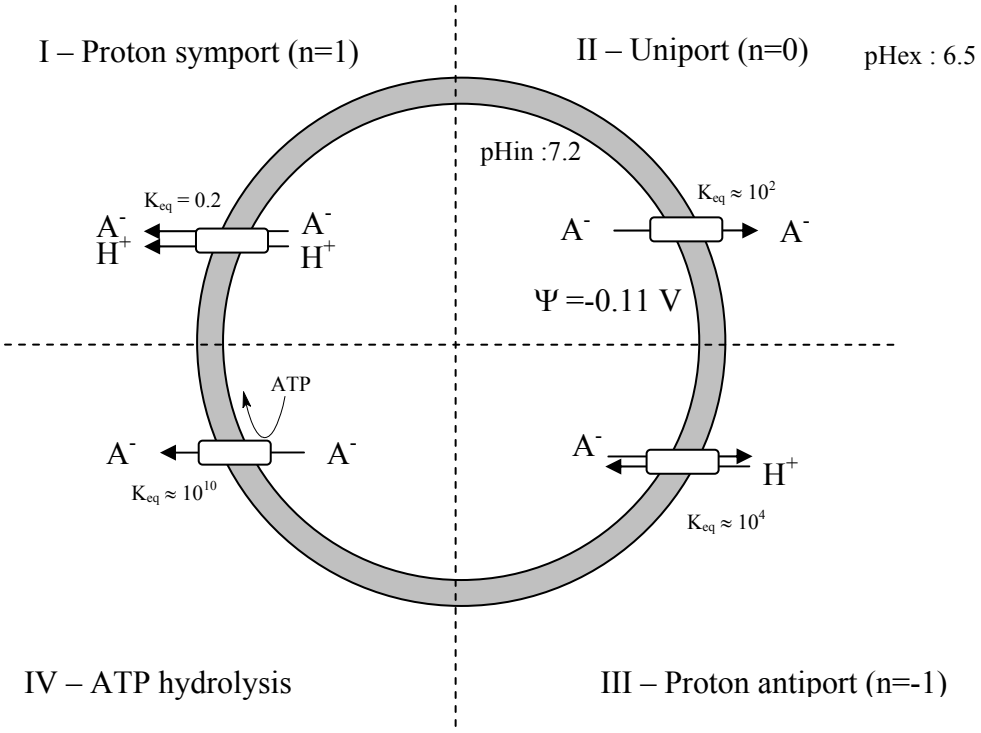

Figure 7.A1: Different types of transport mechanisms for proton coupled export of anions

The equilibrium constants for these four different mechanisms are respectively given by equation no.(A3):

$$K_{eq,uniport,(n=0)} = \frac{C_{ex}}{C_{in}} = e^{\frac{-1 \cdot F \cdot \Psi}{R \cdot T}} \approx 10^2$$

$$K_{eq,symport,(n=1)} = \frac{C_{ex}}{C_{in}} = 10^{pH_{ex} - pH_{in}} = 10^{6.5-7.2} = 0.2 \qquad \text{(A3)}$$

$$K_{eq,antiport,(n=-1)} = \frac{C_{ex}}{C_{in}} = 10^{pH_{in} - pH_{ex}} \cdot e^{\frac{-2 \cdot F \cdot \Psi}{R \cdot T}} \approx 10^4$$

$$K_{eq,ATP-hydrolyis,(n=0)} = \frac{C_{ex}}{C_{in}} = e^{\frac{-1 \cdot F \cdot \Psi + \Delta G_p}{R \cdot T}} \approx 10^{10}$$

Under physiological conditions, the energy gained from ATP hydrolysis (ΔG_p) is approximately -50 kJ·mol^{-1}.

For metabolites carrying -2 charge, K_{eq} values calculated for different mechanisms are given as, for uniport 10^4, for symport 0.04, for antiport ~10^8 and for ATP-hydrolysis ~10^{20}.

7.7.2 Appendix II: Kinetic model

A kinetic model was setup for the product pathway to estimate the capacities of the enzymes and transporters taking part in the formation of ACV. The structure of the kinetic model is described in the Figure 7.16. For the model setup all the concentrations were converted to mmol/m^3 to have uniform units. The intracellular concentrations that were expressed in µmol/gDW can be converted to $\mathrm{mmol/m^3_{IC}}$ by using the specific cell volume V_x, which is taken to be 2.5 x 10^{-6} $\mathrm{m^3_{IC}}$ cells / gDW [131,160]. The discrete cell dry weight C_x data are made continuous by fitting the data to an exponential function and then used as input to the model given by equation,

$$C_x = C_{x,1} + C_{x,2} \cdot e^{\left[\frac{-t}{\tau_{C_x}}\right]} \qquad \text{(A4)}$$

The intracellular bisACV formed can be converted back into ACV in the cell by means of thioredoxin-thioredoxin reductase (TR) system. The kinetics of this enzyme is assumed to be of Michaelis-Menten type [159] with $K_{m,bisACV} = 125$ µM [36]. In the current model, however, the fluxes through TR system cannot be identified and therefore conversion of ACV to bisACV is assumed to be only in one direction, hence $v_{TR} = 0$.

ACVS enzyme kinetics

The kinetics of the ACVS is extensively studied and is assumed to follow Michaelis-Menten type kinetics involving the three amino acids. In addition, the kinetics is also influenced by noncompetitive inhibition by bisACV and ACV [159,161]. By comparing the experimental intracellular concentrations and the K_m values of the precursor aminoacids, and also from recent studies performed by Deshmukh et al. (thesis chapter 4), we can assume that the ACVS kinetics is independent of the three precursor aminoacids. Thus, the ACVS kinetics can be described by, the following equation, taking only the inhibition terms into account as

$$v_{ACVS} = \frac{k_{ACVS}(enzyme\,capacity)}{\left(1 + \frac{C_{ACV,IC}}{K_{i,ACV}}\right) \cdot \left(1 + \frac{C_{bisACV,IC}}{K_{i,bisACV}}\right)} \qquad \text{(A5)}$$

From the measurements of ACVS levels, we observed that the ACVS enzyme capacity falls five fold in time in an exponential fashion. Thus, the enzyme level can be expressed with an exponential time function

$$k_{ACVS} = k_{ACVS,1} + k_{ACVS,2} \cdot e^{\left[\frac{-t}{\tau_{ACVS}}\right]} \qquad \text{(A6)}$$

ACV transporter kinetics

The thermodynamic equilibrium ratio (EC/IC) for ACV for proton coupled transport is given by equation A1. At neutral pH in *P. chrysogenum*, intracellular ACV carries one negative charge and therefore secretion of ACV is expected to be coupled to the transport of a proton. This can be through either proton symport, or proton antiport, or uniport (intracellular proton is pumped out through ATP-ase). At a temperature of 25 °C, an average membrane potential of -0.11V, a extracellular (pH:6.5) and intracellular (pH:7.2) pH difference of -0.7 and assuming complete dissociation of ACV in and out of the cell, the equilibrium constants of these three transport mechanisms can be calculated. The equilibrium constants calculated from equation A1 for the three possible mechanisms of ACV are shown in Table 7.A1. All the three transport mechanisms are possible, however, for the kinetic model we assume that secretion of ACV^- occurs by irreversible antiport mechanism ($K_{eq,ACV} \approx 2.6 \times 10^4$).

Table 7.A1: Equilibrium constants of uniport, symport and antiport transport of an anion carrying a charge of -1 calculated for the conditions T=298K, Ψ= - 0.11V, an intracellular pH of 7.2 and an extracellular pH of 6.5

Mechanism	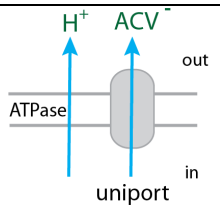	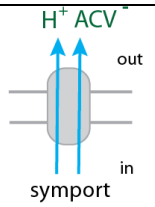	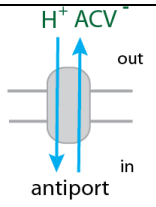
K_{eq} (EC/IC)	73	0.2	2.6×10^4

Mass action kinetics was applied to describe the biomass specific secretion rate of ACV as described by Douma et al. [44] as

$$q_{sec,ACV} = k_{sec,ACV} \cdot \left(C_{ACV,IC} - \frac{C_{ACV,EC}}{K_{eq,ACV}} \right) \qquad \text{(A7)}$$

bisACV transporter kinetics

In order to obtain the fit the mass balances of the compounds, it was also necessary to include the secretion of bisACV. bisACV carries -2 charge, thus will have different K_{eq} values than for -1 charged species. The K_{eq} values calculated for bisACV for different mechanisms are for uniport is 5265, for symport is 0.04 and for antiport is ~10^8. The measured EC/IC ratio of bisACV was, however, lower than all the three K_{eq} and all the three mechanisms were possible. Therefore $bisACV^{-2}$ secretion was also described by antiport mass action kinetics ($K_{eq,bisACV} \approx 10^8$)

$$q_{sec,bisACV} = k_{sec,bisACV} \cdot \left(C_{bisACV,IC} - \frac{C_{bisACV,EC}}{K_{eq,bisACV}} \right) \quad \text{(A8)}$$

Kinetics of bisACV formation from ACV

bisACV is formed spontaneously in presence of oxygen when the thiol bonds of two ACV combine with each other. Thus, the kinetics of bisACV formation is described by the following equation.

$$v_{bisACV,EC/IC} = k_{bisACV,ACV} \cdot C_{O_2,EC/IC}^{0.5} \cdot C_{ACV,EC/IC}^{2}$$

However, the dissolved oxygen concentration was constant throughout the fermentation, therfore the concentration of oxygen can be absorbed in the rate constant. Thus, the modified equation used in the model is

$$v_{bisACV,IC} = k_{bisACV,IC} \cdot C_{ACV,IC}^{2} \quad \text{(A9)}$$

$$v_{bisACV,EC} = k_{bisACV,EC} \cdot C_{ACV,EC}^{2} \quad \text{(A10)}$$

Kinetics of other thiol compound formation from ACV

As observed from the experimental data that the extracellular total ACV obtained from summation method (ACV+ 2 x bisACV) is not similar to the total ACV obtained by addition of reducing agent (TCEP). The rest of the ACV then probably forms unknown compounds by reacting with the other thiol compounds. The kinetics of the formation of these unknown compounds is assumed to follow hyperbolic function given as

$$v_{other\_thiols} = \frac{k_{other\_thiols}}{1 + \frac{K_{m,other\_thiols}}{C_{ACV}}} \cdot \tag{A11}$$

The balance for intracellular metabolites follows as (mmol/ $m^3_{,IC}$. h)

$$\frac{dC_{ACV,IC}}{dt} = v_{ACVS} - v_{bisACV,IC} - q_{sec,ACV} - \mu \cdot C_{ACV,IC} \tag{A12}$$

$$\frac{dC_{bisACV,IC}}{dt} = v_{bisACV,IC} - q_{sec,bisACV} - \mu \cdot C_{bisACV,IC} \tag{A13}$$

The balance of extracellular metabolites follows as (mmol/ m^3_{EC}. h)

$$\frac{dC_{ACV,EC}}{dt} = q_{sec,ACV} \cdot C_x \cdot V_x - v_{bisACV,EC} - v_{other\_thiols} - \frac{\phi_{out}}{V} \cdot C_{ACV,EC} \tag{A14}$$

$$\frac{dC_{bisACV,EC}}{dt} = q_{sec,bisACV} \cdot C_x \cdot V_x + v_{bisACV,EC} - \frac{\phi_{out}}{V} \cdot C_{bisACV,EC} \tag{A15}$$

Table 7.A2: Kinetic parameters of the model

Parameters	*Value*	*unit*	*Equation No.*	*Reference*
$k_{ACVS,1}$	765 ± 40	$mmol/m^3_{IC}.h$	A6	This study
$k_{ACVS,2}$	6350 ± 860	$mmol/m^3_{IC}.h$	A6	This study
τ_{ACVS}	88.0 ± 7.9	h	A6	This study
$k_{bisACV,IC}$	(6.49 ± 0.55) x 10^{-7}	m^3_{IC}/mmol.h	A9	This study
$k_{bisACV,EC}$	< 6.3 x 10^{-4}	m^3_{EC}/mmol.h	A10	This study
$k_{sec,ACV}$	0.0250± 0.0013	h^{-1}	A7	This study
$k_{sec,bisACV}$	0.0270 ± 0.0031	h^{-1}	A8	This study
k_{other_thiols}	7.4 ± 1.1	$mmol/m^3_{EC}.h$	A11	This study
$K_{m,other\_thiols}$	4.1 ± 1.6	$mmol/m^3_{EC}$	A11	This study
$K_{eq,bisACV}$	10^8	[-]	A8	Thermodynamic calculation
$K_{eq,ACV}$	2.6 x 10^4	[-]	A7	Thermodynamic calculation
$K_{i,ACV}$	>10^4	$mmol/m^3_{IC}$	A5	This study
$K_{i,bisACV}$	>10^4	$mmol/m^3_{IC}$	A5	This study
ACV_{IC} start value	21320 ± 3120	$mmol/m^3_{IC}$	A12	This study
$bisAC_{IC,}$ start value	4560 ± 460	$mmol/m^3_{IC}$	A13	This study
$ACV_{EC,}$ start value	67 ± 31	$mmol/m^3_{EC}$	A14	This study
$bisACV_{EC,}$ start value	65 ± 15	$mmol/m^3_{EC}$	A15	This study
V_x	2.5 x 10^{-6}	m^3_{IC} / gDW	A15	[131]
$C_{x,1}$	5587	gDW/m^3_{EC}	A4	This study
$C_{x,2}$	1507	gDW/m^3_{EC}	A4	This study
τ_{C_x}	216.7	h	A4	This study
μ	0.05	h^{-1}	A12, A13	Experimental condition
ϕ_{out}	200 x 10^{-6}	m^3_{EC} / h	A14, A15	Experimental condition
V	4 x 10^{-3}	m^3_{EC}	A14, A15	Experimental condition

The kinetic parameters obtained are shown in Table 7.A2. With these parameter values, the model description was satisfactory. The parameters $k_{ACVS,1}$ and $k_{ACVS,2}$ are influenced by the values selected for $K_{i,ACV}$

For intracellular concentrations, the model estimates are obtained in mmol/m^3_{IC} that is converted into μmol/gDW by using the specific cell volume V_x. For intracellular fluxes, the model estimates obtained in mmol/m^3_{IC}.h are first converted to mmol/gDW.h using specific cell volume V_x and then converted to mmol/Cmol.h by using C-molar biomass weight of 28.05 gDW/Cmol. For extracellular fluxes, the model estimation obtained in mmol/m^3_{EC}.h is first converted by biomass C_x (gDW/m^3) per time point to mmol/gDW.h and then converted to mmol/Cmol.h by using C-molar biomass weight. The predictions of the model are shown in Figure 7.17.

7.7.3 Appendix III: Secretion rates, uptake rates and intracellular fluxes

Fluxes were calculated using the following fermentation broth balances (constant volume):

For product :

$$\frac{dC_i}{dt} = q_{i,\text{sec}} \cdot C_x - \frac{\phi_{out}}{V} \cdot C_i \qquad \text{(A14)}$$

For substrate :

$$\frac{dC_i}{dt} = -q_{i,up} \cdot C_x + \frac{\phi_{in}}{V} \cdot C_{i,in} - \frac{\phi_{out}}{V} \cdot C_i \qquad \text{(A15)}$$

Intracellular balance :

$$\frac{dX_i}{dt} = v_{i,produced} - v_{i,consumed} - q_{i,\text{sec}} - \mu \cdot X_i \qquad \text{(A17)}$$

Where dC_i/dt stands for the change of extracellular concentration over time, q_i is the flux of i compound in mmol/Cmol.h, q_{sec} the secretion rate mmol/Cmol.h, q_{up} the uptake rate in mmol/Cmol.h, C_x the biomasss concentration in Cmol/L, $C_{i,in}$ the concentration of the compound in the inflow in mmol.L^{-1}, and C_i the concentration of the compound in the outflow/broth in mmol/L assuming ideal mixing, ideal outflow. dX_i/dt stands for the change of intracellular amounts over time. v_i is the intracellular flux in mmol/Cmol.h. These equations were used in determining the secretion rate of ACV (q_{secACV} in mmol/Cmol.h), intracellular

flux through ACVS (v_{ACVS} in mmol/Cmol.h) and the secretion rate of OPC (q_{OPC} in mmol/Cmol.h)

7.7.4 Appendix IV: Data reconciliation

Data reconciliation on the two states in chemostat 1 and chemostat 2 is shown in Table 7.A3

Table 7.A3: Comparison of reconciled biomass specific conversion rates for state 1 and state 2 for chemostat cultivation of DS62824 (expressing only ACVS) for chemostat 1 and chemostat 2. The ACV production rate is calculated based on total ACV present in the system (sum of total intracellular ACV and extracellular ACV as determined through TCEP addition); hence the bisACV secretion rate is zero.

	Chemostat 1		***Chemostat 2***	
Rates	***State 1***	***State 2***	***State 1***	***State 2***
μ	49.6 ± 1.1	49.4 ± 1.1	50.2 ± 1.1	50.2 ± 1.1
q_S	-17.37 ± 0.46	-20.21 ± 0.53	-16.96 ± 0.41	-18.95 ± 0.47
q_{O_2}	-41.7 ± 1.7	-58.2 ± 2.1	-38.5 ± 1.3	-50.3 ± 1.7
q_{CO_2}	46.2 ± 1.8	62.5 ± 2.1	43.2 ± 1.4	54.6 ± 1.8
q_{ACV}	0.1918 ± 0.0077	0.0851 ± 0.0039	0.223 ± 0.026	0.0666 ± 0.0062
q_{bisACV}	-	-	-	-
q_{OPC}	0.01063 ± 0.00097	0.00465 ± 0.00032	0.0113 ± 0.0013	0.00185 ± 0.00022
$q_{byproducts}$	5.62 ± 0.39	8.20 ± 0.33	5.15 ± 0.49	7.97 ± 0.36

Specific rates of biomass growth and by-product formation are expressed mCmol/Cmol·h other rates are expressed in mmol/Cmol. h
Chemostat 1 - State 1: A period of fermentation from 58 h to 107 h of maximum production of ACV, assumed to be in pseudo steady state for chemostat 1 having average cell dry weight of 6.48 ± 0.10 gDW/L.
Chemostat 1 - State 2: A period of fermentation from 327 h to 395 h of minimum production of ACV, assumed to be in pseudo steady state for chemostat 1 having average cell dry weight of 5.88 ± 0.06 gDW/L.
Chemostat 2 - State 1: A period of fermentation from 23 h to 120 h of maximum production of ACV, assumed to be in pseudo steady state for chemostat 1 having average cell dry weight of 6.75 ± 0.07 gDW/L.
Chemostat 2 - State 2: A period of fermentation from 310 h to 380 h of minimum production of ACV, assumed to be in pseudo steady state for chemostat 1 having average cell dry weight of 5.99 ± 0.07 gDW/L.

Specific rates of glucose uptake, oxygen uptake and CO_2 production increased from state 1 to state 2. ACV and OPC production rates decreased and the byproducts increased from state 1 to state 2. For ACV production rates, total ACV present in the system was taken for calculations.

7.7.5 Appendix V: Total ACV determination

Without the addition of any reducing agent, the quantification of ACV was very difficult. A comparison of extracellular ACV without addition of TCEP (filled circles) and with addition

of TCEP (open circles) is shown in Figure 7.A2-A for chemostat 1 samples. To determine the total level of extracellular ACV, there were two approaches available. The first approach (Figure 7.A2-B) termed as measured extracellular total ACV was by the addition of an excess of reducing agent TCEP to the samples (open triangles), which reduced all thiol bonds present in the sample for chemostat 2. Thus, the measured extracellular total ACV contained free ACV, ACV obtained by reducing bisACV and ACV obtained by reducing the ACV attached to other thiol compounds. While in the second approach (Figure 7.A2-B) termed as calculated extracellular total ACV, shown by filled triangles, the total ACV was obtained by summation of concentration of free ACV and twice the concentration of bisACV. Calculated extracellular total ACV level as determined by this second approach, also used by Theilgaard et al. [160], ignored ACV bound to other thiol compounds. Therefore, the summation approach gave a lower level of extracellular total ACV than extracellular total ACV level obtained by using TCEP. Figure A2-B points out that of all the extracellular dimerized ACV molecules, only 20-40% of ACV molecules formed self-dimers in the extracellular space, while the bigger part was in fact bound to other thiol compounds (Figure 7.A2-C). This ratio was determined using the equation below.

$$\text{Yield of bisACV} = \frac{2 \cdot [\text{bisACV}_{EC}]}{[\text{Total ACV}_{EC,TCEP}] - [\text{ACV-EM}_{EC}]} = \frac{\text{Total ACV converted to bisACV}}{\text{Total ACV converted}}$$

However, the situation is different for the intracellular environment, where the measured intracellular total ACV is close to the calculated intracellular total ACV (Figure 7.7).

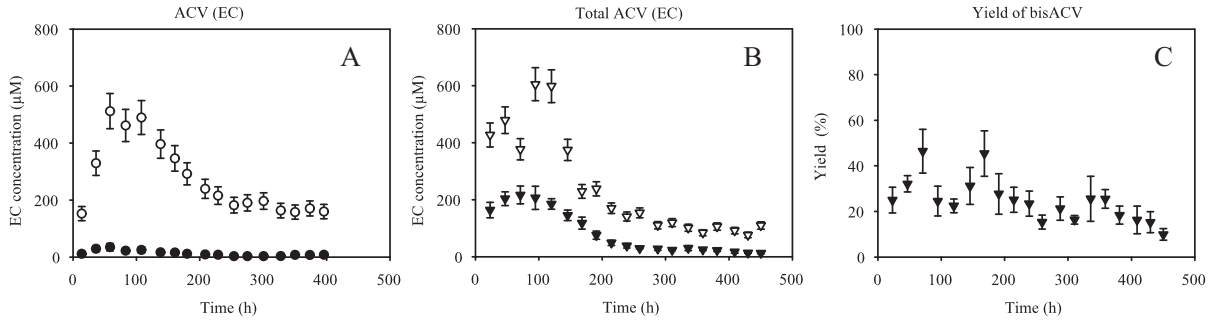

Figure 7.A2: [A] Comparison of measured extracellular total ACV determined by addition of a reducing agent TCEP (open circles) to extracellular ACV without using any reagent for chemostat 1 samples (filled circles). [B] Comparison of measured extracellular total ACV determined by addition of a reducing agent TCEP (open triangle) to that calculated extracellular total ACV (filled triangle) determined by summation of [ACV] + 2 x [bisACV] for chemostat 2 samples. [C] Yield of extracellular ACV in self-dimers (bisACV) compared to the total amount of dimerized ACV (in bisACV or with other thiol compounds) for chemostat 2.

7.8 Supplementary material

7.8.1 Supplementary I: Materials & Methods

Construction of a pcbAB expression plasmid

To enable easy cloning of the *P. chrysogenum pcbAB* gene in the Gateway vector DONR221, we first created a pDONR221 derivative with suitable restriction sites. For this, we isolated an 1125 bps DNA fragment of the *P. chrysogenum atg15* cDNA by PCR with primers AKR0013 and AKR0014 using DNA from a *P. chrysogenum* cDNA library as template [87]. Gateway technology was used to recombine this fragment into pDONR221 yielding pDONR221_STUFFER. We cloned the *P. chrysogenum pcbAB* gene into pDONR221_STUFFER in two steps. First, a 3 kb *Hin*dIII-*Bgl*II DNA fragment containing the 5' region of *pcbAB* was isolated from pHIPZ4-pcbAB [57] and cloned between the *Hin*dIII and *Bgl*II sites of pDONR221_STUFFER resulting in plasmid pDONR221_5'ACVS_3'STUFFER. Subsequently, an 8.5 kb *Bgl*II-*Sma*I DNA fragment containing the 3' region of *pcbAB* was isolated from pHIPZ4-pcbAB and cloned between the *Bgl*II and *Sma*I sites of pDONR221_5'ACVS_3'STUFFER resulting in pENTR221_ACVS.

To create a vector overexpressing *pcbAB*, a novel destination vector carrying the phleomycin-resistance (*ble*) gene as well as a unique restriction site for linearization was required. First, a *Not*I site was introduced into the pDEST R4-R3/AMDS vector as follows: Two 28 bps overlapping DNA fragments of 1 kb and 0.5 kb were synthesized by PCR with the primer combinations AKR0015+ AKR0016 and AKR0017+AKR0018, respectively, using pDEST R4-R3/AMDS as template. After purification, the two PCR fragments were used as templates in an overlap PCR with primers AKR0015 and AKR0018. From the resulting PCR product, a 1286 bps *Xba*I fragment was isolated and cloned into *Xba*I-digested pDEST R4-R3/AMDS, resulting in pDEST R4-R3/AMDS(NotI). Next, in this plasmid the *amdS* expression cassette was replaced by the *ble* gene. To this effect, a 1.5 kb DNA fragment comprising the P_{pcbC}-*ble*-T_{CYC1} cassette was isolated by PCR with primers AKR0019 and AKR0020 using pENTR221-phleo as template. The PCR fragment was digested with *Kpn*I and *Nde*I and cloned into *Kpn*I + *Nde*I-digested pDEST R4-R3/AMDS(NotI), yielding pDEST R4-R3/phleo(NotI).

Finally, the *pcbAB* expression plasmid was constructed by Gateway technology by recombining pENTR41-PpcbC, pENTR221_ACVS, pENTR23-HIS8TpenDE and pDEST R4-R3/phleo(NotI), resulting in plasmid pDEST R4-R3(phleo)_PpcbC_ACVS_Tat.

Construction of a P. chrysogenum strain producing ACVS

For the construction of a strain expressing only the *pcbAB* gene of the penicillin gene cluster, plasmid pDEST R4-R3(phleo)_PpcbC_ACVS_Tat was linearized with *Not*I and transformed into protoplasts of *P. chrysogenum* DS55153, a strain lacking all penicillin biosynthesis gene clusters [65]. Phleomycin-resistant transformants were selected and analyzed by colony PCR using primers AKR0041 and AKR0042, which exclusively yields a 905 bps fragment in *pcbAB*-containing clones. Positive transformants were cultured on PPM. Subsequently, crude extracts were prepared and analyzed by western blotting to demonstrate production of ACVS by the transformants. Two independent clones producing significant levels of ACVS (#1-11 and #1-17) were used for further study.

Table 7.S1: Oligonucleotide primers used in this study

AKR0013	5' GGGGACAAGTTTGTACAAAAAAGCAGGCTACAAGCTTTGCTTGCTTCATCCAGTCCTCTCA 3'
AKR0014	5' GGGGACCACTTTGTACAAGAAAGCTGGGTTCCCGGGGCTTCGGAAGAACTTCCAGAGTTC 3'
AKR0015	5' ACGCTGCTTCATAGCATACCTC 3'
AKR0016	5' GTTGTAAAACGGCGGCCGCTGAATTATC 3'
AKR0017	5' GATAATTCAGCGGCCGCCGTTTTACAAC 3'
AKR0018	5' ACCATGCCATGCTACGAAAGAG
AKR0019	5' GGAATTCCATATGGAGGTCGACTACATGTATCTGCATG 3'
AKR0020	5' CGGGGTACCGGTTTGCAAATTAAAGCCTTCGAGCGTC 3'
AKR0041	5' CAGCAATGGCATCTTCAAGC 3'
AKR0042	5' TGTCTTCATGCCGTTCAACC 3'

Table 7.S2: Plasmids used in this study

pDONR221	Gateway vector; Kan^R	Invitrogen
pDONR221_STUFFER	pDONR221 containing part of *P. chrysogenum atg15* cDNA as stuffer fragment; Kan^R	This study
pHIPZ4-pcbAB	contains *P. chrysogenum pcbAB* gene; Amp^R, Zeo^R	[57]
pDONR221_5'ACVS_3'STUFFER	pDONR221_STUFFER containing 5'end of *pcbAB* gene replacing part of the *atg15* stuffer fragment; Kan^R	This study
pENTR221_ACVS	pDONR221 containing *pcbAB* gene; Kan^R	This study
pDEST R4-R3/AMDS	pDEST R4-R3 containing P_{gpdA}-*amdS*-T_{penDE} cassette; Amp^R; Cam^R	[88]
pDEST R4-R3/AMDS(NotI)	pDEST R4-R3/AMDS containing additional *Not*I site; Amp^R; Cam^R	This study
pDEST R4-R3/phleo(NotI)	pDEST R4-R3 containing P_{pcbC}-*ble*-T_{CYC1} cassette; Amp^R; Cam^R	This study
pENTR221-phleo	pDONR221 containing P_{pcbC}-*ble*-T_{CYC1} cassette; Kan^R	[91]
pENTR41-PpcbC	pDONR P4-P1R containing *pcbC* promoter; Kan^R	[127]
pENTR23-HIS8TpenDE	pDONR P2R-P3 containing *penDE* terminator; Kan^R	[88]
pDEST R4-R3(phleo)_PpcbC_ACVS_Tat	pDEST R4-R3-phleo(NotI) containing P_{pcbC}-*pcbAB*-T_{penDE} expression cassette; Amp^R	This study

Key: Amp^R;, ampicillin resistant; Kan^R, kanamycin resistant; Cam^R, chloramphenicol resistant; Zeo^R, zeocin resistant.

Chapter 8

Outlook

This thesis was aimed to comprehensively understand the mechanism of the enzymes/transporters in the penicillin biosynthesis pathway in *P. chrysogenum* under *in vivo* conditions and propose metabolic engineering targets for improvement. This was achieved by combining a proper data set and understanding the enzyme kinetics and possible bottlenecks in the pathway by constructing a kinetic model. A step by step approach to construct a comprehensive kinetic model was undertaken. First a model was developed for PAA and PenG transport, secondly the effect of extra availability of the precursor amino acids (α-AAA) and cysteine (results not shown) on pathway flux was checked and then a dynamic data set was generated involving all the metabolites of the pathway. This data set was then used to estimate parameters for the comprehensive kinetic model. The model is based on the mechanisms of the enzymes/transporters in the penicillin biosynthesis pathway and identifies possible bottlenecks.

Several metabolic engineering targets were identified in this study to improve the yield and productivities of PenG. One of the first metabolic engineering targets was elimination of the active PAA exporter. This will decrease the energy consumed by futile cycling of PAA and thus increase the energetic efficiency (and the product yield) of the strain and saving substantial substrate and O_2 costs for industrial production of PenG. One such transporter was identified and a mutant strain lacking the transporter (ΔABC40)[181] was studied in our lab (not published). A PAA wash-in experiment was performed whereby the mutant *P. chrysogenum* strain (ΔABC40) was cultivated in a chemostat without supply of PAA. After reaching a pseudo steady state, PAA medium (5 mM) was supplied and extra- and intracellular samples were taken. The results did not show any significant difference when compared with the wild type strain with respect to qCO_2, qO_2, q_{PAA} and q_{PenG}. This indicates that probably there is more than one transporter for the active export of PAA. Thus, in the future identifying and eliminating other transporters for PAA export is essential to increase the energetic efficiency of penicillin production.

The often overlooked issue of transport of pathway metabolites across the cell membrane was one of the main focuses in this thesis. The studies offer the methodologies to understand the mechanism of transport of metabolites based on thermodynamics by comparing equilibrium constants of proposed mechanisms with the experimental EC/IC ratios of metabolites. Limitations with such an approach remain in the assumption of values of intracellular

membrane potential, intracellular pH and intracellular volume of the cell. Proper methods must be developed to measure their *in vivo* values.

Other metabolic engineering targets that were suggested were identification and enhancing the capacity of PenG exporter and identifying and removing transporters of 6APA and IPN. These steps are expected enhance the flux towards the production of penicillin.

Finally, ACVS was found to control the flux in the pathway because its level of activity is decreasing (degenerating) over the period of cultivation. The studies on degeneration have been performed on the wild type strain [42], however, no concrete reasons for the degeneration of the enzymes were pointed out. Degeneration of ACVS was also found for the ACV producing strain. Further, research into the degeneration pattern of ACVS would therefore be highly relevant. Understanding the phenomenon of degradation and how to reduce it will enable more sustainable production of PenG in future. The modular structure of NRP synthetases could be utilized to improve ACVS through genetic engineering, or construct an ideal ACVS enzyme through synthetic biology. Thus, improvement by finding the cause of its genetic and/or protein instability is the most important task in the future.

In conclusion, this study offers an experimental design and modeling approach to generate dynamic data and understand and parameterize *in vivo* kinetics of enzymes and transporters. Furthermore, it also offers a scheme to develop a cell factory and to understand possible bottlenecks for the production of the desired product. This approach can be utilized to understand similar problems with other strains and other pathways.

References

1. Abraham EP, Chain E, Fletcher CM, Gardner AD, Heatley NG, Jennings MA, Florey HW (1941). Further observations on penicillin. Lancet, 238 (6155):177-189.

2. Affenzeller K, Jacklitsch WM, Hönlinger C, Kubicek CP (1989). Lysine biosynthesis in *Penicillium chrysogenum* is regulated by feedback inhibition of α-aminoadipate reductase. FEMS Microbiol Lett, 58 (2-3):293-297.

3. Aharonowitz Y, Bergmeyer J, Cantoral JM, Cohen G, Demain AL, Fink U, Kinghorn J, Kleinkauf H, MacCabe A, Palissa H, Pfeifer E, Schwecke T, van Liempt H, von Döhren H, Wolfe S, Zhang J (1993). δ-(L-α-aminoadipyl)-L-cysteinyl-D-valine synthetase, the multienzyme integrating the four primary reactions in β-lactam biosynthesis, as a model peptide synthetase. J Biotechnol, 11 (7):807-810.

4. Alvarez E, Cantoral JM, Barredo JL, Díez B, Martín JF (1987). Purification to homogeneity and characterization of acyl coenzyme A:6-aminopenicillanic acid acyltransferase of *Penicillium chrysogenum*. Antimicrob Agents Chemother, 31 (11):1675-1682.

5. Alvarez E, Meesschaert B, Montenegro E, Gutiérrez S, Díez B, Barredo JL, Martín JF (1993). The isopenicillin-N acyltransferase of *Penicillium chrysogenum* has isopenicillin-N amidohydrolase, 6-aminopenicillanic acid acyltransferase and penicillin amidase activities, all of which are encoded by the single penDE gene. Eur J Biochem, 215:323-332.

6. Amarnath K, Amarnath V, Amarnath K, Valentine HL, Valentine WM (2003). A specific HPLC-UV method for the determination of cysteine and related aminothiols in biological samples. Talanta, 60 (6):1229-1238.

7. Andersson I, Terwisscha van Scheltinga AC, Valegård K (2001). Towards new β-lactam antibiotics. Cell Mol Life Sci, 58 (12):1897-1906.

8. Andrade AC, Van Nistelrooy JGM, Peery RB, Skatrud PL, De Waard MA (2000). The role of ABC transporters from *Aspergillus nidulans* in protection against cytotoxic agents and in antibiotic production. Mol Gen Genet, 263 (6):966-977.

9. Antonenkov VD, Hiltunen JK (2006). Peroxisomal membrane permeability and solute transfer. Biochim Biophys Acta, Mol Cell Res, 1763 (12):1697-1706.

10. Aryanchira S (2010). Overcoming antibiotic-resistant bacteria. Gen Eng Biotechnol News, 30 (15):18.

11. Ates B, Ercal BC, Manda K, Abraham L, Ercal N (2009). Determination of glutathione disulfide levels in biological samples using thiol–disulfide exchanging agent, dithiothreitol. Biomed Chromatogr, 23 (2):119-123.

12. Bailey J (1991). Toward a science of metabolic engineering. Science, 252 (5013):1668-1675.

13. Bainbridge ZA, Scott RI, Perry D (1992). Oxygen utilisation by isopenicillin N synthase from *Penicillium chrysogenum*. J Chem Technol Biotechnol, 55 (3):233-238.

14. Banko G, Wolfe S, Demain AL (1986). Cell-free synthesis of δ-(L-α-aminoadipyl)-L-cysteine, the first intermediate of penicillin and cephalosporin biosynthesis. Biochem Biophys Res Commun, 137 (1):528-535.

15. Barreiro C, Martín JF, García-Estrada C (2012). Proteomics shows new faces for the old penicillin producer *Penicillium chrysogenum*. J Biomed Biotechnol, doi: 10.1155/2012/105109, Epub 2012 Jan 19.

16. Bartoszewska M, Kiel JAKW, Bovenberg RAL, Veenhuis M, van der Klei IJ (2010). Autophagy deficiency promotes ß-lactam production in *Penicillium chrysogenum*. Appl Environ Microbiol, 77 (4):1413-1422.

17. Batchelor FR, Doyle FP, Nayler JHC, Rolinson GN (1959). Synthesis of penicillin: 6-aminopenicillanic acid in penicillin fermentations. Nature, 183 (4656):257-258.

18. Bezstarosti K, Ghamari A, Grosveld FG, Demmers JAA (2010). Differential proteomics based on ^{18}O labeling to determine the cyclin dependent kinase 9 interactome. J Proteome Res, 9 (9):4464-4475.

19. Bhattacharjee JK (1985). α-Aminoadipate pathway for the biosynthesis of lysine in lower eukaryotes. Crit Rev Microbiol, 12 (2):131-151.

20. Bourbouloux Ae, Shahi P, Chakladar A, Delrot S, Bachhawat AK (2000). Hgt1p, a high affinity glutathione transporter from the yeast *Saccharomyces cerevisiae*. J Biol Chem, 275 (18):13259-13265.

21. Brakhage AA (1998). Molecular regulation of β-lactam biosynthesis in filamentous fungi. Microbiol Mol Biol Rev, 62 (3):547-585.

22. Brakhage AA, Spröte P, Al-Abdallah Q, Gehrke A, Plattner H, Tüncher A (2004). Regulation of penicillin biosynthesis in filamentous fungi In: Advances in Biochemical Engineering/Biotechnology. Springer-Verlag Berlin / Heidelberg, 88:45-90.

23. Bruggink A, Roos EC, de Vroom E (1998). Penicillin acylase in the industrial production of ß-lactam antibiotics. Org Process Res Dev, 2 (2):128-133.

24. Brundidge SP, Gaeta FCA, Hook DJ, Sapino C, Elander RP, Morin RB (1980). Association of 6-oxo-piperidine-2-carboxylic acid with penicillin-v production in *penicillium-chrysogenum* fermentations. J Antibiot, 33 (11):1348-1351.

25. Burgstaller W (1997). Transport of small ions and molecules through the plasma membrane of filamentous fungi. Crit Rev Microbiol, 23 (1):1-46.

26. Burns JA, Butler JC, Moran J, Whitesides GM (1991). Selective reduction of disulfides by tris(2-carboxyethyl)phosphine. J Org Chem, 56 (8):2648-2650.

27. Byford MF, Baldwin JE, Shiau C-Y, Schofield CJ (1997). The mechanism of ACV synthetase. Chem Rev, 97 (7):2631-2650.

28. Caboche S, Leclère V, Pupin M, Kucherov G, Jacques P (2010). Diversity of monomers in nonribosomal peptides: towards the prediction of origin and biological activity. J Bacteriol, 192 (19):5143-5150.

29. Camera E, Picardo M (2002). Analytical methods to investigate glutathione and related compounds in biological and pathological processes. J Chromatogr B, 781 (1-2):181-206.

30. Cantoral JM, Díez B, Barredo JL, Alvarez E, Martín JF (1987). High-frequency transformation of *Penicillium chrysogenum*. Nat Biotech, 5 (5):494-497.

31. Casqueiro J, Bañuelos O, Gutiérrez S, Martín JF (2001). Metabolic engineering of the lysine pathway for β-lactam overproduction in *Penicillium chrysogenum*. In: Novel Frontiers in the Production of Compounds for Biomedical Use, Focus on Biotechnology. Springer, Netherlands, 1:147-159.

32. Casqueiro J, Gutiérrez S, Bañuelos O, Hijarrubia MJ, Martín JF (1999). Gene targeting in *Penicillium chrysogenum*: Disruption of the *lys2* gene leads to penicillin overproduction. J Bacteriol, 181 (4):1181-1188.

33. Chain E, Florey HW, Gardner AD, Heatley NG, Jennings MA, Orr-Ewing J, Sanders AG (1940). Penicillin as a chemotherapeutic agent. Lancet, 236 (6104):226-228.

34. Christensen LH, Mandrup G, Nielsen J, Villadsen J (1994). A robust liquid chromatographic method for measurement of medium components during penicillin fermentations. Anal Chim Acta, 296 (1):51-62.

35. Clutterbuck PW, Lovell R, Raistrick H (1932). Studies in the biochemistry of micro-organisms: The formation from glucose by members of the *Penicillium chrysogenum* series of a pigment, an alkali-soluble protein and penicillin-the antibacterial substance of Fleming. Biochem J, 26 (6):1907-1918.

36. Cohen G, Argaman A, Schreiber R, Mislovati M, Aharonowitz Y (1994). The thioredoxin system of *Penicillium chrysogenum* and its possible role in penicillin biosynthesis. J Bacteriol, 176 (4):973–984.

37. de Jonge LP, Buijs NAA, ten Pierick A, Deshmukh A, Zhao Z, Kiel JAKW, Heijnen JJ, van Gulik WM (2011). Scale-down of penicillin production in *Penicillium chrysogenum*. Biotechnol J, 6 (8):944–958.

38. de Jonge LP, Douma RD, Heijnen JJ, van Gulik WM (2012). Optimization of cold methanol quenching for quantitative metabolomics of *Penicillium chrysogenum*. Metabolomics, 8 (4):727-735.

39. de Jongh WA, Nielsen J (2007). Filamentous fungi as cell factories for metabolite production. In: Food Mycology, Mycology. CRC Press:163-182.

40. Demain AL, Elander RP (1999). The β-lactam antibiotics: past, present, and future. Antonie Van Leeuwenhoek, 75 (1):5-19.

41. Díez B, Gutiérrez S, Barredo J, van Solingen P, van der Voort L, Martín J (1990). The cluster of penicillin biosynthetic genes. Identification and characterization of the *pcb*AB gene encoding the α-aminoadipyl-cysteinyl-valine synthetase and linkage to the *pcb*C and *pen*DE genes. J Biol Chem, 265:16358 - 16365.

42. Douma RD, Batista JM, Touw KM, Kiel JA, Krikken AM, Zhao Z, Veiga T, Klaassen P, Bovenberg RA, Daran J-M, Heijnen JJ, van Gulik WM (2011). Degeneration of penicillin production in ethanol-limited chemostat cultivations of *Penicillium chrysogenum*: A systems biology approach. BMC Systems Biology, 5:132.

43. Douma RD, de Jonge LP, Jonker CTH, Seifar RM, Heijnen JJ, van Gulik WM (2010). Intracellular metabolite determination in the presence of extracellular abundance: Application to the penicillin biosynthesis pathway in *Penicillium chrysogenum*. Biotechnol Bioeng, 107 (1):105-115.

44. Douma RD, Deshmukh AT, de Jonge LP, de Jong BW, Seifar RM, Heijnen JJ, van Gulik WM (2012). Novel insights in transport mechanisms and kinetics of phenylacetic acid and penicillin-G in *Penicillium chrysogenum*. Biotechnol Prog, 28 (2):337-348.

45. Douma RD, Verheijen PJT, de Laat WTAM, Heijnen JJ, van Gulik WM (2010). Dynamic gene expression regulation model for growth and penicillin production in *Penicillium chrysogenum*. Biotechnol Bioeng, 106 (4):608-618.

46. Ellison I, Richie Jr JP (2012). Mechanisms of glutathione disulfide efflux from erythrocytes. Biochem Pharmacol, 83 (1):164-169.

47. Emri T, Pócsi I, Szentirmai A (1997). Phenoxyacetic acid induces glutathione-dependent detoxification and depletes the glutathione pool in *Penicillium chrysogenum*. J Basic Microbiol, 37 (3):181-186.

48. Eriksen SH, Jensen B, Schneider I, Kaasgaard S, Olsen J (1995). Uptake of phenoxyacetic acid by *Penicillium chrysogenum*. Appl Microbiol Biotechnol, 42 (6):945-950.

49. Evers ME, Trio H, van den Berg MA, Bovenberg RAL, Driessen AJM (2004). Compartmentalization and transport in β-lactam antibiotics biosynthesis. In: Advances in Biochemical Engineering/Biotechnology. Springer-Verlag Berlin Heidelberg, 88:111-135.

50. Fell DA (1992). Metabolic control analysis - a survey of its theoretical and experimental development. Biochem J, 286:313-330.

51. Feng B, Friedlin E, Marzluf GA (1994). A reporter gene analysis of penicillin biosynthesis gene expression in *Penicillium chrysogenum* and its regulation by nitrogen and glucose catabolite repression. Appl Environ Microbiol, 60 (12):4432-4439.

52. Fernández-Cañón JM, Reglero A, Martínez-Blanco H, Luengo JM (1989). Uptake of phenylacetic acid by *Penicillium chrysogenum* wis 54-1255: A critical regulatory point in benzylpenicillin biosynthesis. J Antibiot, 42 (9):1398-1409.

53. Fierro F, Barredo J, Díez B, Gutiérrez S, Fernández F, Martín J (1995). The penicillin gene cluster is amplified in tandem repeats linked by conserved hexanucleotide sequences. Proc Natl Acad Sci USA, 92:6200-6204.

54. Fleming A (1929). On the antibacterial action of cultures of a Penicillium, with special reference to their use in the isolation of *B. influenza*. Exp Pathol, 10:226-236.

55. Friedrich CG, Demain AL (1978). Uptake and metabolism of α-aminoadipic acid by *Penicillium chrysogenum* wis 54-1255. Arch Microbiol, 119 (1):43-47.

56. García-Estrada C, Vaca I, Lamas-Maceiras M, Martín J (2007). *In vivo* transport of the intermediates of the penicillin biosynthetic pathway in tailored strains of *Penicillium chrysogenum*. Appl Microbiol Biotechnol, 76 (1):169-182.

57. Gidijala L, Kiel JAKW, Douma RD, Seifar RM, van Gulik WM, Bovenberg RAL, Veenhuis M, van der Klei IJ (2009). An engineered yeast efficiently secreting penicillin. PLoS One, 4 (12):e8317.

58. Gidijala L, van Der Klei IJ, Veenhuis M, Kiel JAKW (2007). Reprogramming *Hansenula polymorpha* for penicillin production: expression of the *Penicillium chrysogenum* pcl gene. FEMS Yeast Res, 7 (7):1160-1167.

59. Gonzalez B, François J, Renaud M (1997). A rapid and reliable method for metabolite extraction in yeast using boiling buffered ethanol. Yeast, 13 (14):1347-1355.

60. Grunau S, Mindthoff S, Rottensteiner H, Sormunen RT, Hiltunen JK, Erdmann R, Antonenkov VD (2009). Channel-forming activities of peroxisomal membrane proteins from the yeast *Saccharomyces cerevisiae*. FEBS J, 276 (6):1698-1708.

61. Guan X, Hoffman B, Dwivedi C, Matthees DP (2003). A simultaneous liquid chromatography/mass spectrometric assay of glutathione, cysteine, homocysteine and their disulfides in biological samples. J Pharm Biomed Anal, 31 (2):251-261.

62. Gunnarsson N, Eliasson A, Nielsen J (2004). Control of fluxes towards antibiotics and the role of primary metabolism in production of antibiotics. In: Molecular Biotechnolgy of Fungal beta-Lactam Antibiotics and Related Peptide Synthetases.137-178.

63. Gutierrez S, Marcos AT, Casqueiro J, Kosalkova K, Fernandez FJ, Velasco J, Martín JF (1999). Transcription of the *pcbAB*, *pcbC* and *penDE* genes of *Penicillium chrysogenum* AS-P-78 is repressed by glucose and the repression is not reversed by alkaline pHs Microbiology, 145 (2):317-324.

64. Harris DM, Diderich JA, Krogt ZA, Luttik MA, Raamsdonk LM, Bovenberg RAL, van Gulik WM, van Dijken JP, Pronk JT (2006). Enzymic analysis of NADPH metabolism in in β-lactam-producing *Penicillium chrysogenum* : presence of a mitochondrial NADPH dehydrogenase Metab Eng, 8 (2):91-101.

65. Harris DM, van der Krogt ZA, Klaassen P, Raamsdonk LM, Hage S, van den Berg MA, Bovenberg RAL, Pronk JT, Daran J-M (2009). Exploring and dissecting genome-wide gene expression responses of *Penicillium chrysogenum* to phenylacetic acid consumption and penicillinG production. BMC Genomics, 10 (1):75.

66. Harris DM, Westerlaken I, Schipper D, Krogt ZA, Gombert AK, Sutherland J, Raamsdonk LM, Berg MA, Bovenberg RAL, Pronk JT, Daran J-M (2009). Engineering of *Penicillium chrysogenum* for fermentative production of a novel carbamoylated cephem antibiotic precursor. Metab Eng, 11:125-137.

67. Hazelwood LA, Tai SL, Boer VM, de Winde JH, Pronk JT, Daran J-M (2006). A new physiological role for Pdr12p in *Saccharomyces cerevisiae*: export of aromatic and branched-chain organic acids produced in amino acid catabolism. FEMS Yeast Res, 6:937-945.

68. Henriksen CM, Christensen LH, Nielsen J, Villadsen J (1996). Growth energetics and metabolic fluxes in continuous cultures of *Penicillium chrysogenum*. J Biotechnol, 45 (2):149-164.

69. Henriksen CM, Holm SS, Schipper D, Jørgensen HS, Nielsen J, Villadsen J (1997). Kinetic studies on the carboxylation of 6-amino-penicillanic acid to 8-hydroxy-penillic acid. Process Biochem, 32 (2):85-91.

70. Henriksen CM, Nielsen J, Villadsen J (1998). Cyclization of α-aminoadipic acid into the δ-lactam 6-oxo-piperidine-2-carboxylic acid by *Penicillium chrysogenum*. The Journal of Antibiotics, 51 (2):99-106.

71. Hillenga DJ, Versantvoort HJ, Driessen AJ, Konings WN (1996). Basic amino acid transport in plasma membrane vesicles of *Penicillium chrysogenum*. J Bacteriol, 178 (14):3991–3995.

72. Hillenga DJ, Versantvoort HJM, van der Molen S, Driessen AJM, Konings WN (1995). *Penicillium chrysogenum* takes up the penicillin G precursor phenylacetic acid by passive diffusion. Appl Environ Microbiol, 61 (7):2589-2595.

73. Hönlinger C, Kubicek CP (1989). Metabolism and compartmentation of α-aminoadipic acid in penicillin-producing strains of *Penicillium chrysogenum*. Biochim Biophys Acta, General Subjects, 993 (2-3):204-211.

74. Hönlinger C, Kubicek CP (1989). Regulation of δ-(L-α-aminoadipyl)-L-cysteinyl-D-valine and isopenicillin N biosynthesis in *Penicillium chrysogenum* by the α-aminoadipate pool size. FEMS Microbiol Lett, 65 (1-2):71-75.

75. Jacklitsch WM, Hampel W, Röhr M, Kubicek CP (1986). α-Aminoadipate pool concentration and penicillin biosynthesis in strains of *Penicillium chrysogenum*. Canadian Journal of Microbiology, 32 (6):473-480.

76. Jaklitsch WM, Kubicek CP (1990). Homocitrate synthase from *Penicillium chrysogenum*. Localization, purification of the cytosolic isoenzyme, and sensitivity to lysine. Biochem J, 269 (1):247–253.

77. Jami M-S, Barreiro C, García-Estrada C, Martín J-F (2010). Proteome analysis of the penicillin producer *Penicillium chrysogenum*. Molecular & Cellular Proteomics, 9 (6):1182-1198.

78. Jensen SE, Westlake DWS, Wolfe S (1988). Production of the penicillin precursor δ-(L-α-aminoadipyl)-L-cysteinyl-D-valine (ACV) by cell-free extracts from *Streptomyces clavuligerus*. FEMS Microbiol Lett, 49 (2):213-218.

79. Jørgensen H, Nielsen J, Villadsen J, Møllgaard H (1995). Analysis of penicillin V biosynthesis during fed-batch cultivations with a high-yielding strain of *Penicillium chrysogenum*. Appl Microbiol Biotechnol, 43 (1):123-130.

80. Jørgensen H, Nielsen J, Villadsen J, Møllgaard H (1995). Metabolic flux distributions in *Penicillium chrysogenum* during fed-batch cultivations. Biotechnol Bioeng, 46 (2):117-131.

81. Kacser H (1983). The control of enzyme-systems invivo - elasticity analysis of the steady-state. Biochem Soc Trans, 11 (1):35-40.

82. Kacser H, Burns JA, Fell DA (1995). The control of flux. Biochem Soc Trans, 23 (2):341-366.

83. Kadima TA, Jensen SE, Pickard MA (1995). Production of δ-(l-α-aminoadipyl)-l-cysteinyl-d-valine by entrapped ACV-synthetase from *Streptomyces clavuligerus* J Ind Microbiol Biotechnol, 14 (1):35-40.

84. Kardos N, Demain AL (2011). Penicillin: the medicine with the greatest impact on therapeutic outcomes. Appl Microbiol Biotechnol, 92 (4):677-687.

85. Keller DA, Menzel DB (1985). Picomole analysis of glutathione, glutathione disulfide, glutathione S-sulfonate, and cysteine S-sulfonate by high-performance liquid chromatography. Anal Biochem, 151 (2):418-423.

86. Keller NP, Turner G, Bennett JW (2005). Fungal secondary metabolism - from biochemistry to genomics. Nat Rev Micro, 3 (12):937-947.

87. Kiel JAKW, Hilbrands RE, Bovenberg RAL, Veenhuis M (2000). Isolation of *Penicillium chrysogenum PEX1* and *PEX6* encoding AAA proteins involved in peroxisome biogenesis. Appl Microbiol Biotechnol, 54 (2):238-242.

88. Kiel JAKW, van den Berg MA, Fusetti F, Poolman B, Bovenberg RAL, Veenhuis M, van der Klei IJ (2009). Matching the proteome to the genome: the microbody of penicillin-producing *Penicillium chrysogenum* cells. Functional & Integrative Genomics, 9 (2):167-184.

89. Kleijn RJ, Liu F, van Winden WA, van Gulik WM, Ras C, Heijnen JJ (2007). Cytosolic NADPH metabolism in penicillin-G producing and non-producing chemostat cultures of *Penicillium chrysogenum*. Metab Eng, 9 (1):112-123.

90. Kleinkauf H, von Döhren H (1990). Nonribosomal biosynthesis of peptide antibiotics. Eur J Biochem, 192 (1):1-15.

91. Koetsier MJ, Gombert AK, Fekken S, Bovenberg RAL, van den Berg MA, Kiel JAKW, Jekel PA, Janssen DB, Pronk JT, van der Klei IJ, Daran J-M (2010). The *Penicillium chrysogenum* aclA gene encodes a broad-substrate-specificity acyl-coenzyme A ligase involved in activation of adipic acid, a side-chain precursor for cephem antibiotics. Fungal Genet Biol, 47 (1):33-42.

92. Koetsier MJ, Jekel PA, van den Berg MA, Bovenberg RAL, Janssen DB (2009). Characterization of a phenylacetate-CoA ligase from *Penicillium chrysogenum*. Biochem J, 417 (2):467-476.

93. Koffas M, Roberge C, Lee K, Stephanopoulos G (1999). Metabolic Engineering. Annu Rev Biomed Eng, 1 (1):535-557.

94. Krämer R (1996). Analysis and modeling of substrate uptake and product release by prokaryotic and eukaryotic cells. In: Metabolic Engineering, Advances in Biochemical Engineering/Biotechnology. Springer Berlin / Heidelberg, 54:31-74.

95. Kresnowati MTAP, Suarez-Mendez C, Groothuizen MK, van Winden WA, Heijnen JJ (2007). Measurement of fast dynamic intracellular pH in *Saccharomyces cerevisiae* using benzoic acid pulse. Biotechnol Bioeng, 97 (1):86-98.

96. Kresnowati MTAP, van Winden WA, van Gulik WM, Heijnen JJ (2008). Energetic and metabolic transient response of *Saccharomyces cerevisiae* to benzoic acid. FEBS J, 275 (22):5527-5541.

97. Krijt J, Vacková M, Kožich V (2001). Measurement of homocysteine and other aminothiols in plasma: Advantages of using tris(2-carboxyethyl)phosphine as reductant compared with tri-n-butylphosphine Clin Chem, 47 (10):1821-1828.

98. Lange HC, Eman M, van Zuijlen G, Visser D, van Dam JC, Frank J, Teixeira de Mattos MJ, Heijnen JJ (2001). Improved rapid sampling for in vivo kinetics of intracellular metabolites in *Saccharomyces cerevisiae*. Biotechnol Bioeng, 75 (4):406-415.

99. Lautru S, Challis GL (2004). Substrate recognition by nonribosomal peptide synthetase multi-enzymes. Microbiology, 150 (6):1629-1636.

100. Legerton TL, Kanamori K, Weiss RL, Roberts JD (1983). Measurements of cytoplasmic and vacuolar pH in *Neurospora* using nitrogen-15 nuclear magnetic resonance spectroscopy. Biochemistry (Mosc), 22 (4):899-903.

101. Legiša M, Kidrič J (1989). Initiation of citric acid accumulation in the early stages of *Aspergillus niger* growth. Appl Microbiol Biotechnol, 31 (5):453-457.

102. Luengo JM, Revilla G, López MJ, Villanueva JR, Martín JF (1980). Inhibition and repression of homocitrate synthase by lysine in *Penicillium chrysogenum*. J Bacteriol, 144 (3):869–876.

103. Martín JF, Casqueiro J, Kosalková K, Marcos AT, Gutiérrez AFFS (1999). Penicillin and cephalosporin biosynthesis: Mechanism of carbon catabolite regulation of penicillin production. Antonie Van Leeuwenhoek, 75 (1):21-31.

104. Martín JF, Casqueiro J, Liras P (2005). Secretion systems for secondary metabolites: how producer cells send out messages of intercellular communication. Curr Opin Microbiol, 8 (3):282-293.

105. Martín JF, Liras P (1989). Organization and expression of genes involved in the biosynthesis of antibiotics and other secondary metabolites. Annu Rev Microbiol, 43:173-206.

106. Martín JF, Ullán RV, García-Estrada C (2010). Regulation and compartmentalization of β-lactam biosynthesis. Microb Biotechnol 3(3):285-299.

107. Mashego MR, van Gulik WM, Vinke JL, Heijnen JJ (2003). Critical evaluation of sampling techniques for residual glucose determination in carbon-limited chemostat culture of *Saccharomyces cerevisiae*. Biotechnol Bioeng, 83 (4):395-399.

108. Mashego MR, van Gulik WM, Vinke JL, Visser D, Heijnen JJ (2006). In vivo kinetics with rapid perturbation experiments in *Saccharomyces cerevisiae* using a second-generation BioScope. Metab Eng, 8 (4):370-383.

109. Mashego MR, Wu L, Van Dam JC, Ras C, Vinke JL, Van Winden WA, Van Gulik WM, Heijnen JJ (2004). MIRACLE: mass isotopomer ratio analysis of U-13C-labeled extracts. A new method for accurate quantification of changes in concentrations of intracellular metabolites. Biotechnol Bioeng, 85 (6):620-628.

110. Medema MH, Blin K, Cimermancic P, de Jager V, Zakrzewski P, Fischbach MA, Weber T, Takano E, Breitling R (2011). antiSMASH: rapid identification, annotation and analysis of secondary metabolite biosynthesis gene clusters in bacterial and fungal genome sequences. Nucleic Acids Res, 39 (Web Server issue):W339-W346.

111. Meredith MJ (1983). Analysis of protein-glutathione mixed disulfides by high performance liquid chromatography. Anal Biochem, 131 (2):504-509.

112. Mohimani H, Liu W-T, Yang Y-L, Gaudencio SP, Fenical W, Dorrestein PC, Pevzner PA (2011). Multiplex de novo sequencing of peptide antibiotics. J Comput Biol, 18 (11):1371-1381.

113. Mortensen P, Gouw JW, Olsen JV, Ong S-E, Rigbolt KTG, Bunkenborg J, Cox Jr, Foster LJ, Heck AJR, Blagoev B, Andersen JS, Mann M (2009). MSQuant, an open source platform for mass spectrometry-based quantitative proteomics. J Proteome Res, 9 (1):393-403.

114. Moyer AJ, Coghill RD (1946). Penicillin: Production of penicillin in surface cultures J Bacteriol, 51 (1):57-78.

115. Moyer AJ, Coghill RD (1946). Penicillin: The laboratory scale production of penicillin in submerged cultures by *Penicillium notatum* Westling (NRRL 832). J Bacteriol, 51 (1):79-93.

116. Moyer AJ, Coghill RD (1947). Penicillin: The effect of phenylacetic acid on penicillin production J Bacteriol, 53 (3):329-341.

117. Muller WH, Vanderkrift TP, Krouwer AJJ, Wosten HAB, Vandervoort LHM, Smaal EB, Verkleij AJ (1991). Localization of the pathway of the penicillin biosynthesis in *Penicillium-chrysogenum*. EMBO J, 10 (2):489-495.

118. Nasution U, van Gulik WM, Kleijn RJ, van Winden WA, Proell A, Heijnen JJ (2006). Measurement of intracellular metabolites of primary metabolism and adenine nucleotides in chemostat cultivated *Penicillium chrysogenum*. Biotechnol Bioeng, 94 (1):159-166.

119. Nasution U, van Gulik WM, Proell A, van Winden WA, Heijnen JJ (2006). Generating short-term kinetic responses of primary metabolism of *Penicillium chrysogenum* through glucose perturbation in the bioscope mini reactor. Metab Eng, 8 (5):395-405.

120. Nasution U, van Gulik WM, Ras C, Proell A, Heijnen JJ (2008). A metabolome study of the steady-state relation between central metabolism, amino acid biosynthesis and penicillin production in *Penicillium chrysogenum*. Metab Eng, 10 (1):10-23.

121. Nelson DL, Cox MM (2000) Lehninger Principles of Biochemistry Thrid Edition ed edn. Worth Publishers, New York, NY.

122. Nielsen J (1997). Physiological engineering aspects of *Penicillium chrysogenum*. In. World Scientific, Singapore:1-9.

123. Nielsen J (1998). The role of metabolic engineering in the production of secondary metabolites. Curr Opin Microbiol, 1 (3):330-336.

124. Nielsen J, Jørgensen HS (1995). Metabolic control analysis of the penicillin biosynthetic pathway in a high-yielding strain of *Penicillium chrysogenum*. Biotechnol Prog, 11 (3):299-305.

125. Nielsen J, Jørgensen HS (1996). A kinetic model for the penicillin biosynthetic pathway in *Penicillium chrysogenum*. Control Eng Pract, 4 (6):765-771.

126. Nijland JG, Ebbendorf B, Woszczynska M, Boer R, Bovenberg RAL, Driessen AJM (2010). Nonlinear biosynthetic gene cluster dose effect on penicillin production by *Penicillium chrysogenum*. Appl Environ Microbiol, 76 (21):7109-7115.

127. Nijland JG, Kovalchuk A, van den Berg MA, Bovenberg RAL, Driessen AJM (2008). Expression of the transporter encoded by the cefT gene of *Acremonium chrysogenum* increases cephalosporin production in *Penicillium chrysogenum*. Fungal Genet Biol, 45 (10):1415-1421.

128. Nikerel IE, Canelas AB, Jol SJ, Verheijen PJT, Heijnen JJ (2011). Construction of kinetic models for metabolic reaction networks: Lessons learned in analysing short-term stimulus response data. Mathematical and Computer Modelling of Dynamical Systems, 17 (3):243-260.

129. Opaliński Ł, Bartoszewska M, Fekken S, Liu HY, de Boer R, van der Klei I, Veenhuis M, Kiel JAKW. De novo peroxisome biogenesis in *Penicillium chrysogenum* is not dependent on the Pex11 family members or Pex16. PLoS One, 7 (4):12.

130. Packer H. L. TCR (1990). Morphological measurements on filamentous microorganisms by fully automatic image analysis. Biotechnol Bioeng, 35 (9):870-881.

131. Packer HL, Keshavarz-Moore E, Lilly MD, Thomas CR (1992). Estimation of cell volume and biomass of *Penicillium chrysogenum* using image analysis. Biotechnol Bioeng, 39 (4):384-391.

132. Peñalva MA, Rowlands RT, Turner G (1998). The optimization of penicillin biosynthesis in fungi. Trends Biotechnol, 16 (11):483-489.

133. Pfennig S, Stubbs MT (2012). Flexing and stretching in nonribosomal peptide synthetases. Chem Biol, 19 (2):167-169.

134. Pilatus U, Techel D (1991). 31P-NMR-studies on intracellular pH and metabolite concentrations in relation to the circadian rhythm, temperature and nutrition in *Neurospora crassa*. Biochim Biophys Acta, Mol Cell Res, 1091 (3):349-355.

135. Pissara PdN, Nielsen J, Bazin MJ (1996). Pathway kinetics and metabolic control analysis of a high-yielding strain of *Penicillium chrysogenum* during fed batch cultivations. Biotechnol Bioeng, 51 (2):168-176.

136. Prinz WA, Åslund F, Holmgren A, Beckwith J (1997). The Role of the thioredoxin and glutaredoxin pathways in reducing protein disulfide bonds in the *Escherichia coli* cytoplasm. J Biol Chem, 272 (25):15661-15667.

137. Ramos FR, Lopez-Nieto MJ, Martín JF (1985). Isopenicillin N synthetase of *Penicillium chrysogenum*, an enzyme that converts δ-(L-α-Aminoadipyl)-L-Cysteinyl-D-Valine to Isopenicillin N. Antimicrob Agents Chemother, 27 (3):380-387.

138. Raper KB (1946). The development of improved penicillin-producing molds. Ann N Y Acad Sci, 48 (2):41-56.

139. Raper KB, Alexander DF, Coghill RD (1944). Penicillin II. Natural variation and penicillin production in *Penicillium notatum* and allied species. J Bacteriol, 48:639-659.

140. Rizzi M, Baltes M, Theobald U, Reuss M (1997). In vivo analysis of metabolic dynamics in *Saccharomyces cerevisiae*: II. Mathematical model. Biotechnol Bioeng, 55 (4):592-608.

141. Rodriguez-Saiz M, Barredo J, Moreno M, Fernandez-Canon J, Penalva M, Diez B (2001). Reduced function of a phenylacetate-oxidizing cytochrome P450 caused strong genetic improvement in early phylogeny of penicillin-producing strains. J Bacteriol, 183:5465 - 5471.

142. Rokem JS, Lantz AE, Nielsen J (2007). Systems biology of antibiotic production by microorganisms. Nat Prod Rep, 24 (6):1262-1287.

143. Rolinson GN, Batchelor FR, Butterworth D, Cameron-Wood J, Cole M, Eustace GC, Hart MV, Richards M, Chain EB (1960). Formation of 6-aminopenicillanic acid from penicillin by enzymatic hydrolysis. Nature, 187:236-237.

144. Sambrook J, Fritsch EF, Maniatis T (1989) Molecular cloning: a laboratory manual. Cold Spring Harbor Laboratory Press, Cold Spring Harbor, NY.

145. Sanders D, Slayman CL (1982). Control of intracellular pH—Predominant role of oxidative metabolism, not proton transport, in the eukaryotic microorganism *Neurospora*. J Gen Physiol, 80:377–402.

146. Schofield CJ, Baldwin JE, Byford MF, Clifton I, Hajdu J, Hensgens C, Roach P (1997). Proteins of the penicillin biosynthesis pathway. Curr Opin Struct Biol, 7 (6):857-864.

147. Schönberg A (1935). Über einige neue Reaktionen organischer Disulfide, sowie über die Oxydation organischer Verbindungen bei Gegenwart von Disulfiden (Vorläuf. Mitteil.). Berichte der deutschen chemischen Gesellschaft (A and B Series), 68 (1):163-164.

148. Schwarzer D, Finking R, Marahiel MA (2003). Nonribosomal peptides: From genes to products. Nat Prod Rep, 20:275–287.

149. Seifar RM, Deshmukh AT, Heijnen JJ, van Gulik WM (2012). Determination of δ-[L-α-aminoadipyl]-L-cysteinyl-D-valine in cell extracts of *Penicillium chrysogenum* using ion pair-RP-UPLC-MS/MS. J Sep Sci, 35 (2):225-230.

150. Seifar RM, Ras C, van Dam JC, van Gulik WM, Heijnen JJ, van Winden WA (2009). Simultaneous quantification of free nucleotides in complex biological samples using ion pair reversed phase liquid chromatography isotope dilution tandem mass spectrometry. Anal Biochem, 388 (2):213-219.

151. Seifar RM, Zhao Z, van Dam J, van Winden W, van Gulik W, Heijnen JJ (2008). Quantitative analysis of metabolites in complex biological samples using ion-pair reversed-phase liquid chromatography-isotope dilution tandem mass spectrometry. J Chromatogr, 1187 (1-2):103-110.

152. Seiwert B, Karst U (2007). Simultaneous LC/MS/MS determination of thiols and disulfides in urine samples based on differential labeling with Ferrocene-based maleimides. Anal Chem, 79 (18):7131-7138.

153. Shimada K, Mitamura K (1994). Derivatization of thiol-containing compounds. Journal of Chromatography B, 659 (1-2):227-241.

154. Sieber SA, Marahiel MA (2005). Molecular mechanisms underlying nonribosomal peptide synthesis: Approaches to new antibiotics. Chem Rev, 105 (2):715-738.

155. Stefaniak JJ, Gailey FB, Jarvis FG, Johnson MJ (1946). The effect of environmental conditions on penicillin fermentations with *Penicillium chrysogenum X-1612*. J Bacteriol, 52 (1):119-127.

156. Steghens JP, Flourie F, Arab K, Collombel C (2003). Fast liquid chromatography-mass spectrometry glutathione measurement in whole blood: micromolar GSSG is a sample preparation artifact. Journal of Chromatography B-Analytical Technologies in the Biomedical and Life Sciences, 798 (2):343-349.

157. Svardal AM, Mansoor MA, Ueland PM (1990). Determination of reduced, oxidized, and protein-bound glutathione in human plasma with precolumn derivatization with monobromobimane and liquid chromatography. Anal Biochem, 184 (2):338-346.

158. Teusink B, Passarge J, Reijenga CA, Esgalhado E, van der Weijden CC, Schepper M, Walsh MC, Bakker BM, van Dam K, Westerhoff HV, Snoep JL (2000). Can yeast glycolysis be understood in terms of in vitro kinetics of the constituent enzymes? Testing biochemistry. Eur J Biochem, 267 (17):5313-5329.

159. Theilgaard HA, Nielsen J (1999). Metabolic control analysis of the penicillin biosynthetic pathway: the influence of the lld-ACV:bisACV ratio on the flux control. Antonie Van Leeuwenhoek, 75 (1):145-154.

160. Theilgaard HA, van den Berg MA, Mulder CA, Bovenberg RAL, Nielsen J (2001). Quantitative analysis of *Penicillium chrysogenum* Wis54-1255 transformants overexpressing the penicillin biosynthetic genes. Biotechnol Bioeng, 72 (4):379-388.

161. Theilgaard HB, Kristiansen KN, Henriksen CM, Nielsen J (1997). Purification and characterization of δ-(L-α-aminoadipyl)-L-cysteinyl-D-valine synthetase from *Penicillium chrysogenum*. Biochem J, 327 (1):185–191.

162. Theobald U, Mailinger W, Baltes M, Rizzi M, Reuss M (1997). In vivo analysis of metabolic dynamics in *Saccharomyces cerevisiae* : I. Experimental observations. Biotechnol Bioeng, 55 (2):305-316.

163. Theodoulou FL, Zhang X, Marcos Lousa C, Nyathi Y, Baker A, Geisler M, Venema K (2011). Peroxisomal transport systems: Roles in signaling and metabolism transporters and pumps in plant signaling. In, Signaling and Communication in Plants. Springer Berlin Heidelberg, 7:327-351.

164. Thykaer J, Nielsen J (2003). Metabolic engineering of ß-lactam production. Metab Eng, 5 (1):56-69.

165. Trip H, Evers ME, Kiel JAKW, Driessen AJM (2004). Uptake of the β-Lactam precursor α-aminoadipic acid in *Penicillium chrysogenum* is mediated by the acidic and the general amino acid permease. Appl Environ Microbiol, 70 (8):4775–4783.

166. Ullán R, Liu GL, Casqueiro J, Gutiérrez S, Bañuelos O, Martín J (2002). The *cefT* gene of *Acremonium chrysogenum* C10 encodes a putative multidrug efflux pump protein that significantly increases cephalosporin C production. Mol Genet Genomics, 267 (5):673-683.

167. Ullán R, Teijeira F, Martín J (2008). Expression of the *Acremonium chrysogenum cefT* gene in *Penicillum chrysogenum* indicates that it encodes an hydrophilic ß-lactam transporter. Curr Genet, 54 (3):153-161.

168. van de Kamp M, Driessen AJM, Konings WN (1999). Compartmentalization and transport in β-lactam antibiotic biosynthesis by filamentous fungi. Antonie Van Leeuwenhoek, 75 (1):41-78.

169. van den Berg MA (2010). Functional characterisation of penicillin production strains. Fungal Biology Reviews, 24 (1-2):73-78.

170. van den Berg MA (2011). Impact of the *Penicillium chrysogenum* genome on industrial production of metabolites. Appl Microbiol Biotechnol, 92 (1):45-53.

171. van den Berg MA, Albang R, Albermann K, Badger JH, Daran J-M, Driessen AJM, García-Estrada C, Fedorova ND, Harris DM, Heijne WHM, Joardar V, Kiel JAKW, Kovalchuk A, Martín JF, Nierman WC, Nijland JG, Pronk JT, Roubos JA, van der Klei IJ, van Peij NNME, Veenhuis M, von Döhren H, Wagner C, Wortman J, Bovenberg RAL (2008). Genome sequencing and analysis of the filamentous fungus *Penicillium chrysogenum*. Nat Biotechnol, 26 (10):1161-1168.

172. van den Berg MA, Bovenberg RAL, Driessen AJM, Konings WN, Nieboer M, Schuurs TA, Westerlaken I (2001) Enhancing secretion of beta-lactam compounds from a micro-organism by enhancing adenosine triphosphate-binding cassette transporter activity, useful for producing e.g. penicillin and cephalosporins. WO2001/32904, 2001.

173. van der Lende TR, Breeuwer P, Abee T, Konings WN, Driessen AJM (2002). Assessment of the microbody luminal pH in the filamentous fungus *Penicillium chrysogenum*. Biochim Biophys Acta, Mol Cell Res, 1589 (2):104-111.

174. van der Rest ME, Kamminga AH, Nakano A, Anraku Y, Poolman B, Konings WN (1995). The plasma-membrane of *Saccharomyces-cerevisiae*- structure, function, and biogenesis. Microbiol Rev, 59 (2):304-322.

175. van Gulik WM, Antoniewicz MR, deLaat WTAM, Vinke JL, Heijnen JJ (2001). Energetics of growth and penicillin production in a high-producing strain of *Penicillium chrysogenum*. Biotechnol Bioeng, 72 (2):185-193.

176. van Gulik WM, de Laat WTAM, Vinke JL, Heijnen JJ (2000). Application of metabolic flux analysis for the identification of metabolic bottlenecks in the biosynthesis of penicillin-G. Biotechnol Bioeng, 68 (6):602-618.

177. Veiga T, Solis-Escalante D, Romagnoli G, ten Pierick A, Hanemaaijer M, Deshmukh AT, Wahl A, Pronk JT, Daran JM (2012). Resolving phenylalanine metabolism sheds light on natural synthesis of penicillin G in *Penicillium chrysogenum*. Eukaryot Cell, 11 (2):238-249.

178. Verheijen PJT (2010). Data reconciliation and error detection. In: The Metabolic Pathway Engineering Handbook. Fundamentals. CRC Press, Boca Raton, FL:8:1-12.

179. Visser D, van Zuylen GA, van Dam JC, Oudshoorn A, Eman MR, Ras C, van Gulik WM, Frank J, van Dedem GWK, Heijnen JJ (2002). Rapid sampling for analysis of in vivo kinetics using the BioScope: A system for continuous-pulse experiments. Biotechnol Bioeng, 79 (6):674-681.

180. von Döhren H, Keller U, Vater J, Zocher R (1997). Multifunctional peptide synthetases. Chem Rev, 97 (7):2675-2706.

181. Weber SS, Kovalchuk A, Bovenberg RAL, Driessen AJM (2012). The ABC transporter ABC40 encodes a phenylacetic acid export system in *Penicillium chrysogenum*. Fungal Genet Biol, 49 (11):915-921.

182. Weber SS, Polli F, Boer R, Bovenberg RAL, Driessen AJM (2012). Increased penicillin production in *Penicillium chrysogenum* production strains via balanced overexpression of isopenicillin N acyltransferase. Appl Environ Microbiol, 78 (19):7107-7113.

183. Whitaker A (1976). Amino acid transport into fungi: An essay. Trans Br mycol Soc, 67 (3):365-376.

184. Wiechert W, de Graaf AA (1997). Bidirectional reaction steps in metabolic networks: I. Modeling and simulation of carbon isotope labeling experiments. Biotechnol Bioeng, 55 (1):101-117.

185. Wiechert W, Siefke C, de Graaf AA, Marx A (1997). Bidirectional reaction steps in metabolic networks: II. Flux estimation and statistical analysis. Biotechnol Bioeng, 55 (1):118-135.

186. Wu L, Mashego MR, van Dam JC, Proell AM, Vinke JL, Ras C, van Winden WA, van Gulik WM, Heijnen JJ (2005). Quantitative analysis of the microbial metabolome by isotope dilution mass spectrometry using uniformly 13C-labeled cell extracts as internal standards. Anal Biochem, 336 (2):164-171.

187. Xu H, Andi B, Qian J, West A, Cook P (2006). The α-aminoadipate pathway for lysine biosynthesis in fungi. Cell Biochem Biophys, 46 (1):43-64.

188. Yang S, Sadilek M, Lidstrom ME. Streamlined pentafluorophenylpropyl column liquid chromatography-tandem quadrupole mass spectrometry and global C-13-labeled internal standards improve performance for quantitative metabolomics in bacteria. J Chromatogr, 1217 (47):7401-7410.

189. Zhang J, Demain AL (1992). ACV synthetase. Crit Rev Biotechnol, 12 (3):245-260.

190. Zhang J, Wolfe S, Demain AL (1992). Biochemical studies on the activity of δ-(L-α-aminoadipyl)-L-cysteinyl-D-valine synthetase from *Streptomyces clavuligerus*. Biochem J, 283 (3):691-698.

191. Zhao Z, Kuijvenhoven K, van Gulik WM, Heijnen JJ, van Winden WA, Verheijen PJT (2011). Cytosolic NADPH balancing in *Penicillium chrysogenum* cultivated on mixtures of glucose and ethanol. Appl Microbiol Biotechnol, 89 (1):63-72.

192. Zhu P, Oe T, Blair IA (2008). Determination of cellular redox status by stable isotope dilution liquid chromatography/mass spectrometry analysis of glutathione and glutathione disulfide. Rapid Commun Mass Spectrom, 22 (4):432-440.

Publications

Cornelissen S, Liu, S, Deshmukh AT, Schmid A and Bühler B (2011). Cell physiology rather than enzyme kinetics can determine the efficiency of cytochrome P450-catalyzed C–H-oxyfunctionalization, Journal of Industrial Microbiology and Biotechnology, 38,1359-1370.

de Jonge LP, Buijs NAA, ten Pierick A, Deshmukh AT, Zhao Z, Kiel JAKW, Heijnen JJ, van Gulik WM (2011). Scale-down of penicillin production in *Penicillium chrysogenum*. Biotechnology Journal, 6, 944-958.

Douma RD, Deshmukh AT, de Jonge LP, de Jong BW, Seifer RM, Heijnen JJ, van Gulik WM (2012). Novel insights in transport mechanisms of phenyl acetic acid and penicillin G in *P. chrysogenum,* Biotechnology progress, 28 (2), 337-348.

Seifar Maleki R*, Deshmukh AT*, Heijnen JJ, van Gulik WM (2012). Determination of δ-(L-α-aminoadipyl)-L-cysteinyl-D-valine in cell extracts of *Penicillium chrysogenum* using Ion Pair-RP-UPLC-MS/MS, Journal of separation science, 35, 225-230 (* : equal contribution).

Veiga T, Solis-Escalante D, Romagnoli GA, ten Pierick A, Hanemaaijer MJ, Deshmukh AT, Wahl AS, Pronk JT, Daran J-MG (2012). Resolving phenylalanine metabolism sheds light on natural synthesis of penicillin G in *Penicillium chrysogenum,* Eucaryotic cell, 11 (2):238-24

Deshmukh AT, van der Hoek C, Maleki Seifar R, ten Pierick A, Heijnen JJ and van Gulik WM L-α-Aminoadipate is not the limiting precursor aminoacid in the penicillin biosynthetic pathway in a high producing *P. chrysogenum* strain *(Submitted for publication)*

Deshmukh AT, Maleki Seifar R, ten Pierick A, Heijnen JJ and van Gulik WM. *In vivo* analysis of dynamics in metabolome, fluxome and secretion of the penicillin biosynthesis pathway metabolites in *Penicillium chrysogenum (Submitted for publication)*

Deshmukh, AT, Verheijen, PJT, Heijnen JJ and van Gulik WM. A complete *in vivo* kinetic model of the penicillin biosynthesis pathway in *Penicillium chrysogenum (Submitted for publication)*

Deshmukh AT, de Reus PE, Maleki Seifar R, Kralt A, Pieterse M, Pinkse MWH, Verhaert PDEM, Verheijen PJT, van der Klei IJ, Heijnen JJ and van Gulik WM. Production of δ-[L-α-aminoadipyl]-L-cysteinyl-D-valine as a model non ribosomal peptide in *P. chrysogenum*
(Submitted for publication)

Maleki Seifar R, Ras C, Deshmukh AT, Bekers KM, Suarez Mendez C, da Cruz ALB, van Gulik WM, Heijnen JJ. Quantitative analysis of intracellular coenzymes in *Saccharomyces cerevisiae* using ion pair reversed phase ultrahigh performance liquid chromatography tandem mass spectrometry.
(Submitted for publication)

Oral presentations

Understanding *in vivo* kinetics and transport through stimulus response experiments: *Penicillium chrysogenum* as host strain, *Metabolic Engineering IX conference*, Biarritz, France, 5th June 2012

Transport mechanisms for PAA and PenG in *Penicillium chrysogenum, 3rd Kluyver Centre Programme Meeting Day*, Wageningen, Netherlands, 23rd September 2010.

The in-vivo kinetics of ACV-synthetase and connected enzymes in *Penicillium chrysogenum.*, *TransACTS Symposium*, Lunteren, Netherlands, 12th January 2011.

Simulation of temperature distribution along the length of pin fin in natural & forced convection, *National Conference on Recent Advances in Mechanical Engineering (RAME-2004)*, Nashik, India, 16-17 January 2004.

QFD and SWOT-An effective tool for education system. *International Conference on Recent Advances in Education System*, Tiruchirapalli, India, 23rd February 2003.

Poster presentations

Deshmukh AT, Verheijen PJT, Maleki Seifar R, Heijnen JJ & van Gulik WM. Unraveling *in vivo* kinetics of penicillin biosynthesis pathway. *Metabolic Engineering IX conference*, Biarritz, France, 3-7 June, 2012.

Deshmukh AT, Verheijen PJT, Maleki Seifar R, Heijnen JJ & van Gulik WM. Understanding *in vivo* kinetics and transport through stimulus response experiments: *Penicillium chrysogenum* as host strain. *Metabolic Engineering IX conference*, Biarritz, France, 3-7 June, 2012.

Deshmukh AT, van der Hoek C, Maleki Seifar R, ten Pierick A, Heijnen JJ & van Gulik WM. L-α-aminoadipate is not the limiting precursor aminoacid in the penicillin biosynthetic pathway in a high producing *P. chrysogenum* strain, *ESF-EMBO Symposium on 'Synthetic Biology of Antibiotic Production'*: Sant Feliu de Guixols, Spain, 2-7 October, 2011.

Maleki Seifar R, Deshmukh AT, van Gulik WM, Heijnen JJ. Determination of δ-(L-α-aminoadipyl)-L-cysteinyl-D-valine in cell extracts of *Penicillium chrysogenum* using IP-RP-UPLC-MS/MS. *27th Asilomar conference on mass spectrometry*: USA, 30 September- 4 October, 2011.

Deshmukh AT, Maleki Seifar R, Bovenberg RAL, Heijnen JJ & van Gulik WM. Elucidation of the in-vivo kinetics of the penicillin biosynthesis pathway in *Penicillium chrysogenum* through stimulus response experiments. *Metabolic Engineering VIII conference*: Jeju Island, South Korea, 13-17 June, 2010.

Deshmukh AT, Maleki Seifar R, Bovenberg RAL, Heijnen JJ & van Gulik WM. Elucidation of the in-vivo kinetics of the penicillin biosynthesis pathway in *Penicillium chrysogenum* through stimulus response experiments. *International Conference on Systems Biology*: Edingburgh, UK, 10-15 October, 2010.

Deshmukh A.T., van Gulik W.M., Maleki Seifar R., Heijnen J.J. In vivo kinetic study of ACV synthetase in *Penicillium chrysogenum*, 5th DRC-LST / BSDL symposium, Delft , Netherlands, 4 November 2009.

Deshmukh AT. *et.al*. Integration of advanced oxidation technologies and biological processes: Recent developments, trends, and advances", *International Conference on Advances in Industrial Wastewater Treatment*, Chennai, India, 9-11 February 2005.

Curriculum Vitae

Amit T. Deshmukh was born on 10th April 1979 in Kotul, Akole, Maharashtra, India. He completed his secondary school from St. Xavier's High School and higher secondary school from K.T.H.M. College of science, situated in Nashik, India. He pursued further education from 1996 to 2000 to obtain Bachelors in Chemical Engineering at the University of Pune, India. From 2001 until 2005, he worked as Lecturer in Chemical Engineering at engineering institutes affiliated to University of Pune, India. First, during 2001-2002 at S. V. M. Engineering College and later from 2002 until 2005 at K. K. Wagh Institute of Engineering Education and Research. During this period, he was involved in conducting lectures and practicals for undergraduate students of chemical engineering, counseling and mentoring students, laboratory development and assisting research. From 2005 until 2007, he did his MSc. in Chemical Engineering with specialization in Bio-chemical engineering from the faculty of Biochemical and Chemical Engineering, Technische Universität Dortmund, Germany. During his master thesis, he worked in the field of intensification of a biotechnological process using whole cell bacterial strains in the group of Prof. Andreas Schmid at Technische Universität Dortmund, Germany. From July 2008, he worked as PhD researcher in the group of Prof. J.J. (Sef) Heijnen at the Delft University of Technology, Delft, The Netherlands. During his PhD, he was working on elucidating in-vivo enzyme kinetics of the penicillin biosynthesis pathway in *P. chrysogenum*. Currently he is working as an associate scientist at DSM, Delft, The Netherlands.

Acknowledgements

Any kind of accomplishment requires the effort of many people and the fruitful completion of this Ph.D. thesis is no different. First of all I would like to thank my promoter Sef Heijnen who gave me the opportunity to work in his group under his guidance. In these four years I have not seen anyone else as energetic as him. I have often tried to emulate his way of thinking and his enthusiasm for work. And I am happy to say that he is my "Guru" from whom I have learned a lot, not only technical aspects of the subject but also the way to follow the passion for work.

I would also like to thank my direct supervisor and co-promotor Walter van Gulik, with whom I had very good understanding on technical and personal front. We spent together many hours of fruitful discussions and his feedback on experimental design and later for the writing skills were helpful that has resulted in a good piece of PhD work. I also worked under his supervision for the KIT project. I foresee that we will have much collaboration in the future as well. I thank him for all his fruitful suggestions and guidance which kept the flow of the thesis in spite of many shortcomings.

I am also highly indebted to Peter Verheijen for sharing all his wits and years of experience in mathematics and statistics as well as in Matlab programming. I always admire the modelling and programming skills of him and he has helped me tremendously to carry out parameter estimation routines, which is a major part of this thesis. With his support I could make the work performed at TU Delft "statistically significant".

I sincerely thank Ida van der Klei, Lars Blank, Henk Noorman, Jean-Marc Daran, Marcel Zwietering, Luuk van der Wielen for accepting to be part of my PhD defense committee and for their valuable comments on my thesis.

Aljoscha Wahl and I, we both joined TU delft in the same month of 2008 and we flourished over the years. I also thank him to allow me to be a part of IGEM 2010 and suggesting fruitful inputs for the research and providing tools for analysis of labeling experiments data.

My association with the analytical group was very pleasant, be it the promptness of Angie or technical and personal chats with Cor, Jan, Zhen, and later with Patricia. They helped me a lot

by analysing hundreds of samples that I produced during my PhD work and later for the KIT project. Most notably was my association with Reza, with whom I shared “buddy” kind of relationship although he is much more experienced. We had a lot of discussion on accurately quantifying thiol compounds and this association nicely culminated in publications. We will continue this relationship even after I leave TU Delft. I also thank Johan for providing analysis of TOC. The whole thesis is based on the metabolomics data and therefore the analytical team from my perspective has contributed significantly for the completion of the thesis.

Most of the chapters in my thesis contain stimulus response experiments that needed rapid sampling, thus this work has also the contribution of the rapid sampling team members who helped at some point or other for rapid sampling: Lodewijk, Rutger, Emrah (first timer), Andre Canelas, Zheng, Elaheh, Zhen, Camilo, Katelijne, Luisa, Hugo (second timer), Mihir, Jinrui, Anisha, Reza, Angie, Patricia, Rob, Dirk, Aljoshca, Walter, master students - Mark, Klaas, Andre, Kai, Janneke, Robin, David, Tom, Oscar, Robin and Bouke, guest researchers - Joel, Christina, as well as members from other groups - Sushil, Camilo Lopez Garzon, Ishwar. I acknowledge their efforts to produce high quality data from the experiments.

The important part is to generate the data in the lab and with the help of fermentors and they are very well nurtured and mentored by Rob Kerste and Dirk Geerts and also for some period by Mario Pronk. These people were always there to help and to solve any kind of technical issues regarding the working of chemostat cultivations. With Dirk I also gave LST practicals and our cooperation was very nice.

I had close association with Lodewijk from whom I actually learned the chemostat cultivation of *P. chrysogenum*. I would like to thank him as I shared a lot of laboratory floor along with him. I also thank long discussions with Zheng with whom I also shared office for two years. I also had nice interactions with Rutger with whom I shared the same goal to find out transport mechanisms for PAA and PenG. Luisa and I shared the same room for the first 2 years of my PhD, starting and finishing almost at the same time, we shared nice moments of our PhD’s together. Katelijne and Camilo helped a lot during the KIT project to share their knowledge regarding yeast metabolism and I thank both of them. Camilo notably helped me to conduct labeling experiments and also for data processing techniques. Camilo is my paranymph for the thesis defense.

During these four years I had several colleagues who directly or indirectly had influence on my work. I enjoyed their company and that made working in the lab and in the office very satisfactory. They include most notably Andre Canelas, Emrah, Elaheh (helped especially for the KIT project), Hilal, Lodewijk, Luisa, Katelijne (also helped to translate propositions), Camilo, Hugo, Rutger, Sergio, Domenico, Marco and Zheng. Most importantly the Latin Americans (Camilo and Hugo) brought a bit of fun in the lab, which otherwise was strictly Dutch. I also thank colleagues from other groups who directly or indirectly made the department a cheerful place to work and helped me whenever necessary most notably members from IMB group Jean-Marc, Ton, Pascale, Erik, Marijke, Tania, Daniel, Marit, Stefan, Rintze, Benjamin, Nakul, Ishwar and Victor. I also thank members from BST group Adrie, Maria, Rob, Marcel, Stef, Max, Kedar, Sreekant, Camilo, Carol, Cagri, Beckley, Esteban and Sushil.

I thank Sjaak, Robert, Jos, Arno & workshop team, Herman, Hans, Astrid, Apilena, and Jannie for providing excellent co-ordination between people in the department and providing facilities needed in the lab, office and in the kitchen. I also thank our secretary, first Anette and then in the later years Jenifer (who also kept the looks of the department tall, dark, tough and stubble), for arranging the departmental formalities as and when necessary. I also shared some nice chatting with Kawita occasionally.

During my PhD I supervised two Bachelor students - Christiaan and Elise and they both contributed significantly for their part. Elise also helped me to translate the summary of the thesis in Dutch. I thank both of them for active participation in the research work.

Association with other groups and discussions with the faculty members was essential to overcome some the questions raised during the research work. I worked in collaboration with other groups either from TU Delft or from other universities. Especially the collaboration with Tania Vegia and Jean-Marc Daran from IMB resulted into a nice publication. I also worked with mutants especially strains prepared by Annemarie Kralt (RUG) and Stefan Weber (RUG). I also had collaboration with Pieterse M. and Martijn Pinkse for determining ACVS enzyme level. Adrie Straathof (BST group) provided inputs and insights for 6APA production. I thank them all, for providing help when needed.

I received lot of productive feedback during the IBOS and Kluyver centre meetings. Most notably from the people who were related to my project such as Jack Pronk and Jean-Marc Daran from IMB group at TU Delft, Ida van der Klei, Arnold Driessen, and Jan Kiel from RUG. I also thank the industrial partner of this project, DSM, who financially supported this project in cash and kind, and arranged for the strains necessary for the research. They also contributed valuable suggestions for the fulfilment of the research especially Roel Bovenberg, Wouter van Winden and Remon Boer.

And most important are the friends who always stood by me and my wife when we are away from our home and gave us the comfort of not been far away from our relatives and family and parents. I would like to mention Sushil (BST group) who is a very close friend of mine from last 7 years and was always there at any time not only socially but also for helping during rapid and weekend sampling. Other friends with whom I share some of the memorable moments are Amol, Somnath, Sameer Patwardhan, Amit Patil, Sudam, and Krishna with whom I spent many weekends and evenings of my first year of PhD. With my friends Kedar, Sreekant, Samir, Somnath, Sushil, Amol, Nishant and Nilesh I enjoyed weekend "Galli Cricket" in Netherlands. Friends from back home Satish, Santosh, Santosh Kadam, Nilesh Rao, Pravin also encouraged me from time to time.

My family friends that include most importantly Singare family, Lawand family, Sable family, Gaykawad family, Bajaj family, Mahashabde family, Sandesh-Manjushree family, Pisat family, Patil Amol family, Kulkarni Samir family, Wadekar family and Patil Deepak family with whom I have spent many weekends and memorable vacation/fietsen trips. They were always besides me during the high and low times and provided support in all forms during my stay in Delft. Also, we celebrated together many Indian festivals that brought Indian nostalgia in the foreign lands, and we have now become a one "Delft Indian family".

I would also like to mention my Dutch language tutor, Wil Castenmiller with whom I share my Friday evenings and exchange our cultural traits and have improved my language skills very much. Also, to mention Theo and Marijke Kaspenburg who are our Dutch family friends, which whom we share our culture and festivities and who have helped us to integrate in the Dutch society.

If inadvertently I have not mentioned any name I would like to express my gratitude to all those who made my stay at TU and in Delft a memorable one.

In the end I would like to mention my wife - Swati, whose patience and support during the high and low times of my PhD was instrumental in accomplishing this task. She was the one who stood by me literally day and night and I hope to get her support till death parts us.

And last but not the least I would like to thank my parents and family members who were behind me and encouraging me always to take challenges in life and giving me comfort when considered necessary. My grandfather passed away during the course of my PhD and could not see this day, therefore I dedicate my thesis to him. My parents and family once had a dream to see me as a doctor and I am happy to finally fulfill their dream. They in reality gave me the strength to come up to this turning point in my life and complete one of the stepping stone in the form of Doctoral degree……

- Amit T. Deshmukh
July 2013, Delft